AN INTELLIGENT ENGINE CONDITION MONITORING SYSTEM

by

Osama Esmail Mahmoud Esmail

This thesis is submitted in fulfilment of the requirements for the degree of Doctor of Philosophy

School of Mechanical and System Engineering
Newcastle University, UK

February 2009

CONTAINS A PULLOUT

ABSTRACT

The main focus of the work reported here is in the design of an intelligent condition monitoring system for diesel engines. Mechanical systems in general and diesel engines in particular can develop faults if operated for any length of time. Condition monitoring is a method by which the performance of a diesel engine can be maintained at a high level, ensuring both continuous availability and design-level efficiency. A key element in a condition monitoring program is to acquire sensor information from the engine, and use this information to assess the condition of the engine, with an emphasis on monitoring causes of engine failure or reduced efficiency.

A Ford 70PS 4-stroke diesel engine has been instrumented with a range of sensors and interfaced to a PC in order to facilitate computer controlled data acquisition and data storage. Data was analyzed to evaluate the optimum use of sensors to identify faults and to develop an intelligent algorithm for the engine condition monitoring and fault detection, and in particular faults affecting the combustion process in the engine. In order to investigate the fault-symptom relationships, two synthetic faults were introduced to the engine. Fuel and inlet air shortage were selected as the faults for their direct relationship to the combustion process quality. As a subtask the manually operated hydraulic brake was adapted to allow automatic control to improve its performance. Two modes of controlling were designed for the developed automatic control of the hydraulic brake system.

A robust mathematical diesel engine model has been developed which can be used to predict the engine parameters related to the combustion process in the diesel engine, was constructed from the basic relationships of the diesel engine using the minimum number of empirical equations. The system equations of a single cylinder engine were initially developed, from which the multi-cylinder diesel engine model was validated against experimental test data. The model was then tuned to improve the predicted engine parameters for better matching with the available engine type. The final four-cylinder diesel engine model was verified and the results show an accurate match with the experimental results.

Neural networks and fuzzification were used to develop and validate the intelligent condition monitoring and fault diagnosis algorithm, in order to satisfy the requirements of on-line operation, i.e. reliability, easily trained, minimum hardware and software requirements. The development process used a number of different neural network architecture and training techniques. To increase the number of the parameters used for the engine condition evaluation, the Multi-Net technique was used to satisfy accurate and fast decision making. Two neural networks are designed to operate in parallel to accommodate the different sampling rate of the key parameters without interference and with reduced data processing time. The two neural networks were trained and validated using part of the measured data set that represents the engine operating range. Another set of data, not utilized within the training stage, has been applied for validation. The results of validation process indicate the successful prediction of the faults using the key measured parameters, as well as a fast data processing algorithm.

One of the main outcomes of this study is the development of a new technique to measure cylinder pressure and fuel pressure through the measurement of the strain in the injector body. The main advantage of this technique is that, it does not require any intrusive modification to the engine which might affect the engine actual performance. The developed sensor was tested and used to measure the cylinder and fuel pressure to verify the fuel fault effect on the combustion process quality. Due to high sampling rate required, the developed condition monitoring and fault diagnosis algorithm does not utilize this signal to reduce the required computational resources for practical applications.

ACKNOWLEDGMENT

It is not easy to list the many people who have helped me during the course of this project, as it is now presented. But my first thanks and grateful are to Dr. Robert Bicker, my supervisor, for his continues support and help, but most of all, for his constructive technical advice and many suggestions throughout this project, which has been invaluable.

Special thanks must be directed to the Egyptian Government whose support this study financially and academically through the Educational and Culture Bureau in London.

I would also like to thank the Robotic Laboratory group in the Mechanical and System School, especially Dr. Jack Hill for making available one of the data acquisition card. Thanks are also due to all the technicians who have helped and support during this project.

Finally I would like to thank and dedicate this thesis to my family, especially my wife, and my kids Mahmoud, and Mariam. Especial thanks to my mother for her support and encouragement during my whole life.

CONTENTS

LIST OF FIGURE

LIST OF TABLES

NOMENCLATURE

Symbol	Meaning	Unit
A	Cylinder inner surface area	m^2
A, B, C, D	Matrices defining physical relationships	
A_p	Piston area	m^2
A_v	Valve area	m^2
b_1, b_2	Length ratio	
C_d	Discharge coefficient	
F	Equivalence ratio	
f	Actual fuel-air ratio	
$fmep$	Friction mean effective pressure	bar
f_s	Stoichiometric fuel-air ratio	
H_o	The total stagnation enthalpy	kJ
h_o	Specific stagnation enthalpy	kJ/kg
ID	Ignition delay	ms
J	Engine inertia	$Kg.m^2$
J_1	Dynamometer inertia	$Kg.m^2$
J_c	Moment of inertia of crankshaft	$Kg.m^2$
J_R	Moment of inertia of connecting rod	$Kg.m^2$
k	Thermal conductivity	kW/m^2 K
L	Connecting rod length	m
L	Valve lift	mm
M	Mass of the piston assembly	kg
m	Mass	kg
m_a	Air mass	kg
m_{bf}	Mass of burnt fuel	kg
m_c	Mass of the crankshaft	kg
m_R	Mass of the connecting rod	kg
m_p	Mass of the piston	kg
$(\acute{m}_f)_{diff}$	Normalized fuel burning rate in diffusion mode	
$(\acute{m}_f)_{norm}$	Normalized total fuel burning rate	
$(\acute{m}_f)_{pre}$	Normalized fuel burning rate in the premixed mode	
N	Crankshaft rotational speed	RPM
N_p	Mean piston speed	m/sec
P	Pressure	kPa
P_{atm}	Atmospheric pressure	kPa
Q	Heat transfer	kW
Q_a	Air flow rate	kg/s
$\acute{Q}_{ht}$	Total heat transfer rate	kW

Symbol	Meaning	Unit
$\dot{Q}_{ht1}$	Convective heat transfer rate at the gas to cylinder wall interface	kW
r	Crank radius	m
R	Gas constant	kJ/kg K
R_w	Thermal resistance for conduction	W/(m^2 K)
R_{wc}	The thermal resistance from wall to coolant fluid	W/(m K)
s	Function of the valve lift to valve diameter ratio	mm
ST	Piston stroke value	m
t	Time	sec
T	Temperature	K
t	Wall thickness	mm
T_1	Exhaust gas temperature of cylinder one	K
T_2	Exhaust gas temperature of cylinder two	K
T_3	Exhaust gas temperature of cylinder three	K
T_4	Exhaust gas temperature of cylinder four	K
T_5	Total exhaust gas temperature	K
T_a	Inlet air temperature	K
T_f	Mechanical friction torque	Nm
T_f	Injected fuel temperature	Nm
T_i	Indicated torque	Nm
T_L	Applied external load torque	Nm
T_D	damping torque for dynamometer	Nm
T_r	Reciprocating torque	Nm
T_{rad}	(Bulk) radiant temperature	K
T_s	Stiffness torque for dynamometer	Nm
T_{wall}	The inside wall surface temperature of the cylinder head, piston or liner	K
u	Input to the system	
U	Internal energy	kJ/K
u	Specific internal energy	kJ/kg
V	Cylinder volume	m^3
V_o	Measured output voltage	Volt
V_s	The voltage supplied	Volt
W	Work done by the system	kJ
x	A vector containing the states of the system	
y	Output of the system	
y	Piston displacement	m

Greek Symbol	Meaning	Unit
θ	A vector of parameters.	
β	Connecting rod (small end) angle	rad
δ	Pin offset	mm
ϕ	Connecting rod (big end) angle	rad
λ	Geometric factor	
γ	Specific heat ratio	kJ/kg K
β	Burning factor	
σ	Stephan-Boltzman constant	
ε	The apparent grey body emissivity	
θ_1	Crankshaft angle	rad
ω_1	Angular velocity of the engine crankshaft	rad/s
ω_2	Angular velocity of dynamometer shaft	rad/s
θ_2	Dynamometer angular position	rad
θ_{com}	The combustion duration angle	degree
θ_{ign}	The angle at ignition	degree
θ_{inj}	The angle at injection	degree
θ_{norm}	Non-dimensional normalized angle	

Abbreviation	Meaning
A/F	Air-fuel ratio
ADALINE	Adaptive liner element
AI	Artificial intelligence
ANA	Artificial neural network
ART	Adaptive resonance theory
BP	Back propagation
BPM	Back propagation with momentum
CCEM	Cylinder-by-cylinder engine model
CMAC	Cerebellar model articulation controller
CMFD	Condition monitoring and fault diagnosis
DIAS1	Diagnosing expert system
DMLP	Dynamic multilayer Perceptron
DSP	Digital signal processor
EBF	Ellipsoidal basis function
EXEDS	Expert engine diagnosis system
FCEM	Four cylinders engine model
FLN	Functional link neural
FLP	Fuel pump lever position
FPN	Functional polynomial network
GD-FNN	Generalized dynamic fuzzy neural network
GMDH	Group method data handing

Abbreviation	Meaning
IECM	Intelligent engine condition monitoring
IFAC	International Federation of Accountants
LMS	Perceptron learning and least mean squares
LOLIMOT	Local linear model type
MLP	Multilayer Perceptron
MLR	Multiple linear regression
MSOM	Modified self-organizing map network
MVEM	Mean value engine model
NN	Neural network
NPERG	Nonlinear parity equation residual generation
PNN	Polynomial neural network
PNNS	Probabilistic neural networks
PRBS	Pseudo-random binary sequence
RBF	Radial basis function
RNN	Recurrent neural network
SAILOR	Seoul national university artificial intelligent language with objects and rules.
SBDS	Service bay diagnosis system
SCEM	Single cylinder engine model
TDC	Top dead centre
TSK	Takagi-Sugeno-Kang fuzzy system

CHAPTER 1

INTRODUCTION

The history of the diesel engine extends back to the end of the nineteenth century when Dr. Rudolf Diesel began his pioneering work on air blast injected stationary engines, and maintains a dominant position in many applications throughout industry and transport such as, marine, automotive, and power generation plants. The diesel engine is capable of further improvement and will continue to have an assured place as the most efficient liquid fuel burning prime mover yet devised, Baranescu, [1999]. They have a very wide operating range and engine performance depends mainly on the operating conditions which change due to variations in load, speed, rate of fuel consumption, as well as environmental conditions. To maintain engine performance as high as possible, it is vital to adjust the engine parameters within an optimum range, corresponding to its wide operating envelope, and keep the engine operating in an efficient, safe and reliable way.

The reasons for the diesel engines success can be summarised by simple operation, fuel availability, high reliability, high thermal efficiency, and low fuel consumption. The continuous availability of the engine is vital where safety is important and depends upon it. This investigation focuses on achieving continuous availability and reliability of the diesel engine at highest efficiency using condition monitoring and fault diagnosis. During condition monitoring information is collected from the engine whilst in operation, and compared against prior knowledge from a healthy engine. An evaluation is then carried out to meaningfully interpret the actual engine condition and includes the ability to identify any degradation that may result in reduced performance or equipment malfunction. In the fault diagnosis stage, the collected data is used to support a decision on the source of fault and its level. How long the machine can continue to be safely operated can also be evaluated. With this kind of knowledge, the engine can serve the owner with high efficiency and continuous availability, and furthermore, there may be no need to perform any periodic maintenance that is usually required to ensure the highest reliability.

1.1 BACKGROUND TO CONDITION MONITORING AND FAULT DIAGNOSIS

The traditional method of condition monitoring was carried out using manual inspection, relying on the expertise of a technician to monitor and check the engine performance. For example, when the technician observes a reduction in the generated power, he will undertake a sequence of inspections which may involve measuring the off-line cylinder compression pressure. A reduction in the peak pressure might indicate leakage from the cylinder which could be attributable to damaged valves, rings, or cylinder head gasket. To ascertain the specific fault it will then be necessary for the technician to dismantle the cylinder head and inspect the condition of the internal parts. By introducing continuous on-line condition monitoring, it is possible to measure the condition and performance of the diesel engine whilst it is running. At the same time, measurements can identify when it is necessary to renovate or replace engine parts. This measurement data could therefore be uploaded to an automated system that evaluates the engine condition and can predict the possible fault cause and level.

Many researchers and manufacturers have paid close attention to developing a variety of fault diagnosis methods or systems. Among these, the researcher's effort is focused on robust and economic condition monitoring and fault diagnosis systems for the overall diesel engine or a specific subsystem. Most of the engine condition monitoring and fault diagnosis systems that have been reviewed are based on off-line testing and analysis. Since the 1980s, many scientists and researchers have developed models using knowledge based diagnostic reasoning that can solve various types of problem. Conventional models have bottlenecks, such as knowledge acquisition, complexity, and required a large knowledge base. Recently researchers have carried out considerable work using a diagnostic approach based on neural networks, fuzzy logic, or a combination of the two. Because of its high compatibility with non-linear complex systems, the neural network was selected for the proposed engine condition monitoring and fault diagnosis system. In addition, neural networks offer a promising solution that can mimic the human information processing capability. Fuzzification, which is only part of the fuzzy logic structure, was utilized to develop a simple output that gives the user a simple recommended action.

A data acquisition system has been constructed to collect information using appropriate sensors on an existing four cylinder Ford 4-stroke diesel engine. The collected information is used to monitor the engine condition as well as detect any changes that may develop and cause a mechanical fault or reduction in performance. The acquired data was used to construct a Neural Network algorithm that can evaluate the engine condition and detect a fault before it develops to a severe level. A review of previous research in this field shows that the most suitable neural network architectures for the non-linear system are the Radial Basis Function (RBF) and Multi-Layer Perceptron (MLP). A comparison between the two topologies was carried out to evaluate the optimum architectures for the diesel engine application, with the aim of minimizing the number of sensors for the condition monitoring and fault diagnosis system algorithm. This was evaluated by only using the key parameters that is able to detect and evaluate the engine condition and possible faults.

The neural network accuracy depends primarily upon the amount of available data. However, to increase the testing regime an analytical engine model has been constructed using the chemical, thermodynamic and dynamic mathematical relationships that govern the different engine processes. This model was verified and then utilized to investigate the effect of various changes in the engine parameters, as well as being used to generate another set of data for evaluating the condition monitoring and fault diagnosis algorithm. The proposed model was constructed using general relationships that can be adopted to suit high speed medium size diesel engines.

1.2 AIM, OBJECTIVES AND HYPOTHESIS

The aim of this research is to design and develop an intelligent engine monitoring system using a set of sensors to establish the engine status. This information was used to arrive at an informed decision regarding the continued operation and status of the engine and to predict the likely mode of failure. The hypothesis of this work is whether it is possible to implement a condition monitoring and fault diagnosis system using a limited number of low cost sensors coupled to a Neural Networks system to predict the mode of failure. As the system is in the development stage it was designed for use in a maintenance shop environment taking into account the

future application of the system in an on-line engine CMFD. This aim and hypothesis in addition to the basis of condition monitoring and fault diagnosis (CMFD) systems for diesel engine prompted the author to set the objectives of the research as follows:

* Review the past and current practice and application of condition monitoring and fault diagnosis (CMFD) systems in the area of diesel engine application.
* Integrate an available diesel engine with appropriate sensors to monitor its condition under different operating conditions.
* Design and implement a data acquisition system for an automotive diesel engine.
* Design and implement an analytical model for the diesel engine system that has the capability to investigate the effect of physical parameters change on the engine performance.
* Construct a neural network algorithm that has the ability to evaluate the engine condition according to the minimum possible sensor signals.

In order to design and validate a new CMFD, an experimental test facility was developed and instrumented with the required sensors. An existing four cylinder Ford 4-stroke diesel engine (Type 70PS) was utilized for the experimental test programme. The engine was connected to a manually controlled Froude DPX3 200hp sluice plate hydraulic dynamometer to provide the engine load. It was decided to automate the brake control to provide the test system with the facility of actual load simulation throughout the evaluation of the proposed CMFD algorithm.

Following the engine instrumentation, the data acquisition code was designed using Labview (National Instruments) utilizing a high speed data acquisition card. After implementing and testing the whole system, the performance of the engine was fully investigated to establish the ability of the engine CMFD system to diagnose faults. Synthetic faults were introduced on the engine to simulate the actual situation, and the ability of the CMFD system to detect the fault nature was then explored.

Because of the non-linearity and complex dynamic characteristics of the diesel engine, neural networks and fuzzy logic techniques were selected for the fault diagnosis algorithm. Little or almost no process knowledge is required, and the neural networks rely on the fact that knowledge about fault patterns is already embedded in the measured sensor signals. Therefore, this technique requires extensive training sets of data to cover all of the possible operating conditions. The time and cost of collecting all of the data experimentally was an issue and it was decided to develop an analytical engine model that is capable to work in parallel with the actual engine to increase the amount of the available data for training and testing process of the proposed CMFD algorithm of the diesel engine. The model was designed to be applicable for most medium size diesel engine types; and was constructed using MATLAB/SIMULINK (Mathworks).

1.3 RESEARCH OUTCOME

As a result of the presented work, all of the above objectives and the hypothesis had been achieved as well as subtasks challenges raised through the research progress. The main outcomes can be summarized as follows:

* Developments of a new technique for cylinder and injection fuel pressure measurements.
* Evaluate the key parameters to detect the presence of air inlet and fuel blockage faults.
* Development a neuro-fuzzy engine CMFD algorithm that is able to utilize the key parameters of the engine to detect the air inlet and fuel blockage faults and evaluate its severity level.
* Building up of analytical simulation model of diesel engine that had the capability of predicting the main parameters of the diesel engine.

1.4 OVERVIEW OF THE THESIS CONSTRUCTION

The thesis comprises seven chapters as follows:

The background as well as the aims, objectives and hypotheses of the research have been introduced in the Chapter One. A detailed literature review and discussion of the previous research in the field of condition monitoring and fault

diagnosis of the diesel engine is covered in Chapter Two, and aims to give the reader a classification of the different methods used to construct a condition monitoring and fault diagnosis systems starting from early in the 1970s until the recent available techniques. The limitations and the reasons for the selection of neural network for the proposed algorithm are summarised at the end of the chapter.

In Chapter Three, a detailed explanation of the experimental diesel engine testing system is covered. The hydraulic brake modification to improve loading performance with sensors, actuator and control system is discussed. The selected measured parameters and the appropriate sensors used for the engine condition monitoring and fault diagnosis testing system are introduced. The hardware and software requirements for the data acquisition system are also explained, and the Labview software developed for the data collection program is described in detail.

Chapter Four includes all experimental results. The data is analysed and different operating conditions compared. The discussion leads to a selection of the physical parameters that reveal the engine condition under different operating conditions. The data was subsequently used for the verification of the constructed analytical model.

Chapter Five focuses on the proposed engine model and explains the rational and mathematical relationships used for the model. The relationships are classified into two main sections. The dynamics of the engine form one part while the thermodynamic and chemical subsystems of the diesel engine represent the second part. The proposed model is constructed in the MATLAB/SIMULINK environment. The simulation results are presented at the end of this chapter.

The main outcome of the present work comprises Chapter Six, where the engine condition monitoring and fault diagnosis algorithm are described in detail. This chapter aims to explain the principle on which the neural network topology was selected, and how it satisfies the complex requirements and non-linearity of the diesel engine. In addition, a detailed description of the technique used to train the Neural Network for fault detection and diagnosis is also included. The validation and testing steps using experimental results of the engine are evaluated. A brief

discussion of the possible applications of the developed engine condition monitoring and fault diagnosis algorithm is included.

A summary of the outcome from the present work is given in Chapter Seven, along with suggestions for future work. The technical specifications for the components used in the test system are listed in Appendix A and a detailed description of the designed electronic circuits required for the signal processing of the measured signal is given in Appendix B. Appendix C details the mathematical calculations used within the design of the new pressure sensor utilized for measuring the cylinder and injection fuel pressures. The calculations include both the design equations and calculations used for conversion of measured signal. Finally, additional experimental results, which had not been included in the thesis context, are included in Appendix D.

CHAPTER 2

LITERATURE REVIEW

Engine health monitoring, more commonly described as performance or condition monitoring, has been totally revolutionized by the development of the microprocessor and associated software programs. Condition monitoring has perhaps always had higher priority on ships at sea and power plant units than in any other application; for obvious reasons since here an engine failure can result in large loss in life and money. The engine room log sheet, in which the watch keeper records many parameters such as loads, speeds, key pressures and temperatures and the results of occasional manual checks on such measurements as maximum cylinder pressures, is a primitive example of condition monitoring. Such monitoring however has many limitations.

Most of these limitations may now be transcended as a result of two main developments; the vast range of robust and reasonably cheap transducers that are now available, and the ready availability of computer systems capable of storing and handling a vast amount of data, with the ability to recognize complex patterns and trends of behaviour that may represent deterioration or actual danger, as well as the capability of issuing appropriate warnings.

Nevertheless, when making the change from a manned to an unmanned or partially manned system it is well to be aware of what may be lost, as well as what it is hoped to be gained. In a manned installation, the 'expert man system', the engineer, is capable of a range of diagnostic skills and responses that cannot be fully equalled artificially; he will be, for example, have the ability to use historical background experience with the engine to evaluate the meaning of the measurements.

It will be evident that the 'intelligence' of an automated or so-called 'expert' system will be only as good as the model embodied in the computer software; there are many possible models just as there are many possible engine installations. An engineer responsible for choosing such a system for a given application should

check that it is capable of recognizing all the types of malfunction and deterioration that he can foresee, also that it has sufficient built-in flexibility to allow development as experience with the particular installation is accumulated.

Moving from a traditional method of condition monitoring, which is carried out by means of inspection, to a modern condition monitoring system began in the 1970s, where Langballe et al., [1975], describe the development of instrumentation systems for monitoring diesel engines. The development of these condition monitoring systems involved details research into the failure mechanisms in diesel engines and how they behave under wide range of service conditions over a long period of time. It had been shown that it was possible and advantageous to monitor the process and the components directly by means of special sensors to provide more efficient condition monitoring performance than relying on derived information from indirect physical measurements.

Sletmo, [1978], introduce the CYLDET-CM system for condition monitoring of marine diesel engines built up from modules in the alarm system and microcomputer-based digital electronic system DS-8. This system was based on the use of a number of different transducers for the direct, continuous measurements of the cylinder parameters such as combustion pressure and liner surface temperature. Due to the available computational resources at this time, many limitations were found through the development of this system such as low processing speed and utilization of intrusive and unreliable sensors. However, the results were promising and forward looking to the different challenges.

Since then, many researchers have been focused on complete Condition Monitoring and Fault Diagnosis (CMFD) systems for the diesel engine such as, Tjong et al., [1993] Jones and Li, [2000]; Yin et al., [2003]; and Jiang et al., [2008]. The CMFD developer has access to many techniques, such as expert systems, feature extraction, parameter estimation, neural networks, and model-based CMFD systems to monitor the diesel engine condition. Both off-line and on-line CMFD were investigated indicating the advantage and disadvantage of each method.

This chapter covers previous literature in the main areas relating to the diesel engine condition monitoring and fault diagnosis systems. A brief discussion of the different fault detection and diagnostic techniques had been introduced. A review of the different methods used for the diesel engine simulation modeling is included and discusses the advantages and disadvantages of each method. As the neural networks represent one of the most promising techniques in the building of CMFD for internal combustion engines in general and diesel engine specifically, a detailed discussion of the general considerations required for the design and training processes is also explained. The classification of the neural networks topology is covered as well as the training methods for neural networks. A summary of the main outputs of the chapter is also included.

2.1 FAULT DETECTION AND DIAGNOSTIC TECHNIQUES

In this section, a number of techniques proposed for computerised decision making are presented. Note that some conditions can be identified with relative ease if there is a readily available variable for measurement that relates directly to the fault. An example of this is the flow through the oil filter. This condition may be evaluated through the differential pressure over the oil filter, the higher it is the dirtier the filter. Such straightforward condition monitoring techniques are useful to identify, and the required sensors may be fitted and inspected after doing a cost – necessity analysis. As an example, the sensors are usually fitted to evaluate the condition of a lubrication oil filter, but not in the case of an air filter. This is because the health of the engine is more vulnerable to a lack of oil than a shortage in air, i.e. the engine will not be permanently damaged from limited air supply. Other faults may not be directly related to a simple measurable quantity, or a suitable sensor may not be fitted due to restraints in space or resources. The intention of the following section is to review some techniques that help to identify these faults based on more indirect information that is simply measured using reasonable cost sensors.

2.1.1 Expert system

An expert system is a computer program in which the knowledge of an expert on a specific subject can be incorporated in order to solve problem or give advice and thus is capable of emulating human cognitive skills such as problem solving,

visual perception and language understanding. An expert system usually consists of a knowledge base, an interface mechanism, an explanation component, a user interface and acquisition component. Expert system can capture the knowledge of an expert in a particular area, computerize it into some software then transfer it to others users. Similar to human expert, expert system can reason logically, make decisions and explain the final conclusions.

Some engine manufacturers have been conducting extensive research to produce an efficient engine that satisfies customer requirements and complies with environmental legislation. For example, the Ford Motor Company has designed a Service Bay Diagnosis System (SBDS), an expert system to replace traditional printed service manuals and analogue test devices, Bielawski and Lewand, [1991]. A DIAgnosing expert System DIAS1 is being developed using the Seoul national university Artificial Intelligent Language with Objects and Rules (SAILOR) expert shell, which is an expert diagnosis system for ECU controlled automobile engines produced by Hyundai Morots Corporation in Korea, Yoo and Kim, [1992].

Later, Gelgele and Wang, [1998], introduce EXpert Engine Diagnosis System (EXEDS) which is a prototype intelligent diagnostic for automobiles engines. The objective is to help mechanics and car drivers in systematic diagnosis of their daily engine failure and be able to give both low-level and expert assistance in fixing engine malfunctions. It consists of diagnostic rules that progressively led to the possible causes of failure by utilizing a decision tree that represent the expertise in a clear and compact way.

In general, all expert systems face the same problem where knowledge acquisition was the first and most difficult task in the developing process. The knowledge should not only based on correct facts and data, but should also include all possible alternatives to avoid any incorrect diagnosis that leads to unnecessary repair or replacements. In addition, the rule processing mechanism chosen are of primary importance in determining the performance of the entire system. Different types of problems require different type of inference mechanisms that must be adapted to the problem to be solved, Kalogirou, [2003].

2.1.2 Parameter estimation approach

From a theoretical point of view, any linear dynamic system may be represented as a coupled set of first order differential equations:

$$x' = Ax + Bu \tag{2-1}$$

$$y = Cx + Du \tag{2-2}$$

Here x is a vector containing the states of the system. The states are any selected physical variables in time which will fully define the system, e.g. for a second order system mass-spring system, two states, typically position and velocity, are required. u represent the input and y represent the output of the system. A, B, C, and D are matrices defining physical relationships. The matrix D is usually zero, and will be omitted in the following discussion. In the case of D = 0, the states are easily found from equation (2-2) thus

$$x = C^{-1}y \tag{2-3}$$

This simple relationship is only valid if C is invertible, i.e. only for linear systems. In the more likely general case the system equations take the following form

$$x' = f_1(x, u, t, \theta) \tag{2-4}$$

$$y = g_1(x, u, t, \theta) \tag{2-5}$$

where f_1 and g_1 are non-linear equations. θ is a vector of parameters, equivalent to the coefficients of the matrices A, B, C and D. In the general case these coefficients may change, hence the system behaviour will change.

The presence of faults will cause the system to change its behaviour, i.e. the θ vector will change. In the linear system analogy, when this system of matrices A, B, and C could change. Any model of the healthy engine will produce incorrect states and output vector in the case of a fault. Thus the faults or abnormal situation

can be identified. Pursuing this idea, the model could be adjusted such that it will give an output that is more like the actual engine output by changing the parameter vector θ; the values that gives the minimal errors is considered to best describe the engine. By correlating the values of the parameters and a range of faults, successful diagnostics is achieved.

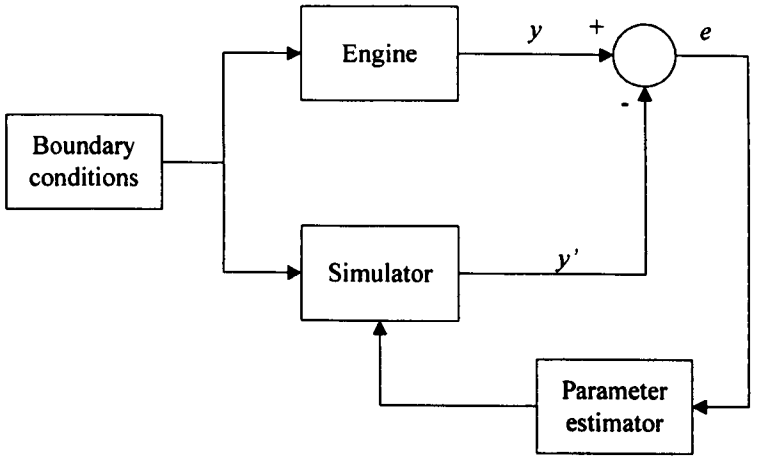

Figure 2.1 Parameter estimation approach to fault diagnosis.

A block diagram of this approach is given in Figure 2.1. The engine itself will at all times run under specific boundary conditions, e.g. set speed and load. The same conditions are fed into a comprehensive simulator model of the engine. The engine produces measured outputs, such as a range of temperatures and pressures, speed etc. The simulator has the same outputs. By comparing these, the validity of the current model can be assessed, and identified parameters or coefficients in the model are changed, based on the output error vector e. The new parameters are fed into the simulator, and the process iterates until the convergence is reached. The values of the parameters are used to identify the faults. However, convergence of parameters may be difficult to achieve since the engine system provides an unpredictable disturbance. In addition, a particular fault may not correlate to any specific parameter, with the result that the fault will not be found and that a residual error e will remain. The presence of such a residual error can serve as a mechanism for novelty detection. Novelty detection is an approach that does not aim at identifying which fault is emerging, but simply identify that something abnormal has happened, requiring further inspection.

Kim et al., [1998], utilized this technique in the estimation of unmeasured or un-measurable physical parameters of the engine for the control and diagnosis processes. Based on the Nonlinear Parity Equation Residual Generation (NPERG) diagnosis scheme, the input and state observers were used to provide fault detection and isolation using dynamic models of the system. the observer was configured such that sensors faults are detected and isolated using (nonlinear) output estimators, while input and plant parameter faults are isolated using (nonlinear) input estimators. The NPERG observer configuration successfully diagnosis faults caused by position sensor fault and fuel injector faults which were considered to demonstrate the diagnosis methods used.

2.1.3 Feature extraction and pattern recognition

Feature extraction and pattern classification algorithms have been used for analyzing signals and for classifying (parts of) the signal into classes Grimmelius et al., [1999]. The classification is done by matching (part of) the signal with a set of reference signals. The isolation of interested parts of the signal is called the feature extraction process. By reducing the signal, noise and parts of the signal that originates from an irrelevant process can be removed. By targeting the feature extraction towards identified fault, one at the time, several faults can be detected independently using the same signal. The matching process, where the conditioned signal is compared to a set of reference signals and assigned to the class that it matches most closely, is termed pattern recognition.

Using the same signal for detecting multiple fault conditions has in theory the potential of reducing the number of sensors used. Alternatively, this benefit can be achieved without performing of state or parameter estimation as discussed above in order to deduce more information than that is directly available from the fitted sensors. Thus the method is suitable for monitoring machinery where a suitable model is not available. The method requires a mathematical model or a lookup table for each feature corresponding to a fault, over a wide operating condition range. Process knowledge is only needed to indicate the (expected) behaviour of the sensor signals, or extensive testing with simulated faults can be conducted.

An advantage of this method is that a library of fault-condition features can be extended over time, spreading the cost of implementation. Another advantage is

that, depending on the actual algorithms, insight into the decision process is possible. Disadvantages include the large effort required to supply reference data and development of algorithms and high-performance computing required depending on the complexity of the signals.

In order to draw the full potentials out of these techniques, a lot of process details must be embedded in the signals, indicating that they must be complex. Signals that may be useful in this context fall into two categories:

* Rapid time-variant signals such as, acoustic emission and dynamic pressure information.
* Group of signals that are static and not interesting in isolation e.g. air and exhaust temperatures and mean velocity measurements.

2.1.4 Neural networks

Neural networks are able to perform a classification similar to the feature extraction and pattern classification technique, although the method by which this is done is different. A neural network is built up from a large set of simple neurons in a network, and simple calculations are associated with each neuron. The advantage with neural networks is that, once properly trained, they are able to differentiate between subtle relationships and features of the incoming signal, whilst also being quite robust to noise in the signal.

Figure 2.2 shows how information is processed through a single node. The node receives weighted activation of other nodes through its incoming connections. First, these are added up (summation). The result is then passed through an activation function; the outcome is the activation of the node. For each of the outgoing connections, this activation value is multiplied with the specific weight and transferred to the next node. By learning, it means that the system adapts (usually by changing suitable controllable parameters) in a specified manner so that, some parts of the system suggests a meaningful behaviour, projected as an output. The controllable parameters have different names such as synaptic weights, synaptic efficacies, free parameters and others.

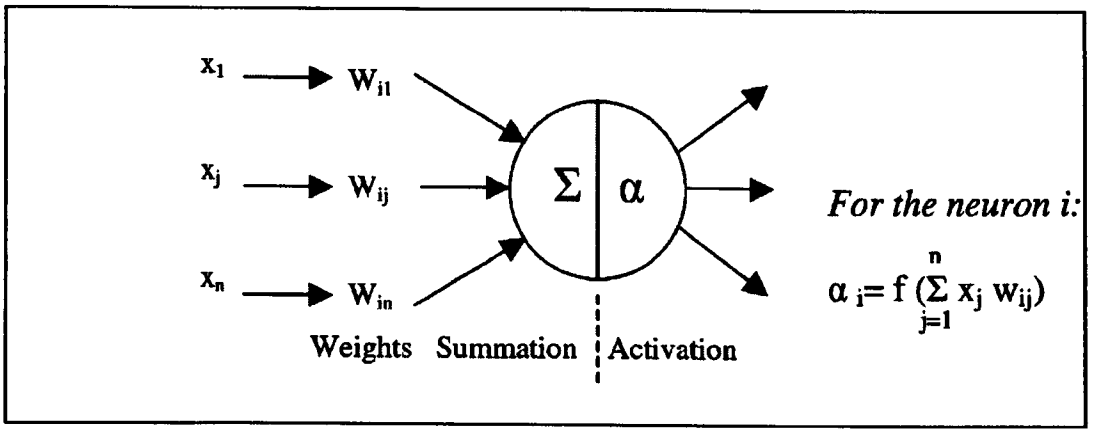

Figure 2.2 Information processing in a neural network unit, Kalogirou, [2003].

There are a number of factors which will influence the ability of a neural network to identify faults when used in a condition monitoring system. Defining a suitable layout is of great importance. This is an inexact science at the moment, and several attempts might be required. Having established a (trial) layout, the network is trained, where a large set of data is required, including many valid data sets for healthy and faulty condition. The test data is fed into the network, and the output is compared with the desired (known) output. The parameters in the network are changed, and the process repeats until a required accuracy is achieved.

Neural networks have the advantage that little or no process knowledge is required, nor is knowledge about fault patterns embedded in the sensor signals. Also, the network will provide no insight into the decision process, as the knowledge is spread over all the nodes in the network. On the other hand, the disadvantages are that extensive training sets are required, the network will only provide valid answers within the trained range, and any change to the system will require retraining.

There has been considerable interest in recent years in the use of neural networks for the modelling and control of combustion processes as well as fault diagnosis of diesel engine because of their ability to represent non-linear systems and their self-learning capabilities. Through the review of research carried out in both areas, many interesting working articles were identified. Morita, [1993], attempted to replace the conventional method used for combustion parameters control, which is called the table looking-up with a neural network method. The control of combustion parameters by neural networks, and especially the learning

characteristics of the networks when the control is adopted on-line control is presented. As a result, it was found that the neural networks are more suitable for on-line control of a car engine than the conventional table look-up map.

Advanced engine control systems require accurate dynamic models of the combustion process, which are substantially non-linear. The application of fast neural network models for engine control design purpose is presented by Hafner et al., [2000]. The special local linear radial basis function (RBF) network is initially introduced followed by a description of the process of building adequate engine dynamic models. These neuro-models were then integrated into an upper-level tool emission optimization tool, which calculated a cost function for exhaust versus consumption/torque and determined optimal settings. The results showed that the system allows a fast application of the optimization tool on the test stand.

The development of a neural network system for fault diagnosis in a marine diesel engine is described in Sharkey et al., [1996]. Neural networks were trained to classify combustion quality on the basis of simulated data. Three different types of data were used: pressure, temperature and combined pressure and temperature. Subsequent to training, three Neural Networks were selected and combined by means of a majority vote to form a system, which achieved 100% generalization to the test set. This performance is attributable to a reliance on the software engineering concept of diversity. Following experimental evaluation of methods of creating diverse neural networks solutions, it was concluded that the best results should be obtained when data is taken from two different sensors (e.g. a pressure and a temperature sensor), or where this is not possible, when new data sets are created by subjecting a set of inputs to non-linear transformations. According to the authors, these conclusions have far reaching implications for other neural network applications.

A multi-network fault diagnosis system designed to provide an early warning of combustion-related faults in a diesel engine is presented by Sharkey et al., [2000b]. Two faults (a leaking exhaust valve and a leaking fuel injector nozzle) were physically induced (at separate times) in the engine. A pressure transducer was used to sense the in-cylinder pressure changes during engine cycles under both of these conditions, and during normal operation. Data corresponding to these

measurements were used to train the neural network to recognize the faults, and to discriminate between them and normal operation. Individually trained networks, some of which were trained on sub-tasks, were combined to form a multi-network system. The multi-network system is shown to be effective when compared with the performance of the component networks from which it was assembled. The system is also shown to outperform a decision-tree algorithm and a human expert. Comparisons presented show the complexity of the required discrimination. The results illustrate the improvements in performance that can come about from the effective use of both problem decomposition and redundancy in the construction of multi-network systems.

Jones and Li, [2000] reviewed some of the used techniques for condition monitoring and fault diagnosis for diesel engines. Firstly, the common faults, fault mechanisms and their expected development and effect of diesel engine performance were summarised. The discussed common faults include power loss, emission changes, lubricating system faults, and mechanical noise. Some of the advanced CMFD techniques are discussed such as, Diesel Engine Fault Diagnosis (DEFD) developed by Lloyd's, Knowledge-Based system for Marine Engine Diagnosis (KBMED) developed by Huazhong University of Science and Technology-China, and Condition/Performance Monitoring and Predictive System for Diesel Engines (CPMPS). A final conclusion indicates that, since the diesel engine is a complex system with highly non-linear characteristics, it is difficult to establish analytical models for the purpose of overall fault diagnosis. However, since neural networks systems mimic the way that humans process information, it is likely that this technique will play an important role in the field of intelligent engine diagnosis.

2.2 DIESEL ENGINE MODELLING

Mathematical modelling of internal combustion engines is a far reaching subject. In the development of engine models over the years we may distinguish three main steps: (1) thermodynamic models based on mass and energy conservation laws have been used since 1950 to help engine design or subsystems matching and to enhance engine processes understanding; (2) Empirical models based on input-output relations were introduced in early 1970s for primary control investigation;

(3) Physically based nonlinear models for both engine simulation and control design. Engine modelling for control tasks involves researchers from different disciplines, i.e. engineering, control and physics. Therefore, several specific nominations may be used for the same class of model in accordance with the framework. To avoid any misunderstanding, Guzzella and Amstutz, [1998] show three categories to classify the different modelling approaches with terminology adapted to the basic principle of the model:

Thermodynamic-based models (known also as, knowledge model, or parametric model, or white box), have been derived using physical first principles and include relatively few physical parameters which are very suitable for control.

Non-thermodynamic models (black-box, or non-parametric model), that use a prior chosen structure, and reflect the input output relationship of the engine based on experimental input-output analysis.

Semi-physical approximate models (or grey-box) which is an intermediate category where the model was built with equations derived from physical laws and which parameters are measured or estimated using identification techniques.

This classification is very helpful but it may be oversimplified because a complete engine model would be a mixture of physical and experimental sub-models. The following section will focus on the first two categories as the third category is mixture of the first two.

2.2.1 Thermodynamic-based model

Thermodynamic diesel engine modelling passed through a long term development as early efforts in the 1950s focused on the closed part of the engine cycle, i.e. the compression/combustion/expansion sequence. These models evolved from the ideal cycle calculations in the 1950s to simple component matching models in the 1960s and multizone and multidimensional combustion models in the 1980s and early 1990s, Chow and Wyszynski, [1999]. High resolution multidimensional models, such as KIVA II 3-D introduced by Mariani and Postrioti, [1996], are often used for specific problem areas in engine design, where details of fluid transport processes or those involving subtle geometry changes dominate. These models are capable of simulating detailed airflow, spray and combustion events in

local geometries. The lower resolution multizone combustion models such as ISIS, discussed by Ball et al., [1999], are able to predict power output, emissions, losses in the engine, fuel consumption and efficiency. Therefore, multizone combustion models are used in the conceptual and development stages of design in order to explore a larger range of alternative within acceptable time and cost limits.

Thermodynamic modelling techniques can be divided into the following groups: (i) quasi-steady, (ii) filling and emptying, and (iii) gas dynamic models. Models that can be adapted to meet the requirement of control systems development are cylinder-by-cylinder (CCEM) and Mean value model (MVEM) while application of the gas dynamic model is very restricted due to its complexity level, Grondin et al., [2004]. The basic classification of thermodynamic models and emergence of models suitable for control are displayed in Figure 2.3.

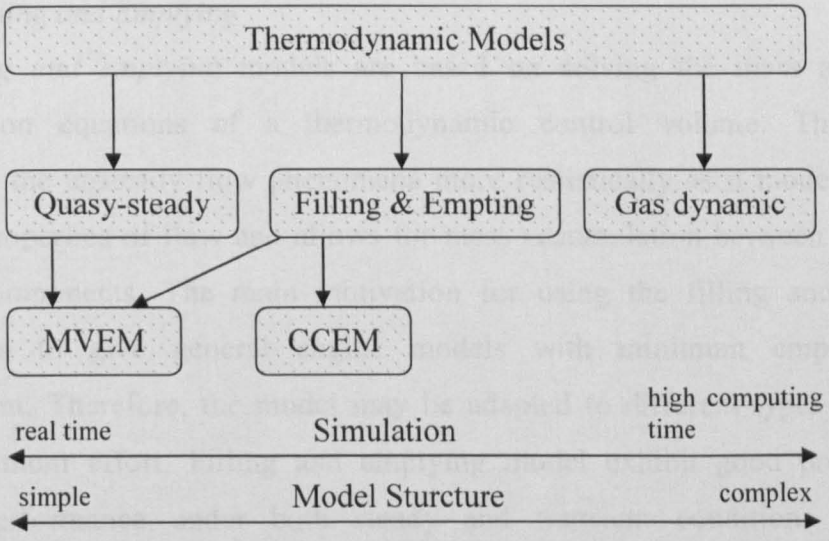

Figure 2.3. Basic classifications for thermodynamic-based models of internal combustion engines, Grondin et al., [2004].

2.2.1.1 Quasi-steady

The first diesel engine simulations using the quasi-steady method were carried out in the early 1970s. The aim of researchers at this time was to develop an engine model as a tool to study and improve the transient performance of the diesel engine. The basic idea behind the quasi-steady technique is to model engine components in term of steady state, where the transient was assumed to be a sequence of steady state points or conditions. The quasi-steady model includes the dynamics of all moving parts such as crankshaft, piston, connecting road and

turbocharger as well as empirical relations representing engine thermodynamics. These simulations are dependent on empirical knowledge and do not allow for mass accumulation between components.

Quasi-steady models are simple and have the advantage of short run times, and for this reason they are suitable for real-time simulation. On the other hand, among the disadvantages of quasi-steady models are their heavy reliance on experimental data and low accuracy. A quasi-steady model requires a large amount of data to obtain empirical relations or maps for each engine component; furthermore, it cannot be transposed to other engines. Complex phenomena such as combustion or gas flow are oversimplified and thus reduce the simulation accuracy. These models do not provide a sufficient level of detail to reflect design change or to predict parameters that influence exhaust emissions Watson, [1984].

2.2.1.2 Filling and Emptying

The *filling and emptying* models are based on solving the mass and energy conservation equations of a thermodynamic control volume. This method represents the unsteady flow phenomena more realistically as it models the time varying properties of flow and allows for mass accumulation between the engine system components. The main motivation for using the filling and emptying method is to give general engine models with minimum empirical data requirement. Therefore, the model may be adapted to different types of engines with minimum effort. Filling and emptying model exhibit good prediction of engine performance under both steady and transient conditions and gives information on parameters known to influence pollutant emissions or noise. However, assumption of uniform state of gas covers up complex acoustic phenomena (resonance). Wave effects inside the manifold can affect engine performance, and thus, the error introduced by filling and emptying method must be considered. The filling and empting model is not suitable to control design application because of their prohibitive computing time, Chow and Wyszynski, [1999].

2.2.1.3 Cylinder-by-cylinder

The *cylinder-by-cylinder* model, based on the filling and emptying method firstly established by Watson, [1984], was of a turbocharged diesel engine simulator

which has been designed to help in the development of an electronic controller. A nonlinear dynamic simulation of a turbocharged diesel engine was presented. The detail of the model was governed by the desire to accurately predict fuel economy of new engine designs currently on the drawing board, but without any empirical input, and respond correctly to changing ambient conditions, design alterations etc. Thus the model treats cylinders and manifolds as thermodynamic control volumes, solving energy and mass conservation equations with subroutines for combustion, heat transfer, turbocharger, dynamic aspects etc. In-cylinder calculations are performed in small engine crank-angle steps so that the correct ignition crank angle is predicted as well as the subsequent fuel burning rate. This enables parameters such as the cylinder pressure and diffusion burning factor to be predicted. It is shown how the run time of a previous model has been reduced by an order of magnitude. The accuracy of the model was tested and verified by comparison between measured and predicted performance over the complete steady state operating range of the engine. Also, the engine response to acceleration and full-load application was tested.

Later, Kao and Moskwa, [1995] improved the accuracy of the Watson model with a formulation adapted to control design. Two main changes were introduced to modify the cylinder-by-cylinder engine model (CCEM). A time varying inertia model derived using Lagrangian principles was introduced to enable the model to reproduce engine speed oscillations. Watson's model does not include such benefit because it was utilizing a simple dynamic model. On the other hand, cylinder-by-cylinder simulation with a detailed combustion model is too slow for real time application. In order to decrease computing times and to make their model compliant with the control formulation, Kao and Moskwa replaced the cylinder model used in Watson's model with a simpler in-cylinder pressure equation relating the cylinder pressure to the fuel mass and cylinder gases properties.

Accurate prediction of in-cycle engine states evolution makes CCEM well suited for fault diagnostic. In-cylinder pressure and fuel burning rate observers based on sliding mode observer theories have been designed from the simplified cylinder-by-cylinder engine model introduced by Kao and Moskwa, [1994]; and Kao and Moskwa, [1995]. In-cylinder pressure is a useful indicator of combustion quality;

therefore, its estimate can be utilized in fault diagnostics schemes instead of employing high cost pressure transducers and intrusive action required for fitting such transducers.

2.2.1.4 Mean Value Engine Modelling

During the early 1990s, the research team at the University of Denmark investigated an alternative technique by introducing non-linear models of reciprocating engines using a concept halfway between quasi-steady and filling and emptying methods. This team named this new class of model mean value engine model (MVEM). The motivation was to reduce computing time compared to more complex phenomenological filling and emptying models. The early publications of the research team is found in Hendricks, [1989a], and introduces the basic idea of the MVEM modelling applied it to a large two stroke turbocharged diesel engine. Mean value models describe dynamically the development of engine physical variables over time periods which are long compared to an engine cycle but short compared to the dominant time constants of the engine. The time scale for the mean value engine model is on the order of 3 to 5 revolutions. It is therefore, fast enough to give an accurate prediction of overall dynamic engine operation. Such models do not include explicitly description of the intake, exhaust or combustion processes but simply represent the overall result of the processes as described by the crank speed, the mean scavenge pressure, the air mass flow rate or a small number of the other measurable engine variables. Cyclic to cyclic variation is implicitly included in the model.

Because of the simplicity of the model it has been possible to expose a number of the details of how the overall system performs and to focus attention on the main performance controlling factors. In particular, it has been possible to give a quantitative description of the turbocharger lag and to map the model engine's transient behaviour over a large range of operating points. Also, it had been shown that the MVEM is a valuable tool in predicting engine frequency response and in forming an idea of what control problem might arise in common operating conditions. The model was verified against experimental data from a large turbocharged two-stroke marine diesel engine and published in Hendricks, [1989b]. A model for a small (1.6 litre) turbocharged indirect injection four stroke diesel engine was introduced by Jensen et al., [1991] based on the MVEM

principle. The model was successfully able to predict all significant engine variables to better than 10% for both transient and steady state operation. Later in the 1990s significant contributions on diesel engine modelling using mean value approach have been published by Kao and Moskwa, [1995]; and Amstutz and Luigi, [1995]. More discussion of the theoretical background can be found in the work proposed by Guzzella and Amstutz, [1998].

2.2.2 Non-thermodynamic models

Complex thermodynamic models are unsuitable for analytical controller design where it used to solve complex differential and algebraic equations; hence simple non-thermodynamic models were the first kind of engine models used for control purposes. Non-thermodynamic, known as black-box, models they were built with the minimum level of knowledge about the system, and no fundamental principles are involved. However, they can include *a priori* information about the engine such as, time delay or engine nonlinearities. These models have to reproduce the input-output behaviour of the system and their structure (transfer function or state-space representation) complies with the control requirement. The modelling procedure consists of four important steps: (1) Experimental data recording, (2) choosing an adequate model structure and the identification algorithm, (3) calculation of the model parameters and (4) validation. In the following section, the "black-box" models of diesel engine will be split into two classes: linear and nonlinear models.

2.2.2.1 Linear models

In the early 1970's, the first linear engine models introduced by Flower and Hazell, [1971]; Hazell and Flower, [1971a] and. Hazell and Flower, [1971b]. This linear discrete engine model was based on the analogy with sampled-data process (see Figure 2.4). For constant speed, the fuel is injected at constant time interval, thus the injector is considered as a pure sampler. The engine converts this fuel mass impulse to a torque pulse at the crankshaft. The inertial load acts as a low pass filter, thus, the torque development can be modelled by a zero-order hold circuit, as shown in Figure 2.5, for a four-cylinder engine. The model output is a stepwise signal with the same area as the experimental torque pulse.

Later, Flower and Windett, [1976], introduced the pseudo-random binary sequence (PRBS) method to identify diesel engine dynamics. PRBS signal is added to the control signal (which is the fuel rack position). This signal and the output signal (the engine speed) are recorded. Samples of input and output are employed to estimate the engine frequency response and to obtain the discrete transfer functions of the engine Jiang, [1994].

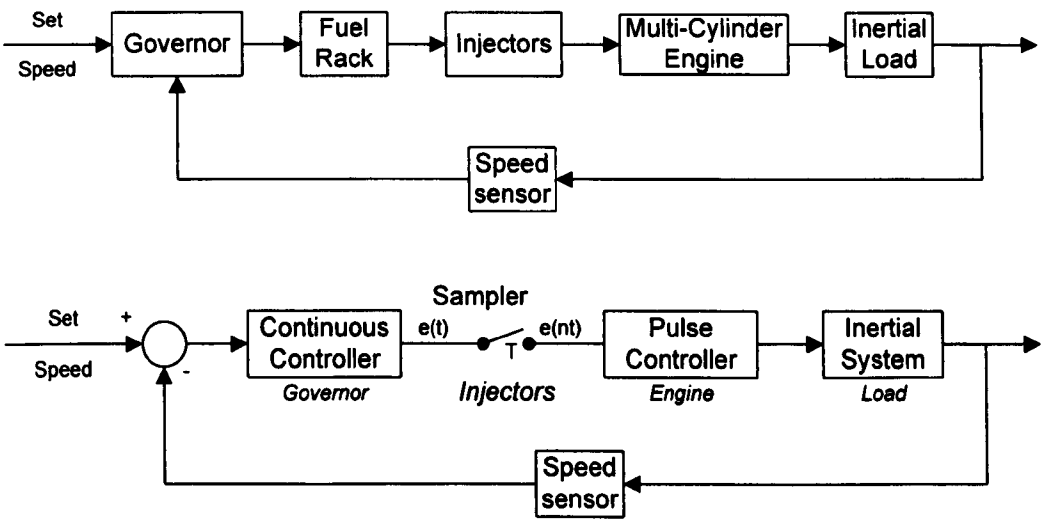

Figure 2.4 Conventional speed control loop (top), equivalent sampled-data model (lower) Hazell and Flower, [1971b].

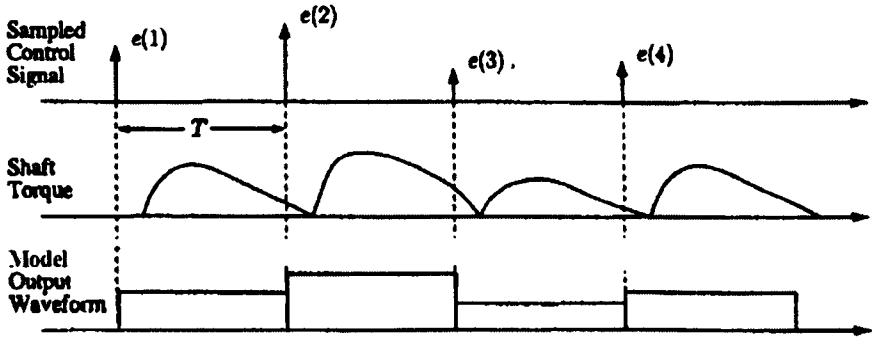

Figure 2.5. Sampled control signal (top), engine torque puls (middle) and model output waveform (bottom) for a four-cylinder engine Hazell and Flower, [1971b].

Closed loop engine speed control is the standard application of the low order linear model. This problem was mentioned in many research papers involving several control techniques. The universal PID (proportion + integration + derivation) controller has been used extensively with linear models and a wide range of modern model-based control techniques have been introduced to enhance control. A few of the theoretical aspects of the control strategies are listed below:

* Optimal control.
* Gain scheduling controller.
* Adaptive and self-tuning controllers.

Whatever type of linear model (continuous or discrete) is employed, it still has the advantage of short run time and simplicity, and is very suitable for analytical controller design. However, validity of linear black-box models is restricted to a narrow operating range and needs to be proceeded by a test on the engine to fit its parameters. In addition, the inherent difficulties are choosing the ideal measurements, the best model architecture, and a good identification method.

2.2.2.2 Non-Linear models

While the linear model can only reproduce the engine dynamics around definite operating points, non-linear models are able to overcome this problem. From the literature, two important directions have been discussed:

- *NARMAX modelling of diesel engine*

In general, NARMAX model can be expressed mathematically in the form of a nonlinear difference equation:

$$y(t) = F\left[y(t-1),.....,y(t-n_y),u(t-1),.....,u(t-n_y)\right] \qquad \textbf{(2-6)}$$

Where F is a nonlinear function of input u and output y. The main problem of the NARMAX approach is the accurate choice of the nonlinear function that correctly represents the engine. In addition, a complex structure may lead to difficult parameter identification. A convenient solution for the parameter identification problem was the use of a polynomial expansion of the function F, but selecting a suitable order of the polynomial is still difficult. The first attempt to model the

diesel engine was carried out by Billing et al, 1988, where they relate the fuel rack position to the engine speed with some nonlinear difference equations.

NARMAX modelling methodology is effective in capturing engine dynamics even when there are complex processes such as pollutant formation. On the other hand, nonlinear models make the control design rather difficult. Nonlinear model predictive control or nonlinear adaptive control using a NARMAX model can be considered, but these problems are still present in diesel engine applications, Glass and Franchek, [1999].

- *Neural networks models*

In the last decade neural networks have become increasingly popular for industrial processes identification. Neural architectures may be characterized by the following statements:

* Inspired by biological neural systems
* Network structure of simple processing nodes
* Usually nonlinear
* Adjustable by training

A basic feed-forward neural network is composed of one input and one output layer with intermediate hidden layers between them, as shown in Figure 2.6.

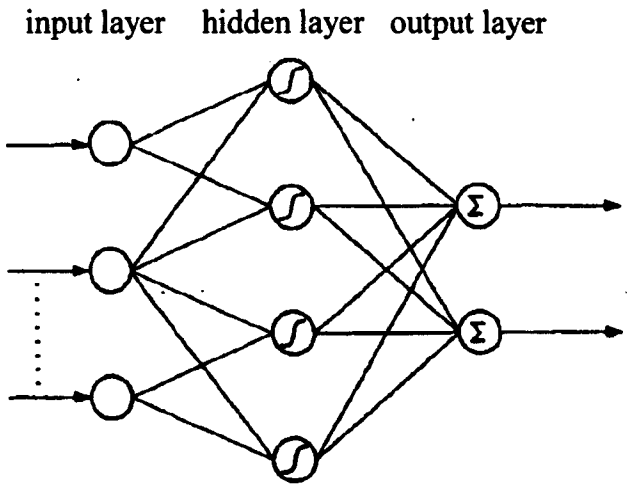

Figure 2.6 Typical feed-forward network with one hidden layer.

The input-layer neurons distribute the inputs to the neurons of the hidden layer. In the neurons of the second layer, the weighted sum of the inputs is passed through an activation function (usually a sigmoid or threshold function). The neurons of the output layer only compute the weighted sum of their inputs. On the other hand, a Radial Basis Function (RBF) network is a two-layer net in which the first layer has radial basis functions while the second consists of linear functions, as illustrated in Figure 2.7.

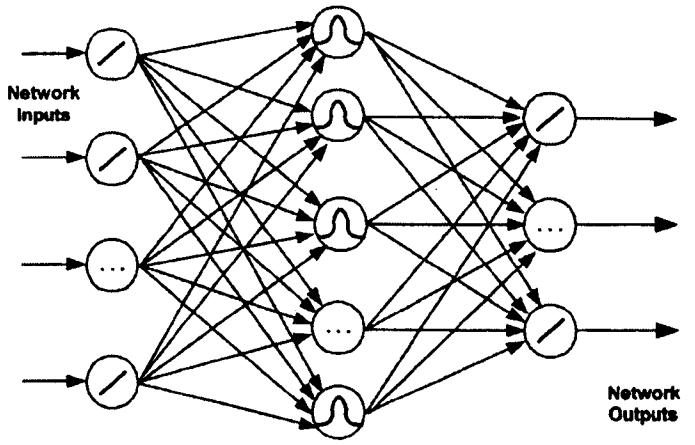

Figure 2.7 Basic Layout of Radial Based Function (RBF) neural network.

To adapt the weights, the input-output data measured on the system are applied to the input layer; this phase is called the learning or training phase. The best parameters are obtained by minimization of a quadratic cost function (i.e. the mean square error between network output and measured output). This nonlinear optimization problem can be solved using Newton's method, a genetic algorithm or other techniques.

Neural network models of compression ignition engines first appeared at the end of the 1990s. Multilayer perceptron (MLP) models have been used to predict crankshaft speed and opacity of a diesel engine. Ayoubi, [1998] and Gamo et al., [1999] demonstrated the potential of Dynamic Multilayer Perceptron (DMLP) to model the charging process of a turbocharged diesel engine, with the neural model giving good prediction of the boost pressure taking the fuel mass and engine speed as inputs. Hafner et al., [1999] and Hafner et al., [2001] developed an exhaust model of turbocharged diesel engine based on an extended radial basis function (RBF) network. Their models predict opacity and NOx emissions using a fast

neural network that accelerates the training phase. The model takes exhaust gas recirculation, injected fuel mass, start of injection angle, variable geometry turbocharger position and oxygen concentration as inputs.

RBF networks offer a flexible and robust approach to the typification of non-linear engine processes. The representation of the data is transparent in so much as the RBF neurons can be regarded as locally applicable sub-models which are linearly combined to reflect the behaviour of the process over the training data range. Moreover, by the use of stabilization techniques, such as regularization, the model can be made robust, Jacob et al., [1999]. Gu et al., [1999], obtained promising results from using the RBF network to engine modelling and cylinder pressure waveform reconstruction. This model assumes that the instantaneous speed signature is the only required input to the model where the external load information is already embedded in the speed signature. This assumption was empirically validated in this study.

- *Fuzzy system*

Control engineering always faces the problem of controlling and modelling nonlinear systems. The diesel engine is a complicated nonlinear system and composed of several subsystems which have complex dynamic characteristics. Therefore, it is very difficult to find an accurate nonlinear model for the real plant. Nevertheless, researchers have proposed some approaches for modelling these engines. Gamo et al., [1998] used the Group Method Data Handing (GMDH) technique for identification of fuel injection system of a diesel engine. Hafner et al., [1999] applied a fast neural network of LOLIMOT (LOcal LInear MOdel) type to model the exhaust gases of a diesel engine. This model was integrated into an upper-level optimization tool to calculate a cost function for exhaust versus consumption of fuel and determine the optimum fuel injection angle. The LOLIMOT algorithm was based on the concept of dividing the input space of nonlinear process into regions with local linear models. The model output was calculated as the weighted sum of all region local linear models.

In the 1990's, a new strategy based on fuzzy logic and neural network provided another solution to model the diesel engine. A variety of different modelling schemes based on neural-fuzzy techniques have been proposed and applied in

engineering practice. Culliere et al., [1995] proposed a neuro-fuzzy model based on a concept of cut-off input space in areas as the first stage in using a fuzzy-module, and then used a multi-layer network, and backpropagation (BP) algorithm to identify local characteristics of the system. The main advantage of the first stage was that it rapidly gives a fuzzy model from the initial network of input space, which can provide more accurate results by increasing the size of the fuzzy set, while the second stage gives the benefit of quickly converging toward the solution, but only if the decomposition base is well chosen. This problem can be avoided by choosing an orthogonal base.

Chen and Linkens, [1998] and Wu and Tam, [1999] introduced a simple and effective method for building a fuzzy model from data using a three-layered RBF network. The advantage of using RBF neurons to construct the fuzzy neural network is the functional equivalence between RBF network and fuzzy inference. However, the equivalence relationship between the models has to satisfy the condition that the number of hidden units in the hidden layer of the RBF network is equal to the number of rules of the fuzzy inference system. Instead of adapting previous clustering-based methods, the structure identification of this approach include input selecting and partition validation implemented on the basis of a class of sub-clusters created by a self-organizing network instead of on raw data. The important input variables which independently and significantly influence the system output can be extracted by a fuzzy neural network. In addition, the optimal number of fuzzy rules can be determined separately via the fuzzy algorithm. Since this method focuses on model simplicity and computing efficiency to satisfactory modelling accuracy, the model produced may not be optimal and will require further improvement.

Another approach for automatically generating fuzzy rules from sample patterns using generalized dynamic fuzzy neural networks (GD-FNNs) was presented by Wu et al., [2001]. The GD-FNN was based on an ellipsoidal basis function (EBF) network combined with a Takagi–Sugeno–Kang (TSK) fuzzy system. The characteristics of the GD-FNN are: (1) structure identification and parameters estimation are performed automatically and simultaneously without partitioning the input space and selecting initial parameters; (2) fuzzy rules can be recruited or

deleted dynamically; (3) fuzzy rules can be generated quickly without resorting to the back-propagation (BP) iteration learning. The GD-FNN is employed in a wide range of applications. Comprehensive comparisons with other latest approaches show that the proposed approach is superior in terms of learning efficiency and performance.

Twiddle and Jones, [2002], developed a fuzzy model based CMFD systems to model the cooling system components of the diesel engine, in parallel with non-linear parameter estimation techniques and neural network classifier approaches. The main disadvantage of only using a neural network classifier approach is that fault condition data must be obtained to train the network. Also, the fault class is defined for the specific magnitude of the fault; therefore, additional data must be acquired to broaden the range of fault magnitudes which may be successfully diagnosed. The fuzzy models were found to be generally effective at generating residuals where deviations from the normal condition are very small, although for larger deviations robustness of models is not guaranteed or expected. In fact, each technique is shown to be capable of producing good results in their respective formats. The fuzzy systems approach has provided a flexible means for incorporating heuristics into both models and diagnostics systems where knowledge of the system was incomplete.

The two stage fault diagnosis system, shown in Figure 2.8, was designed to map the residual vector to one of the number of prescribed system conditions where X represents the input vector to the three fuzzy models, $\hat{y}$ the model outputs, and y the corresponding measured variables. The diagnostic system is designed to output a vector of numbers, d, that represents the truth value of a number of propositions describing possible conditions of the diesel engine cooling system. The diagnosis is defined to be the condition with the highest associated truth value. The magnitude and sign of the residual components of r together with other information regarding the state of the thermostat valve, are used to diagnose the cooling system.

The fuzzy model inputs and outputs have been selected to be representative of the physical system, while the outputs are also suitable reference values for generation of residuals. The developed system offer certain benefits in terms of providing a

CMFD system for an engine cooling system based on a small number of low cost sensors with a success rate ranging from 73 to 98% in the fault diagnosis. Recursive fuzzy models have been shown to be an effective technique for modelling of hysteresis in the thermostatic valve of the cooling system, Twiddle and Jones, [2002].

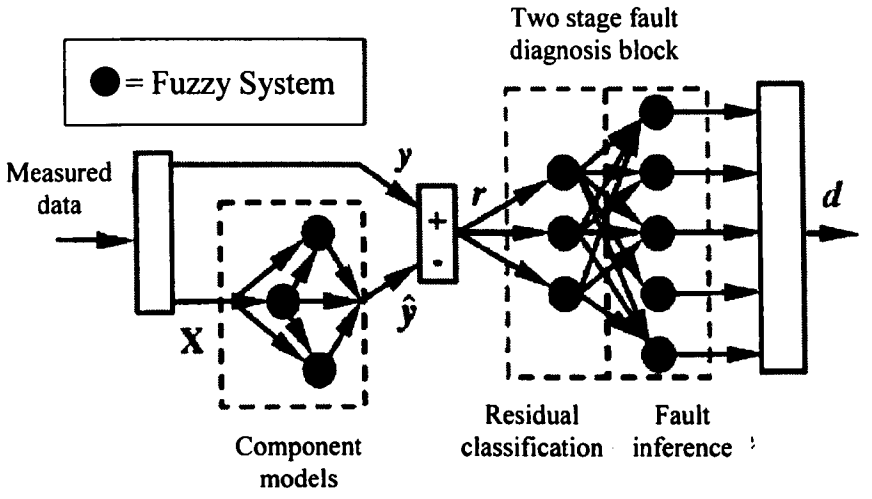

Figure 2.8. Schematic diagram showing the structure of the models and the diagnostic system [Twiddle and Jones, [2002].

Zhang et al., [2003] proposed a new nonlinear fuzzy model for the diesel engine generated using a Modified Self-Organizing Map (MSOM) network. Based on the MSOM, fuzzy rules are determined automatically according to the distribution of training data in the input–output space and the given approximating error. The simulated result indicates that the nonlinear model predicts both the static and dynamic behaviour of the diesel engine accurately and could be used to design the control system of the engine, and help to understand its complex dynamics.

2.3 NEURAL NETWORKS

Before laying out the principles for choosing the best Neural Networks (NN) topology, learning method and data handling, it is important to understand how artificial intelligence (AI) evolved with required computational resources. Artificial intelligence applications have moved away from laboratory experiments to real world implementations, therefore, software complexity also became an issue to withstand the symbolic processing, nondeterministic computations,

dynamic execution, parallel, distributed processing, and management of extensive knowledge bases. In many AI applications, the knowledge needed to solve a problem may be incomplete, because the source of the knowledge is unknown at the time the solution is devised, or the environment may be changing and cannot be anticipated at the design stage. AI systems should be designed with an open concept that allows continuous refinement and acquisition of new knowledge.

Many existing engineering problems require a practically impossible amount of resources to find the perfect solution; therefore, an acceptable solution would be fine. NNs can give good solutions for such classes of problems. In some cases, getting the best NN topology, learning method and data handling could become an engineering approach in itself. The success of using NN for any application depends highly on the data processing, i.e. data handling before or during network operation. Once variables have been identified and data has been collected and is ready to use, it can be processed in several ways, to squeeze more information out and filter it to achieve the optimum condition.

An ANN must be used in problems exhibiting knottiness, nonlinearity, and uncertainties that justify its utilization. They present the following features to cope with such complexities:

* Learning from training data used for system identification; finding a set of connection strengths will allow the network to carry out the desired computation.
* Generalization from inputs not previously presented during the training phase; by accepting an input and producing a reasonable response determined by the internal ANN connection structure makes such a system robust against noisy data, features exploited in industrial applications.
* Mapping of nonlinearities making them suitable for identification in process control applications.
* Parallel processing capability, to allow fast processing for large-scale dynamical systems.
* Applicable to multivariable systems; they naturally process many inputs and have many outputs.

* Used as a black-box approach (no prior knowledge about a system) and implemented on compact processors for space and power constrained applications.

* Several factors have to be considered in order to select a suitable NN configuration for the proposed application. The major points of interest regarding the NN topology selection are related to network design, training, and practical considerations.

Utilization of NN in the field of diesel engine condition monitoring and fault detection covers several areas. Gamo et al., [1999], used a NN to construct a model of the exhaust emission of the diesel engine. The proposed multilayer feedforward neural networks was mainly based on analysis of the sum of square errors on input times delays, orders and number of hidden layer neurons. Sharkey et al., [2000a], utilize a NN in fault detection of diesel engine through a multi-sensor approach which used acoustic emission, cylinder pressure and vibration sensors.

2.3.1 Training considerations

Considerations, such as determining the input and output variables, choosing the size of the training data set, initializing network weights, choosing training parameter values (such as learning rate and momentum rate), and selecting training stopping criteria, are important for several network topologies. There is no generic formula that can be used to choose the parameter values. After a few trials, the network designer should have enough experience to set appropriate criteria that suit his specific problem. The initial weights of a NN are considered as important parameter in the convergence of the training step. It is a common practice to initialize all weights randomly with small absolute values. In linear vector quantization and derived techniques it is usually required to renormalize the weights at every training epoch. A critical parameter is the speed of convergence, which is determined by the learning coefficient. In general, it is desirable to have fast learning, but not so fast as to cause instability of learning iterations. Starting with a large learning coefficient which reduced as the learning process proceeds, results in both fast learning and stable iterations. The momentum coefficients are,

usually, set according to a schedule similar to the one for the learning coefficients Zurada, [1995].

The training data set, number and selection, plays a vital role in the performance of a supervised NN and success of training process. If the number of training examples is not sufficient, then the network cannot correctly learn the actual input–output relation of the system. On the other hand, a large number of training examples will need more time to finish. For some applications, such as real-time adaptive neural control, training time is a critical variable. For others, such as fault detection, the training can be performed off-line and more training data preferred to achieve greater network accuracy. Generally, rather than focusing on volume, it is better to concentrate on the quality and representational nature of the data set. A good training set should contain routine, unusual and boundary condition cases. The generally used criteria to stop NN training are small mean-square training error and small changes in network weights. Selection of how small it should be usually depends on the network designer and is based on the desired accuracy level of the NN. If any prior information about the relationship between inputs and outputs is available and used correctly, the network structure and training time can be reduced and the network accuracy can be significantly improved.

2.3.2 Network design and practical consideration.

The general design considerations for a neural network includes determining the number of input and output nodes to be used, the number of hidden layers in the network and the number of hidden nodes used in each hidden layer. Chow et al., [1993], had introduced a full discussion of the design consideration of NN. The number of input nodes is typically taken to be the same as the number of state variables. The number of output nodes is typically the number that identifies the general category of the state of the system. In the past, it was general practice direction to increase the number of hidden layers, in order to improve training performance. Keeping the number of layers at three and adjusting the number of processing elements in the hidden layer, can achieve the same goal. To determine the number of hidden layer processing elements, a trial-and-error approach was usually adopted, starting with a low number of hidden units and increasing this number as learning problems occur. However, there are some guidelines that can

be used to select the number of hidden layer neurons. It is a common practice to choose a set of training data and a set of testing data that are statistically significant and representative of the system under consideration. The training data set is used to train the NN, while the testing data is used to test the network performance, after the training phase finishes.

Practical considerations regarding the network accuracy, robustness and implementation issues must be addressed, for real-world implementations, for example, for induction motor fault detection, network training is stopped when either the root mean-square error of the training set or the change in network weights is sufficiently small i.e. less than 0.005, Chow et al., [1993]. Since most fault detection schemes are for real-time applications, noise considerations and minor disturbances become important issues. Noise is known to decrease the overall performance fault detectors. Therefore, methods to suppress noise are needed to enhance the accuracy of fault detector of neural networks.

Selection and implementation of the network configuration need to be carefully studied since it is desirable to use the smallest possible number of nodes while maintaining a suitable level of conciseness. Pruning algorithms try to make NNs smaller by trimming unnecessary links or neurons, so the cost of runtime, memory and hardware implementation can be minimized and generalization is improved. Depending on the application, some system functional characteristics are important in deciding which ANN topology should be used. Table 2-1 summarizes the most common ANN structures used for pattern recognition, associative memory, optimization, function approximation, modelling and control, image processing, and classification purposes.

Table 2-1 Organization of NNs based on their functional characteristics.

Function Characteristics	Structure
Pattern Recognition	MLP, Hopfield, Kohonen, PNN
Associative Memory	Hopfield, recurrent MLP, Kohonen
Optimization	Hopfield, ART
Function Approximation	MLP, CMAC, RBF
Modeling and Control	MLP, recurrent MLP, CMAC, FLN, FPN
Image Processing	CNN, Hopfield
Classification (including Clustering)	MLP, Kohonen, RBF, ART, PNN

New and better electronic devices have inspired research to build intelligent machines operating in a fashion similar to the human nervous system. Fascination with this goal started, around the Second World War, when McCulloch and Pitts, in 1943, developed their mind-like machine by interconnecting model based on behaviour of biological neurons, and when Hebb introduced his learning rules. Rosentblatt, [1958], from the Cornell Aeronautical Laboratory put together a learning machine, called the "Perceptron" which was the predecessor of current NNs. The Perceptron received considerable excitement, when it was first introduced, because of its conceptual simplicity. Widrow and Hoff proposed the "ADALINE" (ADAptive LINear Element), a variation on the Perceptron, based on a supervised learning rule (the "error correction rule") which could learn in a faster and more accurate way: synaptic strengths were changed in proportion to the error (what the output is and what it should have been) multiplied by the input, Meireles et al., [2003].

Meireles et al., [2003], summarized the industrial application of NNs up until 2001, (see Figure 2.9), the main purpose of which was to give an idea of the most used ANN topologies and training algorithms and to relate them to common fields in the industrial area. For each entry, the type of the application, ANN topology used, implemented training algorithm, and the main authors are presented. The collected data gives a good picture of what has actually migrated from academic research to practical industrial fields and shows some of the authors and groups responsible for this migration.

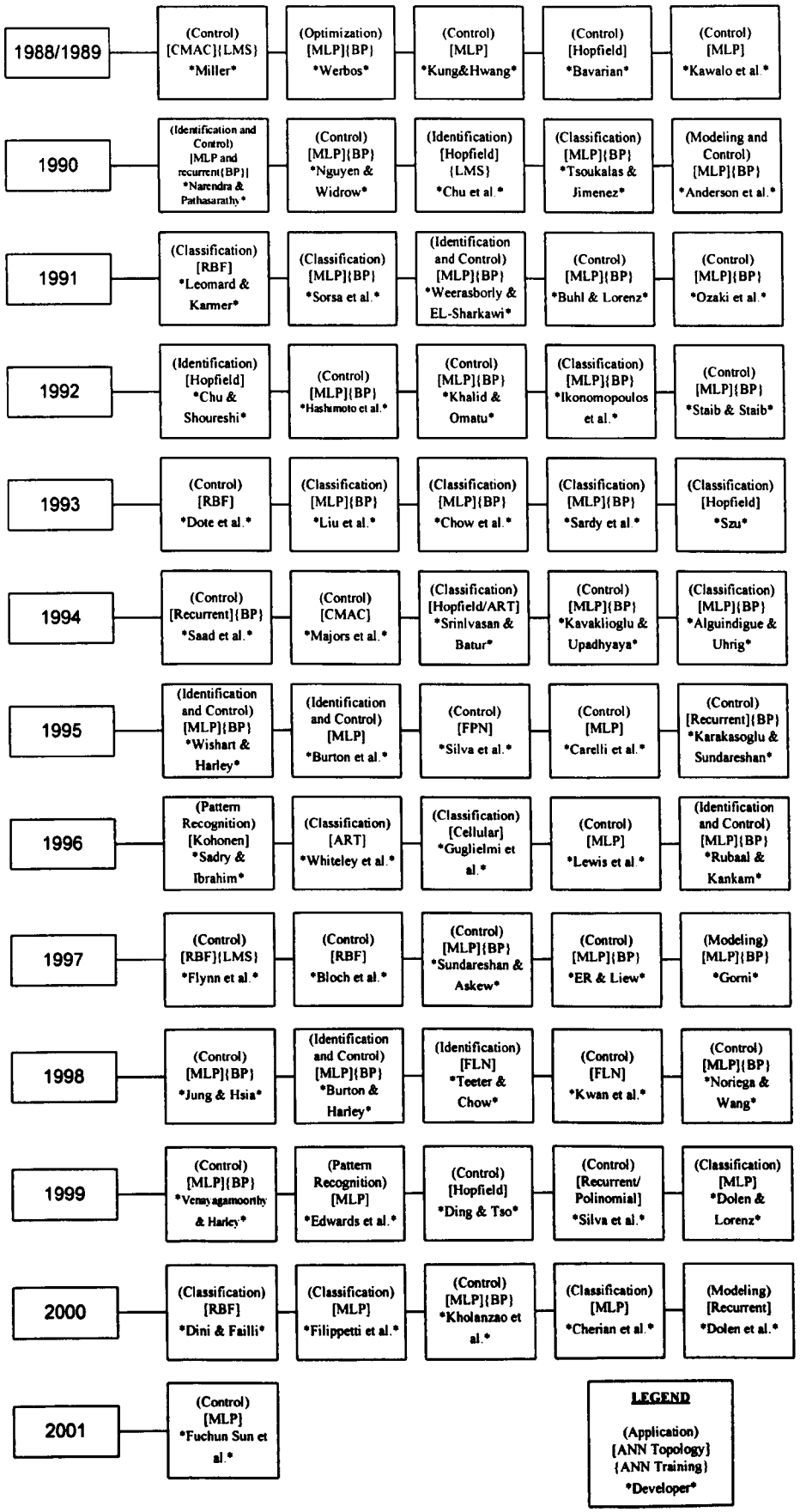

Figure 2.9 Selected industrial applications reported since 1989, Meireles et al., [2003].

2.4 NEURAL NETWORKS CLASSIFICATION

A common classification of ANNs is based on the way in which their elements are interconnected. The following sections try to cover the main types of networks that have been used in the field of engine condition monitoring and fault diagnosis, particularly for use on diesel engines.

2.4.1 Multilayer preceptron (MLP)

In this structure, each neuron output is connected to every neuron in subsequent layers in cascade with no connections between neurons in the same layer. A typical diagram of this structure is detailed in Figure 2.10. MLP has been reported in several applications. Lucking et al., [1994], utilize the MLP neural network for the condition monitoring of gearbox using acoustic signals propagated through the gearbox body. Crowther et al., [1998], use MLP neural network approach in the fault diagnosis of a hydraulic actuator circuit which was trained using a variation of the error back-propagation algorithm. The MPL network was trained using both experimental and computer simulation data. The major challenge was to obtain training data that cover the whole system output vector space for the faults of interest.

In order to improve the dynamic performance of MLP, a new modified version has been introduced known as, Dynamic Multi-layer Preceptron (DMLP). Ludwig and Ayoubi, [1995], compared the performance of a DMLP neural network with the Hammerstein parametric nonlinear dynamic model in diesel engine turbocharger fault detection. The Hammerstein is fast but difficult for the identification process because of the need for both static and dynamic traning data. In addition, physical knowledge of the system is required to construct the transfer function. On the other hand the DMLP is more universal and does not need much system knowledge, except the input and output signals of the identified system. However, the main disadvantage of the DMLP is the high computational resources needed. Later, Ayoubi, [1998], used the DMLP network for the nonlinear process identification of a turbocharged diesel engine. The results showed that identification based on the DMLP needed no *a-priori* information about the process structure, which highlights the flexibility and universality of the model. The MLP is indeed the most utilized structure and spread across several

disciplines such as, identification and defect detection on woven fabrics shown by Sardy et al., [1993]; prediction of paper cure in the papermaking industry introduced by P. J. Edwards et al., [1999]; controller steering backup truck discussed by Nguyen and Widrow, [1990].

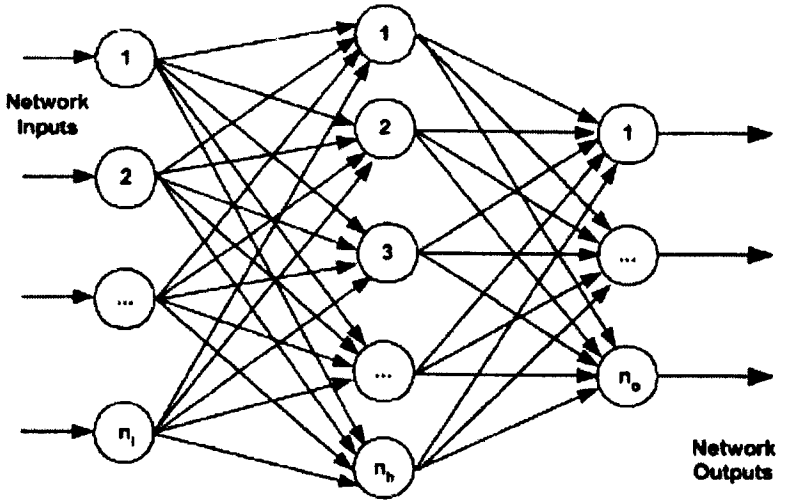

Figure 2.10 MLP basic topology.

2.4.2 Recurrent NNs (RNNs)

Another tool that has been used for temporal classification problems is the recurrent neural network (RNN) which is a modification of a conventional neural network, as shown in Figure 2.11. In this architecture, the inputs to the neurons come from external inputs, as well as from the internal neurons, consisting of both feed forward and feedback connections between layers and neurons. Narendra and Parthasarathy, [1990], demonstrate that the recurrent neural networks can be used effectively for the identification and control of nonlinear dynamical systems. Both static and dynamic back propagation was discussed for the learning process to adjust the different parameters.

Gan and Danai, [1999], show the application of using the model-based RNN in the fault diagnosis of the IFAC (International Federation of Accountants) Benchmark actuator of a speed governor for large diesel engines. As a starting point, the model-based RNN was used for fault detection and isolation solutions and it was improved via training and adapting them to the system's nonlinearity. The result indicates that the model-based recurrent neural network provides better results than black box neural networks. The Hopfield network model is the most popular

type of RNN. It can be used as associative memory and can also be applied to optimization problems. The basic idea of the Hopfield network is that it can store a set of exemplar patterns as multiple stable states. Given a new input pattern, which may be partial or noisy, the network can converge to one of the exemplar patterns nearest to the input pattern. As shown in Figure 2.12, a Hopfield network consists of a single layer of neurons. The network is recurrent and fully interconnected (every neuron in the network is connected to every other neuron). Each input/output takes a discrete bipolar value of either 1 or -1. Szu, [1993], used a modified Hopfield structure to determine the imperfection by the degree of orthogonality between the automated extracted feature, from the send-through image and the class feature of early good samples. The performance measure used for such automatic feature extraction is based on a certain mini-max cost function useful for image classification.

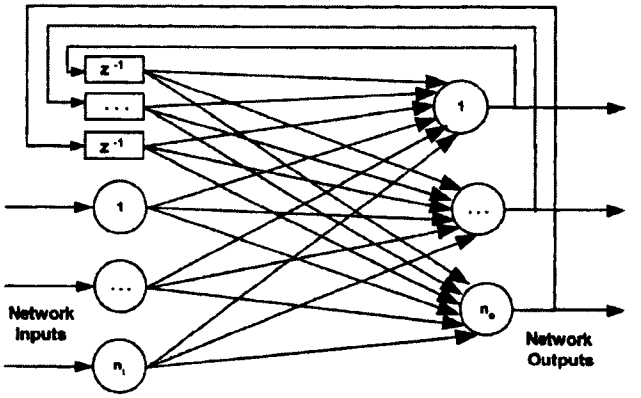

Figure 2.11 Typical recurrent network structure.

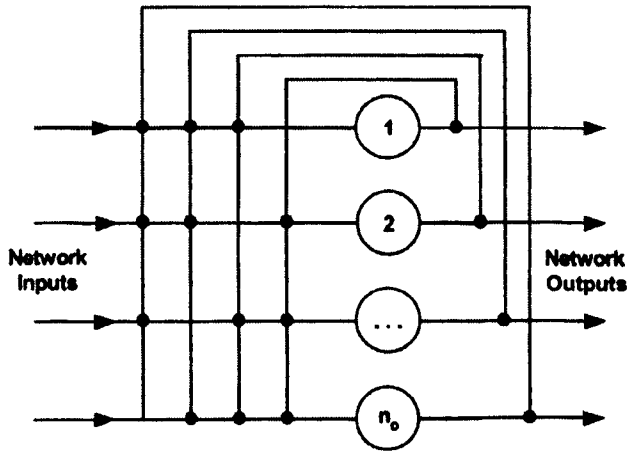

Figure 2.12 Hopfield network structure.

2.4.3 Non-recurrent unsupervised Kohonen networks

The structure of a Kohonen network consists of interconnected processing units that compete for the signal. The learning method is unsupervised learning and consists of a single layer of computational nodes (and an input layer). This network uses lateral feedback, which is a form of feedback, whose magnitude is dependent on the lateral distance from the point of application. Figure 2.13 shows the architecture with two layers. The first layer is the input layer and the second is the output layer, called the Kohonen layer.

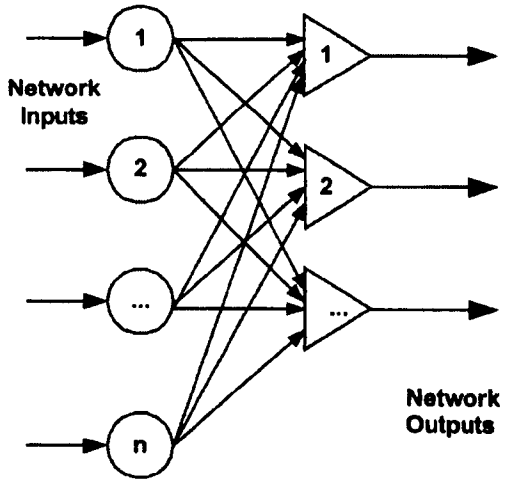

Figure 2.13 Kohonen network structure.

Every input neuron is connected to every output neuron through its associated weight. The network is non-recurrent and input information propagates only from left to right. Continuous (rather than binary or bipolar) input values representing patterns are presented sequentially in time through the input layer, without specifying the desired output. The output neurons can be arranged in one or two dimensions. A neighbourhood parameter, or radius, can be defined to indicate the neighbourhood of a specific neuron.

2.4.4 Cerebellar model articulation controller (CMAC)

The input mapping of the CMAC algorithm can be seen as a set of multidimensional interlaced receptive fields, each one with finite and sharp borders. Any input vector to the network excites some of these fields, while the majority of the receptive fields remain unexcited, not contributing to the corresponding output. On the other hand, the weighted average of the excited

receptive fields will form the network output. Figure 2.14 shows a schematic diagram of this structure, with the nonlinear input mapping by the Albus approach and a hashing operation that can be performed to decrease the amount of memory needed to implement the receptive fields. Majors et al., [1994], developed a methodology to control the air-fuel ratio of automotive fuel injection systems using this type of network. The CMAC was selected because of its function-approximation abilities and its learning and adaptive capabilities. Experimental results showed that the CMAC is very effective in learning the engine nonlinearities and in dealing with the significant time delays inherent in engine sensors. The CMAC controller performance had been improved over the conventional engine control module. Figure 2.15 (a) shows the fluctuation of A/F ratio with time for the engine control module while Figure 2.15 (b) shows the variation of A/F using a CMAC controller with the linear A/F sensor.

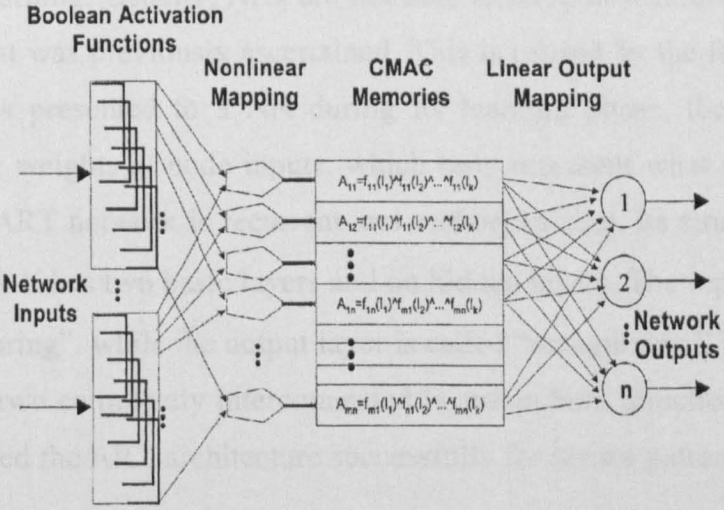

Figure 2.14. CMAC network structure.

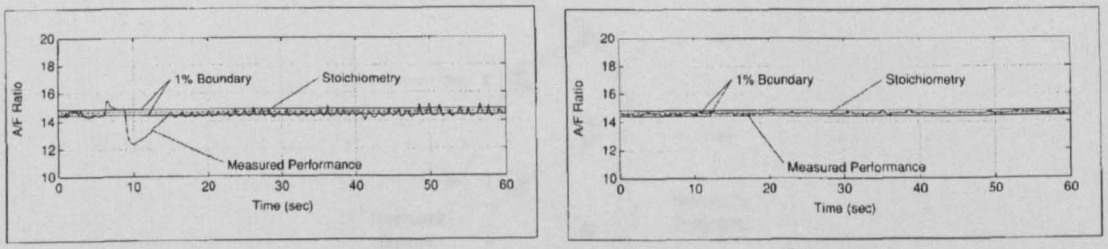

Figure 2.15. The effect of using CMAC controller with linear A/F sensor.

2.4.5 Adaptive resonance theory (ART)

Adaptive Resonance Theory (ART) was developed by Carpenter and Grossberg over the period of 1976-86, during their studies of the behaviour of models of systems of neurons, Whiteley et al., [1996]. They have published a large number of papers, in which they develop the mathematical theory of such models, usually in terms of systems of differential equations, and they have applied this to actual neural systems. Like Kohonen, they have been particularly interested in systems that are capable of organizing themselves. The ART paradigm can be described as a type of incremental clustering. It has the ability to learn without supervised training and is consistent with cognitive and behavioural models. It is an unsupervised paradigm based on competitive learning which is capable of automatically finding categories and creating new ones when they are needed.

The main feature of ART, compared to other similar structures, is its ability to not forget after learning. Usually, NNs are not able to learn new information without damaging what was previously ascertained. This is caused by the fact that when a new pattern is presented to a NN during its learning phase, the network tries modifying the weights at node inputs, which only represent what was previously learned. The ART network is recurrent and self-organizing. Its structure is shown in Figure 2.16. It has two basic layers and no hidden layers. The input layer is also called "comparing", while the output layer is called "recognizing." This network is composed of two completely interconnected layers in both directions. Whiteley et al., [1996], used the ART architecture successfully for sensor pattern interpretation problems.

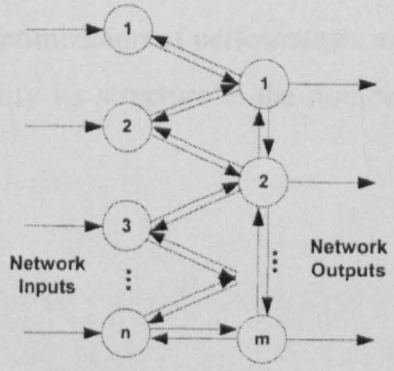

Figure 2.16. Adaptive resonance theory network.

2.4.6 Radial basis function (RBF) networks

Radial-Basis Function Networks used for pattern classification are based on Cover's theorem which states that nonlinearly separable patterns can be separated linearly if the pattern is cast nonlinearly into a higher dimensional space. Therefore we are looking for a network that converts the input to a higher dimension after which it can be classified using only one layer of neurons with linear activation functions. It contains an input layer, a hidden layer with nonlinear activation functions and an output layer with linear activation functions. Figure 2.17 shows the architecture of a RBF neural network.

The RBF network is a popular alternative to the MLP which can offer advantages over the MLP in applications such as fault diagnosis, as it is faster to train because training of the two layers is decoupled. Leonard and Kramer, [1991], utilized the RBF neural networks instead of sigmoid threshold units to overcome the difficulties of a backpropagation network classifier where, under certain conditions, it can produce non-intuitive, non-robust decision surfaces. Results show that RBF networks overcome these difficulties by using a non-monotonic transfer function based on the Gaussian density function. While producing robust decision surface, the RBF also provides an estimate of how close a test case is to the original training data, allowing the classifier to signal that a test case potentially represents a novel class while still presenting the most plausible classification. The adoption of RBF topology was justified by two reasons.

* In most cases, it presents higher training speed when compared with ANN based on back-propagation training methods.
* It allows an easier optimization of performance, since the only parameter that can be used to modify its structure is the number of neurons in the hidden layer.

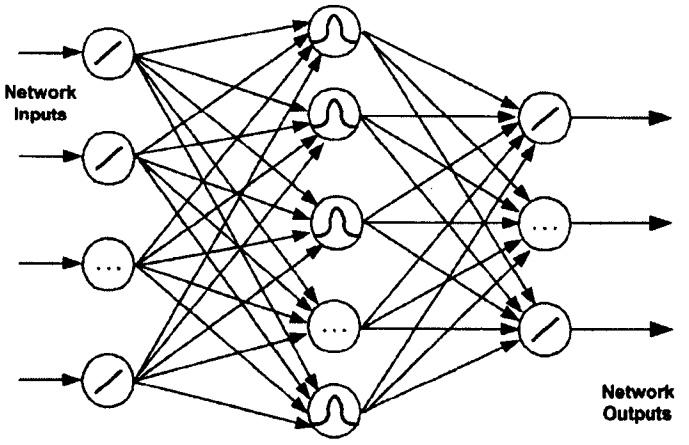

Figure 2.17. RBF network structure.

Leonhardt et al., [1995], introduced a fault detection scheme for monitoring combustion quality and proper injection pump operation. Significant features were extracted for data reduction purposes. By using a RBF neural network, these features were mapped back on the specified (desired) input values by allowing comparisons. Result show that if deviations higher than inherent modelling errors occur, symptoms such as lower fuel mass or premature fuel injection maybe generated. In addition, it was possible to separate fuel mass problems from injection angle failures. RBF had been used successfully to build a model which reconstructs the cylinder pressure using measurement of the instantaneous angular speed of the diesel engine crank shaft. Gu et al., [1996], validated such a model of a four stroke DI diesel engine. The results show that the reconstructed waveform is consistent with the measures pressure over all stages of the pressure process: compression, onset of combustion, peak pressure and the rise and fall of combustion.

Later, Shi et al., [2005], used the RBF neural network for building model of a marine diesel engine generator. The model depends on the fact that the RBF is a universal approximation neural network which has the ability to approximate nonlinear functions. The main advantage of using RBF is that the algorithm is simple and fast, and suitable for digital signal processor (DSP) calculation. The disadvantage of the method is that the generalization of the system is not so satisfactory. Two models are needed for good performance of a RBF neural network, one for the normal operation and the other for fault operation.

2.4.7 Probabilistic NNs (PNNs)

The probabilistic Neural Network, introduced by Donald Specht in 1988, is a three layer, feed forward, one pass training algorithm used for classification and mapping of data, Specht, [1990]. This network provides a general solution to pattern classification problems by following an approach developed in statistics, called Bayesian classifiers. Bayes theory, developed in the 1950's, takes into account the relative likelihood of events and uses *a priori* information to improve prediction. The network paradigm also uses Parzen Estimators which were developed to construct the probability density functions required by Bayes theory. The probabilistic neural network uses a supervised training set to develop distribution functions within a pattern layer. These functions, in the recall mode, are used to estimate the likelihood of an input feature vector being part of a learned category, or class. The learned patterns can also be combined, or weighted, with the *a priori* probability, also called the relative frequency, of each category to determine the most likely class for a given input vector. If the relative frequency of the categories is unknown, then all categories can be assumed to be equally likely and the determination of category is solely based on the closeness of the input feature vector to the distribution function of a class.

PNNs are somewhat similar in structure to MLPs. The basic differences among them are the use of activation by exponential functions and the connection patterns between neurons. In fact, the neurons at the internal layers are not fully connected, depending on the application in turn. Figure 2.18 depicts this structure, showing its basic differences from an ordinary MLP structure. PNN training is normally easy and instantaneous, because of the smaller number of connections. Another practical advantage over other networks is that it operates completely in parallel and the signal flows in a unique direction, without the need for feedback from individual neurons to the inputs.

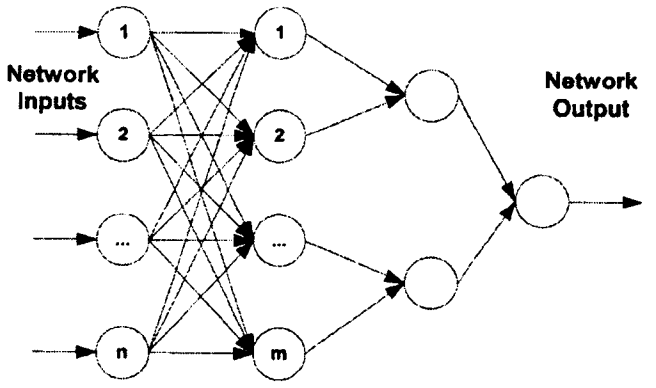

Figure 2.18. Probabilistic ANN structure.

2.4.8 Polynomial networks (PNN)

The PNN is a self-organizing multi-layered iterative algorithm that automatically provides linear and non-linear polynomial regression models. The PNN embodies the advantages of Multiple Linear Regression (MLR) and Artificial Neural Networks (ANNs) into a single entity. It can model both linear and non-linear relationships like ANNs, and it yields a polynomial regression equation as does the MLR for easy interpretation. This algorithm provides robust results in the presence of correlated and irrelative variables or/and outliers. The results of this algorithm can be easily interpreted.

Figure 2.19 depicts a polynomial network. It has its topology formed during the training process. Due to this feature, it is defined as a plastic network. The neuron activation function is based on elementary polynomials of arbitrary order. In some cases, only some of the inputs are used, due to the automatic input selection capability of the training algorithm. Automatic feature selection is very useful in control applications when the plant model order is unknown. Each neuron output can be expressed by a second-order polynomial function. The polynomial coefficients are equivalent to the network weights and the neuron output. The Group Method of Data Handling (GMDH) is a statistics-based training method largely used in modelling economic, ecological, environmental and medical problems. The GMDH training algorithm can be used to adjust the coefficient and evaluate the network structure. This algorithm employs only two sets of data. One for estimating the network weights and the other for testing which neurons should survive during the training process, more details could be found in; Silva et al., [1999].

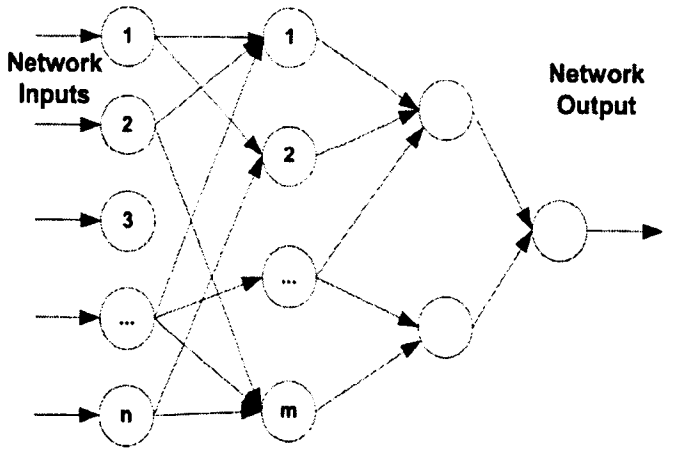

Figure 2.19. Polynomial ANN structure.

2.4.9 Functional link neural (FLN) networks

Functional link neural networks expand the original input space into higher dimensions in an attempt to reduce the burden on the training phase of the networks. This provides the network with a more complete understanding of the input. Basically, the function link acts on an element of an input vector or on all the elements of the input vectors by generating a set of linearly independent functions, and then evaluates these functions with the pattern as the argument. The functions enhance the network's understanding of a given problem and transform the inputs via higher-order functions such as squares, cubes, or sins. It is from the very name of these functions, higher-order or functionally linked mappings, that the two names for this same concept were derived. No new information is added, but the representation of the inputs is enhanced. Higher-order representation of the input data can make the network easier to train. The joint or functional activations become directly available to the model. In some cases, a hidden layer is no longer needed. However, there are limitations to the network model. Many more input nodes must be processed to use the transformations of the original inputs. With higher-order systems, the problem is exacerbated. Yet, because of the finite processing time of computers, it is important that the inputs are not expanded more than is needed to get an accurate solution.

Teeter and Chow, [1998], presented the application of an FLN for identification and control of heating, ventilating, and air conditioning (HVAC) thermal dynamic system. The use of NN provided a means of adapting the online controller, in an effort to minimize a given cost index. The identification networks demonstrated

the capacity to learn changes in the plant dynamics and to accurately predict future plant behaviour. Kwan et al., [1998] introduces a robust ANN controller to the motion control of rigid-link electrically driven robot using an FLN. The use of the FLN has a very important advantage where the robot dynamics was not needed to be exactly known. The structure schematic diagram is shown in Figure 2.20.

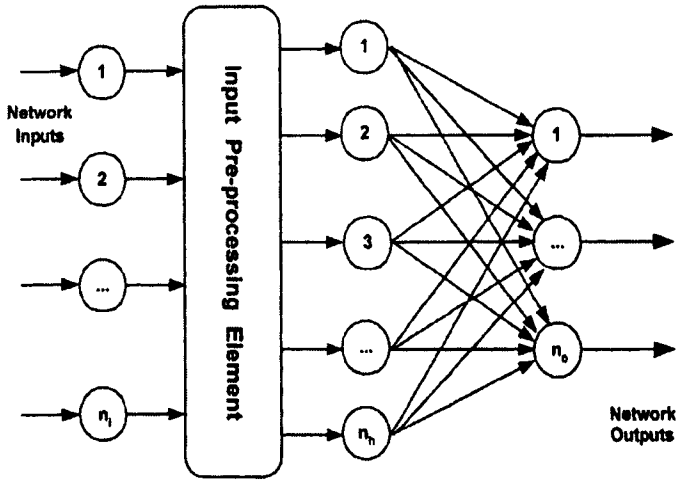

Figure 2.20. Functional link NN structure.

2.4.10 Functional polynomial network (FPN)

This structure was implemented to merge both models of a functional link and polynomial network resulting in a very powerful ANN model due to the automatic input selection capability of the polynomial networks in addition to the fast learning of the functional link networks. The FPN presents advantages such as fast convergence, no local minima problem, structure automatically defined by the training process, and no adjustment of learning parameters.

2.5 TRAINING METHODS

There are basically two main groups of training (or learning) algorithms: supervised learning (which includes reinforcement learning) and unsupervised learning. Once the structure of an NN has been selected, a training algorithm must be attached, to minimize the prediction error made by the network (for supervised learning) or to compress the information from the inputs (for unsupervised learning). In supervised learning, a set of inputs and correct outputs is used to train the network. Before the learning algorithms are applied to update the weights, all the weights are initialized randomly. The network, using this set of inputs,

produces its own outputs. These outputs are compared with the correct outputs and the differences are used to modify the weights, as shown in Figure 2.21. A special case of supervised learning is reinforcement learning, shown in Figure 2.22, where there is no set of inputs and correct outputs. Training is commanded only by signals indicating if the produced output is bad or good, according to a defined criterion. After training, an ANN is tested by giving it only input values, running the ANN and see how close the network comes to outputting the correct target values.

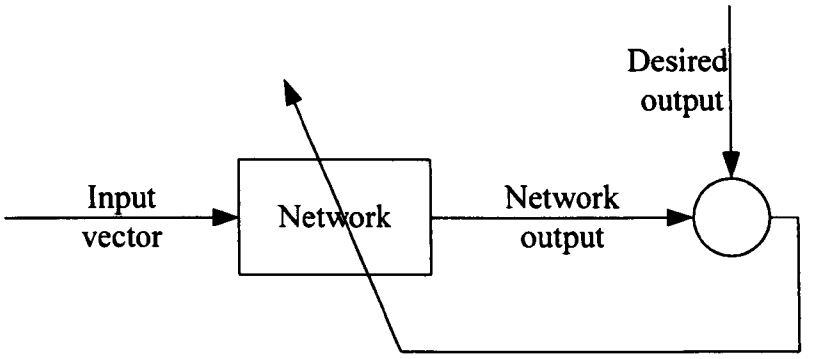

Figure 2.21. Supervised learning scheme.

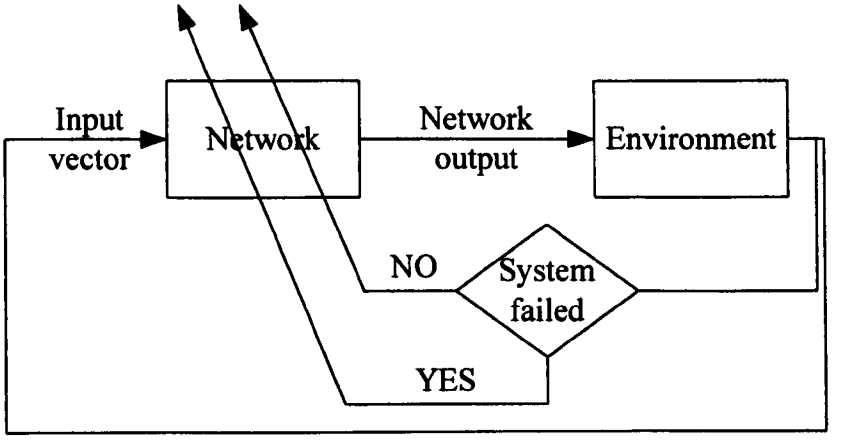

Figure 2.22. Reinforcement learning scheme

Unsupervised learning, also known as self-organized learning, involves no target values; it tries to auto-associate information from the inputs with an intrinsic reduction of data dimension, similar to extracting principal components in linear systems. In other words, by using the correlation of the input vectors, the learning rule changes the network weights to group the input vectors into clusters.

Therefore, similar input vectors will result in similar network outputs since they belong to the same cluster. Figure 2.23 show the principle of the unsupervised learning algorithm.

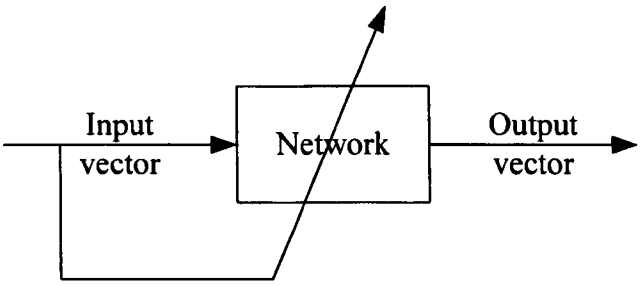

Figure 2.23. Unsupervised learning scheme

In learning algorithms, one should be interested in how the algorithm converges, its speed of convergence, and computational complexity of the algorithm. The error, of a particular configuration of the network, can be determined by running all the training cases through the network and comparing the actual output generated with the desired outputs or clusters. Many methods have been used for the learning algorithm starting from the early supervised learning algorithms such as Perceptron Learning and Least Mean Squares (LMS) also known as Widrow-Hoff Learning. These algorithms were designed for single layer NNs, therefore, they are generally more limited in their applicability. These two algorithms are similar in all of the steps except the error calculation principle. In the Preceptron Learning the error is calculated by the difference between the desired output and the resulting output while in the LMS the error is based on the sum of the inputs to the unit. The linear sum of the input is passed through a bipolar sigmoid function, which produces the output +1 or -1 depending on the polarity of the sum. The LMS algorithm can be used in structures as RBF networks and was successfully applied Leonard and Kramer, [1991]. It has also been used to adapt a complex robotic system involving multiple feedback sensors and multiple commands using CMAC approaches Miller, [1989].

Back Propagation (BP) is a generalization of the LMS algorithm. In this algorithm, an error function is defined as the mean-square difference between the desired output and the actual output of the feedforward network. It is based on steepest

descent techniques extended to each of the layers in the network by the chain rule. Hence, the algorithm computes the partial derivative of the error function with respect to the weights. The error function is defined as half of the square of difference between desired output and network output. The objective is to minimize the error function by taking the error gradient with respect to the parameters or weight vector that is to be adapted. This algorithm is simple to implement and computationally less complex than other modified forms. Despite some disadvantages, it is popular and there are numerous extensions to improve it.

Back Propagation with Momentum (BPM) is the basic improvement to the back propagation algorithm. In this algorithm a momentum term was introduced in the weights equation. This momentum factor is commonly selected between (0 and 1). The adding of momentum term improves the convergence speed and helps the network from being trapped in a local minimum.

2.6 SUMMARY

A survey has been carried out of previously reported research in the field covering most of the areas related to condition monitoring and fault diagnosis of diesel engines. The main outcome of this review indicates the successful utilization of neural networks in CMFD systems for the diesel engine. However, some challenges still face the development of a robust and relatively low cost CMFD algorithm. The number of required sensors as well as their types that suite the diesel engine working environment, increase the implementation cost of proposed system. Therefore, by limiting the number of sensors and using a low cost direct or indirect transducer to evaluate the engine condition represents a good solution.

The utilization of high frequency parameters such as cylinder pressure, in the CMFD algorithm require large computational resources and add some limitations on the possibility of including the constructed algorithm on an embedded controller to suit the future integration in the industrial applications, e.g. market vehicles. Using alternative physical parameters that are indirectly related to the high frequency signals and require less computational resource is a promising solution, e.g. using of instantaneous speed to indicate the cylinder pressure variations, El-Ghamry et al., [2005] and Moro et al., [2002].

The utilization of engine modelling in CMFD systems had met with approved; however, different methods were used to model the engine as a non-linear complex system. Each method has its advantages and disadvantages which have been discussed. One of the most important criteria used for modelling is the number of empirical relations which limit the application range of the model. Therefore, the evaluation of a general engine model that utilizes the minimum possible number of empirical equations and selects a more general empirical relationship that is applicable for a wide range of engines is expected to increase the validity range of the engine model as well as the developed CMFD system based on this model. Whatever, the application area for utilizing the neural networks, the selection of the types of NNs used as well as the training method represents the main keys to evaluating a suitable solution. However, it was not possible to find a specific theoretical basis for such a selection. A useful tool in facing up to this challenge is to utilize previous research as a guide to narrow the selection and compare the commonly used neural networks and training methods.

The idea of using neural networks for fault diagnosis is not a new one. An increased number of successful applications of neural networks to problems of fault diagnosis and condition monitoring have been reported in the literature. There are two main approaches that have been taken in such fault diagnosis and condition monitoring applications: (a) training them to recognise certain known faults and (b) training them to recognise departures from normal operation, i.e. novelty detection. The two approaches are essentially complimentary and in some cases have been used in tandem; novelty detection being particularly useful in cases where few examples of faulty data are available. However, the approach taken in the present study is one of fault diagnosis, since our concern was with the early recognition of subtle faults. A novelty detection approach to the same problem is suggested to be less successful, since, lacking knowledge about possible faults, it would be difficult to set detection levels sensitive enough to detect slight departures from normality. Although there are several examples of the application of ANNs to problems of fault diagnosis, there are fewer examples of their application to fault diagnosis in internal combustion engines. More common applications have been to gear boxes, and bearing faults.

CHAPTER 3

DIESEL ENGINE TEST FACILITY

This chapter provides a full description of the test facility and explains the function of each part in the system and the challenges faced with the selection and integration of different sensors are also covered. The data acquisition system constructed, including the software algorithm, are then discussed in detail. Finally, the testing and calibration of the different sensors are explained.

3.1 TEST SYSTEM LAYOUT

In order to test the proposed condition monitoring technique, it was decided to equip the available engine with extensive instrumentation, including average and instantaneous speed sensors, air and exhaust temperature sensors, and a torque sensor. The parameters to be directly measured were established as a compromise between measured signal importance (with respect to the monitoring objective), cost and availability of transducers, and complexity of fitting into the engine. Figure 3.1 provides an overview of the sensors fitted to the engine and shows the signals measured by the data acquisition system. A signal conditioning circuit was designed and implemented according to the data acquisition system specifications. As the condition monitoring and fault detection were conducted on-line, all data analysis was undertaken using a separate computer on which the proposed CMFD algorithm was developed.

The engine used for the tests is a Ford 70PS 4-stroke 2.5 litre diesel engine. To comply with health and safety regulations within the university, the engine was located in an acoustically insulated test cell. The test engine was integrated with a manually controlled Heenan & Froude DPX3 200hp sluice plate hydraulic dynamometer to simulate the external load during the engine test. To improve the performance of the hydraulic brake, it was decided to integrate the brake with an automatic torque control system. An overview of the design architecture of the brake system is shown in Figure 3.1. The proposed modifications provide the

engine test system with the variable load capability to increase the flexibility for the proposed CMFD algorithm.

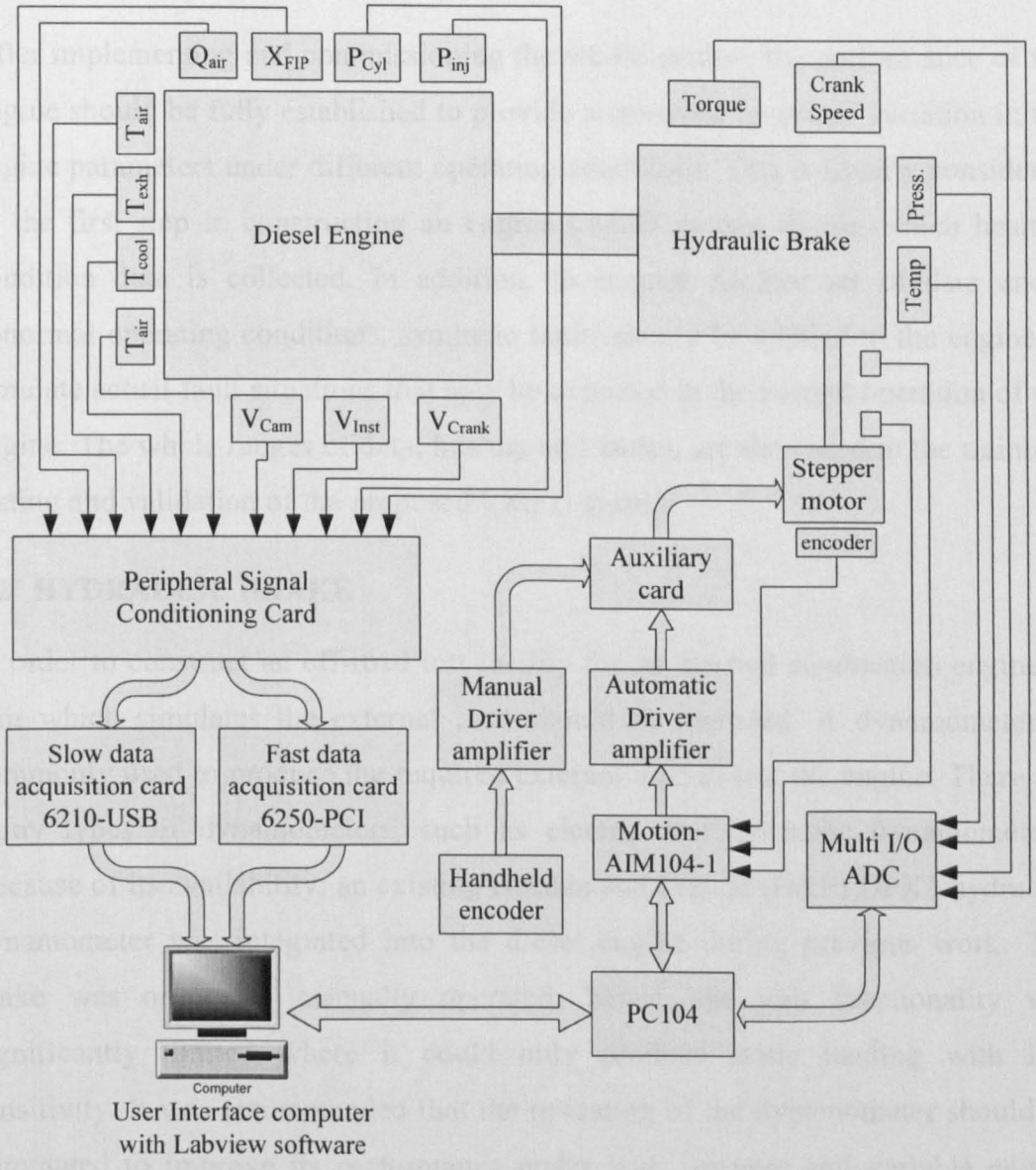

Figure 3.1 The architecture of engine and dynamometer system.

The engine coolant water is circulated by an internal water pump through an automotive radiator mounted on the roof of the test cell. The radiator is air cooled by two integrated battery driven fans. As the test cell is fully enclosed, the fuel tank and accelerator handle are located on the outside wall of the cell. As most of the measured signals required signal conditioning, several electronic circuits were designed and constructed. Full circuit diagrams for the peripheral signal conditioning design are provided in Appendix B. Two data acquisition cards were used to collect the engine data, one for rapidly changing signals and the other for

the slow rate signals. Each card was selected according to the required bandwidth for the measured signals. The data acquisition software was designed using Labview (National Instruments), version 7.5.

After implementing and commissioning the whole system, the performance of the engine should be fully established to provide a complete record of variation in the engine parameters under different operating conditions. This is usually considered as the first step in constructing an engine CMFD system during which healthy condition data is collected. In addition, to acquire another set of data under abnormal operating conditions, synthetic faults should be applied to the engine to simulate actual fault situations that may be expected in the normal operation of the engine. The whole ranges of data, healthy and faulty, are then used in the training, testing and validation of the proposed CMFD system.

3.2 HYDRAULIC BRAKE

In order to construct an off-road test facility for an internal combustion engine, a unit which simulates the external load should be included. A dynamometer is commonly used to produce the required external load to test the engine. There are many types of dynamometers, such as electric and hydraulic dynamometers. Because of its availability; an existing Heenan and Froude (H&F) DPX3 hydraulic dynamometer was integrated into the diesel engine during previous work. The brake was originally manually operated; hence, the unit functionality was significantly limited where it could only produce static loading with low sensitivity. It was recommended that the operating of the dynamometer should be automated to improve its performance under both constant and variable engine loading. The control system design incorporates two control modes: a programmable automatic control mode capable of producing variable load as well as a manual mode. A detailed explanation of both modes is given later in this chapter.

3.2.1 Original dynamometer operation

The hydraulic dynamometer comprises a rotor and two stators. Each stator opposing a rotor face contains a series of semi-circular vanes which accelerate and decelerate water flowing in a toroidial vortex pattern around the working

compartment, as shown in Figure 3.2. The constant momentum exchange of the water creates a torque reaction on the stator/casing which is resisted and measured via a spring-mass mechanism shown in Figure 3.3. The power absorbed by the hydraulic dynamometer is proportional to the rotational speed, the water gap and the mass of water circulating in the working compartment. By adjusting the water passing gap size and flow rate, the power consumption can be regulated. The gap between the stator and the rotor is controlled via a screwed shaft, and the water flow rate is adjusted by the outlet valve.

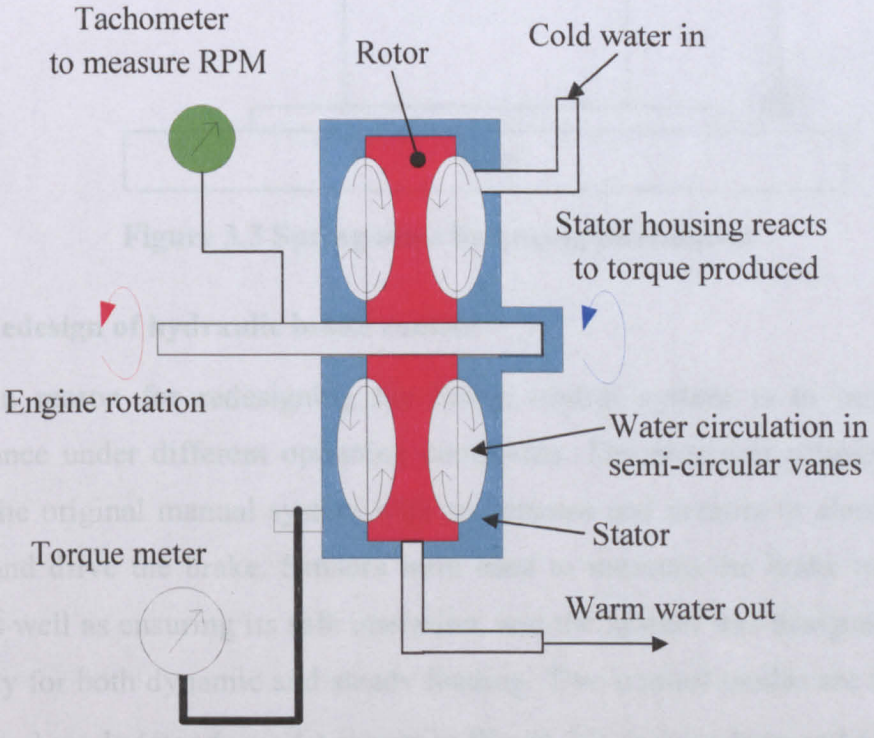

Figure 3.2 Schematic of hydraulic brake internal view.

In action, the rotor discharges water at high speed from its periphery into the pockets formed in the casing liners where the water speed decays. The water returns at diminished speed to the rotor pockets at a point near the shaft. The resistance offered by the water against the rotor motion reacts upon the casing, which tends to turn on its anti-friction roller supports. This tendency is counteracted by means of a lever arm terminating in a loading device or torque metering cell that measure the torque. The water flow is maintained at that level by continuous refilling and draining, which carries away the heat generated by the absorbed energy or horsepower. The heated water is then discharged from the dynamometer to the drain.

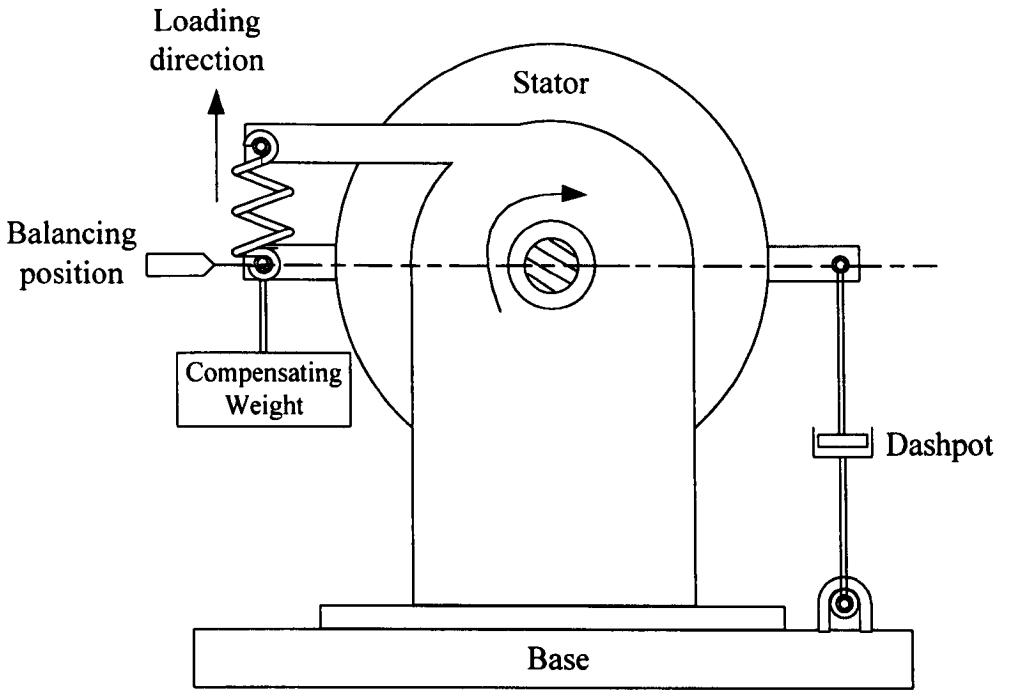

Figure 3.3 Spring mass balancing mechanism

3.2.2 Redesign of hydraulic brake control

The main reason for redesigning the brake control system is to improve its performance under different operating conditions. The proposed solution was to modify the original manual system with an actuator and sensors to electronically control and drive the brake. Sensors were used to measure the brake torque and speed, as well as ensuring its safe operation, and the system was designed to have the ability for both dynamic and steady loading. Two control modes are used. The first manual mode (*steady mode*) shown in Figure 3.4, is open loop and adjusts the screwed shaft to a position that corresponds to the required constant brake load. This configuration is suitable for testing the engine at constant speed conditions, and requires no feedback. The user only needs to monitor the engine speed and adjust the screw shaft position accordingly to achieve the desired speed.

A second control mode was designed to facilitate variable loading which could be pre-programmed to simulate different environmental loading conditions for the engine. The block diagram of the closed loop torque control system is shown in Figure 3.5. To attain reasonable accuracy and rapid response, two control loops were established, using an embedded controller to achieve both easy programming

and reliable performance. In the following subsections more detail of the two control modes are presented, and the control algorithm described.

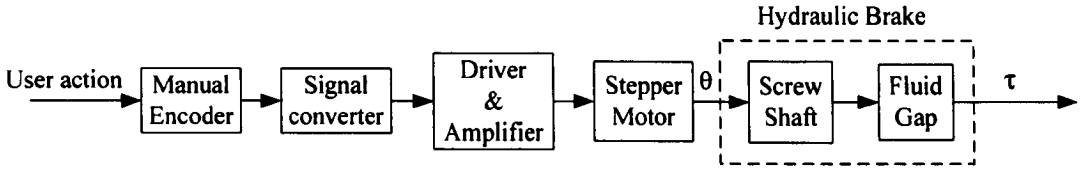

Figure 3.4 Steady mode layout.

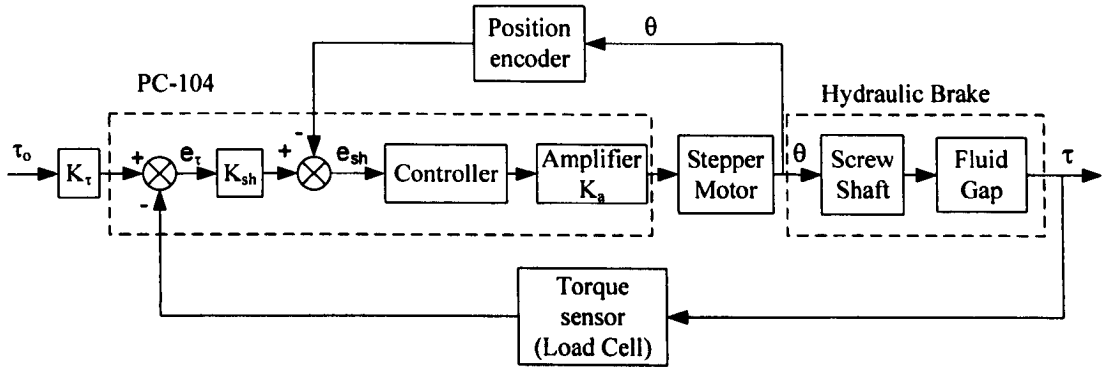

Figure 3.5 Automatic control mode layout.

3.2.2.1 Control modes

- *Manual (steady) mode*

A stepper motor command signal is generated using a two channel manually driven encoder which produces two pulse trains for both rotation angle and direction. This information is interpreted within the manual driver circuit of the stepper motor to produce the appropriate number of steps for the stepper motor movement and direction of rotation, which is detected from the phase difference between the two output channels. An electronic controller/driver circuit was designed to match the stepper motor specifications, in terms of rated current and voltage. The driver utilizes pulse width modulation (PWM) to limit current consumption by the stepper motor, to reduce the possibility of the circuit components overheating. A high input voltage is applied to the motor to reduce the consumed current at the same produced load torque. The PWM protects the motor from the problem of excessive voltage using an internal chopper circuit that chops the output according to the load current. A full schematic diagram of the manual driver circuit is shown in Appendix B.

A manual encoder was mounted in a metal box with a digital display to indicate engine speed in RPM. The handheld box is equipped with a selector button to switch between the different control modes (manual and automatic) using a relay switch contained in an auxiliary circuit. Figure 3.6 shows the handheld unit illustrating the different components. Small led indicators were included to show the control mode selected. The water pressure inside the hydraulic brake is monitored using a pressure switch which is connected to a led which comes on when the water pressure in the brake case reaches the required level. The pressure switch was calibrated against a pressure gauge to switch on at a pressure of 1 bar.

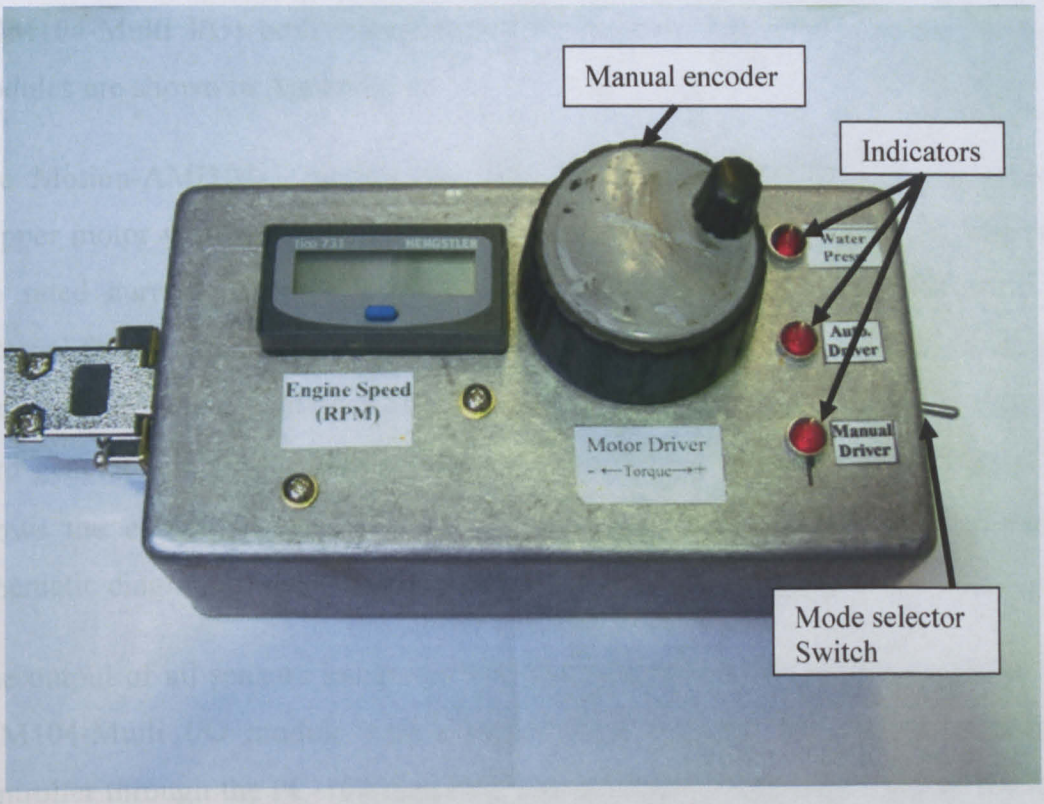

Figure 3.6 Hand held control unit.

- *Automatic control mode*

A torque feedback control configuration was adopted to improve the system's response to desired load variations, programmed according to the engine performance curve or specific operating conditions, such as constant or variable loading. The output torque of the brake was selected as the feedback parameter for the control loop. A load cell was integrated into the brake and its output compared with the desired output torque value to produce the control error signal, as shown

in Figure 3.5. An embedded controller drives the stepper motor, via the motor controller module, to reduce the error.

The automatic control system comprises an Arcom PC-104, AIM104-386EX embedded controller with extension modules, and is intended for specialized embedded computing environments where applications depend on reliable data acquisition despite extreme environments. It was selected for its small size, reliable performance at high temperature and non-clean environments and ease of programming. Two extension modules were integrated to the PC104: a stepper motor driver module (Motion-AIM104-1) and a multi function I/O module (AIM104-Multi I/O) both manufactured by Arcom. Full specifications for both modules are shown in Appendix A.

The Motion-AMI104-1 module has the capability to directly drive a bipolar stepper motor with a maximum rated current of 1A per phase, which is less than the rated current of the stepper motor used (4.6A per phase). Therefore, an external driver was designed and constructed in order to use the pulse train signals generated from the Motion-AMI104-1 module as driving signals. The external card generated a driving signal with a rated current of 5A per phase. Figure 3.7 shows the electronic circuit of the stepper motor external driver. A detailed schematic diagram of the driver circuit is shown in Appendix B.

The output of all sensors integrated into the hydraulic brake are connected to the AIM104-Multi I/O module which capture and transmit the data to embedded controller through the PC-104 data bus. The analogue sensor signals from the load cell passed through a signal conditioning circuit where they were filtered and amplified/attenuated to match the A/D input range. Two auxiliary signal conditioning cards were designed and constructed to fulfil these requirements. The first card amplifies the output signal of the load cell to a reasonable level based on the multi function I/O module specifications. A low-pass filter was integrated with the load cell amplifier circuit to reduce the effect of noise interference on the measured signal before the amplification stage. The filtered signal was amplified using a high accuracy, high gain and low drift amplifier (Analog Devices, AD524).

The load cell-amplifier combination was calibrated in order to adjust the amplifier gain. Based on the load range of the brake, a gain of 50 was selected for the signal amplification in order to achieve a reasonable voltage level according to the maximum allowable input analogue voltage (+5V). The calibration of the load cell with the amplifier was conducted on an Instron tensile test machine. To ensure the repeatability of the load cell, the calibration test was repeated several times and the results showed very good repeatability, as illustrated in Figure 3.8. A correlation equation was deduced using the test results and used to evaluate the measured load using the amplifier output voltage within the data acquisition program. A second auxiliary card was designed and constructed to include a two-way relay and power supply sockets to switch between the two controller modes of manual and automatic. The relay is triggered using the mode selector switch which is included in the hand held control and display unit, as shown in Figure 3.6.

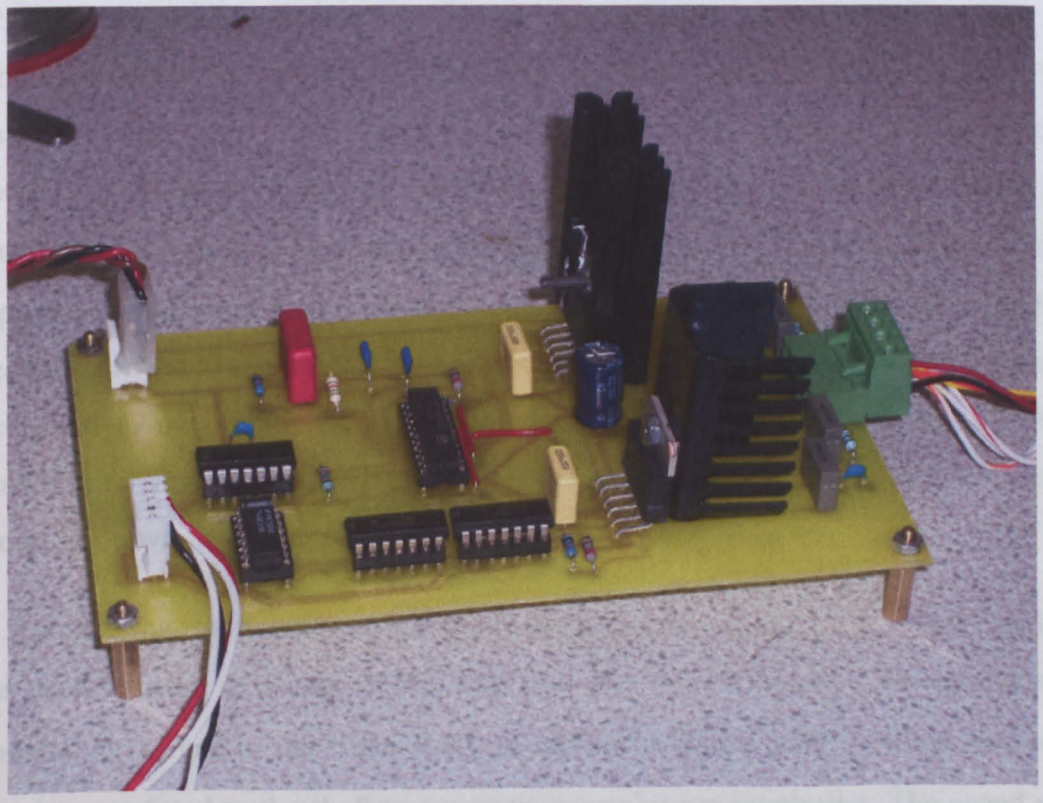

Figure 3.7 Stepper motor automatic external driving card.

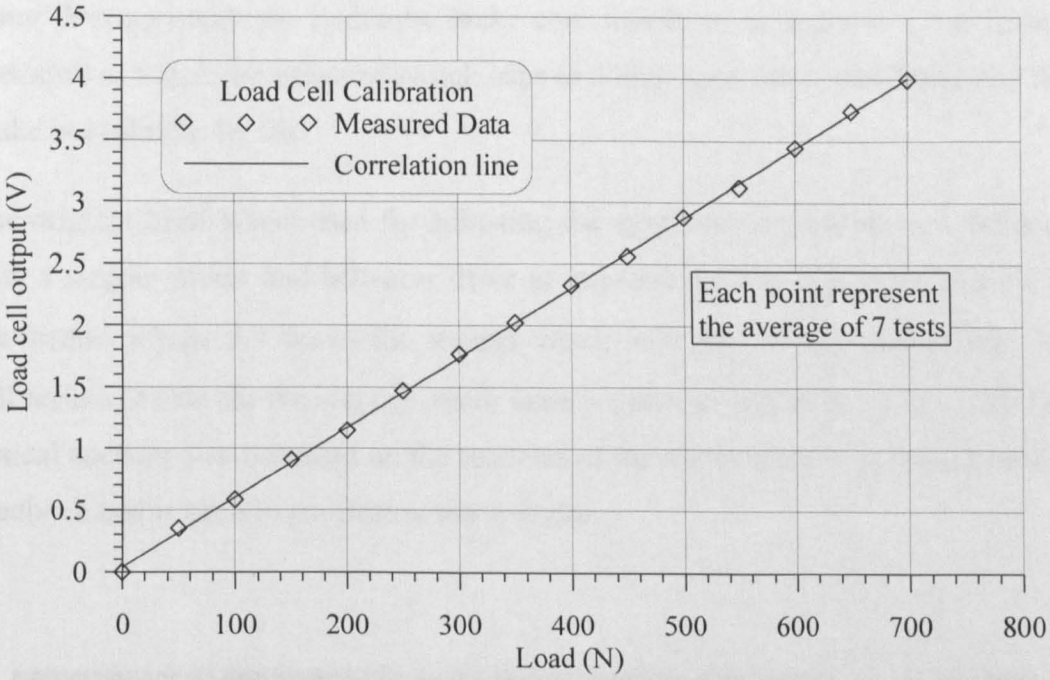

Figure 3.8 Load cell calibration curve.

3.2.2.2 Sensors and actuators

A high accuracy S-shape load cell (OMEGA LCCA-200) was used to measure the brake reaction force. The load cell replaces the original dead-weight system, where it is connected to the spring from one side and to the base frame from the other side, as shown in Figure 3.9. An interface circuit was designed and implemented to amplify the small output voltage of the load cell that is used as feedback for the brake control system. In addition, this signal was also separately connected to the main data acquisition system for engine monitoring. The full specification for the load cell is given in Appendix A; the amplifier schematic circuit is shown in Appendix B.

To measure the rotational speed of the hydraulic brake an optical proximity switch was used because of its reliability, low cost and eases of fitting. The sensor was mounted at the end of the brake shaft, as shown in Figure 3.10. A metal disc with one slot was fitted to the shaft to generate one pulse per revolution. The speed was measured using time interval between two consecutive pulses using a high speed timer counter provided on the multi I/O interface card.

To ensure the water pressure to the brake before applying load; a pressure switch was located at the water outlet point, as shown in Figure 3.11. The pressure of

water flowing inside the hydraulic brake case should be adjusted to 1 bar (gauge pressure) at which the pressure switch trips to a high logic level indicating that the brake is available for use.

The original hand wheel used for adjusting the dynamometer torque was replaced with a stepper motor and belt-gear drive to improve the regulation and control of the torque. Figure 3.9 shows the stepper motor with the driving mechanism. The full technical data for the stepper motor used is given in Appendix A. A 3-channel optical encoder was mounted on the rear end of the motor shaft to provide position feedback and is used to confirm motor rotation.

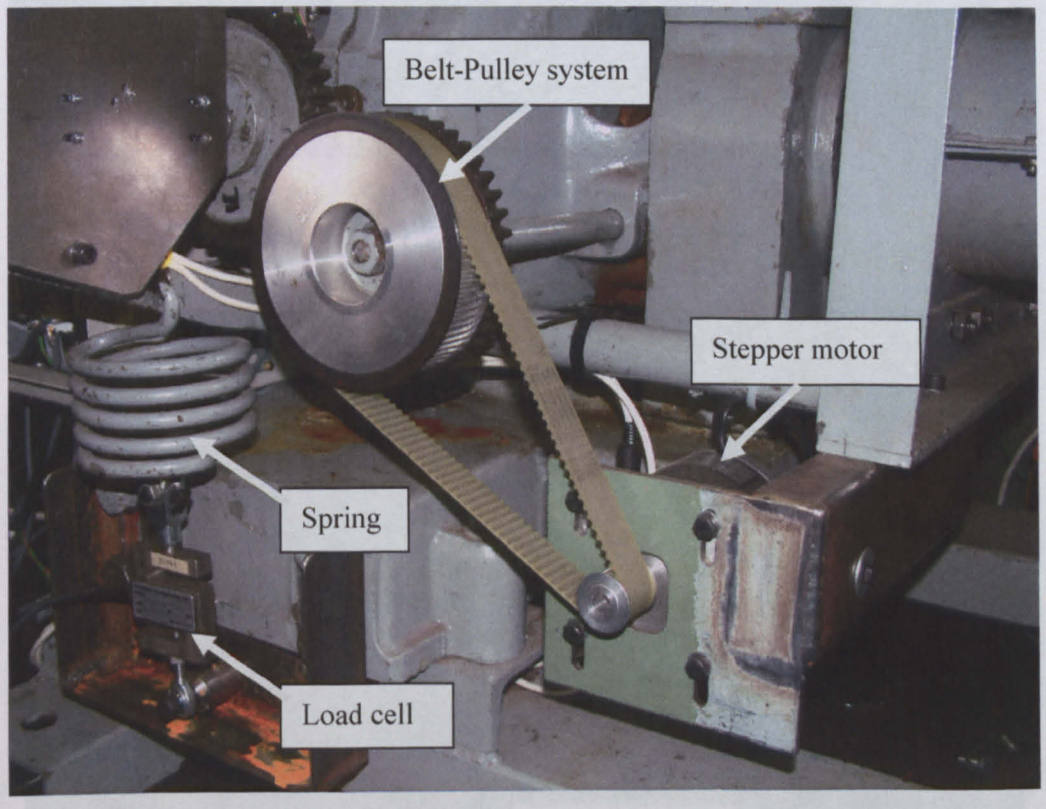

Figure 3.9 The load cell fitting and stepper motor driving mechanism.

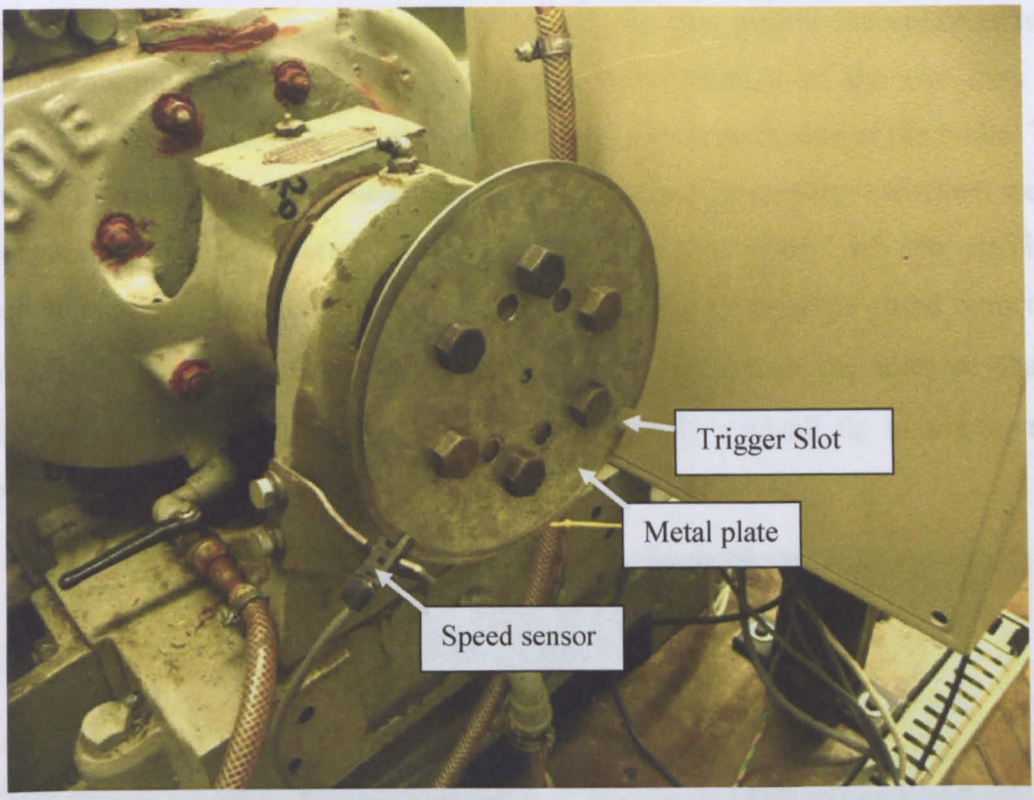

Figure 3.10 Hydraulic brake speed sensor.

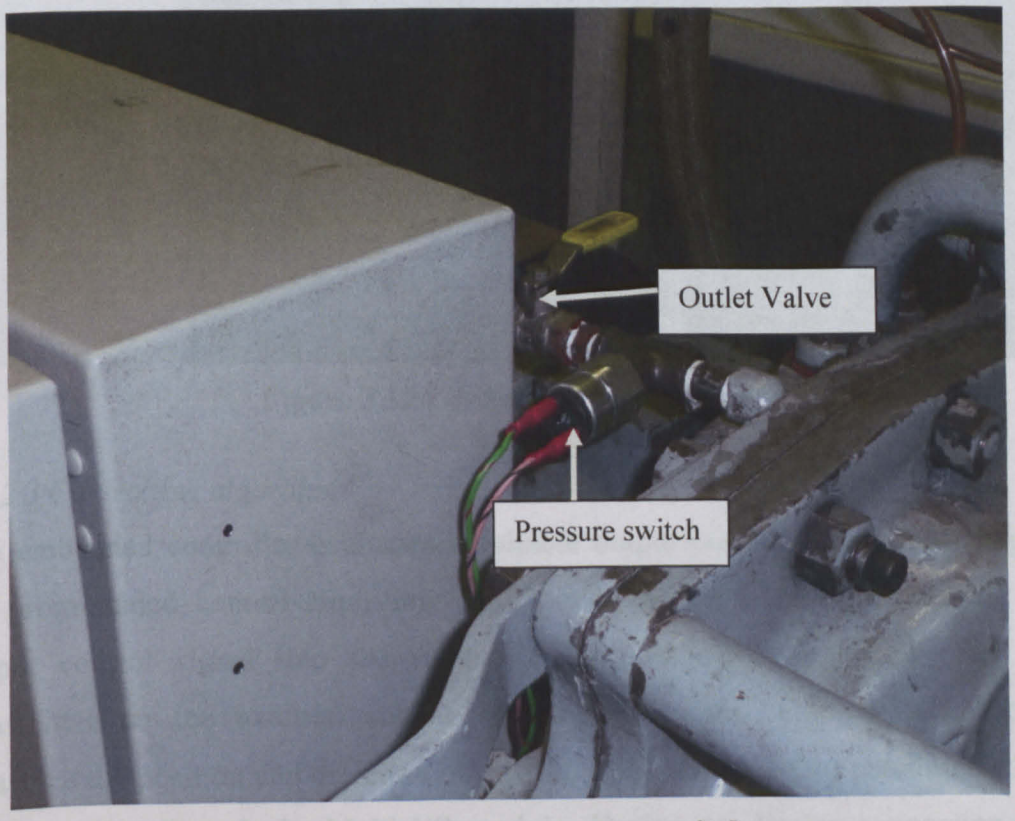

Figure 3.11 Water pressure switch

The design of the transmission used to adjust the two stators incorporates two counter-rotating nuts on a single lead screw. The rotation of the two nuts is coupled to the lead screw through a pair of gears, one at each side of the brake. To restrict the motion of the lead screw, two optical proximity switches were incorporated in the control system to prevent over-travel of the driving mechanism. The proximity switch was mounted on a metal plate fitted onto the brake loading arm, as shown in Figure 3.12. The top end of the screwed shaft, which is connected to the stator, was integrated with a small tip to trigger the proximity switch to prevent from over-travel.

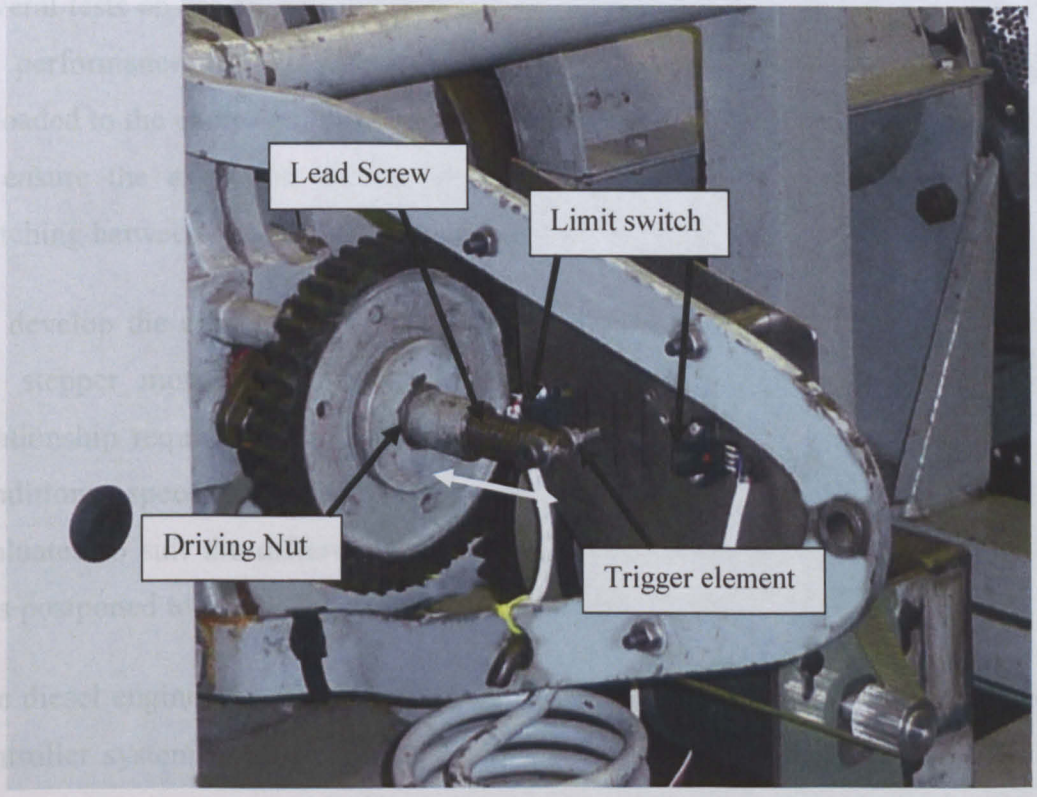

Figure 3.12 Lead screw limit switch

3.2.2.3 Controlling algorithm

The embedded controller evaluates a suitable output control signal according to the programmed control algorithm. The Motion-AIM104-1 module convert the output control signal into the rotation angle and direction signals that are transmitted to the external stepper motor driver card. The optical encoder measures the position and direction of rotation and feed the actual position back to the controller through the Multi-I/O module. Having no display connection and limited memory, the code was written in Borland C++ and compiled on a host PC,

then uploaded to the controller through the serial connection. Figure 3.13 shows the flow chart of the control algorithm code.

As the present study mainly focuses on the diesel engine condition monitoring under steady conditions, only the hardware parts of the automatic control mode were validated. All engine tests were performed under steady state working conditions, and only the manual control mode of the hydraulic brake was used. The development of the automatic control algorithm will be postponed to the future work.

Several tests on the stepper motor control system have been conducted to validate the performance which consisted of a sequence of positions programmed and uploaded to the controller to be performed. The optical encoder feedback was used to ensure the execution of the required positions. These tests show accurate matching between the desired positions and the actual achieved positions.

To develop the complete control algorithm, a load-position relationship between the stepper motor position and resulting brake load was required. Such a relationship requires further tests on the brake system under different operating conditions, speed and load. The optimum controlling technique can then be evaluated to suit the different loading conditions of the diesel engine. This task was postponed to future development due to lack of time in the present research.

The diesel engine was tested only under static loading conditions and the manual controller system used to control the hydraulic brake via the handheld unit. The load cell output was recorded through the main data acquisition system. A more detailed description of the engine data acquisition system is provided later.

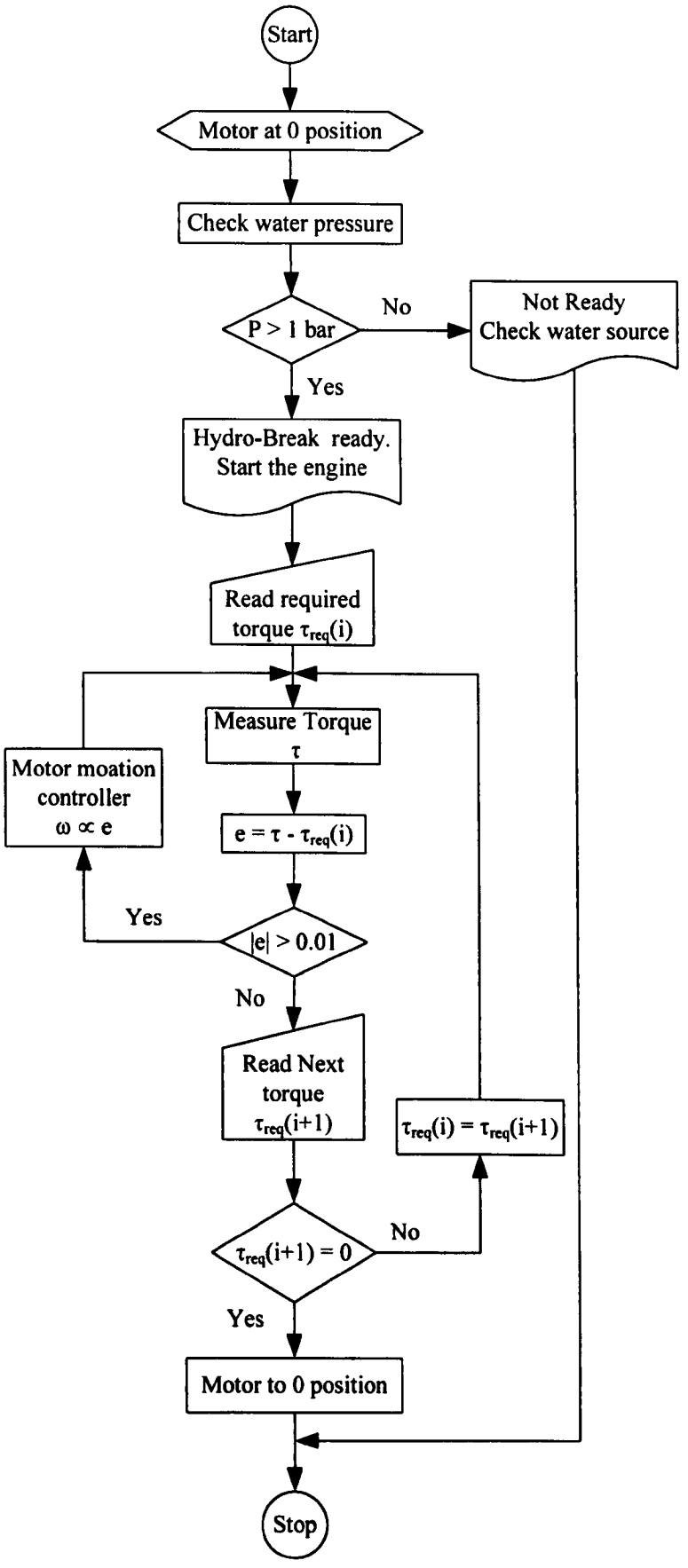

Figure 3.13 The flow chart of the hydraulic brake system controller

3.3 DIESEL ENGINE INSTRUMENTATION

The first step in implementing and testing the condition monitoring and fault detection system was to integrate the engine with appropriate sensors to measure the engine parameters that influence the engine performance and condition. Diesel engine condition monitoring involves many processes and physical parameters which could be measured, including the combustion process, wear, mechanical drivetrain, and exhaust emission. According to various considerations, this study aims to focus attention on the combustion process, and disregard mechanical drivetrain issues as well as auxiliary equipment. There are three reasons for this decision. Firstly, faults affecting the combustion process are believed to represent a major proportion of faults related to performance degradation developing during the running of internal combustion engines. Secondly, a number of conditions affecting combustion are easily simulated without the need for intrusive modifications to the engine parts. Finally, sensors expected to give information about the combustion process were found to be available and easily integrated into the engine, some of which are available in commercially marketed engines. In addition, the reasonable cost of the sensors used is another important factor in the system implementation and the possibility of its future application. In the following subsections, a brief explanation of the physical parameters selected and their importance as well as their relationship to the combustion process are given. In addition, full detailed descriptions of the transducers used, fitting method, and the signal conditioning processes are also included.

3.3.1 Signals measured

There are many physical parameters that have to be measured in order to evaluate the condition and quality of the combustion process. A list of these parameters and their relation to the combustion process are given as follows:

* Cylinder pressure is one of the most important signals that reveal the quality of the combustion process. The rate of change and peak value of cylinder pressure is a key parameter. Any deviation in the cylinder pressure signal could be interpreted to identify particular faults. The pressure inside the cylinder may be measured directly or indirectly. Sensors that directly measure cylinder pressure usually need access holes to the inner space of the

cylinder. Any permanent modification in the cylinder head usually causes changes to the actual displacement and clearance volume, which directly affects engine performance. Also, the harsh environment of high temperature and pressure inside the cylinder of the diesel engine requires the use of expensive direct measuring sensors. To limit the effect on engine performance, specially designed sensors can be integrated with the glue plug to avoid any change in combustion chamber volume; however, the cost of such sensors is still relatively high. Notwithstanding the relatively high cost of special sensors, they are not applicable to the existing Ford engine, which does not have glue plugs. On the other hand, the use of indirect methods to measure cylinder pressure has to be verified using experimental data measured by a direct measuring sensor. A new technique was investigated to measure cylinder pressure without introducing changes to the combustion chamber so that the engine's original performance conditions are unaffected. This challenge was considered as one of the objectives of the present study. A novel technique has been introduced to measure cylinder pressure which satisfies all the above limitations discussed. More details of the new technique are given later in this chapter.

* As a result of variations in cylinder pressure, torque is produced on the crankshaft that drives the different engine parts and the external load at certain rotational speeds. The speed varies with time depending on the pressure level in the cylinder as well as the contributions of each cylinder in a multi-cylinder engine. Instantaneous speed measurement can yield valuable information about the contribution of individual cylinders to the final brake torque produced. It may also be feasible to identify mechanical problems from this signal. In addition, as discussed in the literature review, the instantaneous speed signal can also be used as an indirect method for measuring cylinder pressure. A sensor was used to record the instantaneous speed, which was also able to track the crank angle in real time, and thus aid in providing a reference for other events in the engine cycle monitored by other sensors.

* The high exhaust gases temperature at the exit of the cylinder is a direct result of the combustion; and can help to detect problems such as fuel

starvation, clogged fuel injectors and exhaust valve leaks. However, the range of conditions affecting exhaust gas temperature implies that it would be very difficult to achieve an accurate diagnosis based only on these signals.

* The instantaneous load signal may also provide useful information about the contribution of an individual cylinder; and could also be used to detect combustion problems arising in individual cylinders as well as the drivetrain. In fact, the relationship between engine load and cylinder pressure is much closer, since the available torque is directly proportional to the engines acceleration. The measurement of instantaneous load was thus expected to provide a valuable measure for monitoring and diagnosis of problems in the combustion process at both individual and overall levels.

* Measurement of fuel consumption is one of the most important parameters in evaluating engine performance as well as indicating some of the faults in the fuel injection system. Sensors measuring the flow rate of fuel were found to be very expensive; however, measurement of the fuel lever position was considered an easy and cheap way of estimating fuel consumption.

* It was considered important to measure the inlet air, flow rate and temperature. These parameters represent the boundary conditions of the combustion process. Any change in inlet air condition directly affects the quality of the combustion process and may consequently reduce overall engine performance.

* Although coolant water temperature is not directly related to combustion in the cylinder, it is nevertheless useful to monitor any changes in this temperature, and could also be used as an indication of excessive heat release through the combustion process as well as indicating faults in the cooling system.

3.3.2 Measurement technique and sensors used.

3.3.2.1 Crankshaft speed

As the instantaneous crank speed signal contains useful information about the combustion process, a Hall effect proximity switch (Honeywell 1GT101DC) was selected to measure the instantaneous engine speed for its robustness and low cost. The flywheel, which has 108 gear teeth, was used to trigger the proximity switch.

The flywheel does not need to be magnetised as this switch includes an internal permanent magnet. The sensor has an NPN open collector output, acting as a fast switch, whose change of state depends on the change in distance between the flywheel tooth and the sensor, which has a signal frequency range of 0-100kHz. The position of the proximity sensor is shown in Figure 3.14, while Figure 3.15 shows the actual sensor mounted adjacent to the flywheel.

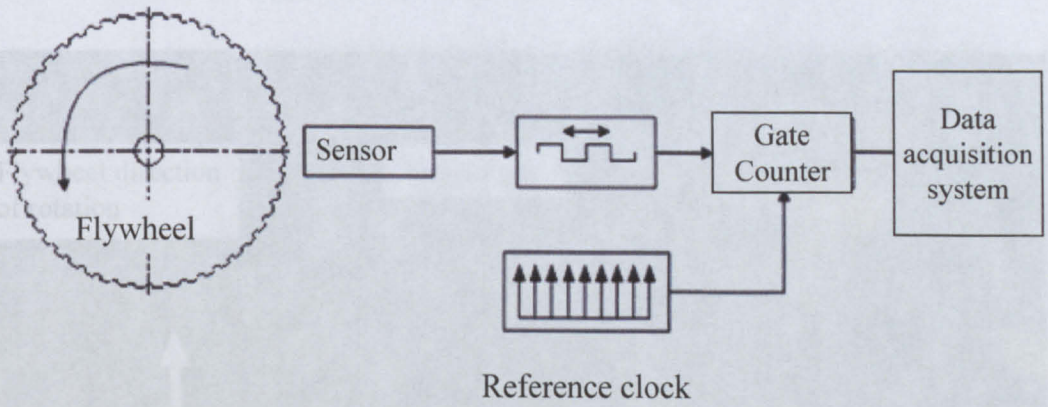

Figure 3.14 Instant speed sensor layout.

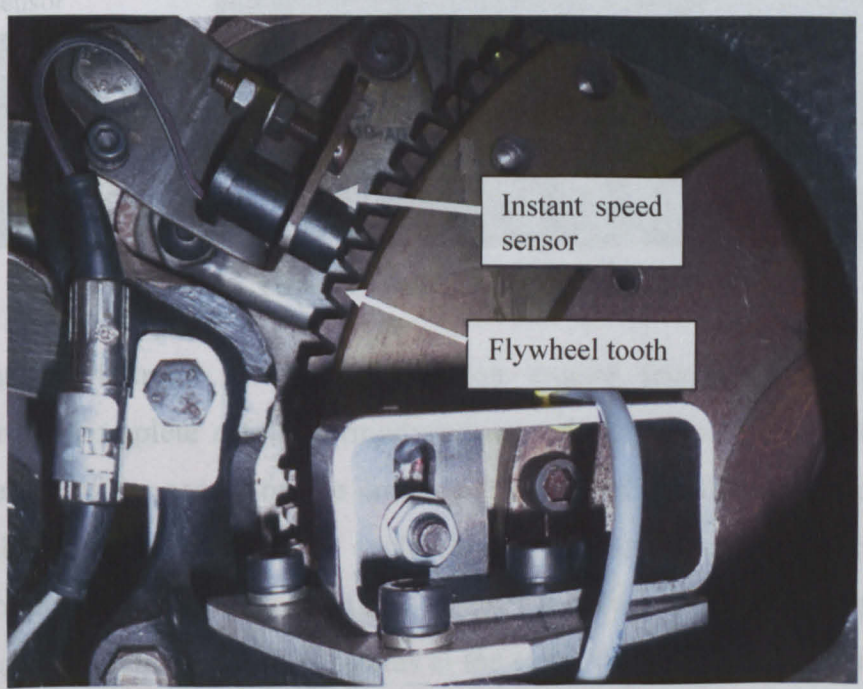

Figure 3.15 The instant speed sensor mounted to the engine.

Average crankshaft speed is also considered an important parameter in evaluating engine performance, and accordingly an optical proximity switch (Omron EE-

SX673) was selected to fulfil this function. Depending on the sensor mounting location, its output can identify the position of the crankshaft relative to any one of the four pistons. An existing threaded hole on the face of the flywheel was found to be in a suitable location relative to cylinder one TDC position. A modified bolt was fitted to trigger the sensor and a pin of equivalent mass (without trigger) was fitted diametrically opposite to maintain balance. Figure 3.16 shows the average speed sensor with the trigger pin passing through it.

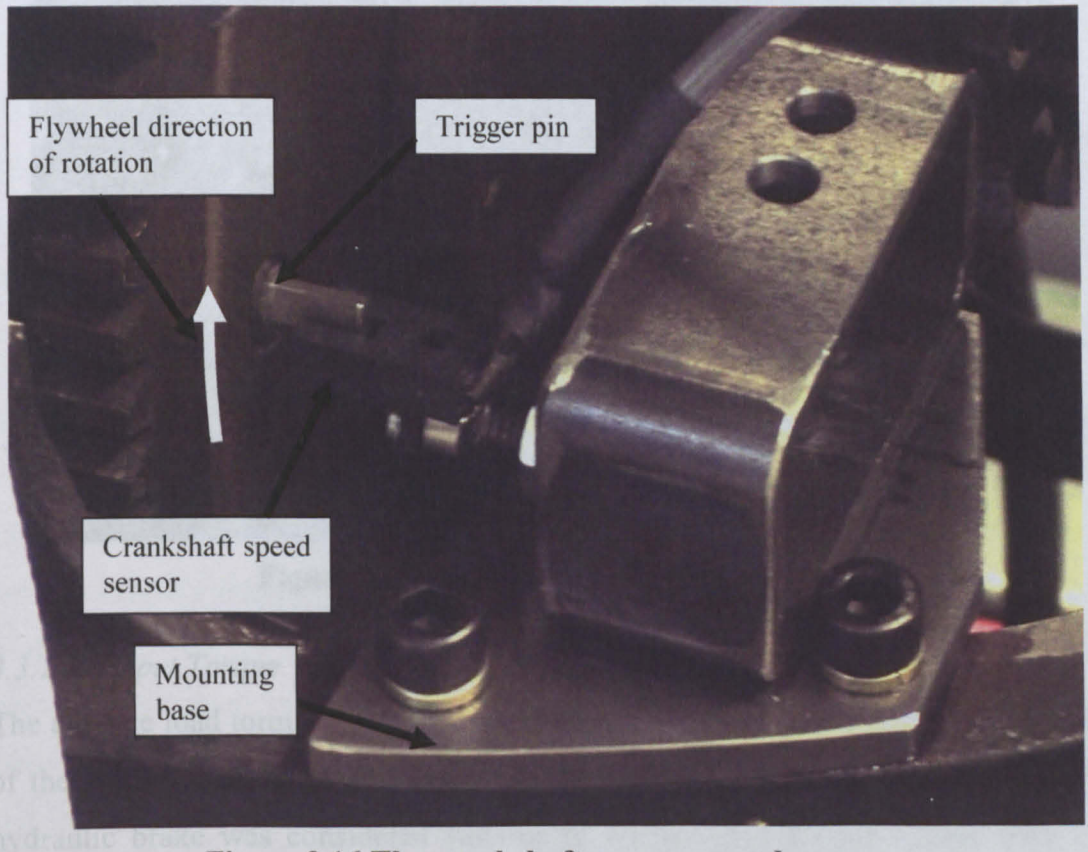

Figure 3.16 The crankshaft average speed sensor.

Given that a 4-stroke internal combustion engine requires two crankshaft revolutions to complete a full thermodynamic cycle, it is readily concluded that the utilisation of the sensor on the crankshaft will not be sufficient to identify in which half of the thermodynamic cycle the cylinder is at, hence, a second Hall effect proximity switch, placed axially against the fuel injection pump driving pulley, was installed. This pulley rotates at the same speed as the camshaft (which rotates at half the crankshaft speed). One of the four bolts fixing the fuel injection pump pulley was extended to provide one pulse per two crank revolutions and this signal was used to indicate the start of the complete thermodynamic cycle. Figure

3.17 shows the camshaft position sensor mounted on the rear pulley cover against the camshaft.

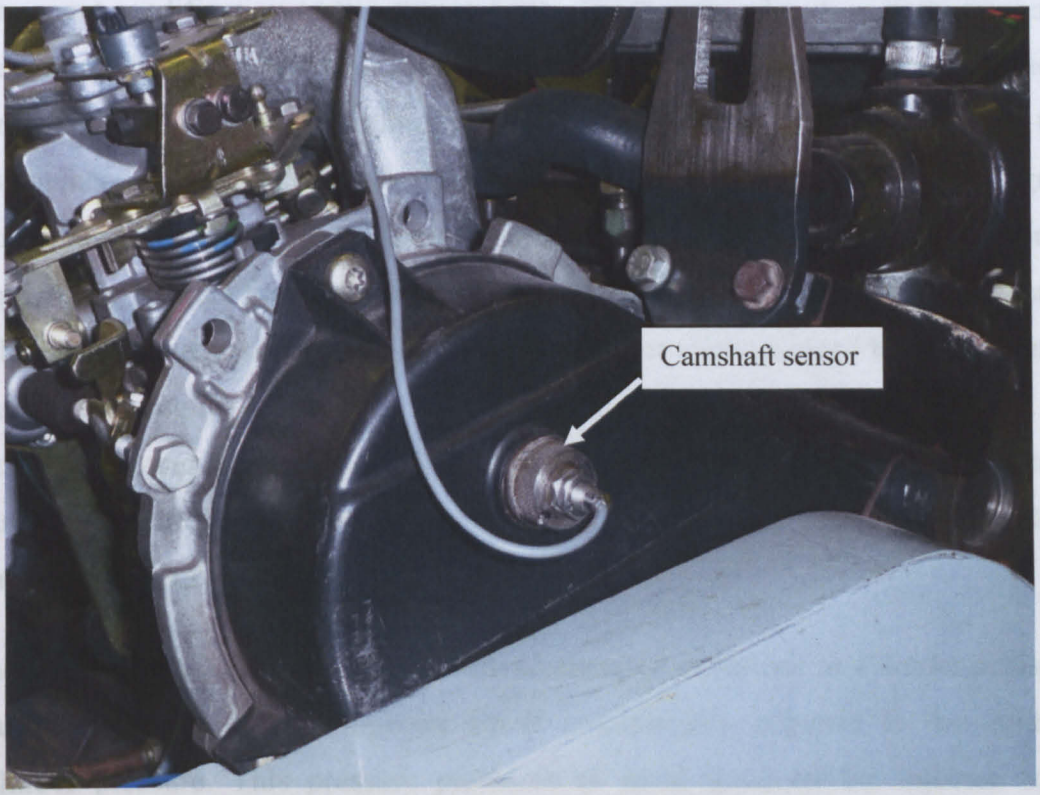

Figure 3.17 The camshaft position sensor.

3.3.2.2 Output Torque

The average load torque value is an essential parameter required for the evaluation of the engine's boundary operating conditions. The load cell integrated with the hydraulic brake was considered suitable to use for load measurements. This of course assumes that the friction load on the dynamometer is small in comparison to the load torque. A parallel connection to the load cell output was established for both the hydraulic brake control system and the engine data acquisition system. A description of the load cell has been given previously in section 3.2.2.2.

3.3.2.3 Cylinder pressure

Researchers, such as El-Ghamry et al., [2005] and Moro et al., [2002], have suggested that cylinder pressure is the most important parameter resulting from the combustion process and is therefore an important parameter in monitoring the efficiency of the combustion process. However, measuring cylinder pressure is not easy because of the difficult harsh environmental conditions that exist inside the

cylinder. This is especially so in a diesel engine where both pressures and temperatures are very high. As previously discussed the direct pressure sensing methods require a sensor fitted into the cylinder through a hole which will cause a permanent modification to the engine body. On the other hand, indirect methods seek a relationship between the cylinder pressure and some other physical parameter that can be measured non-intrusively on the engine, such as the instantaneous crankshaft speed. However, such methods require further signal processing to determine the cylinder pressure. Additional computational power is required for indirect measuring methods, which increases data processing time and reduces the accuracy of results. In addition, indirect methods need to be calibrated against the engine employing a direct measuring sensor. It was decided to establish another method that has the advantages of the direct method without intrusive modification to the engine in order to prevent any effects on the actual combustion process.

The feasibility of using the fuel injector to measure variations in cylinder pressure was explored, as the fuel injector tip is continuously exposed to the internal cylinder pressure. This pressure produces an axial force on the injector body which is rigidly fitted to the engine body and an axial strain will be induced in the body of the injector, and the resulting strain should be a measure of the cylinder pressure. However, the fuel injector is already subjected to the fuel pressure, delivered by the injection pump. This produces a circumferential (hoop) strain on the injector body. Measuring strains in both axial and circumferential directions could be a useful way of determining both the cylinder pressure and fuel pressure respectively. Figure 3.18 illustrates the engine fuel injector.

To obtain measurable axial and hoop strains, it was necessary to reduce the injector wall thickness, as shown in Figure 3.19. Calculations were undertaken to establish the minimum wall thickness, and based on the engine specification, Ford, [1998]. It was considered feasible to reduce the injector outer diameter from 9.5mm to 6.5mm without jeopardizing its integrity. Appendix C details the calculations used to determine the factor of safety. The analysis was based on maximum shear stress failure for thick wall pipes, Kutz, [1998].

Appropriate high temperature strain gauges were attached to the injector (Micro-Measurements WK-06-062AP-350) to form two half-bridges. Two gauges were attached axially and two circumferentially, so as to measure axial strain and hoop strain, respectively. Additional gauges were added to a steel sleeve to provide temperature compensation and configure them as full bridges.

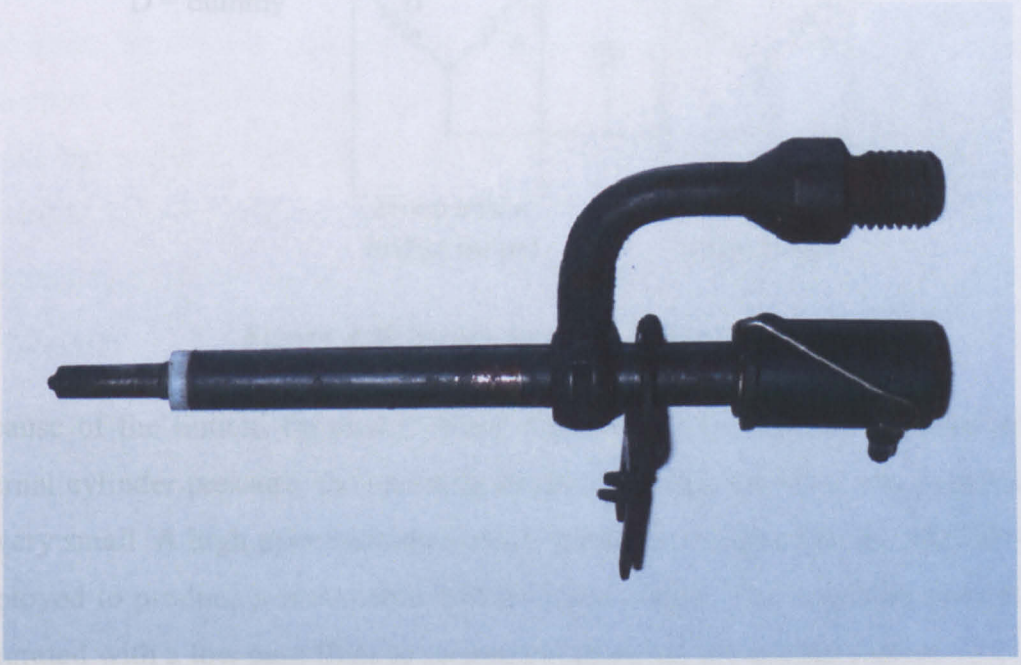

Figure 3.18 The conventional fuel injector.

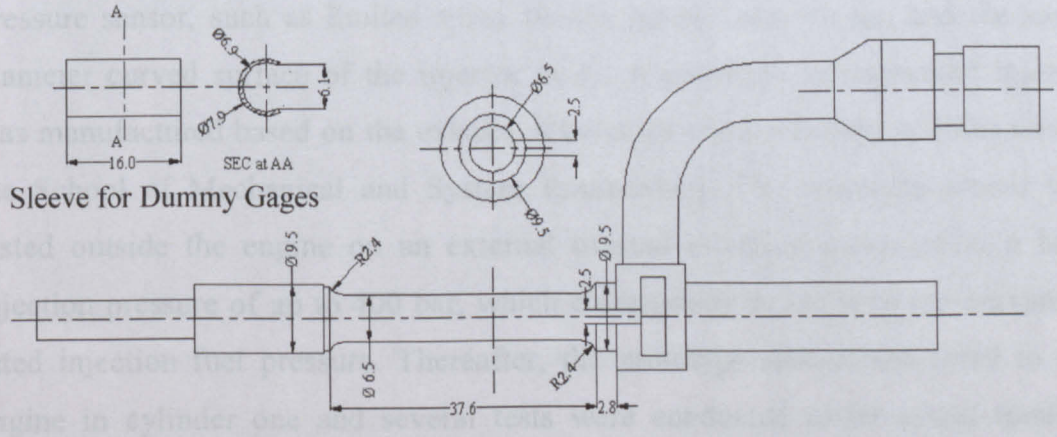

Figure 3.19 The modified fuel injector.

Each bridge contains two dummy gauges (D) that are mounted on the sleeve, as shown in Figure 3.19, which was wrapped around the injector body. The WK-06-062AP-350 strain gauge, with a 350Ω resistance, was selected as it can withstand

high temperature operating conditions, up to 450C (please refer to Appendix A for full specifications). The strain gauge configuration is shown in Figure 3.20.

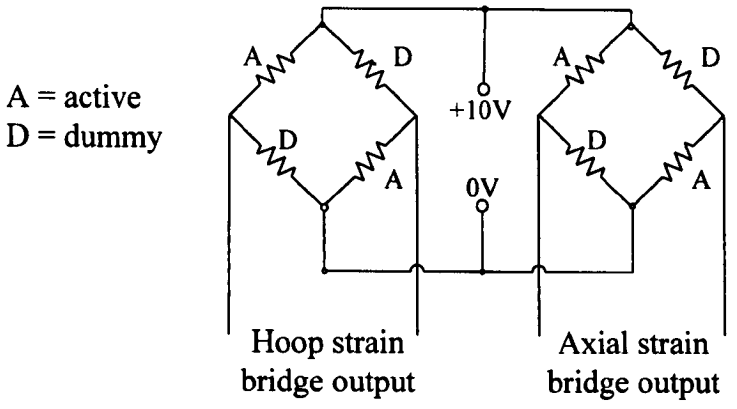

Figure 3.20 Strain gauge configuration

Because of the limited tip area (5.4mm diameter) of the injector exposed to the internal cylinder pressure, the resulting strain in the injector body was expected to be very small. A high gain instrumentation amplifier (Analog Device AD524) was employed to produce a reasonable voltage level output. The amplifier circuit was integrated with a low pass filter to reduce the effect of noise interference.

Many issues arose to challenge the design and implementation of this new cylinder pressure sensor, such as limited space for the gauges and wiring, and the small diameter curved surface of the injector body. A prototype instrumented injector was manufactured based on the existing laboratory and workshop facilities within the School of Mechanical and System Engineering. The prototype sensor was tested outside the engine on an external manual injection pump under a high injection pressure of up to 400 bar, which corresponds to 150% of the maximum rated injection fuel pressure. Thereafter, the prototype sensor was fitted to the engine in cylinder one and several tests were conducted under actual running conditions to evaluate its response. A digital storage scope was used to capture the output signal while using the laboratory linear power supply. The results indicate that a gain of 1000 was capable of reproducing the bridge output signal with a reasonable voltage level that meets the data acquisition card specifications with the minimum noise to signal ratio.

Details of the high accuracy precision differential amplifier IC and low pass filter circuit, specially designed for the strain gauge, are shown schematically in Appendix B. The amplifier unit was located as near as possible to the injector location and enclosed in a grounded metal box to provide a shield against noise. Further testing was conducted to evaluate the performance of the sensor prototype and amplifier circuit in capturing the cylinder pressure under different operating conditions. Whilst initial test results were very promising, unfortunately a fault developed on one of the bridges, and on inspection it proved very difficult to resolve the problem. After some considerable time and effort it was eventually decided to have the strain gauge bridge installed by a specialist company (Micro-Measurements) to the same specifications. Figure 3.21 illustrate the injector final design, currently incorporated in the engine.

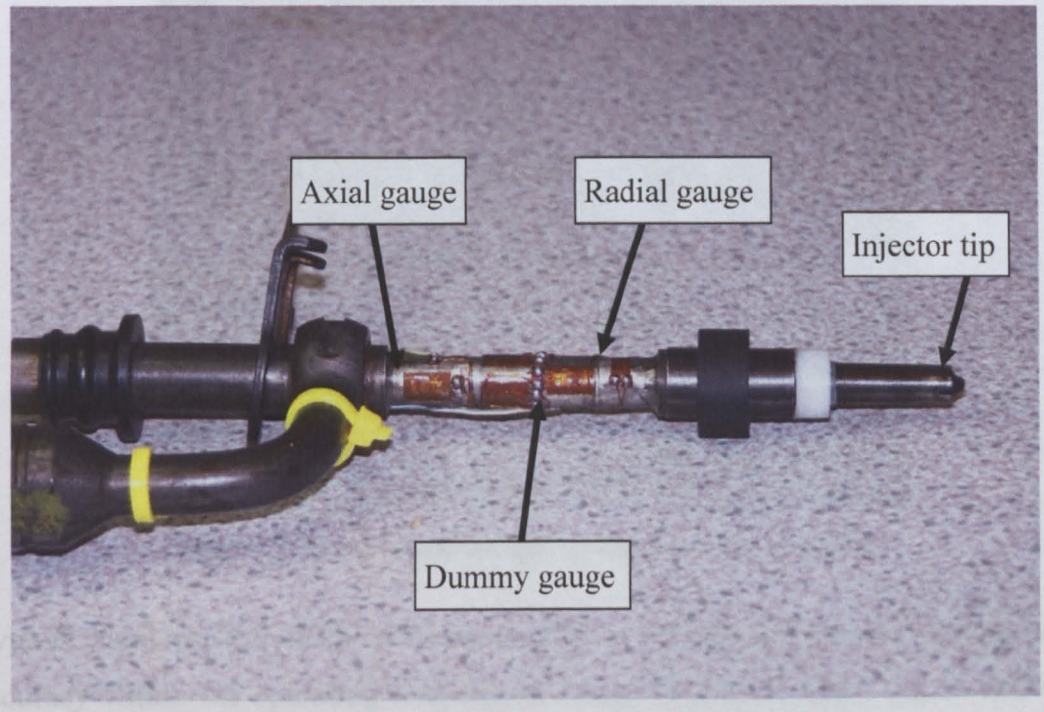

Figure 3.21 The modified injector with the strain gage.

3.3.2.4 Exhaust temperature

The temperature of the exhaust gas (at the exit of each cylinder) is a direct result of the combustion process, and it can indicate misfires and fuel starvation in the individual cylinders. Thermocouples Type-K were thus fitted to the exhaust manifold on each cylinder, mounted as close as possible to the outlet of each cylinder, as shown in Figure 3.22. A fifth thermocouple was also located in the exhaust pipe after the manifold in order to measure the overall exhaust gas

temperature. This last temperature thermocouple can be used to detect any malfunction in the exhaust manifold, such as holes and gasket leakages, which could affect the gas temperature.

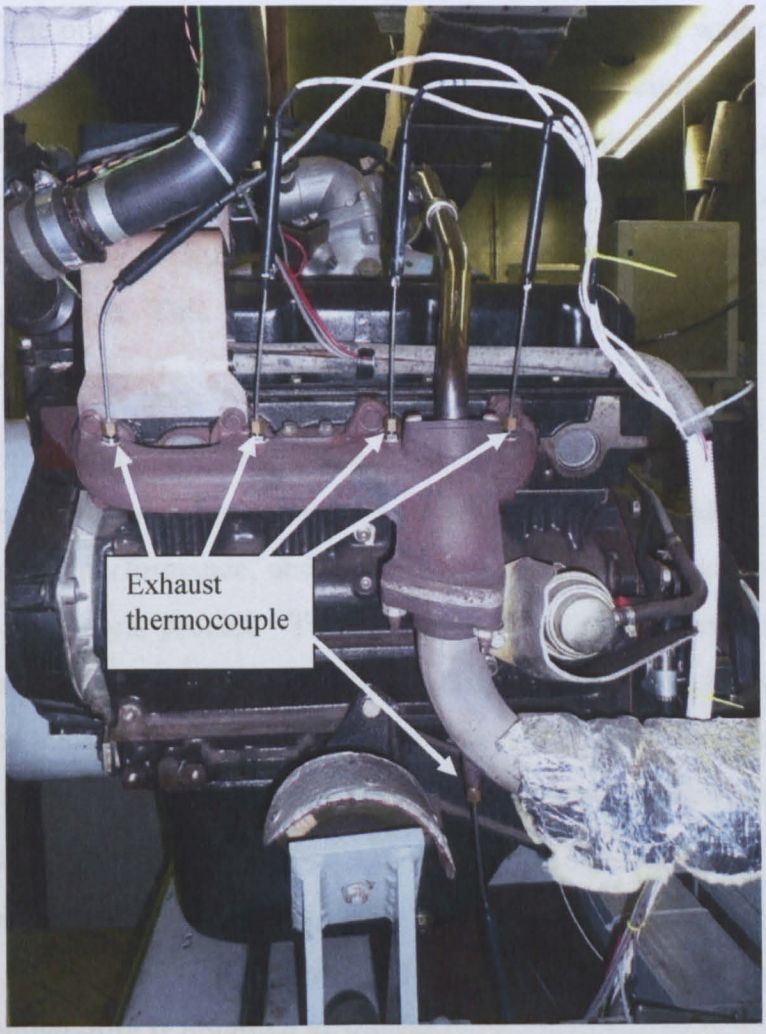

Figure 3.22 The exhaust gas thermocouple location.

Type-K stainless steel shielded thermocouples were selected because of their high accuracy within the operating temperature range of exhaust gases (up to 600°C). The output of the thermocouple sensor is usually a very low voltage signal (mV); so a high accuracy amplifier circuit was used to increase the gain of the signal to the data acquisition system with the minimum possible noise to signal ratio. The circuit, specially designed and implemented, comprises a precision differential amplifier (Analog Devices, AD595) with a low pass filter located before the amplifier to minimise noise. The designed circuit includes a separate amplifier for each thermocouple in order to increase measurement accuracy and avoid common

ground problem. This also overcomes the delay in readings when using a single differential amplifier with a multiplexer to switch between the thermocouples.

During calibration of the shielded thermocouple, a significant time delay was identified, of the order of 23 seconds when immersed in boiling water. To improve the response time, the covering metal shield at the thermocouple's tip was removed to directly exposing the measuring junction to the exhaust gas. The direct contact improved the response time of the thermocouple to <0.02 seconds to reach 100°C from room temperature (20°C). The response time was measured using a digital storage scope. This modification was applied to the four exhaust gas thermocouple sensors.

3.3.2.5 Inlet air flow rate and temperature

The flow rate and temperature of the inlet air are important boundary conditions in evaluating engine performance, and any changes in these parameters will directly affect the combustion process. To measure the inlet air flow rate, a Bosch automotive air flow meter (Bourns 8512) was integrated into the engine intake manifold. The sensor has a rotating vane connected to a potentiometer, and any change in air flow changes the potentiometer resistance, which is measured as a voltage signal via the data acquisition system. Figure 3.23 shows the Bosch sensor integrated with the engine inlet manifold. Based on the calibration information provided by Bosch, the relation between the air flow rate and the output voltage and the air temperature is obtained as follows:

$$Q_a = 12.4\times10^{-3}T_a(V_o/V_s) \qquad \text{for} V_o/V_s < 0.35 \tag{3-1}$$

or

$$Q_a = 261\times10^{-3}T_a(0.49-V_o/V_s) \qquad \text{for} V_o/V_s > 0.35 \tag{3-2}$$

where T_a is the inlet air temperature, V_o is the measured output voltage (also defined in the sensor circuit diagram provided in Appendix B), and V_s is the voltage supplied to the potentiometer, which is 5 V.

The potentiometer signal is passed through a low-pass filter to avoid aliasing in the signal conditioning stage. Tests were carried out while the engine was running

in a steady state condition to ensure that no fluctuation would occur on the output flow rate reading after the filter. The value of the cut-off frequency (2.5 Hz) was selected to compromise between minimising the AC components and the response time. Another consideration was to limit the value of the series resistance in the low pass filter in order to reduce the finite voltage drop across it since the A/D converter does not have infinite input impedance.

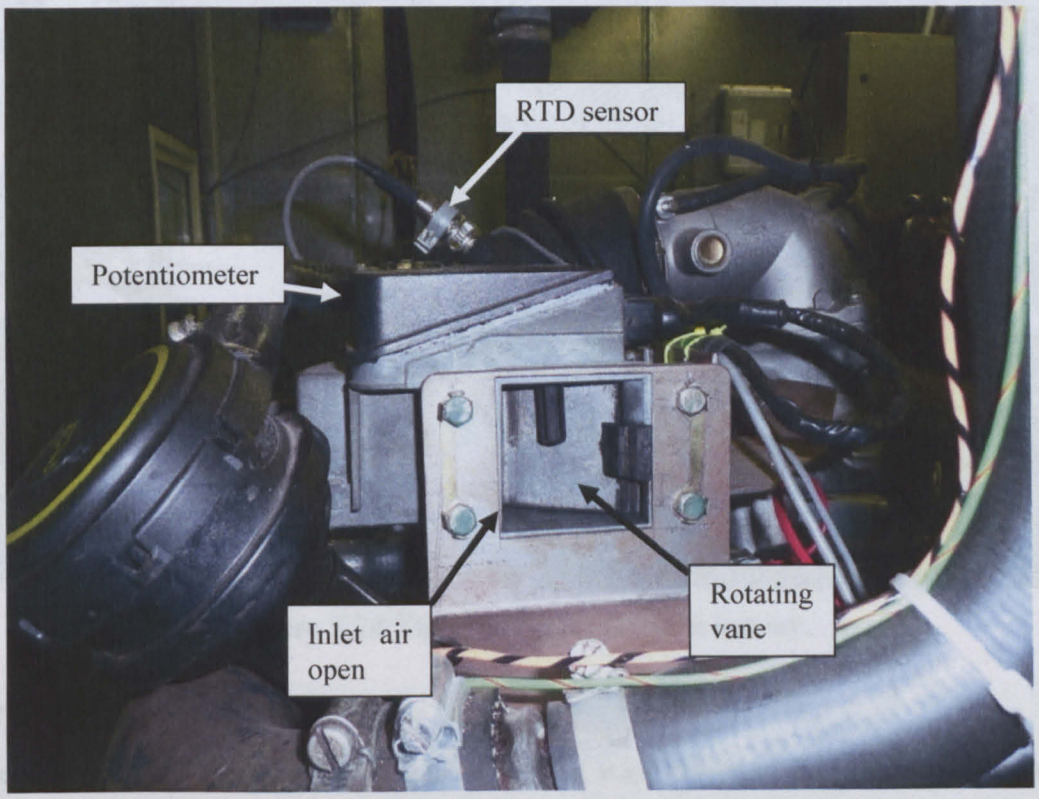

Figure 3.23 The inlet air flow rate and temperature sensor

The Bosch air flow meter also incorporates a thermistor temperature sensor which was connected to the data acquisition system; however in the event this was not used because the calibration data was unavailable. A specially-made probe using a PT100 RTD element was integrated into the air inlet manifold. A change in the air temperature changes the resistance of the RTD element which was then converted to a differential voltage, which was amplified in the signal conditioning stage using a differential amplifier, prior to capture by the data acquisition system. RTD element was selected for its fast response and appropriate measuring range. The RTD sensor was mounted in the air passage to the intake manifold just after the air flowmeter. Figure 3.24 shows the location of the RTD sensor. The detailed

schematic diagram of the designed circuit for inlet air measurements signal conditioning stage is shown in Appendix B.

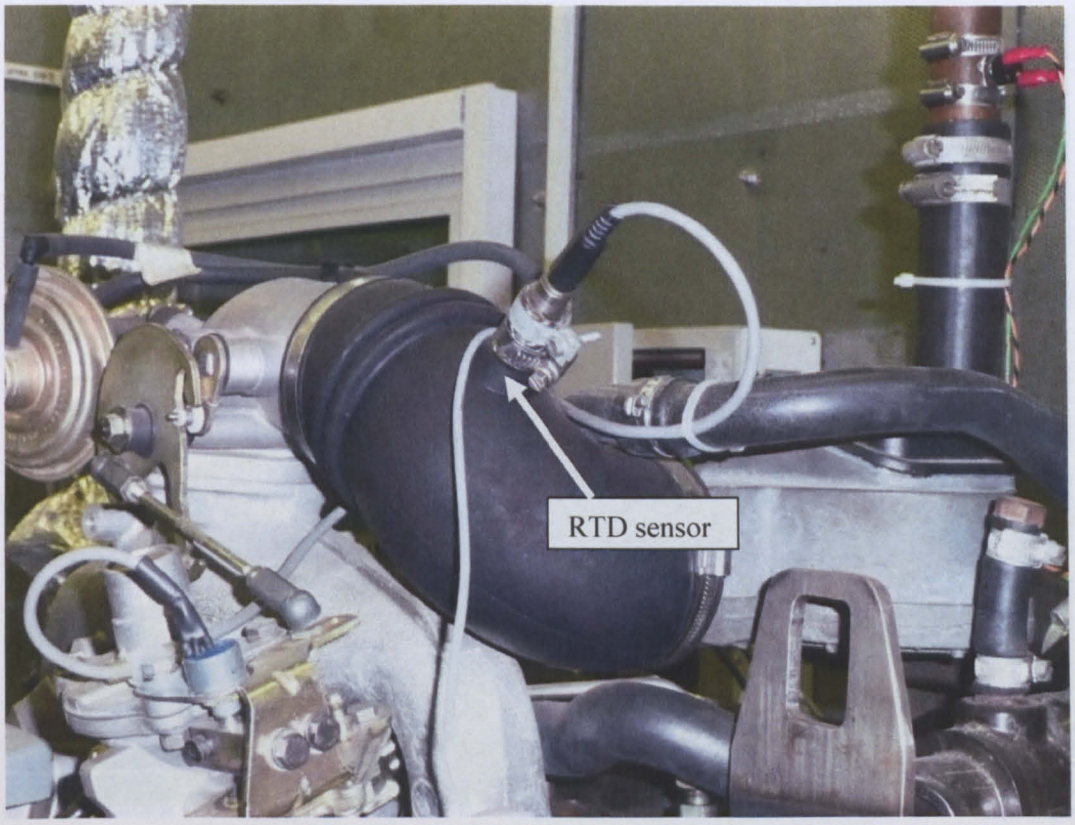

Figure 3.24 The RTD temperature sensor.

3.3.2.6 Fuel consumption flow rate

Fuel is normally supplied to the engine from a wall mounted fuel tank as shown in Figure 3.25. During steady state operation the tank valve is closed to allow the engine to draw the fuel from a 1.0 ml graded glass pipette. By timing a fixed volume of fuel consumed, the fuel consumption rate can be calculated. However, the fuel consumption can only be recorded manually before being processed for the condition monitoring and fault diagnosis algorithm evaluation of the diesel engine.

Alternatively, as the amount of the fuel injected into the engine only depends on the fuel injection pump lever position, measuring the fuel lever position can be considered as an estimation of the fuel consumption or delivered to the cylinder through the injector. An angular potentiometer was integrated on the fuel lever. This sensor only provides an approximate measure of the fuel injected where the governor automatically meters the amount of fuel depending on the average engine

speed at the same fuel lever position. Figure 3.26 shows the angular potentiometer mounted on the pump fuel lever mechanism.

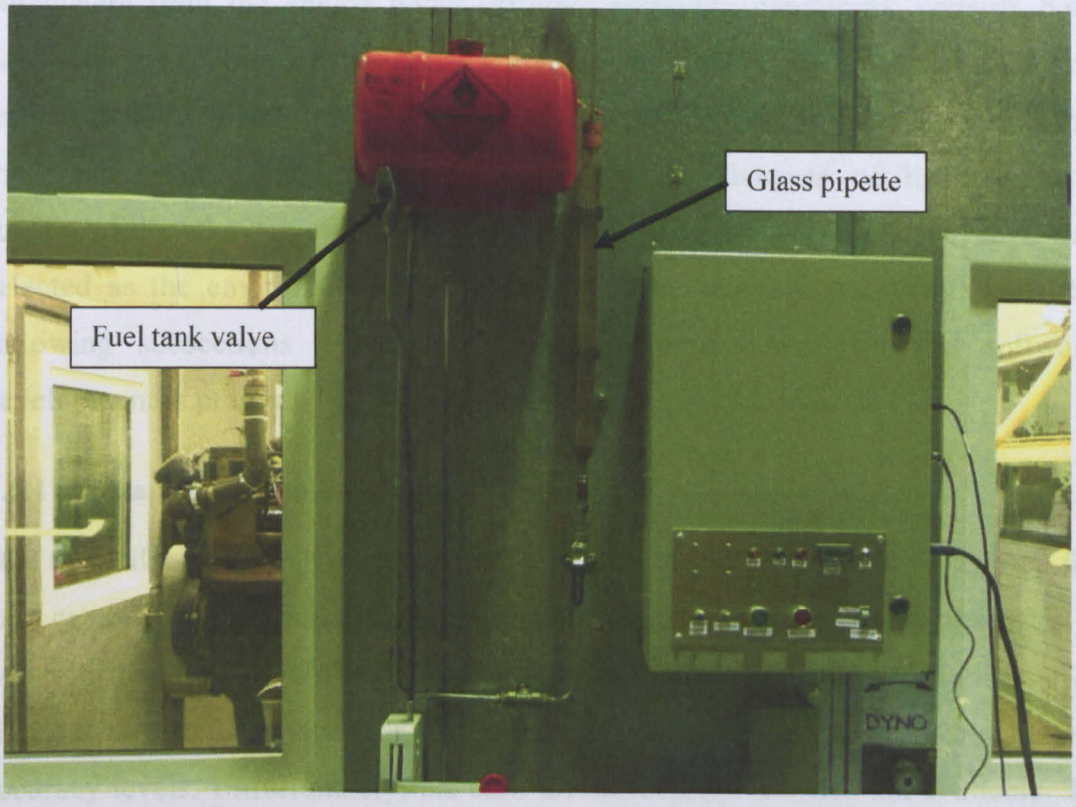

Figure 3.25 Fuel consumption measuring system.

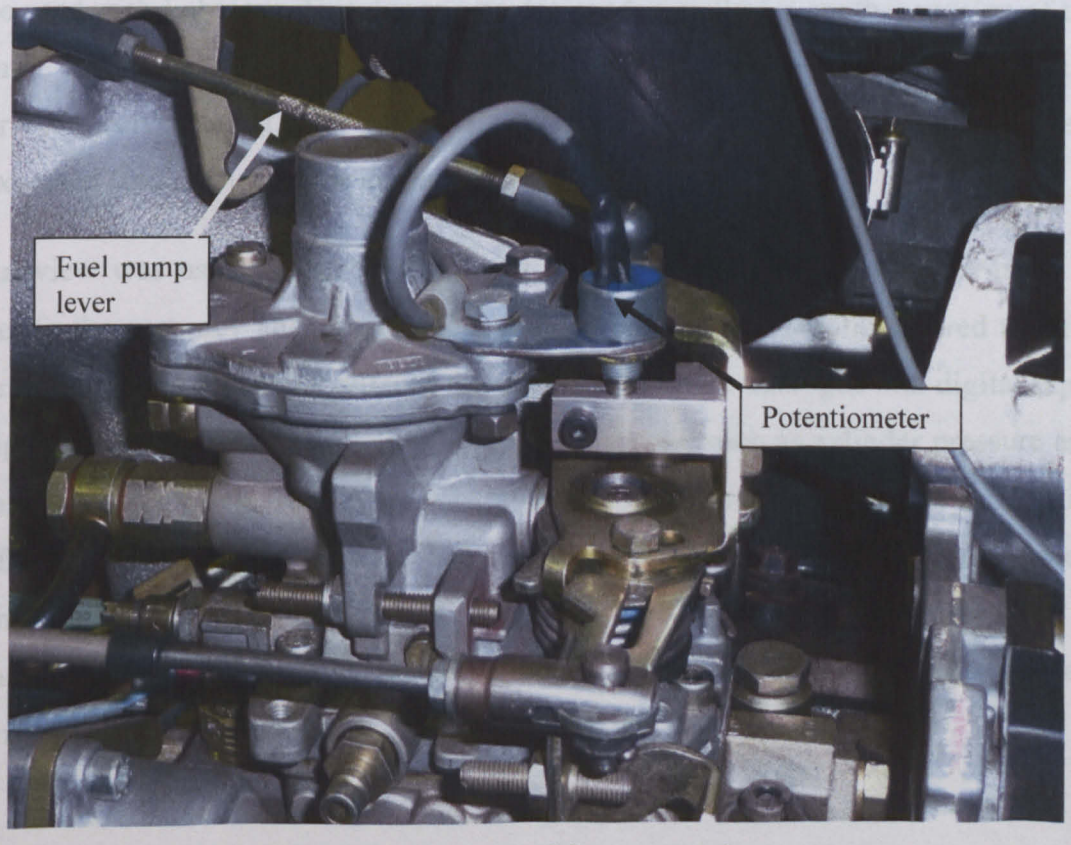

Figure 3.26 Fuel lever position measuring system.

3.4 DATA ACQUISITION SYSTEM

The data acquisition system, used to capture and record the experimental parameters from the engine under different operating conditions, consists both hardware and software. The hardware signal conditioning stage was designed and implemented to match the sensor outputs, the range of the signals measured and the input level of the data acquisition system. Because of its reliability, functionality and availability, NI's Labview graphical programming language was selected as the environment to construct the data acquisition algorithm. In the following subsections a detailed discussion of the hardware and software development is presented to show the selection criteria for each.

3.4.1 Data acquisition hardware

Due to availability, the Advantech PCL-818HG data acquisition card was used for data capture. The technical specification of this card is given in Appendix A. It was considered suitable for the engine data collection according to the range of signal characteristics such as sampling rate, number of input channels and accuracy levels. Unfortunately, the card driver for Labview was not available. To overcome this problem, a compatible driver was supplied by the manufacturer to be used with Labview. This driver was designed initially for another version of the same card series. Hence, it was decided to start a group of primary tests for the driver received using a laboratory signal generator which simulated the different expected frequencies of the engine output signals.

Labview was used to capture the input signals and compared with the input to verify the accuracy and capability of the card driver. The results showed that the driver supplied was only suitable for use with the slow analogue and digital input signals, and could not handle the high speed signals, such as cylinder pressure and instantaneous speed. The driver was proprietary code and there was no possibility of modifying it to deal with the fast signals. In the event, it was decided to select another data acquisition card that satisfied the requirements and specifications of the signals measured and which had the capability to work in a Labview environment.

The signals measured were classified into three different groups. The first group consisted of fast analoge signals (cylinder pressure and instantaneous load), while the second included the slow analoge input signals (exhaust gas temperature, coolant water temperature, inlet air flow and fuel lever position). The last group contained digital signals frequency measurements used to measure both the instantaneous and average speeds of the crankshaft. According to this classification, the data acquisition card selected should have a multi-sampling rate in order to be able to acquire all of the measured signals. Cards with this facility were found to be very expensive; therefore, another solution at reasonable cost was needed. Hence, two separate data acquisition cards were used, one for the fast signals and the other for the slow signals. The cards needed least two counters in order to measure the frequency of the digital signals. The compatibility of the cards with Labview was another restriction that had to be taken into account. The NI-6250-PCI and NI-6210-USB cards were selected.

The NI-6250-PCI internal data acquisition card was selected for the fast analogue signals. It has a high sampling rate of 1.2 MS/s with a 16 bit A/D converter and has two digital counters with a maximum clock speed of 80 MHz at 32 bit resolution which is particularly suitable for the high speed data capture. The technical specification is given in Appendix A. The card was internally fitted in the host desktop computer and connected to the engine through a SHC68-68-EPM shielded cable. A CB-68LP-unshielded wiring board was connected to the cable which was used to connect the different input signals to the selected channels. The card, cable and wiring board are shown in Figure 3.27.

The A/D converter in the NI-6250-PCI card was used for the measurement of the pressure signals coming from the injector; cylinder pressure and fuel pressure, which were connected to channels 1 and 2 respectively. The load cell sensor output used to measure the brake load torque was connected to channel 3 while channel 4 was used to acquire the signal from the camshaft sensor used to indicate the start of the thermodynamic cycle. All four channels were acquired at a rate of 10 kHz, the continuous reading mode was selected for data acquisition and 1000 points were captured each time the loop was executed. The sampling rate was calculated, based on the assumption that at an engine speed of 4000 RPM, the data

acquisition system has the ability to capture at least 50 points through the pressure pulse time. On the other hand, as the rate of variation in the load cell signal is slow in comparison to that of the injector pressure signal, each 10 points of data acquired from the load cell were averaged and represented by only one point in the recorded output data. The remainder of the signals were acquired without any compression in order to get an optimal representation of the signal captured.

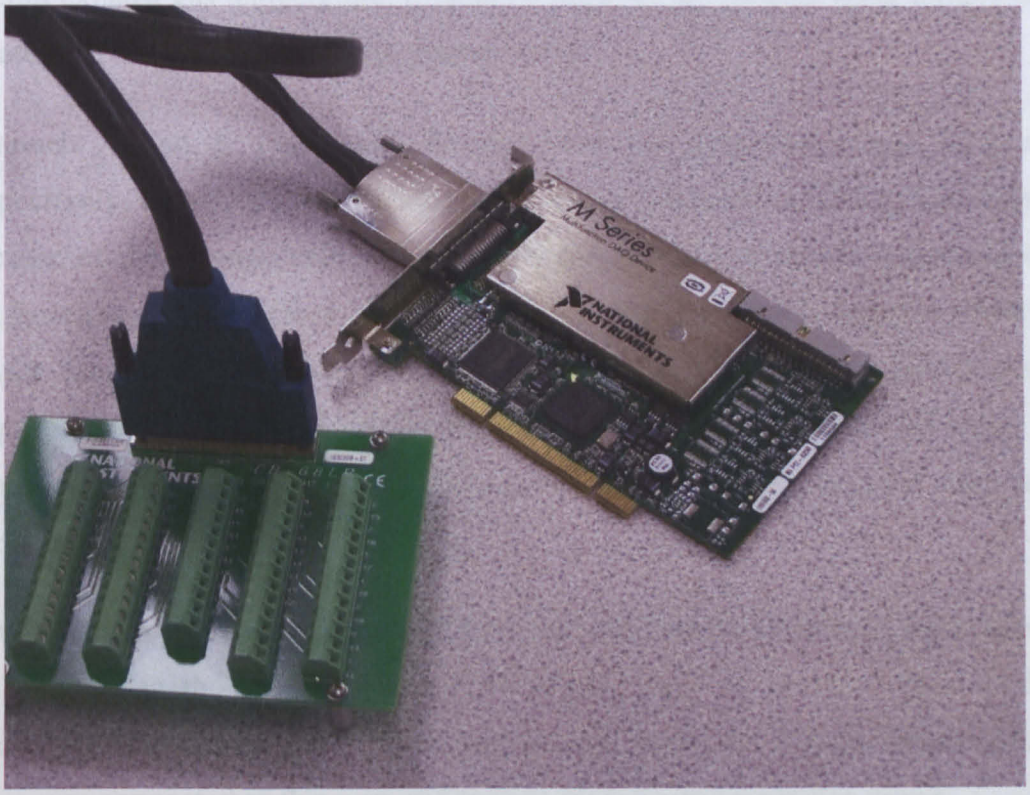

Figure 3.27 The data acquisition card and its accessories.

As the instantaneous speed signal is very important and holds much embedded information, it is very important to capture this signal with the highest possible accuracy and resolution. Counters 1 and 2 were used in series together to increase the resolution of the acquired signal. In this configuration, counter 2 was used to divide each pulse of counter 1 by the divisor value which is controlled through software. The frequency of any two repeated pulses was measured by measuring the time between the consecutive rising edges of the flywheel speed sensor signal. One crankshaft revolution is completed after each 108 readings, which corresponds to the number of teeth on the flywheel.

The NI-6210-USB external data acquisition card was used for acquiring the low rate analogue signals. This card has a 250 kS/s sampling rate with a 16 bit A/D

converter and two digital counters with a maximum clock of 80 MHz of 32 bit resolution. The card uses a USB connector to the desktop computer and is connected directly to the measured signals after the signal conditioning circuit. The analogue input channels from 1 to 6 were connected to the thermocouple amplifier outputs to acquire the temperature readings. Channels 1 to 4 measured the individual cylinder exhaust gas temperatures, while channel 5 was for the overall exhaust gas temperature. Channel 6 acquires the coolant water temperature locate after the cooling water circulation valve.

Channels 7 and 8 were used for the inlet air temperature and flow rate respectively. However the air temperature was not determined using this channel because of the missing calibration relationship for the thermistor integrated into the Bosch sensor. Therefore, channel 9 was used to capture the output of the RTD sensor used to measure the inlet air temperature. The fuel lever position was acquired using channel 10. All analogue input channels were captured using the continuous mode at a rate of 1 kHz with 100 sampling points for each loop executed.

Counter 2 was clocked by an 80 MHz internal clock and was enabled to decrement its value when the gate (GAT) port was high. This configuration was used to accurately time the frequency of the rising pulse on the GAT port. The crankshaft pulse was connected to this port and used to record average engine speed.

3.4.2 Signal conditioning

Each of the sensors used required a regulated power supply as well as signal conditioning for the output signal before connecting to the data acquisition cards to be recorded. The conditioning depends on the dynamic nature and level of the signal measured and the input range of the channel used in the acquisition card. Some of the signals measured required active filter and amplification or attenuation. The signal conditioning stage was divided into three circuit cards; two were mounted in a metal enclosure adjacent to the engine cell and the other as near as possible to the fuel injector.

The fuel injector signal conditioning board was designed to accommodate the signal amplifier of the fuel injector strain gauge. As this amplifier needed a high

gain (1000), the board was mounted on the engine block as near as possible to the injector location to reduce the effect of noise interference and signal loss due to long wires. The other two signal processing cards handled all of the other signals measured. One card supported the air flowmeter, air thermistor, RTD, and fuel lever position signals. In this card, a separate low pass filter and amplifier were used for all of the signals measured. The second card incorporates a single precision differential amplifier for each thermocouple to remove the possibility of common ground error that usually occurs when using a multiplexer with only one amplifier to amplify all thermocouples outputs. The detailed schematic diagrams of these cards are shown in Appendix B.

The metal enclosure containing the last two signal conditioning cards was used to accommodate other peripherals for the engine testing system. Figure 3.28 shows the enclosure containing the USB data acquisition card, the wiring board for the other card, and the two signal conditioning cards. The door of the enclosure was used to mount the control panel for the engine, as shown in Figure 3.29. The panel contains main switch isolation, fuel valve control button to open the fuel valve before starting the engine, push button to start the engine, and finally a shutdown button that disconnects the fuel valve solenoid to close the fuel flow and consequently stop the engine.

In addition, for the purpose of visualization, the panel was integrated with a digital display that shows the average speed of the engine. Some indicator lights were included in the panel for the safe operation of the engine, such as oil warning, cooling fan, and fuel valve indicators. Moreover, the panel contains a manual control button to switch on the radiator cooling fan, in case of any malfunction in the automatic fan switch. The detailed schematic diagram of the panel circuit is included in Appendix B.

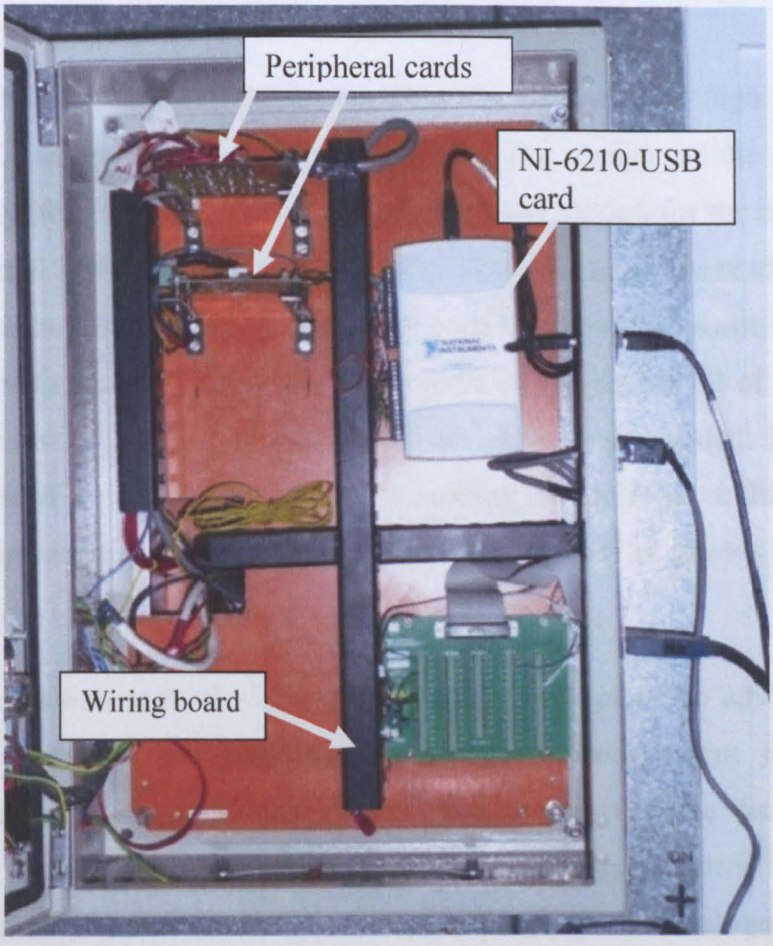

Figure 3.28 Data acquisition and signal conditioning metal enclosure

Figure 3.29 The engine control panel

3.4.3 Data acquisition code

Labview software (National Instruments) has the advantage of high functionality and ease of use for data acquisition systems. The design of the code passed through many iterations to evaluate the most suitable design for the capture of the data. The initial code had a single while loop that contained the read order of the different signals. The testing of this configuration identified some delay in the acquisition of fast signals because the program had to finish all of the different reads for the rest of the slow signals before the while loop repeated. The code was modified to have a separate loop for each reading task to remove this delay from the recording measurements. The Labview code used is shown in detail in Appendix B.

The data acquisition code design was configured to exploit the advantage of the parallel execution of the graphical programming environment that Labview supports. The code had four independent parallel passes of the data processing, where each has its own sampling rate. The first pass acquires the analogue channels of the 6250-PCI card while the second acquires the analogue channels of the 6210-USB card. The two other passes execute the digital measurements of instantaneous speed and average crankshaft speed using the counters of 6250-PCI and 6210-USB cards respectively. The flowchart of the code designed for data acquisition is shown in Figure 3.30.

For the benefit of testing throughout this investigation, a user interface for the measured signals was developed, as shown in Figure 3.31. This interface was used to provide the user detailed information about the values of all signals measured and to enable the starting and stopping of data recording of the engine data acquired. This is controlled through the data storage buttons, where each button corresponds to one of the data groups inside the code (see the detailed code in Appendix B).

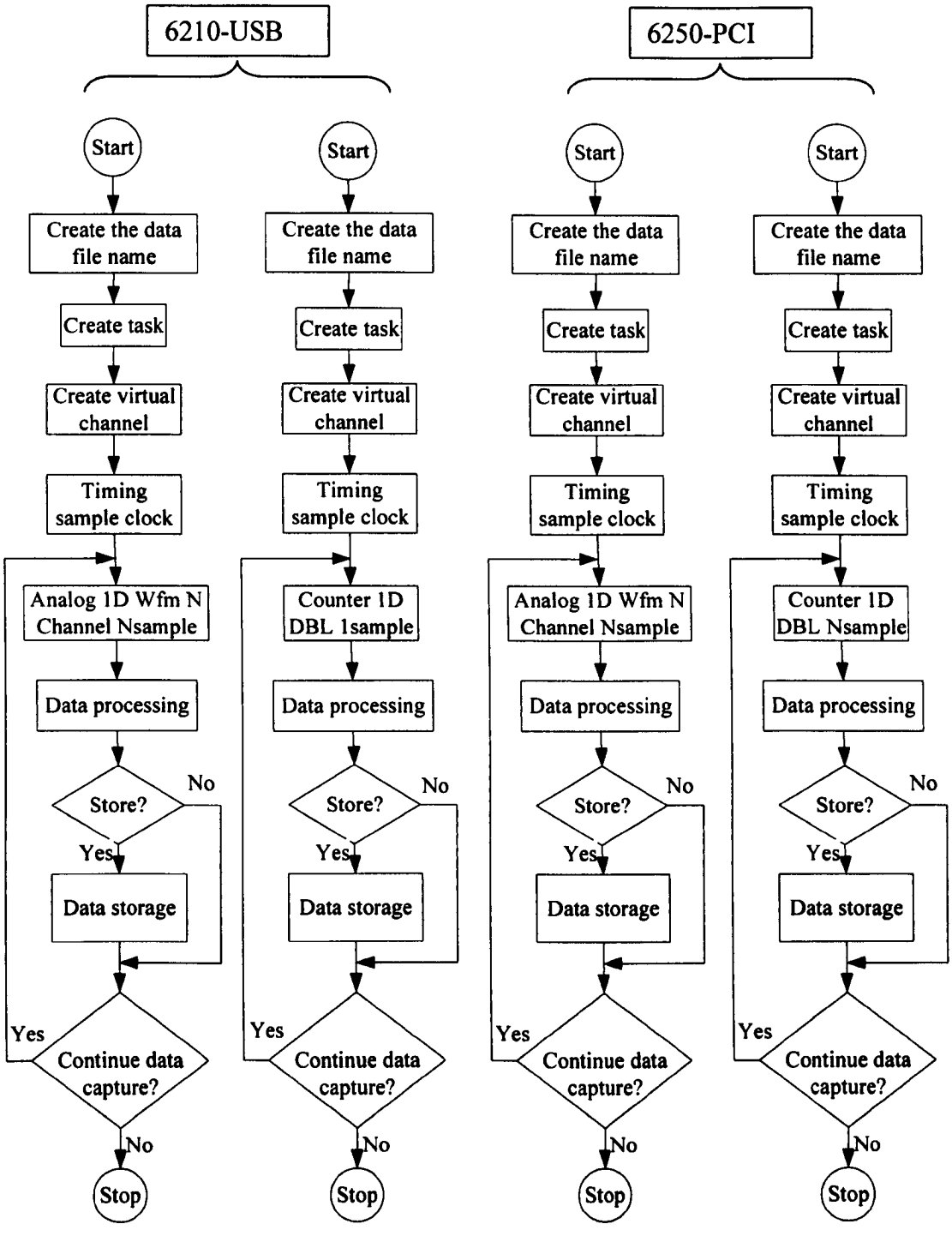

Figure 3.30 Data acquisition code flowchart.

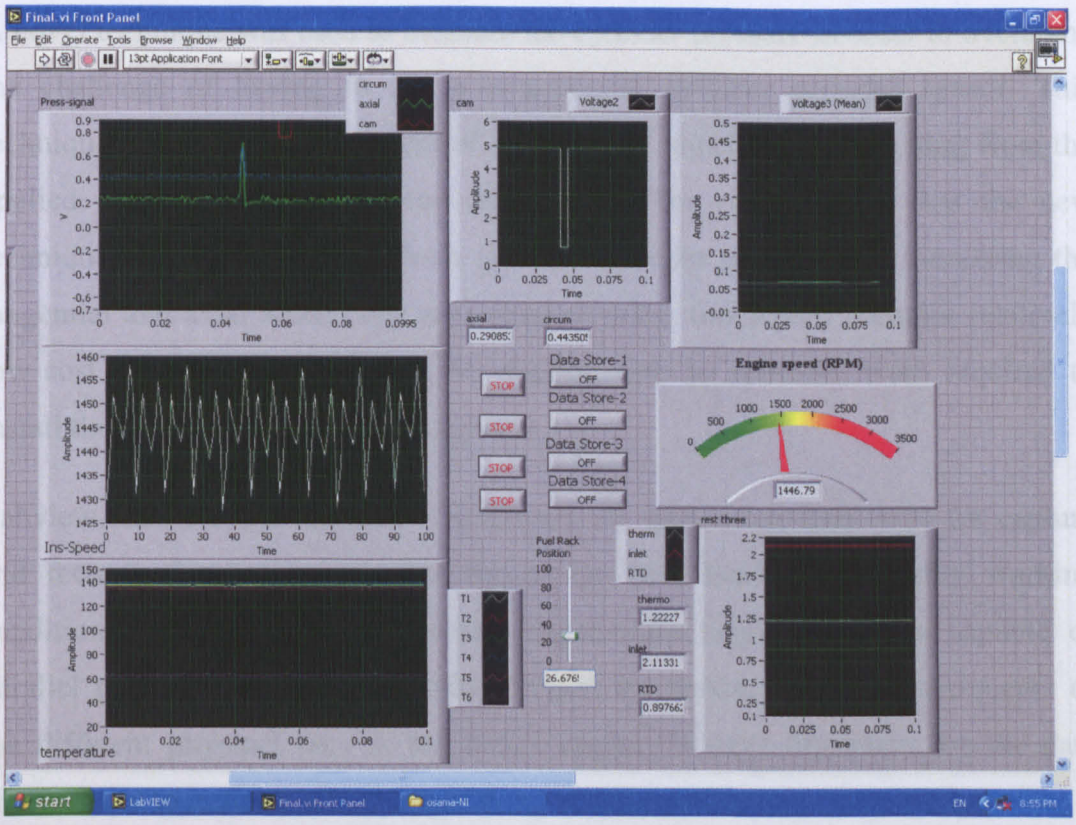

Figure 3.31 The Labview interface screen

3.5 SUMMARY

This chapter provides the reader with a detailed description of the test facility. The context was divided into two sections, firstly, the modifications of the conventional manually driven hydraulic brake into an automatic controlled unit was covered. All the integrated sensors and the required modifications are included. The designed and implemented control system included both automatic programmable mode and steady state control mode to extend the facility of the control system for both static and dynamic loading. Only the static loading mode was used within the present study where the engine was testing under steady state operating condition.

The second section focuses on the diesel engine data acquisition system. The sensor integration as well as required electronic signal conditioning circuit were discussed in detail showing the different criteria used in the design and implementation process. According to the natural of measured physical parameters, two data acquisition cards were used to capture the experimental data of the diesel engine under both healthy and faulty conditions.

A novel technique was used to measure the cylinder pressure in order to overcome the challenge of having to use a commercial cylinder pressure sensor. This technique utilise the measurement of strain in the injector body resulting from the applied cylinder pressure on the injector tip. The results show that the new technique successfully detects both fuel and cylinder pressures by measuring the tangential and axial strain. The advantage of using this sensor includes relatively low cost and easy integration to the engine, with no intrusive work required to install the sensor on commercial engines.

Labview software was utilized to construct the data acquisition code for capture and record of experimental data results for both healthy and faulty working conditions. Labview is a graphical programming language that is capable of parallel programming which is critical point for instantaneous measurements of the different physical data in the diesel engine, is very important for the data analysis and to indicate any changes in the engine performance accurately.

CHAPTER 4

EXPERIMENTAL RESULTS

This chapter presents the results of the diesel engine experimental tests using the constructed data acquisition system and test facilities. The different parameters are discussed and analysed in detail, evaluating their relation to the engine condition as well as the possibility of their use in the CMFD system. The tests were initially performed under 'healthy' conditions, then several synthetic faults were introduced in the engine and the tests repeated at the same operating conditions. To evaluate the engine performance a full mapping of the engine physical parameters was carried out under different operating conditions.

Brake output power and fuel lever position were selected as the mapping coordinates for the engine performance evaluation. As the engine torque is controlled by the hydraulic brake, several different brake torques were selected at each test condition. The fuel lever position (FLP) was changed from idle FLP to the maximum FLP through eight different positions. The idle FLP was adjusted to equal 10% of the maximum FLP; therefore, the engine performance evaluation was undertaken at eight fuel lever positions between 10% to 100%.

Testing was undertaken on the engine under healthy condition to provide the nominal base data for the 'ideal' engine operating condition. As this study mainly focused on establishing faults in the combustion process, fuel and inlet air faults were deliberately introduced in the engine. The fuel fault was simulated by introducing a needle valve in the fuel pipe between the fuel pump and the injector to cylinder 4 of the engine, to reduce the fuel flow in a controllable manner. The inlet air fault to all cylinders was simulated by partially closing the inlet intake. The results were analysed in comparison to the healthy engine data.

In the following sections, the results of the measured parameters will be discussed with respect to the changes in the engine condition and/or the other engine parameters. The understanding of the relationships between the measured parameter and engine condition represent the data from which to evaluate the

Intelligent Engine Condition Monitoring (IECM) algorithm which will be discussed in Chapter 6.

4.1 HEALTHY ENGINE DATA

4.1.1 Instant speed

Instantaneous engine speed provides an excellent indication of the engine condition particularly in identifying faults related specifically to the combustion process and the contribution of individual cylinders. This signal can also provide information about the state of the engine dynamics, cylinder pressure, and fuel burning quality. The fluctuation in crankshaft speed was measured by timing the interval between each tooth on the flywheel. Figure 4.1 illustrates an example of the crank speed variation. The cylinder firing process is clearly indicated by the two peaks per crankshaft revolution for a 4-cylinder 4-stroke. The intermediate troughs between decelerations are a result of the work done in the other cylinders to perform the other strokes i.e. suction of air from intake manifold, fresh air compression and scavenging the exhaust gases out of the cylinder to the exhaust manifold.

An increase in the applied load (at the same FLP), causes the average engine speed to decrease as expected, while the instantaneous speed fluctuation actually increases, as shown in Figure 4.2. This increase in fluctuation can be explained by the decreased ratio between the applied load and stored energy of the flywheel that is recovered within the "no power" period to smooth the crank speed variation. The flywheel inertia is not sufficient to overcome a high brake load and yet continue to rotate the engine smoothly. This results in a rapid deceleration after the end of the power generation stroke, which continues until the next cylinder fires converting more energy to accelerate the engine again.

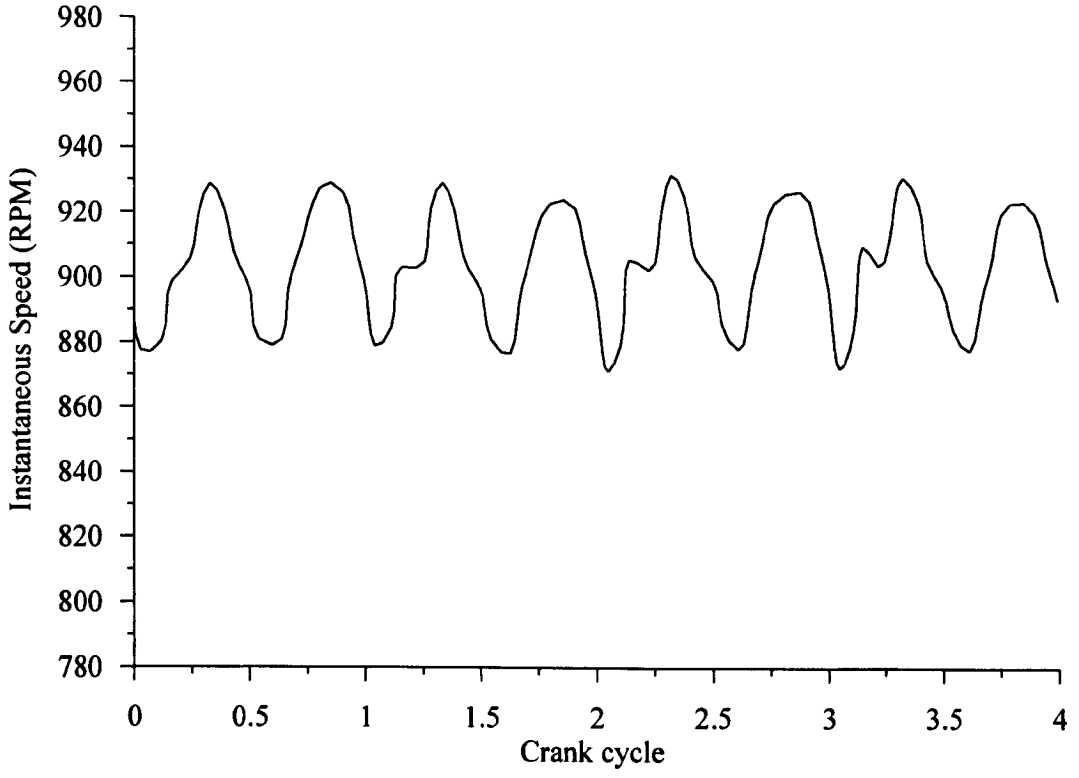

Figure 4.1 Instantaneous speed variation at (15% FLP) - load torque 30 Nm.

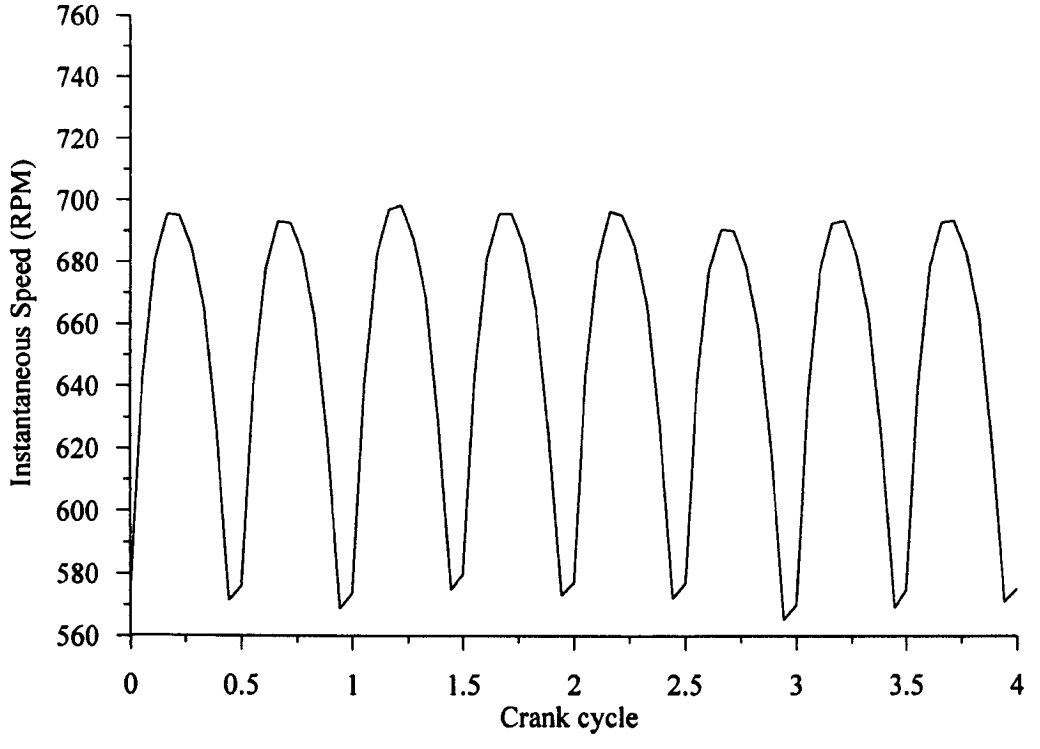

Figure 4.2 Instantaneous speed variation at (15% FLP) - load torque 119 Nm.

The relationship between the instantaneous crankshaft speed and the applied load over a range of different loads has been established. Figure 4.3 shows a sample of two results at fuel lever position of 45%, with applied brake load torque of 13 Nm to 124 Nm. Additional results covering different conditions are given in Appendix D.

It was observed under some operating conditions that the pattern of fluctuation in instantaneous speed was somewhat different as shown in Figure 4.4. At the load condition for Figure 4.4 (a) the crest is much flatter than that of Figure 4.4 (b), where the load torque is much higher. The interpretation is that the stored energy in the flywheel is being dissipated much faster under higher load, thus emphasizing the change in engine load during all four engine strokes.

A comparison with previous experimental measurements, by Leonhardt et al., [1995], of instantaneous speed for a four stroke, 4- cylinder diesel engine obtained from 120 readings per crank cycle, as shown in Figure 4.5, indicates a similar speed fluctuation. The authors suggest that the high speed fluctuation at the peak resulting from the high resolution of the incremental optical speed sensor used. Misfire detection was the main objective of the study, where it was recommended to use the fluctuation in speed between peak and valley as a simple method of detection. Another study, by Sood et al., [1983], utilized a 138 teeth flywheel to experimentally measure the time interval between the flywheel gear teeth of a 6-cylinder in-line 4-stroke diesel engine, which is the inverse of the instantaneous speed. The results shown in Figure 4.6 show the fluctuation in the experimental measurements at high speed (the minimum time). In this study, the measurement fluctuation was found throughout the measuring range.

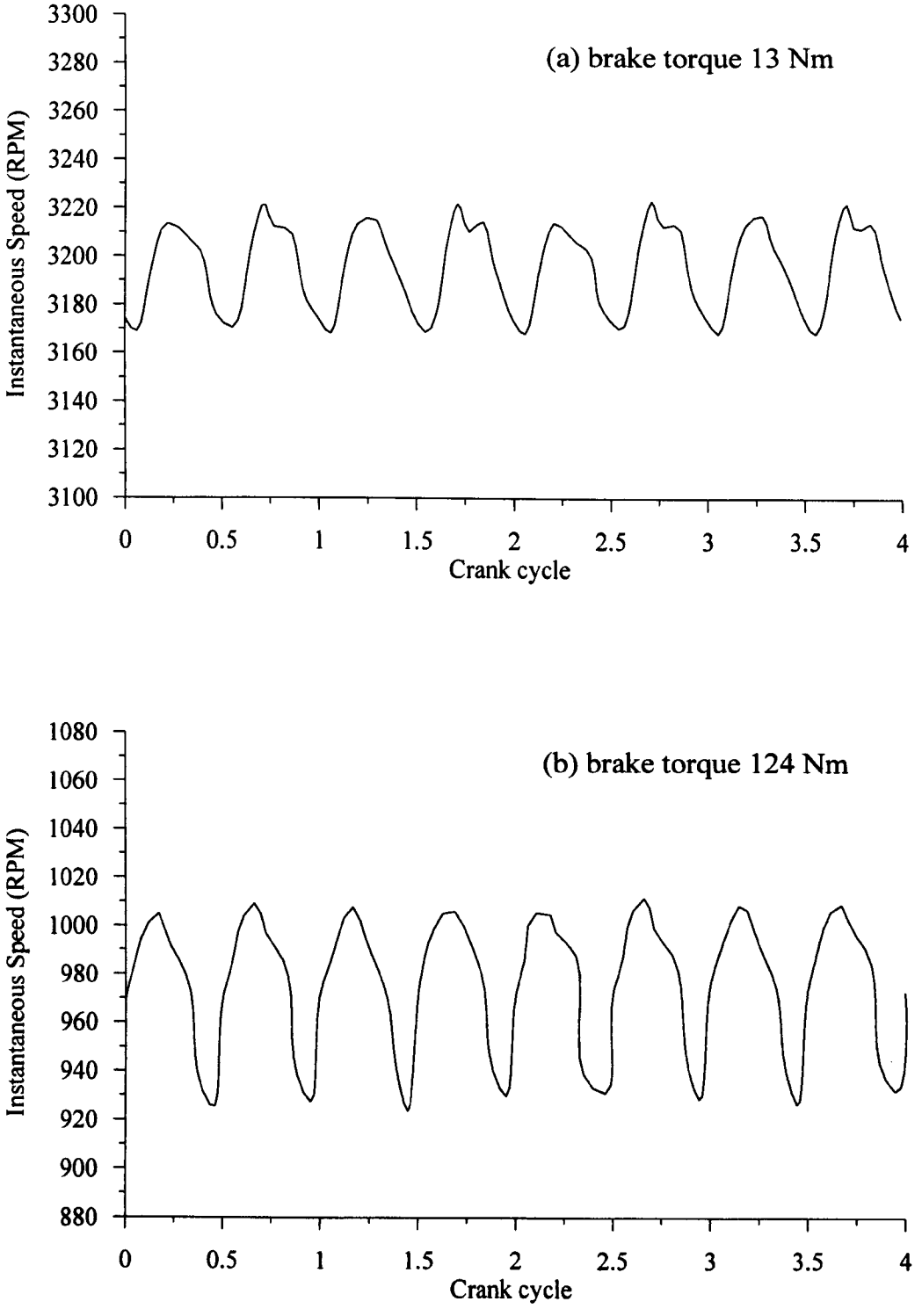

Figure 4.3 Effect of load increase on instantaneous speed at FLP 45%.

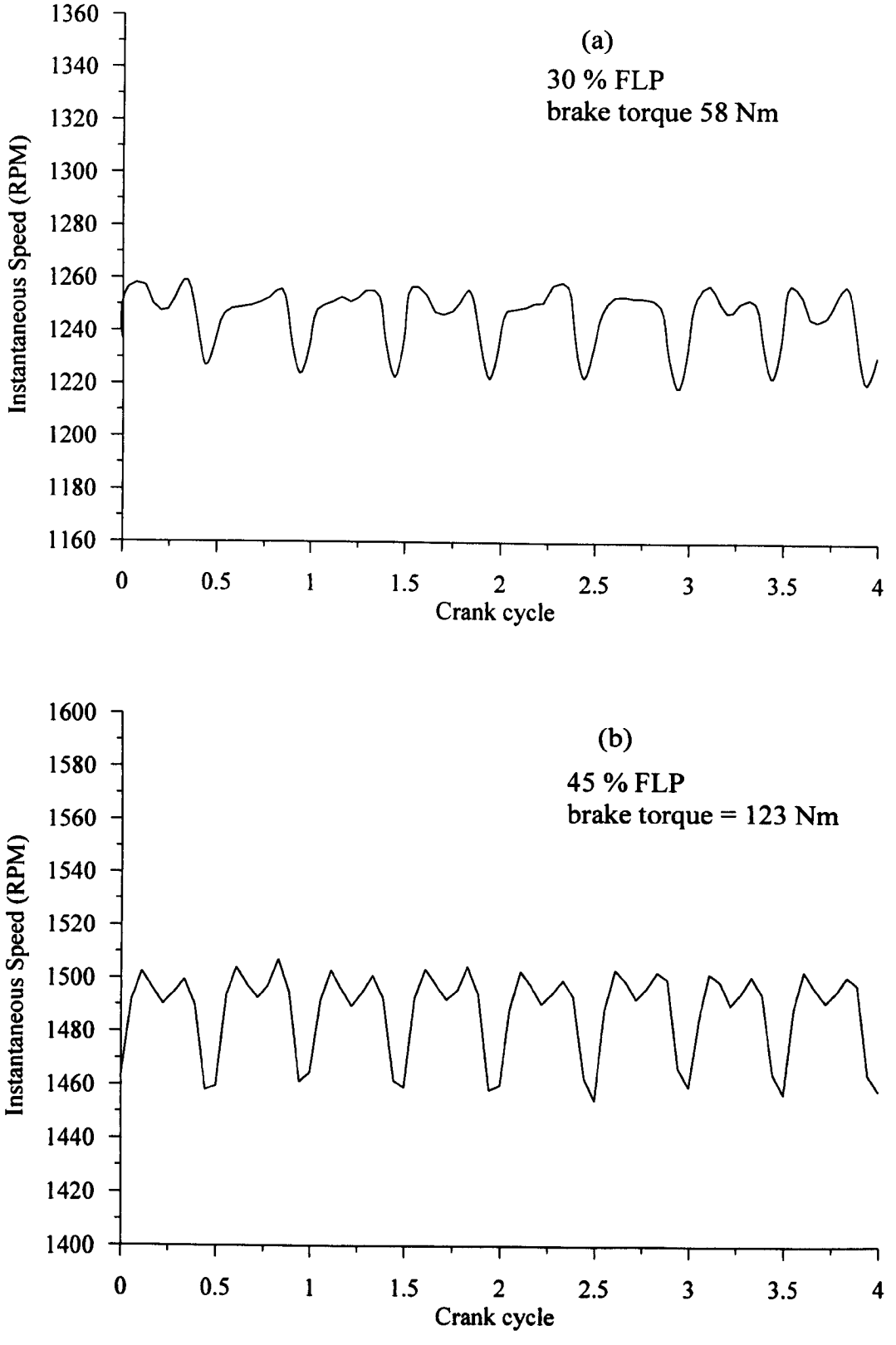

Figure 4.4 Instantaneous Speed variation at high speeds.

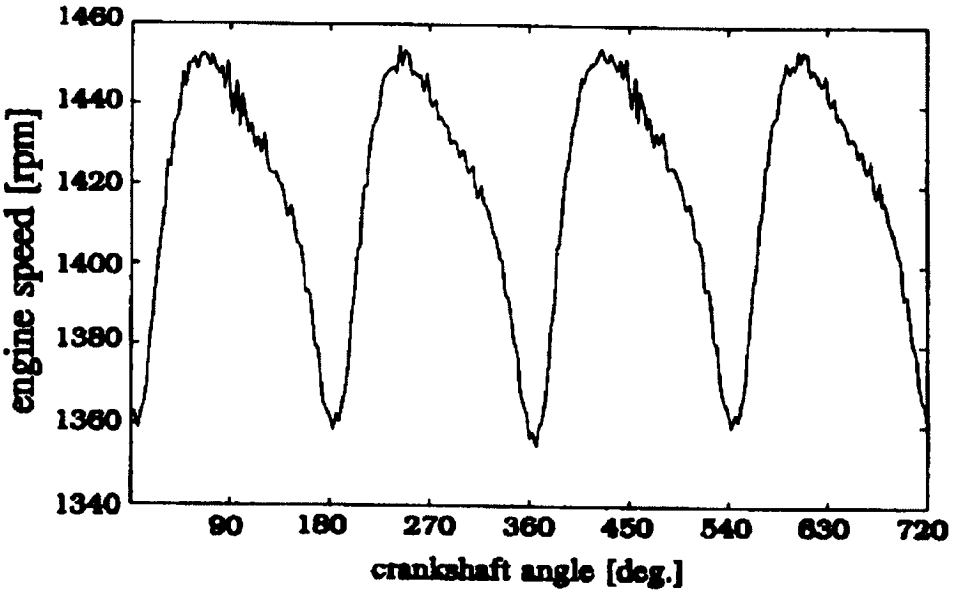

Figure 4.5 Engine speed fluctuations at 1400 RPM; Leonhardt et al., [1995].

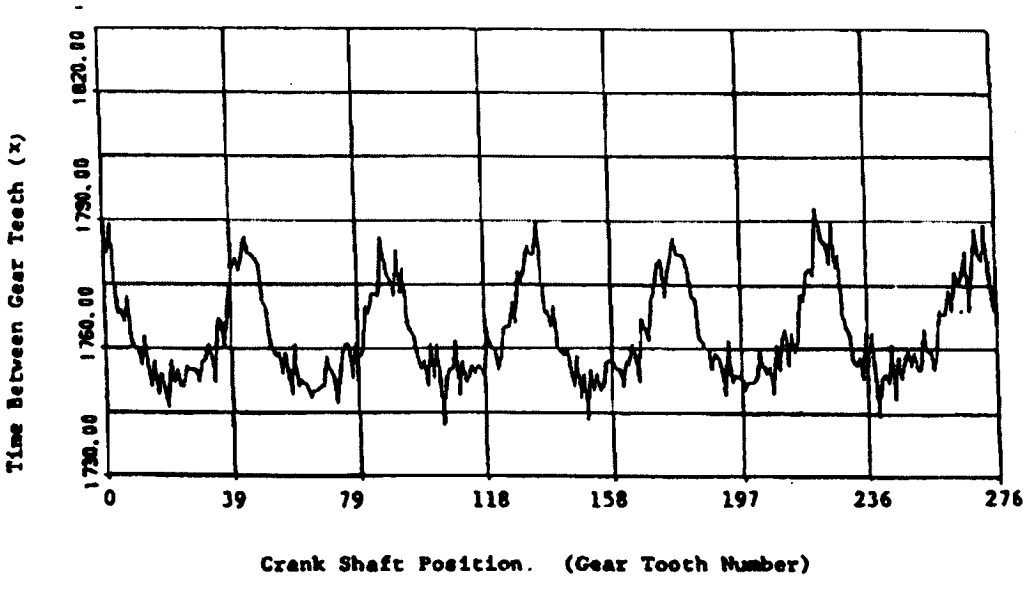

Figure 4.6 The time between flywheel teeth at 1000 RPM of 6-cylinder 4-stroke diesel engine; Sood et al., [1983].

The variation in engine speed under two different load conditions is illustrated in Figure 4.7. At idle (FLP 10%), with a brake load of 58.6 Nm, the nominal speed is 700 RPM, with a fluctuation of 90 RPM. Whereas when the engine is running at a higher speed of 2330 RPM (FLP 45%), under a similar load of 58.2 Nm the speed fluctuation is only 40 RPM, i.e. 1.6%. again illustrating the importance of the flywheel in recovering the engine stored energy, at high speed as well as the

validation of possible use of instantaneous speed as a monitoring tool for the load and speed relations.

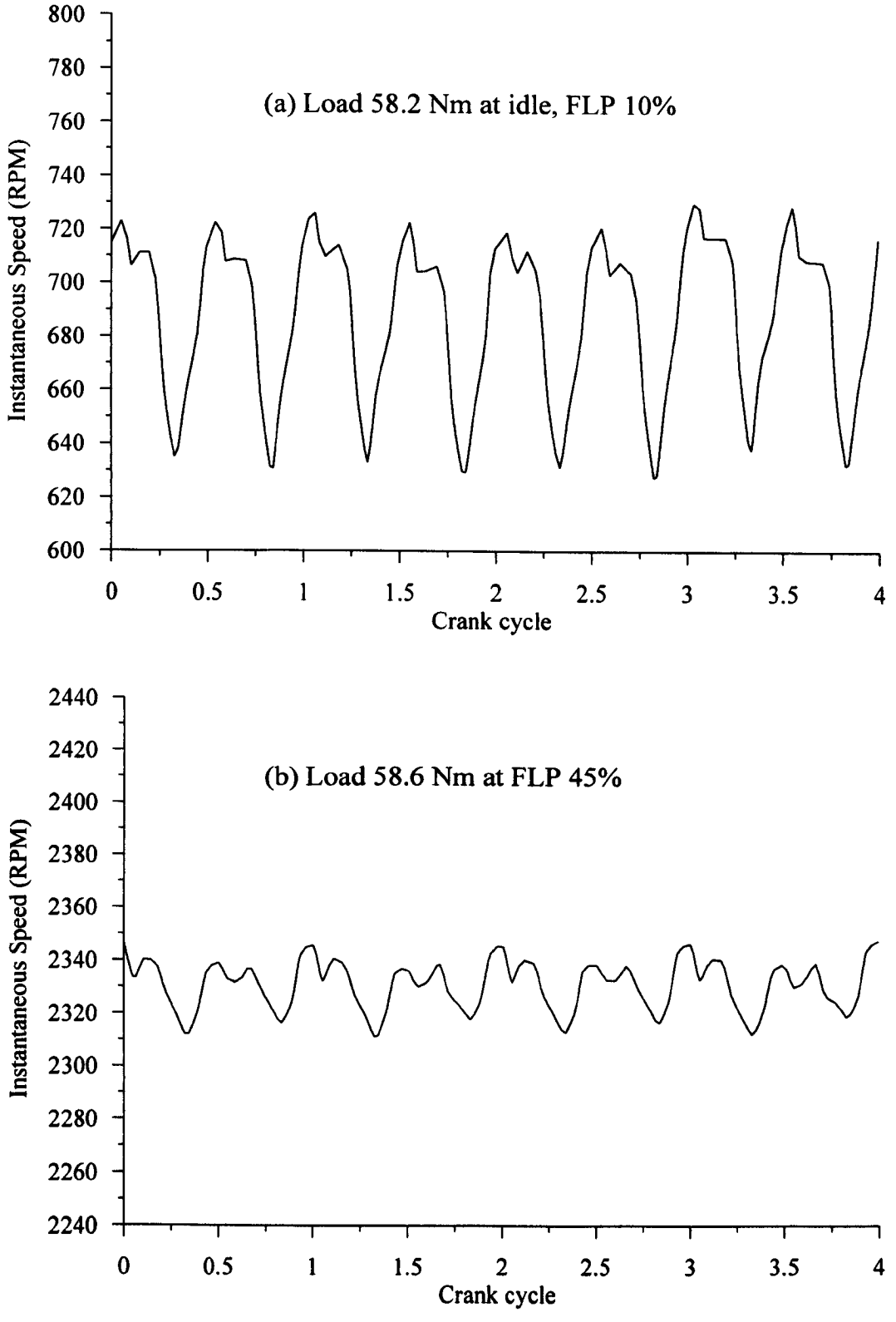

Figure 4.7 Speed fluctuation at constant load.

4.1.2 Exhaust temperature

The temperature measured at the exit of each cylinder helps to monitor the exhaust gas temperature from each cylinder, and is defined according to the thermocouple location shown schematically in Figure 4.8.

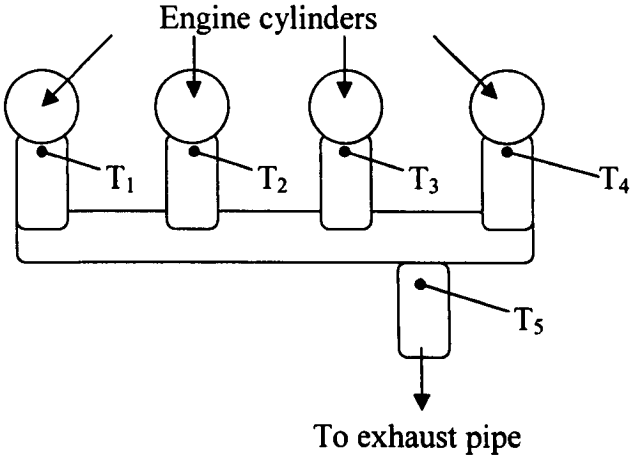

Figure 4.8 Exhaust system schematic diagram showing thermocouple locations.

Figure 4.9 presents the exhaust temperature variation of each cylinder at idle and it can be seen that the temperatures fluctuate due to the exhaust gas flow from the individual cylinders, and are phase shifted due to the cylinder firing order. It can also be noticed that the temperature variation between each individual cylinder is as a result of the exhaust gas flow through the manifold. For example, the flow out of cylinder one will influence temperatures T_2 and T_3 such that the $T_1 < T_2 < T_3$, and $T_4 < T_3$. Temperature T_5 is the composite exhaust gas temperature which as expected shows less cyclic variation.

At idle (FLP 10%), under low load, the average exhaust temperature is relatively low, as shown in Figure 4.9, and any increase in the applied load will directly bring about a significant increase in the cylinder exhaust temperatures, as shown in Figure 4.10. The fuel consumption was increased at idle position from 0.1524 to 0.4434 g/sec as the load was increased from 5 to 118 Nm respectively due to governor effect.

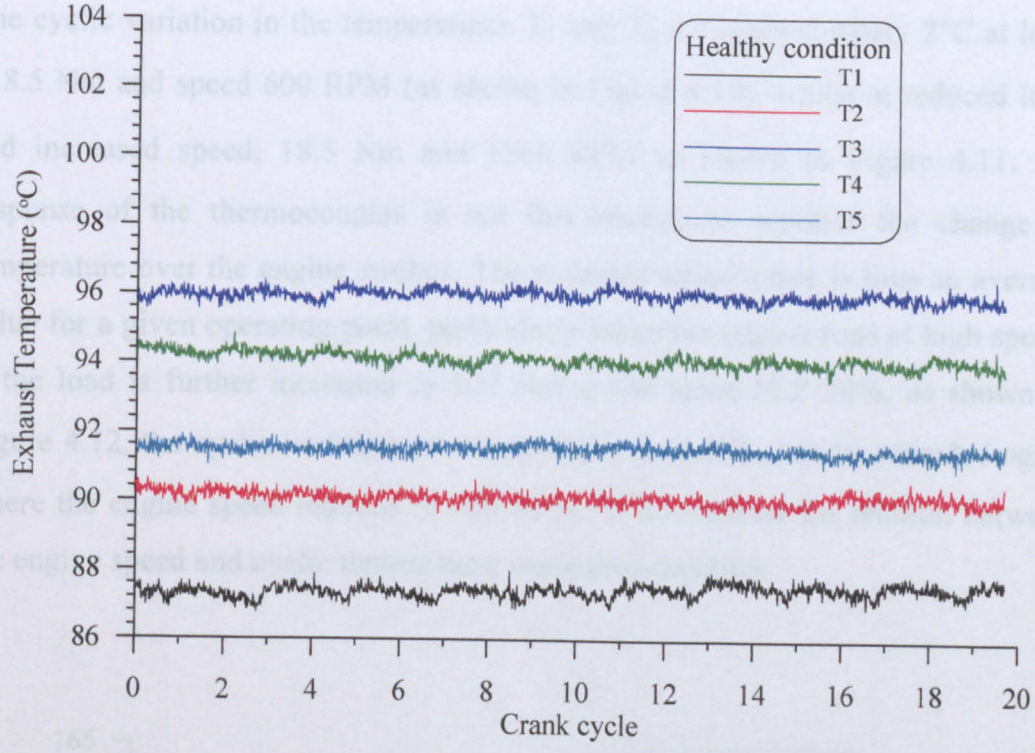

Figure 4.9 Exhaust temperature variation at idle (FLP 10%) - (load 5 Nm, nominal speed 717 RPM).

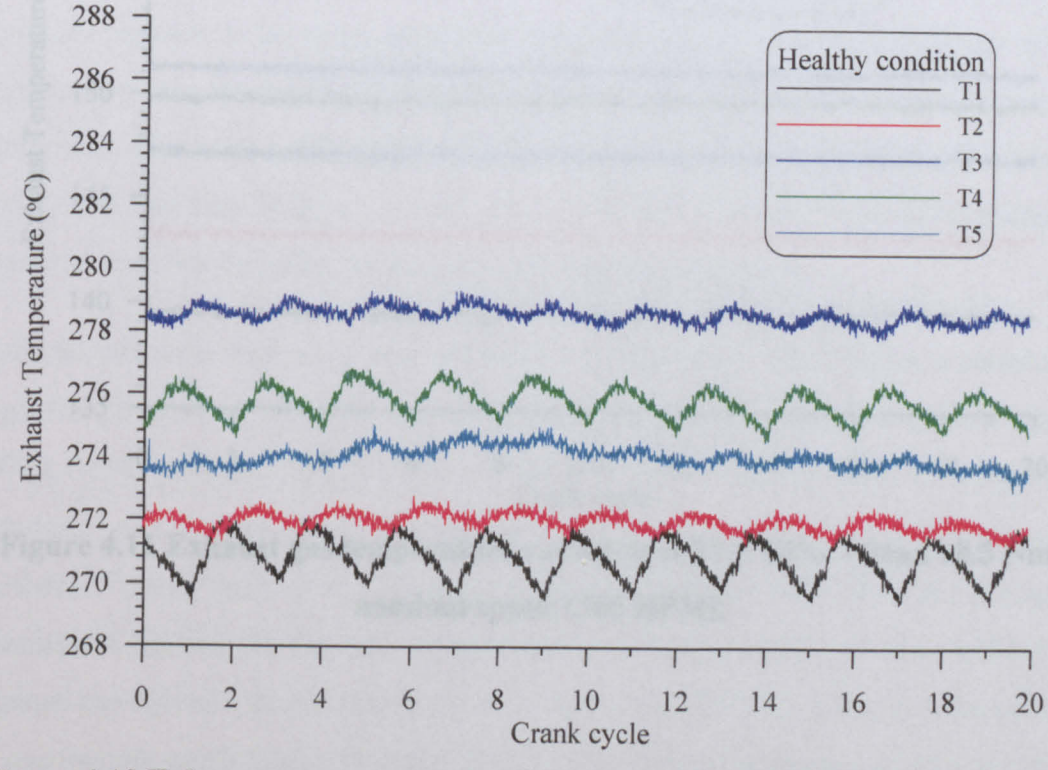

Figure 4.10 Exhaust gas temperature variation at idle (FLP 10%) – (load 118.5 Nm, nominal speed 600 RPM).

The cyclic variation in the temperatures T_1 and T_4 are approximately 2°C at load 118.5 Nm and speed 600 RPM (as shown in Figure 4.10), whilst at reduced load and increased speed, 18.5 Nm and 1360 RPM as shown in Figure 4.11, the response of the thermocouples is not fast enough to monitor the change in temperature over the engine strokes. The recorded temperature is thus an average value for a given operating point, particularly when the engine runs at high speed. If the load is further increased to 107 Nm at the same FLP 30%, as shown in Figure 4.12, the cyclic variation of temperatures T_1 and T_4 can be recorded again where the engine speed reduced to 946 RPM. This confirms the relation between the engine speed and cyclic temperature variation recording.

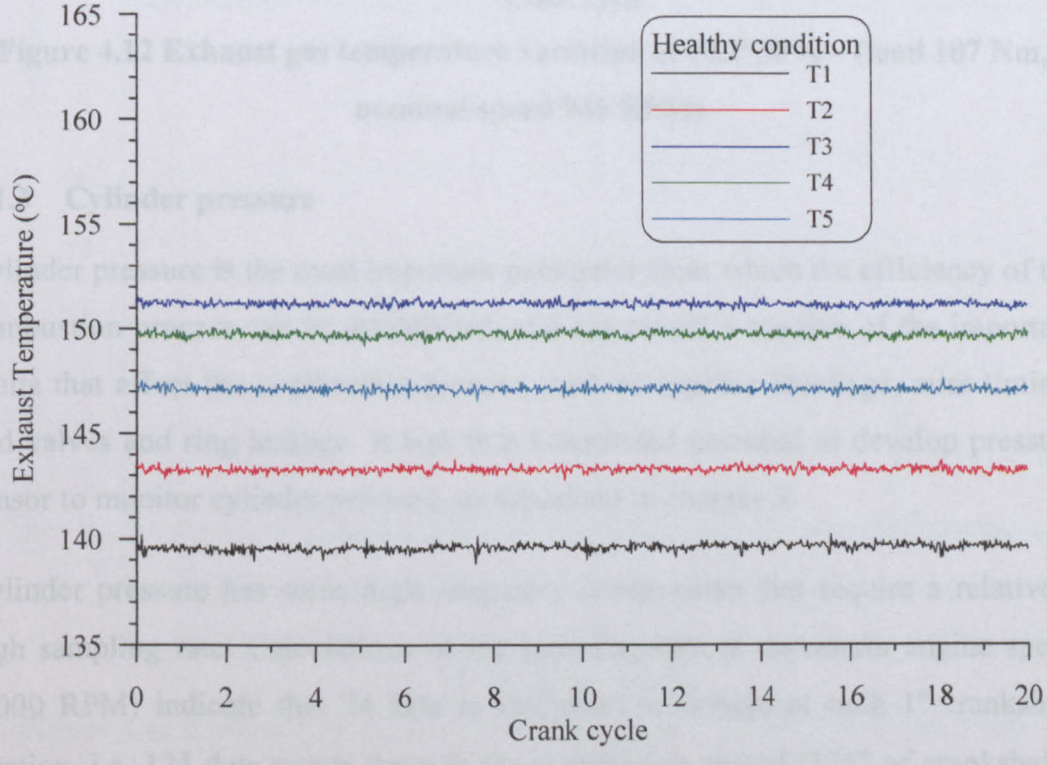

Figure 4.11 Exhaust gas temperature variation at FLP 30% – (load 18.5 Nm, nominal speed 1360 RPM).

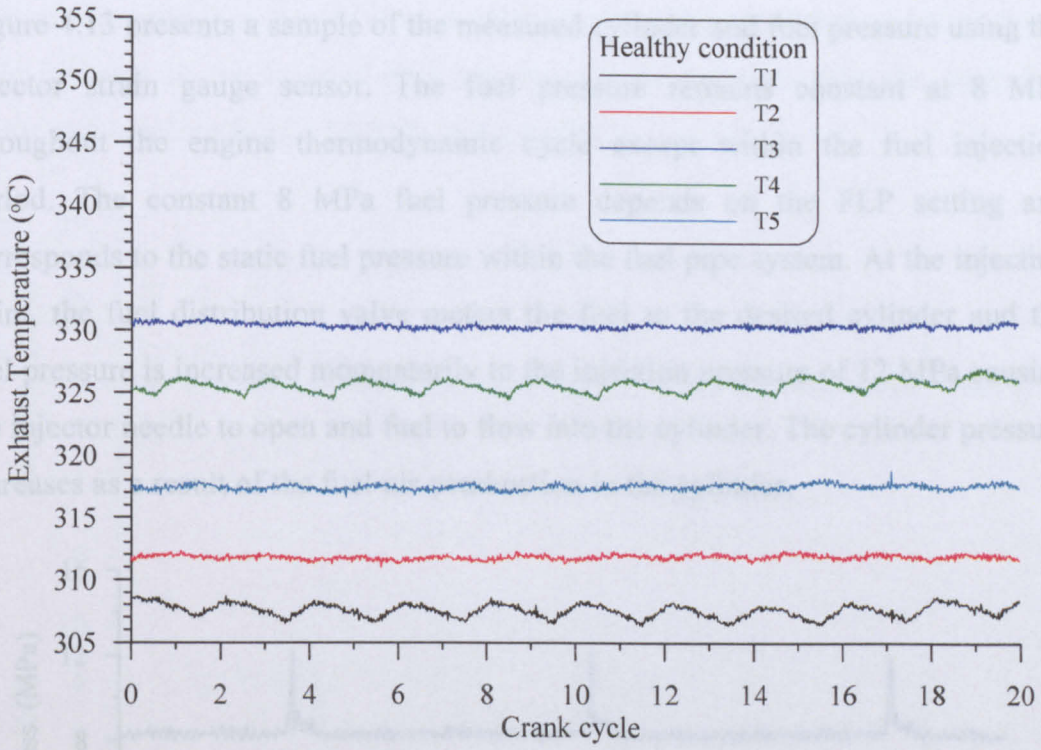

Figure 4.12 Exhaust gas temperature variation at FLP 30% – (load 107 Nm, nominal speed 946 RPM).

4.1.3 Cylinder pressure

Cylinder pressure is the most important parameter from which the efficiency of the combustion process can be established, and can reveal a number of the important faults that affect the combustion process, such as injector blockage, miss timing, and valves and ring leakage. It was thus considered essential to develop pressure sensor to monitor cylinder pressure, as described in chapter 3.

Cylinder pressure has some high frequency components that require a relatively high sampling rate. Calculations of the sampling rate at maximum engine speed (4000 RPM) indicate that 24 kHz is sufficient to sample at each 1° crankshaft rotation, i.e. 125 data points through the combustion period (125° of crankshaft). However, using such a high sampling rate in parallel with the other engine parameters limited the amount of recorded data; consequently, it was decided to capture the cylinder pressure at a lower sample rate of 12 kHz which corresponds to one sample per 2 degree of the crankshaft rotation at maximum engine speed of 4000 RPM.

Figure 4.13 presents a sample of the measured cylinder and fuel pressure using the injector strain gauge sensor. The fuel pressure remains constant at 8 MPa throughout the engine thermodynamic cycle except within the fuel injection period. The constant 8 MPa fuel pressure depends on the FLP setting and corresponds to the static fuel pressure within the fuel pipe system. At the injection point, the fuel distribution valve meters the fuel to the desired cylinder and the fuel pressure is increased momentarily to the injection pressure of 12 MPa causing the injector needle to open and fuel to flow into the cylinder. The cylinder pressure increases as a result of the fuel-air combustion in the cylinder.

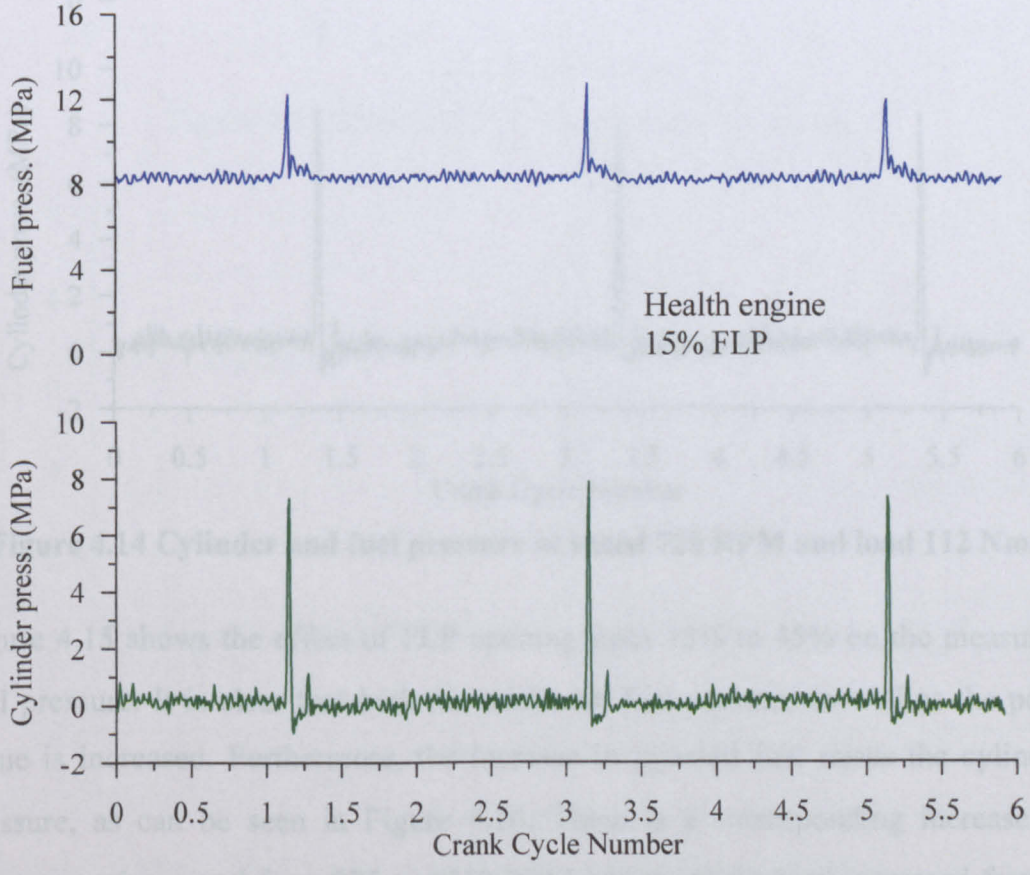

Figure 4.13 Cylinder and fuel pressure at speed 975 RPM and load 8 Nm

With an increase in the applied load from 8 Nm to 112 Nm (at the same fuel lever position FLP 15%), the peak cylinder pressure is increased to 9 MPa as a result of the increase in burnt fuel, as shown in Figure 4.14. Although the FLP is fixed, the amount of injected fuel is increased by the governor to compensate for the applied load change. When the FLP is increased, the fuel valve opens further to allow more fuel to be injected into the individual cylinders. This in turn directly increases the fuel pressure. This is confirmed by monitoring the measured fuel

consumption which increased from 0.1528 g/s to 0.3745 g/s with the load increase. This increase in the injected fuel amount can be detected with the peak fuel pressure increasing from 12.8 MPa to 13.9 MPa.

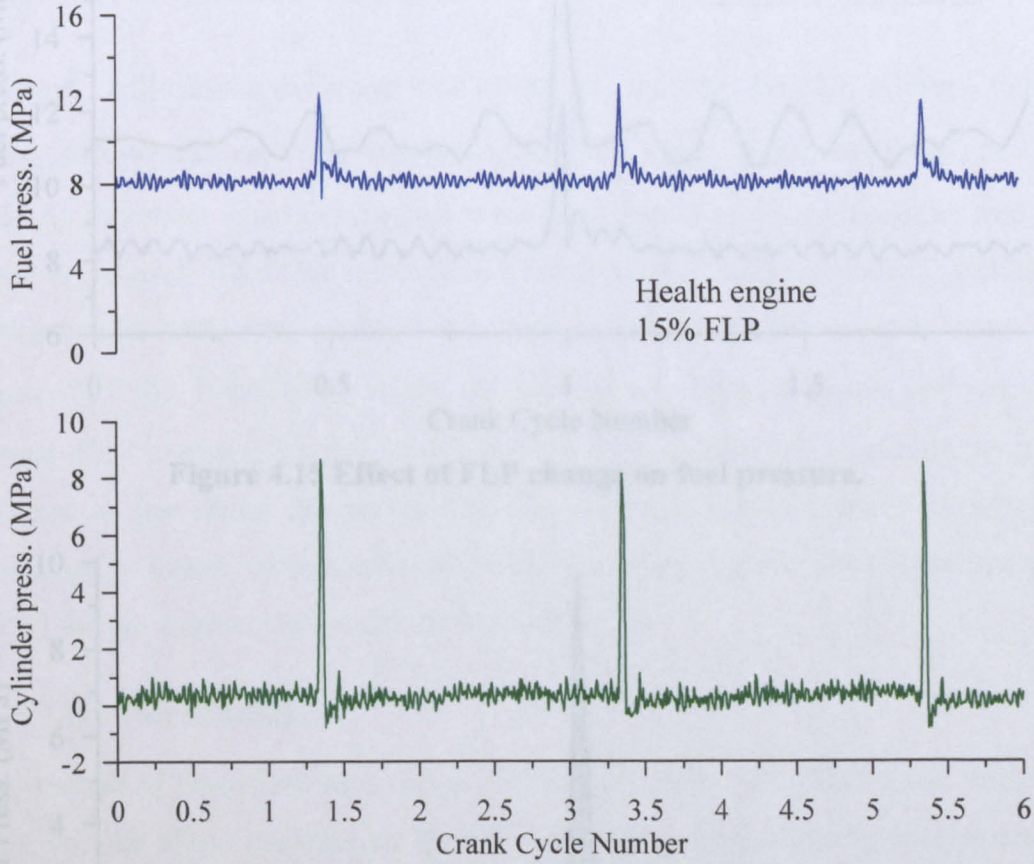

Figure 4.14 Cylinder and fuel pressure at speed 725 RPM and load 112 Nm.

Figure 4.15 shows the effect of FLP opening from 15% to 45% on the measured fuel pressure. It is clear that both the minimum fuel pressure as well as the peak value is increased. Furthermore, the increase in injected fuel raises the cylinder pressure, as can be seen in Figure 4.16. There is a corresponding increase in average engine speed from 975 to 3210 RPM and the brake load increased from 8 to 11.3 Nm.

These results validate the new method used for monitoring the fuel and cylinder pressure in real-time by measuring the circumferential and axial strain in the injector body. Because of the high sampling rates required to accurately capture the sensors output, the measured data will only be used in validating the model results and experimental data analysis, but not for the proposed CMFD.

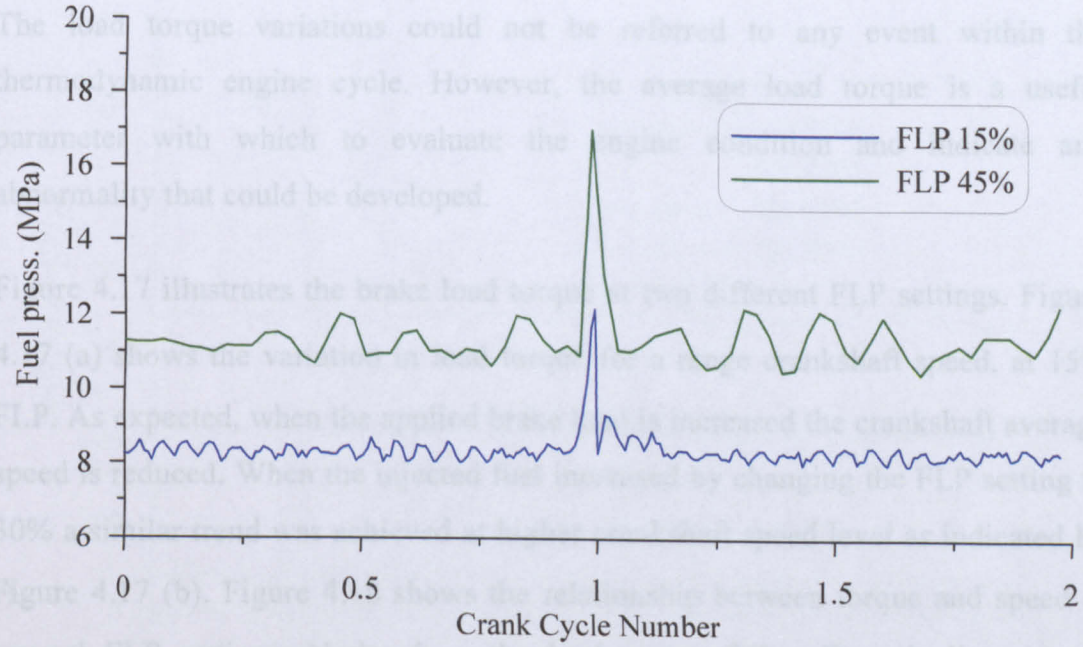

Figure 4.15 Effect of FLP change on fuel pressure.

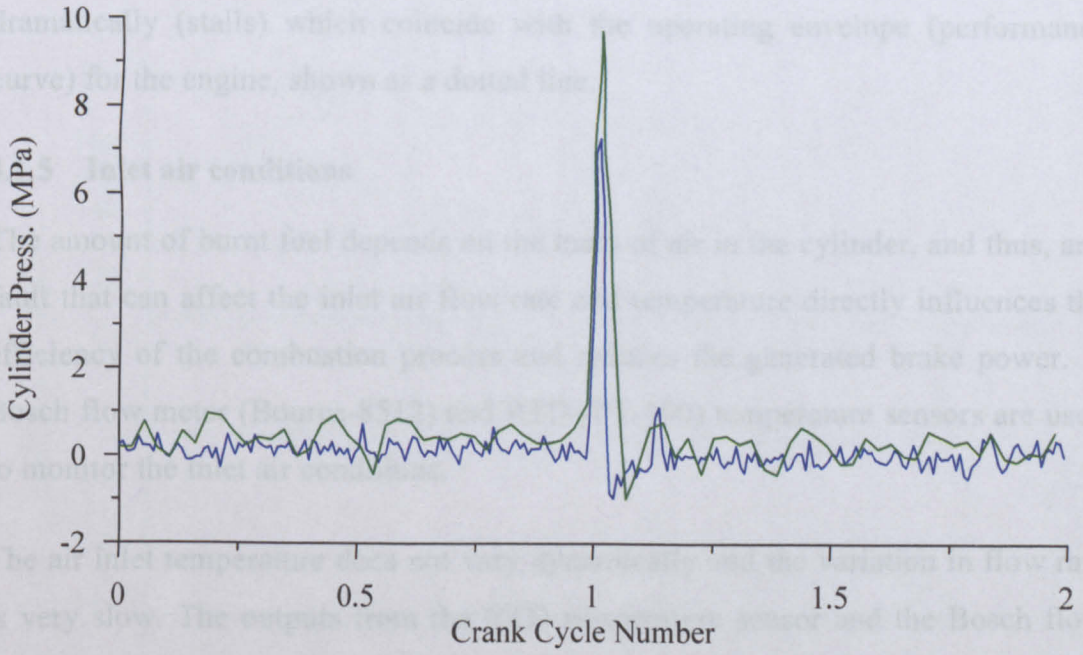

Figure 4.16 Effect of FLP change on cylinder pressure.

4.1.4 Brake load torque

The brake load is the main output of the engine and was measured using the integrated S-type load cell (omega, 200 LBS) to the hydraulic brake. A limited fluctuation was recorded in the measured load torque due to the nature of the hydraulic brake which uses water momentum interchange, which helps to damp out any torque fluctuations. Only small fluctuation (±6% of nominal value) were recorded at high load and low speed due to the low stored energy in the flywheel.

The load torque variations could not be referred to any event within the thermodynamic engine cycle. However, the average load torque is a useful parameter with which to evaluate the engine condition and indicate any abnormality that could be developed.

Figure 4.17 illustrates the brake load torque at two different FLP settings. Figure 4.17 (a) shows the variation in load torque for a range crankshaft speed, at 15% FLP. As expected, when the applied brake load is increased the crankshaft average speed is reduced. When the injected fuel increased by changing the FLP setting to 30% a similar trend was achieved at higher crankshaft speed level as indicated by Figure 4.17 (b). Figure 4.18 shows the relationship between torque and speed at several FLP settings. Notice how the load torque falls off gradually with an increase in the speed (proportionally) up until the point at which it falls off dramatically (stalls) which coincide with the operating envelope (performance curve) for the engine, shown as a dotted line.

4.1.5 Inlet air conditions

The amount of burnt fuel depends on the mass of air in the cylinder, and thus, any fault that can affect the inlet air flow rate and temperature directly influences the efficiency of the combustion process and reduces the generated brake power. A Bosch flow meter (Bourns-8512) and RTD (PT-100) temperature sensors are used to monitor the inlet air conditions.

The air inlet temperature does not vary dynamically and the variation in flow rate is very slow. The outputs from the RTD temperature sensor and the Bosch flow rate meter were sampled at 1 kHz, and a running average filter used to smooth the data. Figure 4.19 illustrate the relationship between the flow meter output (voltage) as a function of engine speed for three different FLP settings, and as expected air flow rate increased with engine speed. The inlet air temperature showed no change throughout the test and only depends on atmospheric conditions on the day of the test.

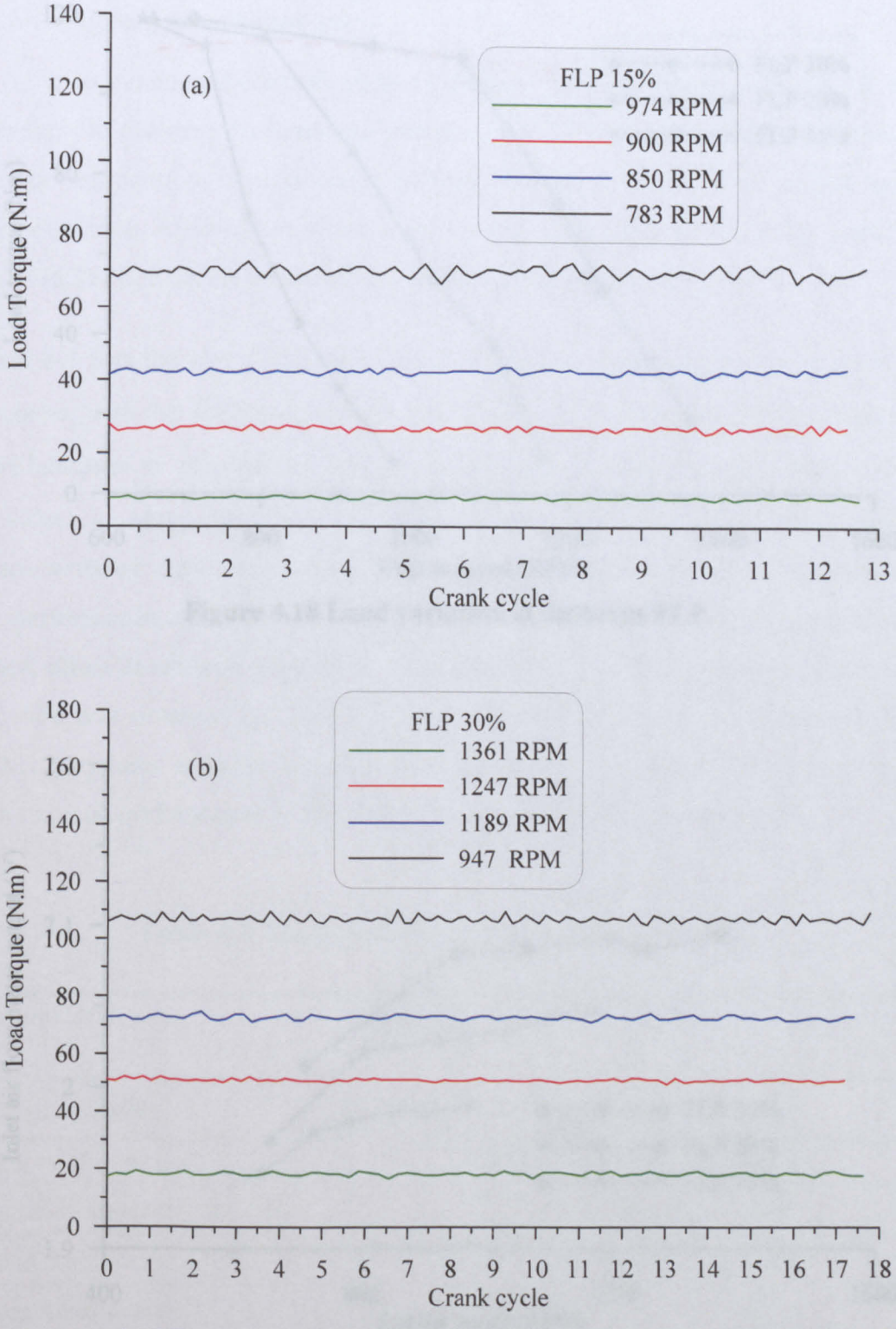

Figure 4.17 Brake load torque variation at different crankshaft speed.

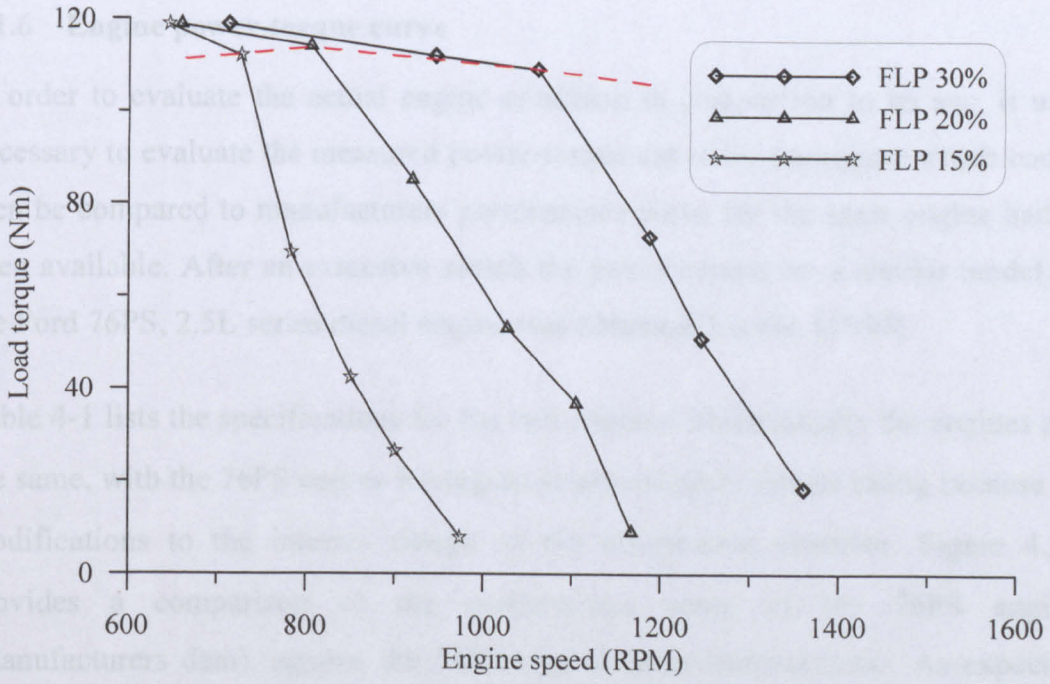

Figure 4.18 Load variation at different FLP.

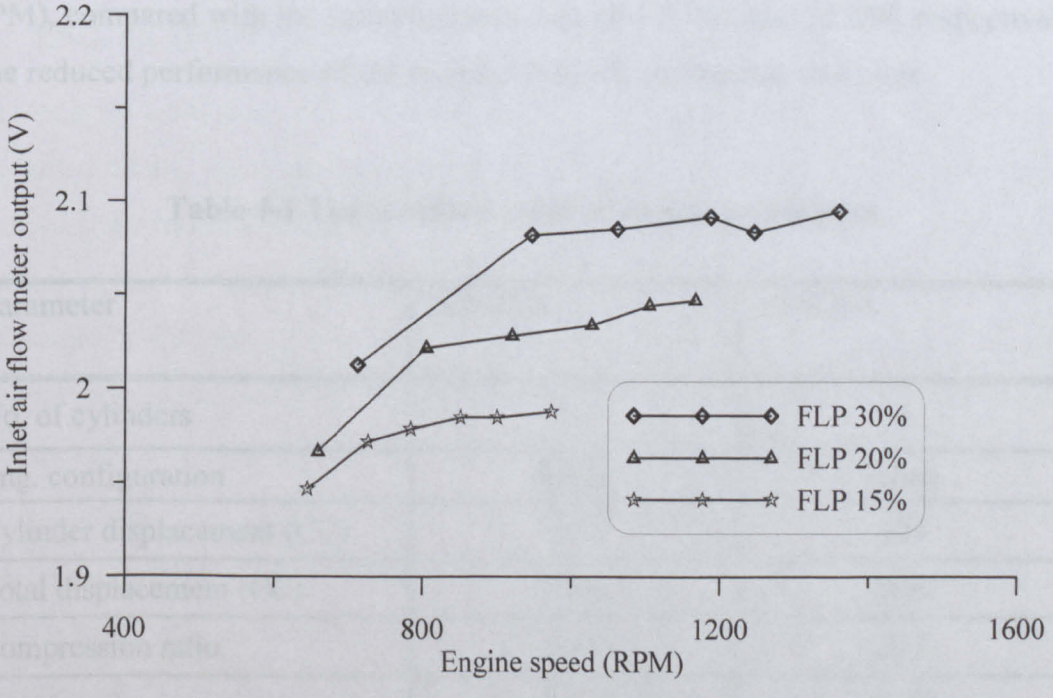

Figure 4.19 Inlet air flow meter signal at different operating conditions.

4.1.6 Engine power-torque curve

In order to evaluate the actual engine condition in comparison to its age, it was necessary to evaluate the measured power-torque curve for the engine which could then be compared to manufacturers performance curve for the same engine had it been available. After an extensive search the power-torque for a similar model of the Ford 76PS, 2.5L series diesel engine was obtained, Lechie, [1999].

Table 4-1 lists the specifications for the two engines. Mechanically the engines are the same, with the 76PS engine having an improved performance rating because of modifications to the internal design of the combustion chamber. Figure 4.20 provides a comparison of the performance curve of the 76PS engine (manufacturers data), against the 70PS engine (experimental data). As expected the performance curve for the torque and power show very similar trends against speed, albeit at reduced magnitude. For the 70PS test engine a maximum torque of 135 Nm was obtained (at 2500 RPM), and maximum power of 49 kW (at 4000 RPM), compared with the manufacturers data of 146 Nm and 52 kW, respectively. The reduced performance of the engine is largely attributable to its age.

Table 4-1 The standard value of engine parameters.

Parameter	70PS NA	76PS NA
No. of cylinders	4	4
Eng. configuration	Inline	Inline
Cylinder displacement (CC)	624	624
Total displacement (CC)	2496	2496
Compression ratio	20.8	20.8
Bore (mm)	93.7	93.7
Stroke (mm)	90.5	90.5
Maximum power (kW) @ 4000 RPM	52	56
Maximum torque (Nm) @ 2500 RPM	146	168

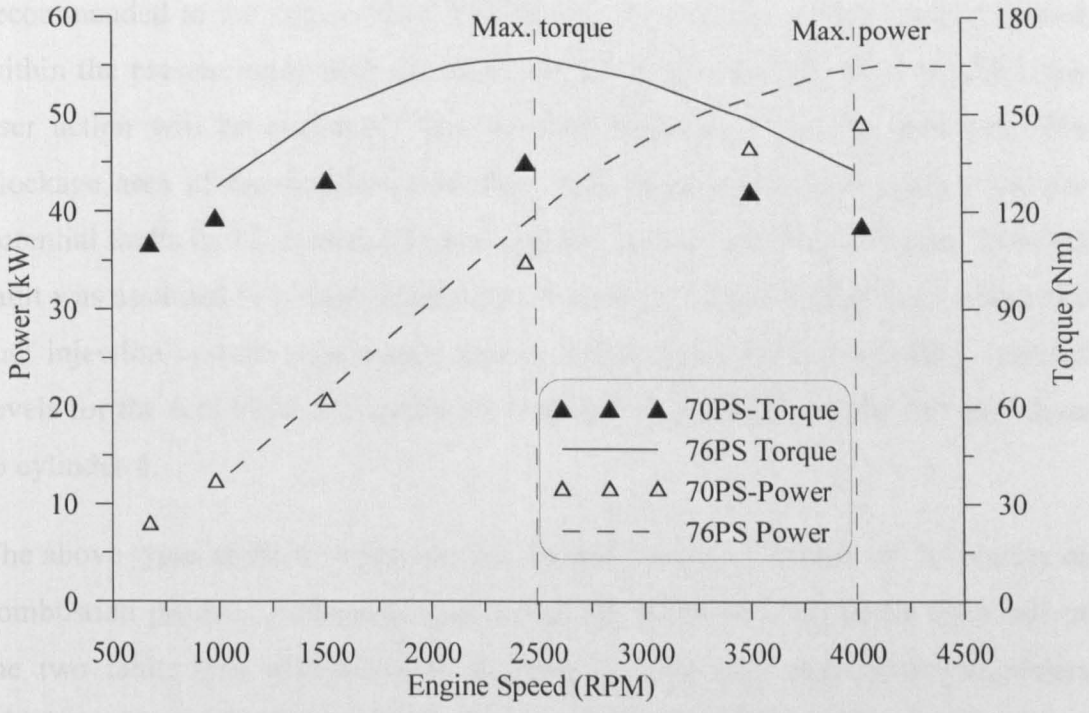

Figure 4.20 Power-torque curve of the engine using experimental data.

4.2 ENGINE DATA UNDER SYNTHETIC FAULTS

The engine data were collected using the data acquisition system and several synthetic faults were introduced to the engine to simulate an actual engine malfunction. In the present study, two types of faults were assessed, injected fuel starvation and inlet air blockage. Fuel starvation could occur as a result of blockage in the piping system between injection pump and injector, blocked injector nozzles or injection pump malfunction. To simulate this, a needle valve was integrated in the fuel line to cylinder 4 of the diesel engine to regulate the amount of fuel injected to that cylinder, as shown in Figure 4.21. Inlet air shortage can be caused by a dirty inlet air filter or blockage in the intake manifold. To simulate the inlet air blockage, the inlet to the flowmeter, mounted on the intake manifold was partially closed as shown in Figure 4.22.

As the present study focus on the development of CMFD system, there is no need to test the engine performance under all of possible fault severity levels where it is only required to evaluate the key parameters at which the fault and its level can be detected. Through many trials and contacts with the engine manufacturers, it was not possible to find out the fault level at which different actions can be

recommended to the engine user. Two levels, for each fault type, were proposed within the present study and considered as the border severity level at which the user action will be evaluated. The air inlet fault was tested at 25% and 50% blockage area of the standard inlet flow area based on the assumption that the potential faults in this system progress rapidly, such as air filter blockage. The fuel fault was assumed to be determent when it reaches higher severity level where the fuel injection system components have a longer service life. Therefore, selected levels for the fuel blockage testing were set at 50% and 80% of the fuel flow area to cylinder 4.

The above types of faults were selected for their strong influence on the quality of combustion process. A detailed analysis of the measured data under each one of the two faults was undertaken to evaluate the optimum measuring parameters which could then be used as a symptom to identify the fault.

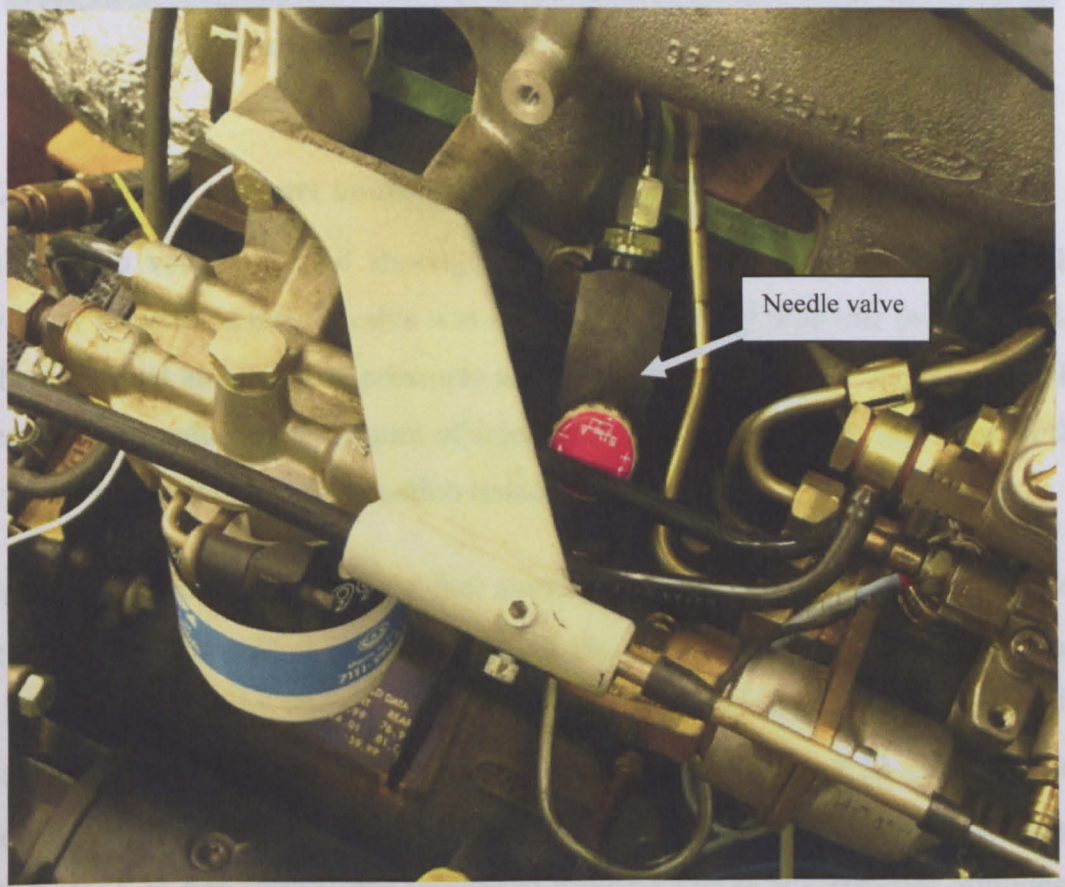

Figure 4.21 Needle valve to control the flow to cylinder 4.

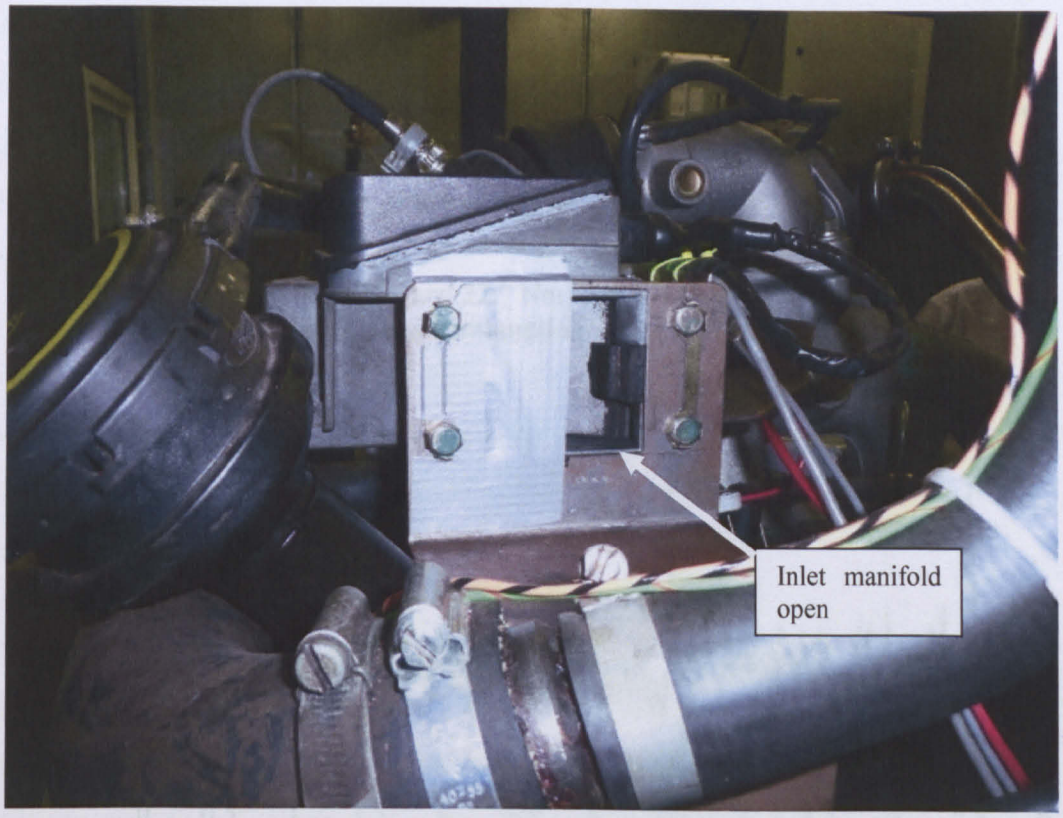

Figure 4.22 Inlet air manifold partially closed.

4.2.1 Cylinder pressure under fuel fault

In order to verify the fuel shortage effect on the combustion process and the cylinder pressure, a needle valve was installed on the fuel pipe line to the cylinder where the fuel and cylinder pressures are measured (cylinder 4). As expected, the needle valve reduces the amount of injected fuel and as a result, the boost in the cylinder pressure due to combustion reduced.

Figure 4.23 shows the effect of fuel shortage to cylinder 4 using the integrated needle valve. It is evident that the peak cylinder pressure has decreased from about 8 MPa in the healthy engine to only 2.3 MPa when the fuel pipe line was 50% blocked, by closing the needle valve, as shown in Figure 4.23 (a). The fuel blockage reduces the injected fuel pressure rise at the injection point to less than 2 MPa which in turn reduce the amount of injected fuel to the cylinder, ultimately producing lower combustion pressure in the cylinder.

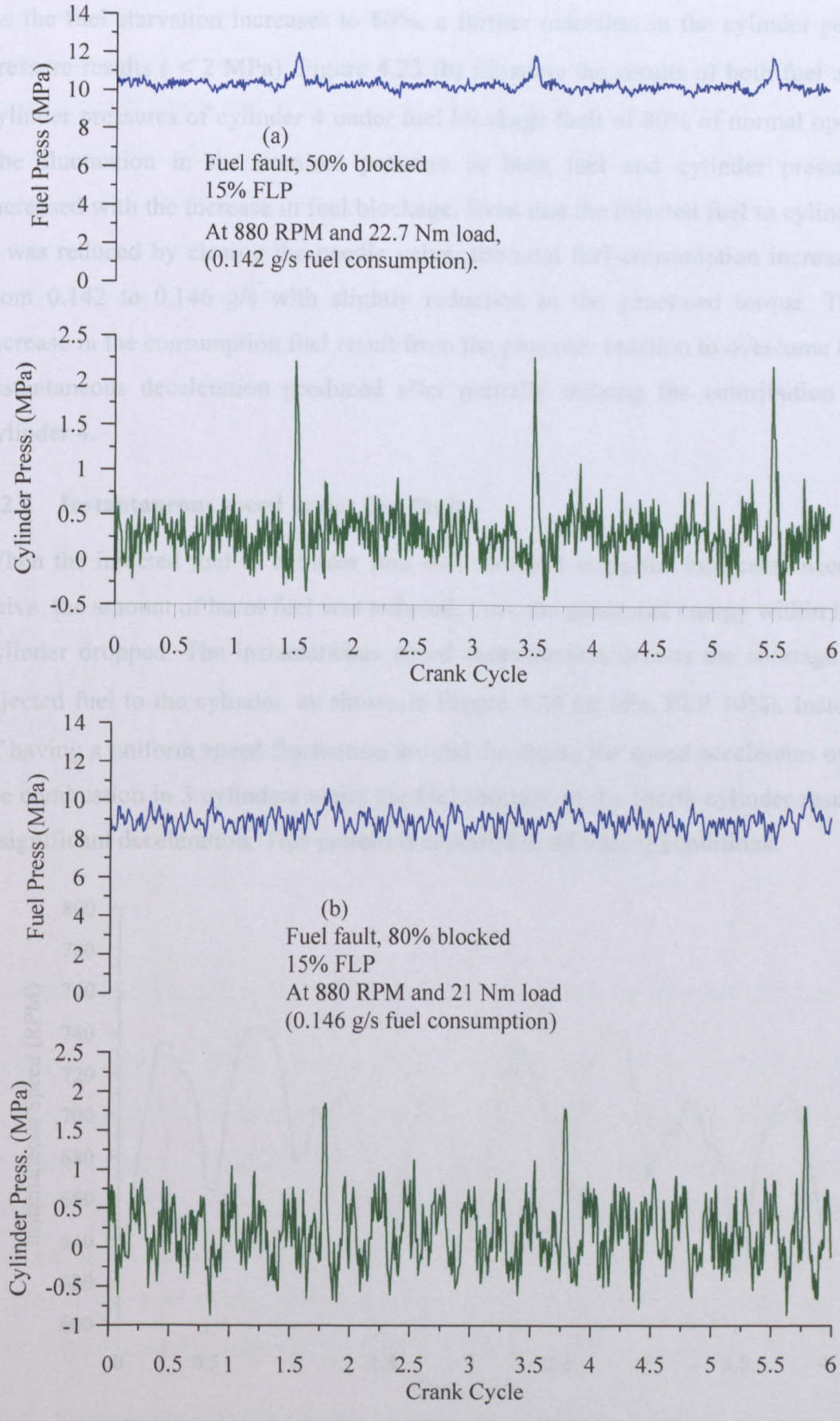

Figure 4.23 Cylinder and fuel pressures under fuel fault condition.

As the fuel starvation increases to 80%, a further reduction in the cylinder peak pressure results (< 2 MPa). Figure 4.23 (b) illustrate the results of both fuel and cylinder pressures of cylinder 4 under fuel blockage fault of 80% of normal open. The fluctuation in the nominal pressure in both fuel and cylinder pressure increased with the increase in fuel blockage. Even that the injected fuel to cylinder 4 was reduced by closing the needle valve, the total fuel consumption increased from 0.142 to 0.146 g/s with slightly reduction in the generated torque. This increase in the consumption fuel result from the governor reaction to overcome the instantaneous deceleration produced after partially missing the contribution of cylinder 4.

4.2.2 Instantaneous speed under fuel fault

When the injected fuel to cylinder four was throttled using the integrated needle valve, the amount of burnt fuel was reduced, thus, the generated energy within this cylinder dropped. The instantaneous speed measurement detects the shortage of injected fuel to the cylinder, as shown in Figure 4.24 (at idle, FLP 10%). Instead of having a uniform speed fluctuation around the mean, the speed accelerates over the combustion in 3 cylinders while the fuel shortage in the fourth cylinder results a significant deceleration. This pattern is repeated in all testing conditions.

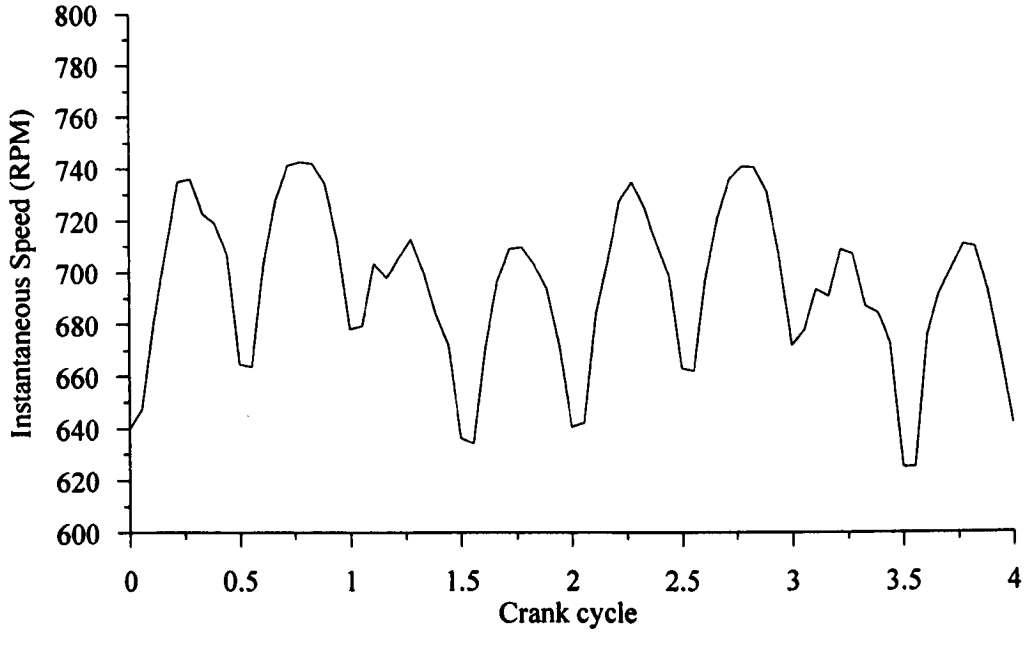

Figure 4.24 Instantaneous speed with 50% block of fuel to cylinder 4, 27.2 Nm and 692 RPM

With an increase in the applied load from 27.2 Nm to 91 Nm (at the same FLP setting) the crankshaft speed is decreased and the fluctuation in the instantaneous speed becomes larger due to the lower energy stored in the flywheel, as shown in Figure 4.25. The affect of the reduced performance in one cylinder at higher load increased the fluctuation in the instantaneous speed. The measurement of instantaneous speed is proved to be very useful tool for detecting a miss-fire or shortage of fuel in the individual cylinder.

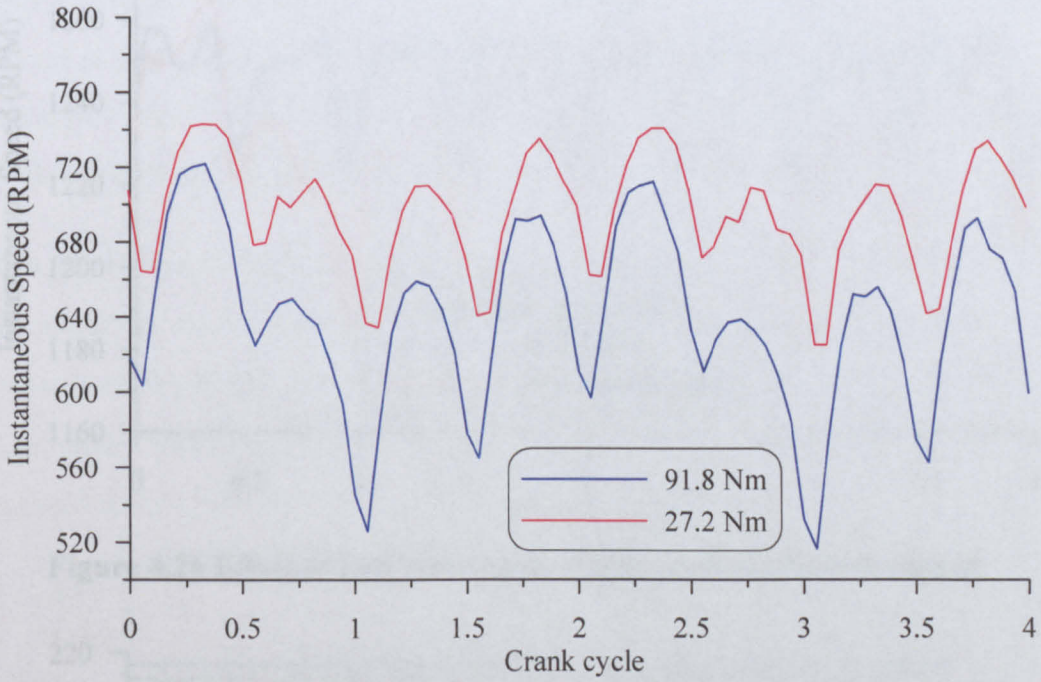

Figure 4.25 The effect of load increase on engine speed at idle FLP (10%).

To clarify the effect of the fuel starvation, a comparison between the healthy and faulty data was utilized at different operating conditions, as shown in Figure 4.26. Both tests were undertaken at FLP 30%, and the mean engine speed decreased from 1250 to 1230 RPM, as a result of the miss-fire. The fuel consumption was also increased from 0.2987 to 0.414 kg/s due to the governor attempting to overcome the loss of the fourth cylinder and keep the engine working at the desired speed. More results were included in Appendix D.

4.2.3 Exhaust gases temperature under fuel fault

The exhaust gas temperature should also help to detect a miss-fire or the fuel shortage in individual cylinders. The reduction of the injected fuel, due to any

block in the injector or pipe system, reduces the energy release from the combustion process, with a corresponding drop in the exhaust gas temperature at the affected cylinder. This was verified by observing the exhaust gas temperatures. Figure 4.27 shows the exhaust gas temperatures when the fuel to cylinder four is throttled to 50%. Temperature T_4 is markedly decreased to about 124°C while the temperature ranges of the remaining cylinders run at between 212 to 222°C. As a result, the total exhaust gas temperature T_5 drops to about 190°C.

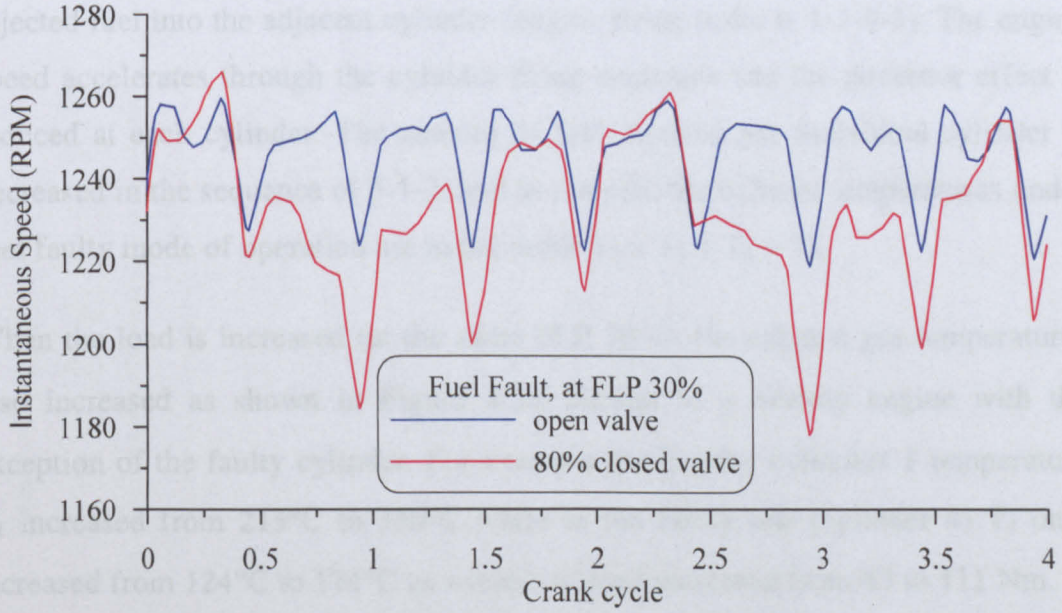

Figure 4.26 Effect of fuel valve open change on instantaneous speed.

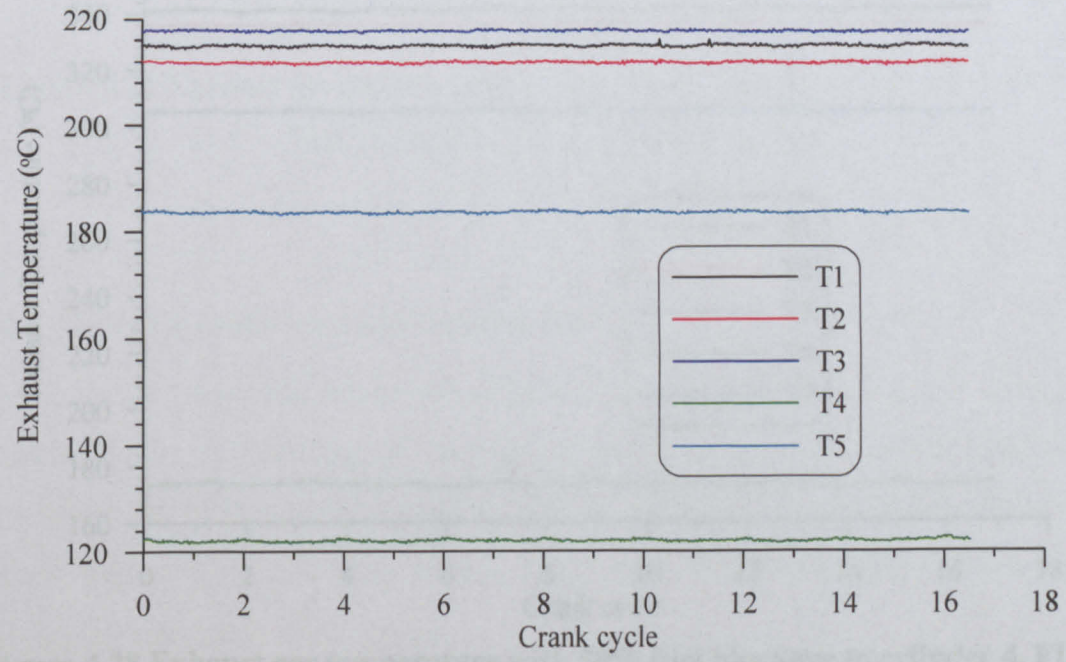

Figure 4.27 Exhaust gas temperature with 50% fuel block to cylinder four, FLP 30%, load 84 Nm and speed 1235 RPM.

Within the health engine operating mode, as discussed before, due to the exhaust manifold configuration the recorded data always shows the $T_3 > T_2 > T_1$. It could be seen that when cylinder 4 is starved of fuel the exhaust gas temperatures of the first three cylinders are $T_3 > T_1 > T_2$. This pattern was confirmed through all recorded data. Extensive analyses of such results indicate that this pattern is a direct result of the governor effect. When cylinder 4 does not provide a normal contribution and begin to open the main fuel valve at the injection pump discharge line to compensate for the drop in the speed. This process increases the amount of injected fuel into the adjacent cylinder (engine firing order is 1-2-4-3). The engine speed accelerates through the cylinder firing sequence and the governor effect is reduced at each cylinder. The amount of fuel injected per individual cylinder is decreased in the sequence of 3-1-2, and as a result, the exhaust temperatures under fuel faulty mode of operation are in the order $T_3 > T_1 > T_2 > T_4$.

When the load is increased (at the same FLP 30%), the exhaust gas temperatures also increased as shown in Figure 4.28, similar to a healthy engine with the exception of the faulty cylinder. For example the healthy cylinders 1 temperature T_1 increased from 213°C to 330°C while in the faulty one (cylinder 4) T_4 only increased from 124°C to 174°C as a result of load increased from 63 to 111 Nm.

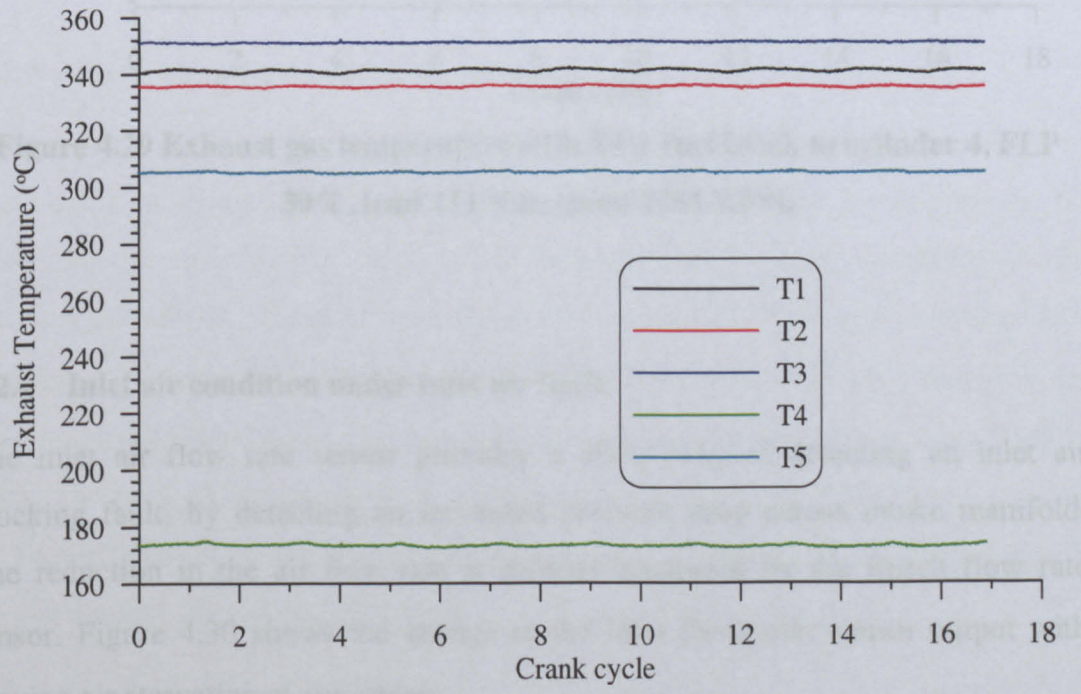

Figure 4.28 Exhaust gas temperature with 50% fuel blockage to cylinder 4, FLP 30%, load 111 Nm, speed 1081 RPM.

With the needle valve closing 80% of the flow area, (at 30% FLP setting) and 111 Nm applied load torque, the exhaust temperatures reduced by about 8°C, as shown in Figure 4.29. A further reduction in the cylinder 4 exhaust gas temperature of up to 12°C even that the thermocouple used is under the influence of the highest exhaust temperature zone within the exhaust manifold which is T_3. The analysis of the exhaust gas temperature of individual cylinders proves it to be a helpful tool in detecting the fuel shortage and combustion faults within individual cylinders.

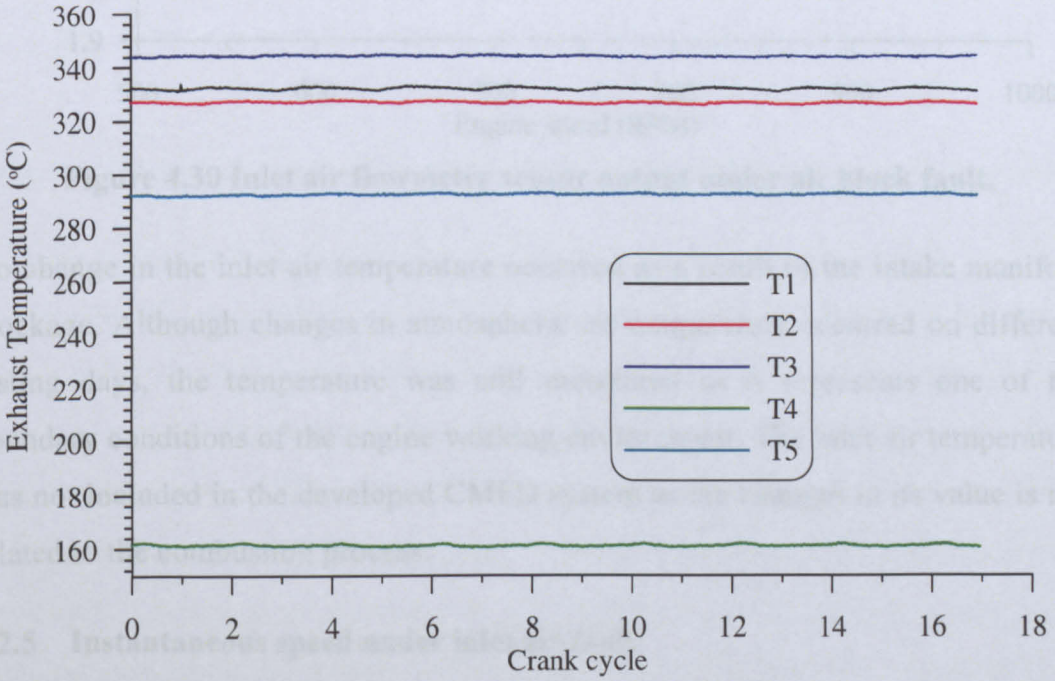

Figure 4.29 Exhaust gas temperature with 80% fuel block to cylinder 4, FLP 30%, load 111 Nm, speed 1081 RPM.

4.2.4 Inlet air condition under inlet air fault

The inlet air flow rate sensor provides a direct way of detecting an inlet air blocking fault, by detecting an increased pressure drop across intake manifold. The reduction in the air flow rate is directly measured by the Bosch flow rate sensor. Figure 4.30 shows the change in the inlet flowmeter sensor output with varying air starvation at any speed.

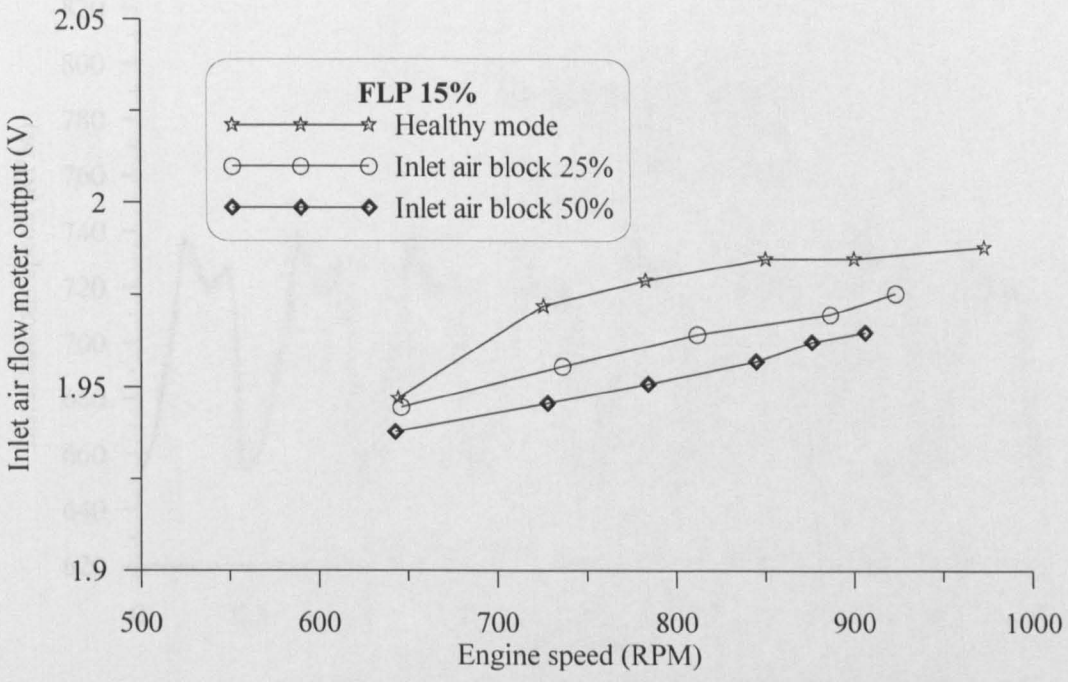

Figure 4.30 Inlet air flowmeter sensor output under air block fault.

No change in the inlet air temperature occurred as a result of the intake manifold blockage. Although changes in atmospheric air temperature occurred on different testing days, the temperature was still monitored as it represents one of the boundary conditions of the engine working environment. The inlet air temperature was not included in the developed CMFD system as the changes in its value is not related to the combustion process.

4.2.5 Instantaneous speed under inlet air fault

As a result of making the engine run under air starvation, the energy generated by the engine is expected to decrease, which will bring about a reduction in the instantaneous speed of the engine. This reduction can be used, in addition to the air flow parameter to evaluate and detect the engine condition under air starvation condition. Figure 4.31 shows that at low speed there is no significant change in the instantaneous speed due to increase in inlet air manifold blockage from 25% to 50%, however, there is a noticeable decrease in the resulting brake torque from 45 to 38 Nm. The drop in the brake torque was a direct result of shortage in available air for combustion in the cylinders.

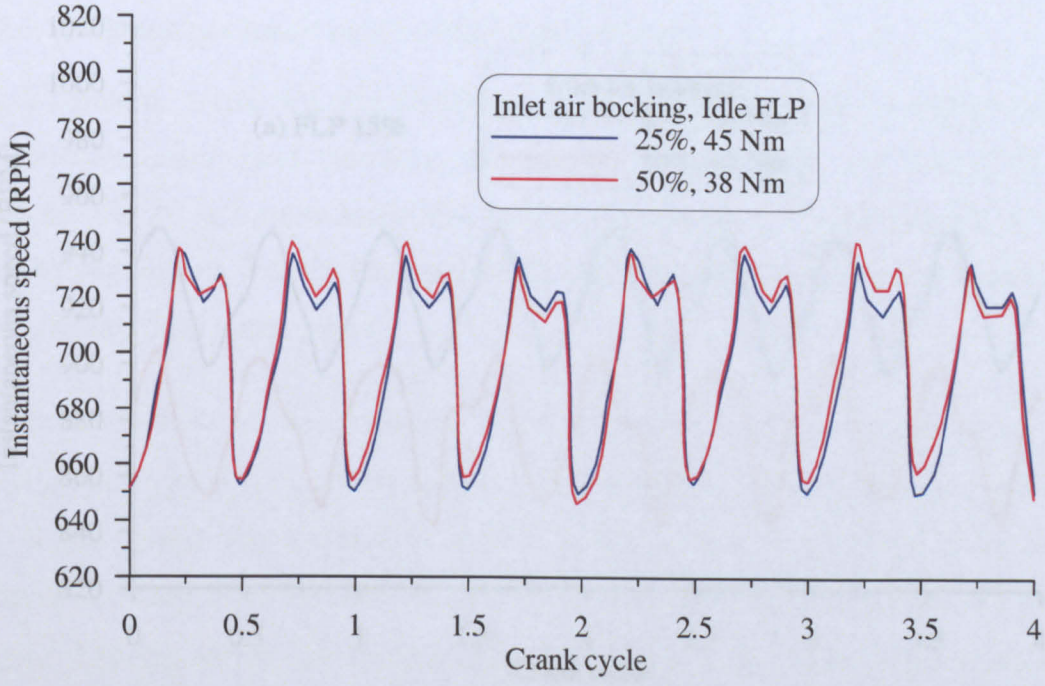

Figure 4.31 Instantaneous speed under inlet air fault at low crankshaft speed.

An increase in the fuel throttle (FLP setting) forces the engine average speed to increase by injecting more fuel to the engine. However, the available air in the engine cylinder controls the actual burnt mass of fuel. With the air inlet blocked the actual mass of fuel burnt is decreased, causing the average engine speed to fall. Figure 4.32 illustrate the effect of reducing the air inlet area of different FLP settings, under various load and speed conditions. Higher speed and brake load generated at lower inlet blocking at any setting of FLP. Similar results were obtained throughout the engine operating range, but only these two examples have been included. These results indicate a strong relationship between air inlet and engine performance, and highlight the use of instantaneous speed parameter to detect this type of engine fault.

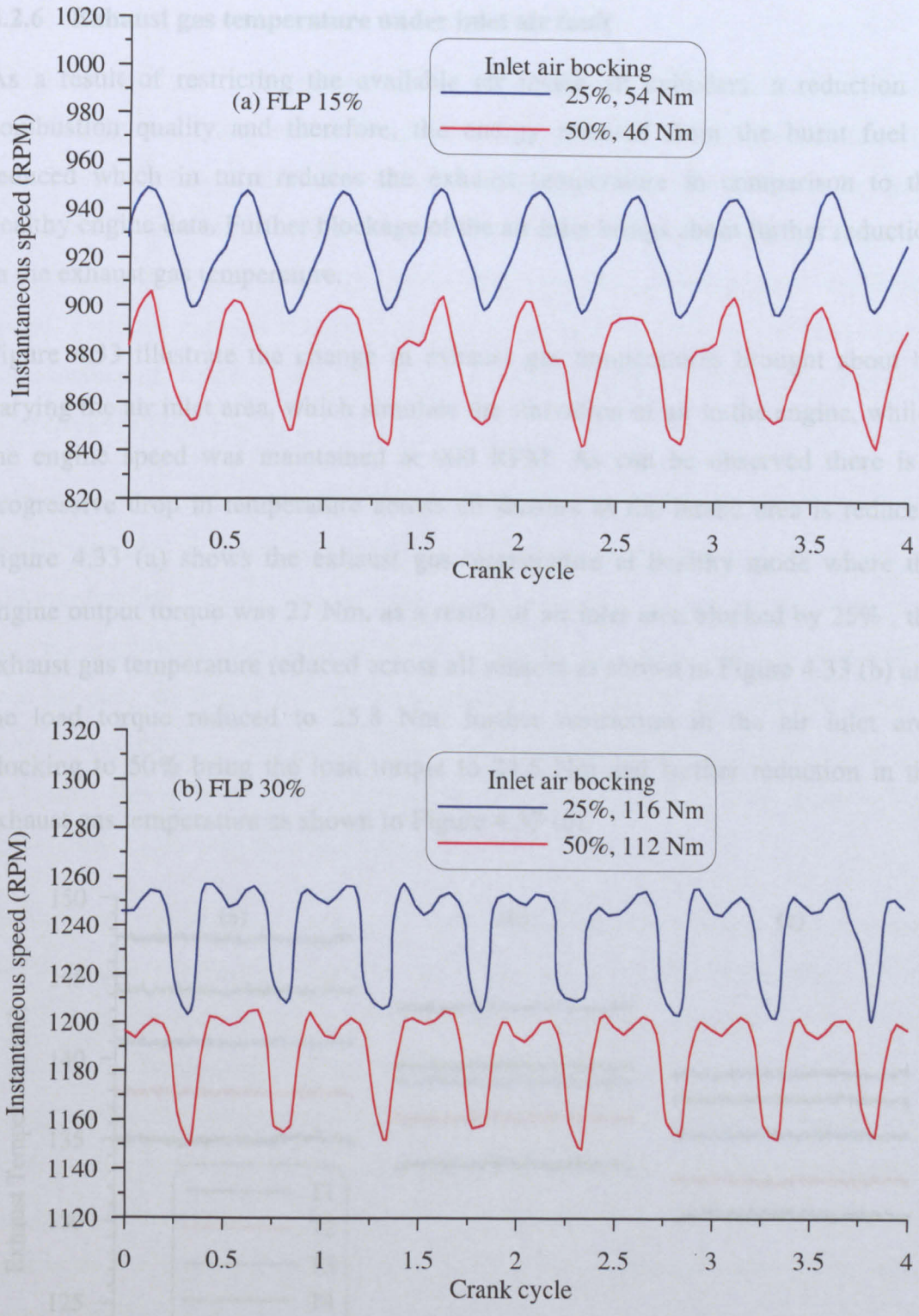

Figure 4.32 Instantaneous speed under inlet air fault at high crankshaft speed.

4.2.6 Exhaust gas temperature under inlet air fault

As a result of restricting the available air inside all cylinders, a reduction in combustion quality and therefore, the energy released from the burnt fuel is reduced which in turn reduces the exhaust temperature in comparison to the healthy engine data. Further blockage of the air inlet brings about further reduction in the exhaust gas temperature.

Figure 4.33 illustrate the change in exhaust gas temperatures brought about by varying the air inlet area, which simulate the starvation of air in the engine, whiles the engine speed was maintained at 900 RPM. As can be observed there is a progressive drop in temperature across all sensors as the intake area is reduced. Figure 4.33 (a) shows the exhaust gas temperature at healthy mode where the engine output torque was 27 Nm, as a result of air inlet area blocked by 25% , the exhaust gas temperature reduced across all sensors as shown in Figure 4.33 (b) and the load torque reduced to 25.8 Nm. further restriction in the air inlet area blocking to 50% bring the load torque to 24.5 Nm and further reduction in the exhaust gas temperature as shown in Figure 4.33 (c).

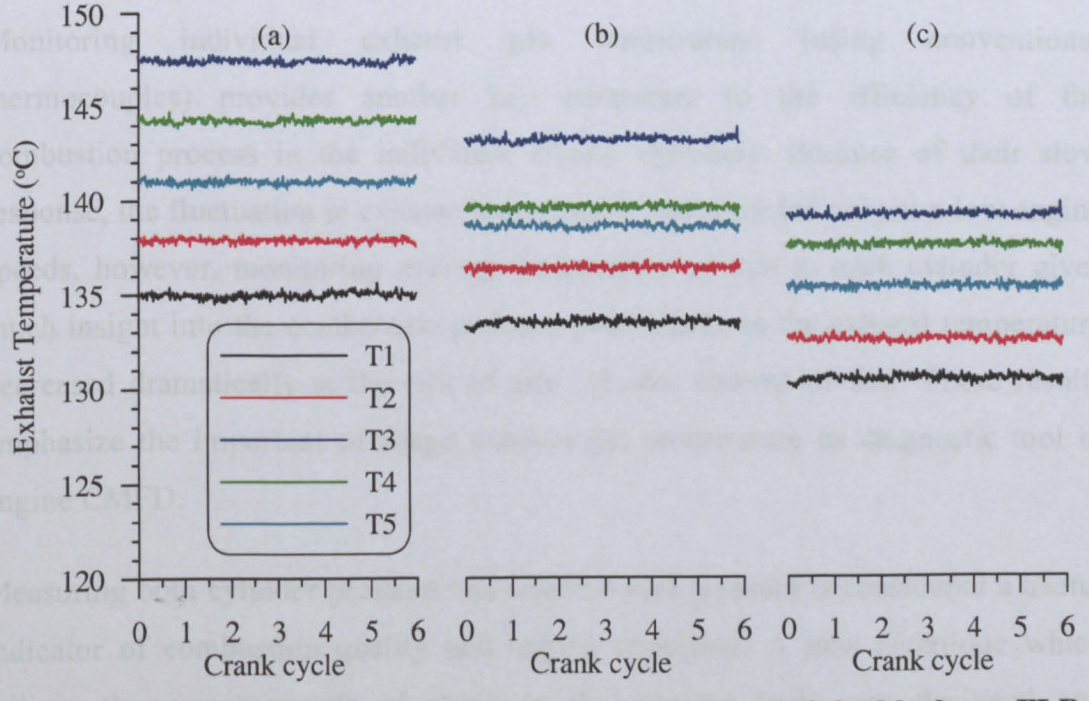

Figure 4.33 Exhaust gas temperature variation due to air inlet blockage, FLP 15%

4.3 SUMMARY

A detailed analysis of the measured experimental data for the diesel engine under both healthy and faulty modes of operation has been covered in this chapter. This was carried out with the purpose of evaluating the key parameters for faults identification within the combustion process which represents the focus interest of the present study. Several key parameters including instantaneous crankshaft speed, cylinder exhaust temperature, fuel lever position (FLP) and load torque, were evaluated, with a view to using them within intelligent CMFD algorithm that is addressed in Chapter 6.

Instantaneous speed measurement is considered a very parameter for use in the CMFD system, as it contains significant information about the engine condition and combustion process. In particular it is possible to detect a malfunction in an individual cylinder. By registering the instantaneous speed with the camshaft, it will be easy to detect a fault in a specific cylinder. It can also be used in conjunction with the inlet air flow rate reading to detect and evaluate any air inlet problems. Being relatively in expensive and easily installed (non-intrusive) the sensors used are a cost effective solution.

Monitoring individual exhaust gas temperature (using conventional thermocouples) provides another key parameter to the efficiency of the combustion process in the individual engine cylinders. Because of their slow response, the fluctuation in exhaust temperature was recorded only at a low engine speeds, however, monitoring average temperature at exit to each cylinder gives much insight into the combustion process, particularly as the exhaust temperature decreased dramatically at the exit of any cylinder starved of fuel. These results emphasize the important of usage exhaust gas temperature as diagnostic tool in engine CMFD.

Measuring both cylinder pressure and injected fuel pressure is considered a useful indicator of combustion quality and engine condition. A new technique which utilizes the measurements of strain in the injector body was designed and validated. The new sensor successfully measure both fuel and cylinder pressure. The main advantage of this technique is that no intrusive work is required for the installation.

However, a high sampling rate is required to accurately capture the pressure-time variation; a lower sampling rate was used within the present study to enable the data acquisition system to capture all engine measured parameters simultaneously. The data was used to evaluate the combustion quality in cylinder 4, and helps to diagnose cylinder faults.

CHAPTER 5

ENGINE MODELLING

Modelling of diesel engines for performance simulation and design has received much research attention in the recent yeas. In addition, with the recent rapid progress of microprocessor technology, it is feasible to use these models for real-time applications, such as state estimation, control and fault detection. However, there is need for further research in modelling techniques, to improve the predictive accuracy of the model to achieve more precise estimation and control.

Early studies into diesel engine modelling relied on the use of empirical data to develop linear dynamic models. These models link steady state experimental data representing engine thermodynamics and gas flow with simple dynamic models of the mechanical components. The major disadvantage of such quasi-linear models is their heavy reliance on experimental data. Furthermore, they poorly represent the transient response of the engine. More recently, non-linear engine simulation models using the filling and emptying method and the method of characteristics have been developed for the purpose of engine design and performance predictions, Watson and Janota, [1982]; Heywood, [1988]; Assanis et al., [1997].

Many models have been developed for the purpose of engine control and parameter estimation. One of these models known as the mean value model, was introduced by Jensen et al., [1991]. This model consists of several empirical algebraic and first-order differential equations in order to achieve a real-time implementation. The main drawback of this type of model is the requirement for empirical test data to fit the model equations and evaluate the suitable model constant values. Another diesel engine model for electronic control was developed by Watson, [1984], where the in-cylinder combustion process was included using a single-zone model and filling and emptying modelling technique. Watson, [1984], introduces several modifications to this model to cut down the computational time; however, it does not predict in-cycle crankshaft angular speed variations. Kao and Moskwa, [1995], introduce a hybrid of two engine models based on a mean torque production model and a simplified cylinder-by-cylinder

model. The hybrid model was investigated in order to provide control engineers with tools for developing control and diagnostic algorithms. The implementation of the mean torque model required empirical test data to fit the model equations; however the simplified cylinder-by-cylinder model is not able to predict accurately the in-cycle variations of the engine states.

In this study, a combined dynamic and thermodynamic engine model is developed and used to predict the in-cycle variation of the engine states. To enable the study of the engine behaviour under loading, a dynamic dynamometer model is also included. Engine events for control and performance estimation are generally periodic with respect to crank angle rather than time, and hence the engine model is totally based on the crank angle domain. The proposed model does not require any empirical inputs for engine performance and takes into consideration the inertia variations of the crankshaft assembly with piston pin offset. The model treats the four stroke cylinder cycle and the manifolds as thermodynamic control volumes by using the filling and emptying method, solving energy and mass conservation equations with subsystem for combustion and heat transfer. The model will be constructed in MATLAB/SIMULINK environment.

In order to construct the model from the basic governing equations, a single cylinder model was initially developed, which represents the main unit in the multi-cylinder engine. As the available engine comprises 4-cylinders, the single cylinder model was tested and validated using experimental results derived from the pressure signal only which is measured within cylinder 4. The single cylinder engine model (SCEM) was utilized to construct the four cylinder engine model (FCEM) assuming that it consists of four identical cylinders working with a phase shift corresponding to the firing order. A modification was required in the SCEM to match the optimum performance of the FCEM, such as the crankshaft balancing under the forces produced from the different cylinders.

The SCEM consists of both dynamic and thermodynamic balancing system. The dynamic part of the model computed the forces relationship of all moving parts of the engine whether rotating or translating. From the resulting equations it was possible to predict the engine indicated torque. The inputs of the dynamic subsystem are crank angle and cylinder pressure and include constants for mass

and inertia. Using the defined engine relationships, the model can predict the instantaneous crankshaft speed variation. The dynamic model was integrated with a simplified formula to estimate the friction torque as a function of engine speed to improve the computed inertia variations of the crankshaft assembly, Rakopoulos and Giakoumis, [1998].

The thermodynamic model is based on the filling and emptying method. Three thermodynamic control volumes are considered: the inlet manifold, the cylinder and the exhaust manifold. A schematic diagram of the engine is shown in Figure 5.1. Equations for the mass and energy conservation, gas property relations and perfect gas law are solved in the crank angle domain. A single-zone combustion model is used for predicting the theoretical fuel burning rate. The cylinder is treated as a single control volume with homogenous temperature and pressure through the whole thermodynamic cycle. The thermodynamic sub-model inputs are the inlet air conditions, crankshaft speed and applied load on the engine.

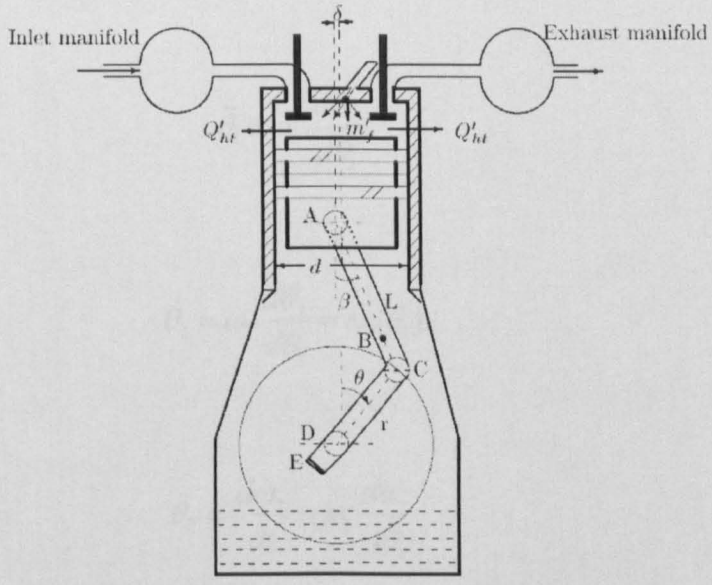

Figure 5.1. Single-cylinder diesel engine.

5.1 DYNAMIC MODELLING

Figure 5.2 shows a simplified model of an engine coupled to a dynamometer. The time domain model was firstly discussed by Zweiri et al., [1998], then a more discussion of the different friction sources were covered in Zweiri et al., [1999]. The time domain adds difficulties for the engine simulation where all the

movements should be defined in the same domain. Crank angle was found to be a more suitable domain for internal engine analysis as most of the simulation parameters are related to the crank angle.

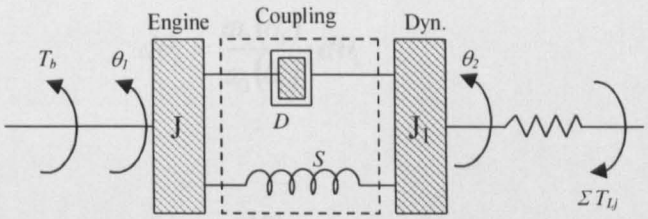

Figure 5.2. Engine coupled to a dynamometer; Zweiri et al., [1999].

To develop an engine dynamic model in the crank angle domain, the crankshaft angle θ_1 is selected to be the independent variable. The coordinate transformations are as follows, Wang et al., [1997]

$$\dot{\theta}_1 = \frac{d\theta_1}{dt} = \omega_1(\theta_1) \tag{5-1}$$

$$\ddot{\theta}_1 = \omega_1 \frac{d\omega_1}{d\theta_1} \tag{5-2}$$

$$\dot{\theta}_2 = \omega_1 \frac{d\theta_2}{d\theta_1} = \omega_2(\theta_1) \tag{5-3}$$

$$\ddot{\theta}_2 = \frac{d\omega_2}{dt} = \omega_1 \frac{d\omega_2}{d\theta_1} \tag{5-4}$$

Where t is time, ω_1 is the angular velocity of the engine crankshaft and ω_2 is the angular velocity of the dynamometer shaft. The relationship between the dynamometer angular position θ_2 and the independent variable θ_1, the crank shaft angular position, is given by:

$$\omega_2(\theta_1)=\omega_1(\theta_1)\frac{d\theta_2}{d\theta_1}$$

$$d\theta_2=\frac{\omega_2(\theta_1)}{\omega_1(\theta_1)}\cdot d\theta_1$$

$$\therefore \theta_2=\int\frac{\omega_2}{\omega_1}\cdot d\theta_1 \qquad \textbf{(5-5)}$$

Depending on this domain transformation and utilizing the Lagrangian principles, the two equations, describing the dynamics of the system in crank angle domain, can be derived as follows

$$\dot{\omega}_1=\frac{1}{J}\left\{T_i(\theta_1)-\frac{1}{2}\cdot\frac{\partial J(\theta_1)}{\partial\theta_1}\cdot\omega_1^2-T_r-\sum T_f-T_S-T_D\right\} \qquad \textbf{(5-6)}$$

$$\dot{\omega}_2=\frac{1}{J_1}(T_D+T_S-T_L) \qquad \textbf{(5-7)}$$

where T_i is the indicated torque, T_f is the mechanical friction torque, T_r is the reciprocating torque, T_L is the applied external load torque, T_S and T_D are the stiffness and damping torque for the dynamometer, J is engine inertia, and J_1 is the dynamometer inertia.

The indicated engine torque T_i, is generated by the conversion of the chemical energy to thermal energy and then into mechanical energy, via the combustion process. The relationship between the indicated torque and the indicated pressure P in the cylinder at any crank shaft position θ_1 is given by the following relation:

$$T_i=(P-P_{atm})A_p rG(\theta_1) \qquad \textbf{(5-8)}$$

where the factor, G, is a function of the piston and cylinder geometry

$$G(\theta_1) = \frac{\sin(\theta_1 + \beta)}{\cos\beta} \tag{5-9}$$

where β is the connection rod angle, r is the crank radius (equal to half of the stroke), L is the connecting rod length, δ is the pin offset, which is very important to balancing forces acting on the piston, and ϕ is the connecting rod angle when the piston is at the top dead centre position. Refer to Figure 5.3.

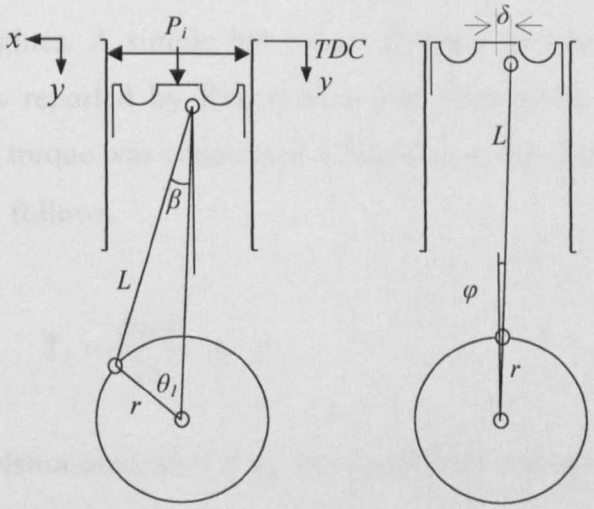

Figure 5.3. Piston-cylinder mechanism including forces and dimensions.

The piston displacement y, is defined as the distance between the piston location at any crank angle and the top dead centre. From the piston-crank geometry (referring to Figure 5.3) y can be given by the following relationship, as a function of the crank angle.

$$y = \sqrt{(r+L)^2 - \delta^2} - [L\cos\beta + r\cos(\theta_1 - \phi)] \tag{5-10}$$

Where the angles ϕ and β are given by

$$\phi = \sin^{-1}\frac{\delta}{r+L} \tag{5-11}$$

$$\beta = \sin^{-1}\frac{\delta + r\sin(\theta_1 - \phi)}{L} \tag{5-12}$$

The mechanical friction torque T_f represents the reduction in the brake output torque due to the mechanical friction in all the moving parts in the engine. Zweiri et al., [2000], introduced a detailed model for the instantaneous friction estimation in different engine parts. This model contains sophisticated detail of the engine lubrication system, bearings, valve train, piston rings, and auxiliaries gears losses. Therefore, many constant values will be required that is usually not available for the commercial engines. A simple but robust formula for the calculation of the friction torque was reported by Rakopoulos and Giakoumis, [1998] where the mechanical friction torque was considered a function of the friction mean effective pressure (*fmep*) as follows.

$$T_f = \frac{fmep}{2\pi} \cdot A_p \cdot r \tag{5-13}$$

where A_p is the piston area and r is the crankshaft radius. The friction mean effective pressure was correlated as a function of engine speed (RPM) and compression ration of the engine.

$$fmep = 0.123 \times CR + 4.774 \times 10^{-4} N \quad \text{(Bar)} \tag{5-14}$$

This formula was used within the present study for its simplicity and validity with the steady state operation mode.

The reciprocating torque T_r, is the torque produced by the motion of the piston assembly including the small end of the connecting rod and is given by:

$$T_r = MrG(\theta_1)\ddot{y} \tag{5-15}$$

The second derivative of the piston displacement can be calculated by differentiating equation (5-10) with respect to time, then the reciprocating torque becomes

$$T_r = MrG(\theta_1)\left[G_1(\theta_1)\dot{\theta}_1^2 + G_2(\theta_1)\ddot{\theta}_1\right] \tag{5-16}$$

where M is mass of the piston assembly including the small end of the connecting rod, and $G_1(\theta_1)$ and $G_2(\theta_1)$ are functions of the engine geometry:

$$G_1(\theta_1) = r\left\{\cos(\theta_1 - \phi)\cdot\left[1 + \frac{(r/L)\cdot\cos(\theta_1 - \phi)}{\sqrt{\lambda(\theta_1)^3}}\right] - \sqrt{\frac{1-\lambda(\theta_1)}{\lambda(\theta_1)}}\cdot\sin(\theta_1 - \phi)\right\} \tag{5-17}$$

$$G_2(\theta_1) = r\left\{\sin(\theta_1 - \phi) + \sqrt{\frac{1-\lambda(\theta_1)}{\lambda(\theta_1)}}\cdot\cos(\theta_1 - \phi)\right\} \tag{5-18}$$

where λ is a geometric factor which is defined as follows:

$$\lambda = 1 - \sin^2\beta \tag{5-19}$$

The torsional stiffness torque T_S, and the damping torque T_D, at the coupling between the engine and the dynamometer are given by

$$T_S = S(\theta_1 - \theta_2) \tag{5-20}$$

and

$$T_D = D(\dot{\theta}_1 - \dot{\theta}_2) \tag{5-21}$$

where, S and D are stiffness and damping coefficients respectively of the coupling between the engine and the dynamometer.

5.1.1 Inertia variation

Reciprocating mechanisms have variable inertia due to the change of geometry through a crank revolution. The piston and connecting rod masses change their position relative to the crankshaft axis and hence change the effective inertia about this axis. The same path is followed by these parts during each revolution of the crankshaft and thus the inertia variation is smooth and periodic. The variable

inertia, as a function of crankshaft position, is used with respect to the crank shaft rotational axis. For a given crank angle, the inertia (with respect to the centre line of the crankshaft) is defined by considering the equivalent inertia of piston, connecting rod and crankshaft assembly. For more details reader can refer to, Rao, [1990]; Hesterman and Stone, [1994]; Drew et al., [1999]; and Li and Stone, [1999]. In this model, the piston pin offset is taken into account during the analysis of the variable inertia. The crank angle varying inertia of an engine crankshaft assembly is derived in detail by Hesterman and Stone, [1994], and can be calculated using the following equation.

$$\begin{aligned} J(\theta_1) = J_C + m_C(b_2 r)^2 + J_R\left[\left(\frac{r}{L}\right)^2 \frac{1}{\lambda(\theta_1)}\cos^2\theta_1\right] \\ + m_P r^2\left[\sqrt{\frac{1-\lambda(\theta_1)}{\lambda(\theta_1)}}\cos\theta_1 + \sin\theta_1\right]^2 \\ + m_R r^2(1-b_1)^2\cos^2\theta_1 + m_R r^2\left[b_1\sqrt{\frac{1-\lambda(\theta_1)}{\lambda(\theta_1)}}\cos\theta_1 + \sin\theta_1\right]^2 \end{aligned} \tag{5-22}$$

and

$$\begin{aligned} \frac{\partial J(\theta_1)}{\partial\theta_1} = 2J_R\left[\left(\frac{r}{L}\right)^3 \frac{\sqrt{1-\lambda(\theta_1)}}{\lambda(\theta_1)^2}\cos^3\theta_1 - \left(\frac{r}{L}\right)^2 \frac{1}{\lambda(\theta_1)}\cos\theta_1\right] \\ - 2m_R(1-b_1)^2 r^2\cos\theta_1\sin\theta_1 \\ + m_R r^2\left[b_1\sqrt{\frac{1-\lambda(\theta_1)}{\lambda(\theta_1)}}\cos\theta_1 - \sin\theta_1\right]\left\{\begin{array}{l} -\left[\frac{rb_1}{L\sqrt{\lambda(\theta_1)^3}}\right]\cos^2\theta_1 \\ -\cos\theta_1 + b_1\sqrt{\frac{1-\lambda(\theta_1)}{\lambda(\theta_1)}}\sin\theta_1 \end{array}\right\} \\ + m_P r^2\left[\sqrt{\frac{1-\lambda(\theta_1)}{\lambda(\theta_1)}}\cos\theta_1 + \sin\theta_1\right]\left\{\begin{array}{l} \left[\frac{r}{L\sqrt{\lambda(\theta_1)^3}}\right]\cos^2\theta_1 \\ -\cos\theta_1 + \sqrt{\frac{1-\lambda(\theta_1)}{\lambda(\theta_1)}}\sin\theta_1 \end{array}\right\} \end{aligned} \tag{5-23}$$

Where J_C is the moment of inertia of the crankshaft, J_R is the moment of inertia of the connecting rod, m_C is the mass of the crankshaft, m_R is the mass of the connecting rod, m_P is the mass of the piston, b_1 is the length ratio of the CB to CA and b_2 is the length ratio of ED to DC as shown in Figure 5.1.

5.1.2 Cylinder volume and surface area

Referring to the piston–crank mechanism, shown in Figure 5.3, and using the geometrical relationships between the different parts, their dimensions and relative motions, the cylinder volume is calculated at any crankshaft angle using the following equation.

$$V = \frac{V_d}{c-1} + \frac{\pi d^2}{4}\left[\sqrt{(r+L)^2 - \delta^2} - \{L\cos\beta + r\cos(\theta_1 - \phi)\}\right] \qquad \textbf{(5-24)}$$

In addition, the internal surface area of the cylinder through which the heat transfer to the surrounding is determined by

$$A = \alpha\frac{\pi d^2}{4} + \pi d\left[\sqrt{(r+L)^2 - \delta^2} - \{L\cos\beta + r\cos(\theta_1 - \phi)\}\right] \qquad \textbf{(5-25)}$$

where $\alpha > 2$ for a non-flat piston and cylinder head and $\alpha = 2$ for a flat piston top and cylinder head bottom. The variation of the cylinder volume with respect to the crankshaft angle can be evaluated by derivation of equation (22) as follows

$$V' = \frac{\pi d^2}{4} r\left[\sin(\theta_1 - \phi) + \frac{\cos(\theta_1 - \phi)[\delta + r\sin(\theta_1 - \phi)]}{\sqrt{L^2 - [\delta + r\sin(\theta_1 - \phi)]^2}}\right] \qquad \textbf{(5-26)}$$

5.2 THERMODYNAMIC MODELLING

The foundation of the diesel engine simulation is the physically-based, thermodynamic, zero-dimensional model introduced by Assanis and Heywood, [1986]. In the simulation, the diesel four-stroke cycle was treated as a sequence of continuous processes: intake, compression, combustion (including expansion), and exhaust. The system of interest is the instantaneous contents of a cylinder. In

general, this system was opened to the transfer of mass, enthalpy, and energy in the form of work and heat. Throughout the cycle, the cylinder is treated as a variable volume plenum, spatially uniform in pressure. Furthermore, the cylinder contents are represented as one continuous medium by defining an average equivalence ratio and temperature in the cylinder at all times.

Quasi-steady, adiabatic, one-dimensional flow equations are used to predict mass flows past the intake and exhaust valves. The intake manifold and the exhaust port are treated as plenums whose pressure and temperature history are specified. The compression process is defined so as to include the ignition delay period, i.e. the time interval between the start of the injection process and the ignition point. The total length of the ignition delay is related to the mean cylinder gas temperature and pressure during this delay period.

Combustion is modelled as a uniformly-distributed heat release process that is assumed to be proportional to the rate of fuel burning which is modelled empirically. Since the diesel combustion process is comprised of a pre-mixed and diffusion-controlled combustion mechanism, the total fuel injected is considered to be the sum of two algebraic functions, one for each combustion mechanism. The fraction of the total fuel injected that is burnt by either mechanism depends on the length of the ignition delay period and the engine load and speed.

Heat transfer is included in all of the engine processes. Convective heat transfer was modelled using an available engine correlation based on turbulent flow in pipes. Radiative heat transfer was added during combustion and exhaust. The combustion chamber surface temperature of the piston, cylinder head, and liner can be either specified or calculated from a specification of the wall structure and energy balance around the wall.

The filling and emptying method was selected to be the basis of the proposed model, where three thermodynamic control volumes are considered: the inlet manifold, the cylinder and the exhaust manifold. A schematic diagram of the engine with the control volume is shown in Figure 5.4. This method ignores the effect of pressure waves inside the control volumes and treats the gases as a homogeneous mixture of ideal gases which are assumed to have a uniform

temperature and pressure at each instant in time. Therefore, the instantaneous state of the mixture is only dependent on the temperature, pressure, and equivalence ratio. Moreover, the mass flows across the boundary of the combustion chamber, during the period when the intake and exhaust valves are closed, are assumed to be limited to the fuel injected to the cylinder. In addition, the injected fuel is assumed to instantaneously evaporate, Watson and Janota, [1982]; and Watson, [1984]. In the following section, a detailed derivation of the governing equation for the thermodynamic model will be carried out.

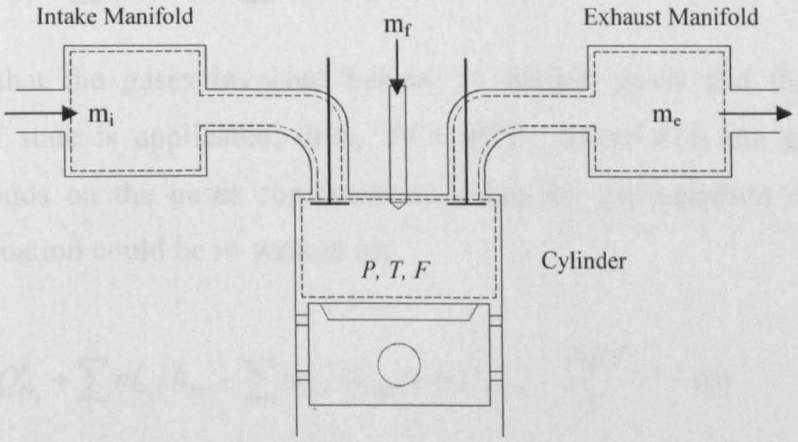

Figure 5.4. Schematic of the engine control volumes.

5.2.1 Conservation of mass and energy

In general, the first law of thermodynamics for open system with respect to time can be written as:

$$U' = Q' - W' + \sum H'_{oi} \qquad \textbf{(5-27)}$$

Where, U is the internal energy, Q heat transfer through system boundary, W work done by the system, H_o the total stagnation enthalpy and i subscript donates different control volume. This equation could be re-written as

$$(mu)' = \sum_j Q'_j - P \cdot V' + \sum m'_i \cdot h_{oi} \qquad \textbf{(5-28)}$$

where the subscript j denotes surface with different rate of heat transfer, m mass, P pressure, T temperature, h_o the specific stagnation enthalpy, u specific internal energy.

Note: Q includes the heat released by combustion, $\sum m_i' \cdot h_{oi}$ represents the enthalpy fluxes through the intake and exhaust valves as well as the enthalpy flux associated with fuel injection.

$$m \cdot u' + u \cdot m' = \sum_j Q_j' - P \cdot V' + \sum m_i' \cdot h_{oi} \qquad \textbf{(5-29)}$$

$$= \sum_j Q_{ht_j}' - P \cdot V' + \sum m_{in}' \cdot h_{oin} - \sum m_{out}' \cdot h_{oout} + m_f' \cdot h_{for}$$

$$mu' = \sum_j Q_{ht_j}' + \sum m_{in}' \cdot h_{oin} - \sum m_{out}' \cdot h_{oout} + m_f' \cdot h_{for} - P \cdot V' - um' \qquad \textbf{(5-30)}$$

Assuming that the gases involved behave as perfect gases and the ideal gas equation of state is applicable, then, $PV = mRT$, where R is the gas constant which depends on the gases composition. Using the gas equation of state, the previous equation could be re-written as,

$$mu' = \sum_j Q_{ht_j}' + \sum m_{in}' \cdot h_{oin} - \sum m_{out}' \cdot h_{oout} + m_f' \cdot h_{for} - \frac{mRT}{V} V' - um' \qquad \textbf{(5-31)}$$

Hence, the specific internal energy variation with time will be:

$$u' = \left(\begin{array}{c} \sum_j Q_{ht_j}' + \sum m_{in}' \cdot h_{oin} - \sum m_{out}' \cdot h_{oout} \\ + m_f' \cdot h_{for} - um' \end{array} \right) \cdot \frac{1}{m} - \frac{RT}{V} V' \qquad \textbf{(5-32)}$$

Watson and Janota, [1982] and Watson, [1984], shows that the internal energy could be assumed as a function of the temperature T and the equivalence ratio F. The effect of pressure will be neglected since the effect of gas dissociation is considered very small and will be neglected; therefore, the specific internal energy could be expressed as:

$$u = u(T, F) \qquad \textbf{(5-33)}$$

This relationship has been proven empirically in the study introduced by Watson and Janota, [1982]. Using a curve fitting of combustion product experimental data as a continuous function, the results show that the internal energy can be calculated using the following empirical equation.

$$u = \frac{k_1(T) - k_2(T) \cdot F}{1 + f_s F} \quad \text{(kJ/kg)} \tag{5-34}$$

where

$$k_1(T) = 0.692T + 39.17 * 10^{-6} T^2 + 52.9 * 10^{-9} T^3 - 228.62 * 10^{-13} T^4 + 277.58 * 10^{-17} T^5 \tag{5-35}$$

and

$$k_2(T) = 3049.39 - 5.7 * 10^{-2} T - 9.5 * 10^{-5} T^2 + 21.53 * 10^{-9} T^3 - 200.26 * 10^{-14} T^4 \tag{5-36}$$

This empirical equation for the internal energy calculation was accepted within the following range of temperatures and equivalence ratios:

$250 < T < 2400$ K and $0 < F < 1.6$, where $F = 0$ for air and $F > 0$ for combustion products.

Using equations (5-32) and (5-33), then

$$\frac{\partial u}{\partial T} T' + \frac{\partial u}{\partial F} F' = \left(\begin{array}{c} \sum_j Q'_{ht_j} + \sum m'_{in} \cdot h_{oin} - \sum m'_{out} \cdot h_{oout} \\ + m'_f \cdot h_{for} - um' \end{array} \right) \cdot \frac{1}{m} - \frac{RT}{V} V' \tag{5-37}$$

This equation is re-arranged to obtain the rate of change of temperature for each control volume as follows:

$$T' = \left\{ \left(\begin{array}{l} \sum_j Q'_{ht_j} + \sum m'_{in} \cdot h_{oin} \\ - \sum m'_{out} \cdot h_{oout} \\ + m'_f \cdot h_{for} - um' \end{array} \right) \cdot \frac{1}{m} - \frac{RT}{V} V' - \frac{\partial u}{\partial F} F' \right\} \Big/ \frac{\partial u}{\partial T} \tag{5-38}$$

Knowing that R is the gas constant for the gas mixture of the air and burned fuel which could be given by the following equation as function of equivalence fuel to air ratio F, and the stoichiometric fuel-air ratio f_s, which is given the value

0.0676 for the average hydrocarbon composition of diesel fuel (C_nH_{2n}), Watson, [1982].

$$R = \frac{0.287 + 0.02F}{1 + f_s F} \tag{5-39}$$

$$F = \frac{f}{f_s} \tag{5-40}$$

where, f is the actual fuel-air ratio.

The equivalence fuel-air ratio is a function of time, where the amount of burning fuel changed with time from zero before the start of combustion until its maximum value at the end of the combustion process in the cylinder. To evaluate the variation of equivalence ratio with respect to time, applying the mass conservation law for both air and fuel using the total mass,

$$m = m_a + m_{bf} \tag{5-41}$$

where m_a is the air mass and m_{bf} is the mass of burnt fuel. Solving equations (5-40) and (5-41), the mass of the burnt fuel is evaluated as,

$$m_{bf} = \frac{mFf_s}{1 + Ff_s} \tag{5-42}$$

By differentiating this equation with respect to time and rearranging for the rate of equivalence ratio change, then

$$F' = \left(\frac{1 + f_s F}{m}\right)\left(\frac{1 + f_s F}{f_s} m'_{bf} - Fm'\right) \tag{5-43}$$

5.2.2 Ports and valves mass flow rates

In order to model the flow process, across the ports and valves through intake and exhaust, a one-dimensional model was used. This model used the analogy of an

orifice having an equivalent area of the valve or port passage. Appling the energy equation from upstream to downstream for isentropic steady flow, and assuming that the inlet velocity is very small and can be neglected for subsonic flow, where $P_d/P_u > [2/(\gamma+1)]^{\gamma/(\gamma-1)}$, the mass flow rate has the form

$$m' = C_d A_v P_u \sqrt{\left(\frac{2\gamma}{\gamma-1}\right)\frac{1}{RT_u}\left[\left(\frac{P_d}{P_u}\right)^{2/\gamma} - \left(\frac{P_d}{P_u}\right)^{\gamma+1/\gamma}\right]} \qquad \textbf{(5-44)}$$

where C_d is the discharge coefficient, γ is the specific heat ratio and A_v is the valve or port area. The discharge coefficient value depends on the curtain area of the valve as s function of the valve lift to valve diameter ratio. For more detail refer to, Heywood, [1988]

Under some operating conditions, the flow would be sonic flow, i.e. when the pressure ratio become ($P_d/P_u \le [2/(\gamma+1)]^{\gamma/(\gamma-1)}$). Under such condition the mass flow rate equation would be

$$m' = C_d A_v P_u \sqrt{\frac{\gamma}{RT_u}\left(\frac{2}{\gamma+1}\right)^{(\gamma+1)/(\gamma-1)}} \qquad \textbf{(5-45)}$$

For cylinder valves, throttles and other control valves where pressure ratios can be large, it is essential to use equations (5-44) or (5-45) as compressible effects can be significant. In order to use the orifice equations, the area and discharge coefficient (or loss factor) must be known for the constricting part of the pipe, in this case a cylinder valve. Another example is a control valve, where the orifice areas varies with time and losses vary with area.

For cylinder valves the variation of flow area is determined by the cam profile and for a particular engine the variation of area will normally be available from measurements in the form of area versus crank angle curves, for inlet and exhaust valves, as shown in Figure 5.5. Often the curves give effective area ($A_v \cdot C_d$) as this can easily be derived from combining test rig measurements of flow with the use of equations (5-44) and (5-45) in reverse. Deriving effective area curves in this

way avoids difficult problems of separately determining actual flow area through the valve and the discharge coefficient. Some organizations prefer to express valve profiles by valve lift versus crank angle, with associated area-lift and C_d -lift curves. The data still coming from flow rig measurements. In this case, care has to be taken in defining 'flow area' as actual flow area through a valve varies with lift in a complex way. Frequently an approximation to flow area is used, the associated C_d values then accounting for the approximation. One common approach is to use the 'curtain area', which is simply defined as

$$\text{Curtain Area} = \pi DL \qquad \textbf{(5-46)}$$

where D is valve head diameter and L the valve lift from flow measurements, C_d values can be obtained again using the orifice equations in reverse. However, it is important to realize that these C_d values go with the curtain areas of (5-46) and must not be used with other definitions of flow area, which will need their own set of C_d-lift curves. By using equations (5-44) and (5-45) in a model the effective flow area is obtained each time step from look-up tables of either effective flow area versus crank angle, or lift versus crank angle with an associated C_d-lift table, using linear interpolation. The pressure ratio is determined by the pressures in the cylinder and either inlet or exhaust manifold at the time step. For steady state operation this is all the data that is often required, but for transient modelling additional information will be needed for the valve's response rate as a real valve will not respond instantaneously to changing conditions. Such information will also be needed for steady state modelling if the valve has a sufficiently fast response to respond to in-cycle changes in engine conditions. For this study the method of effective valve area was used for its simplicity and suitability for the transient modelling.

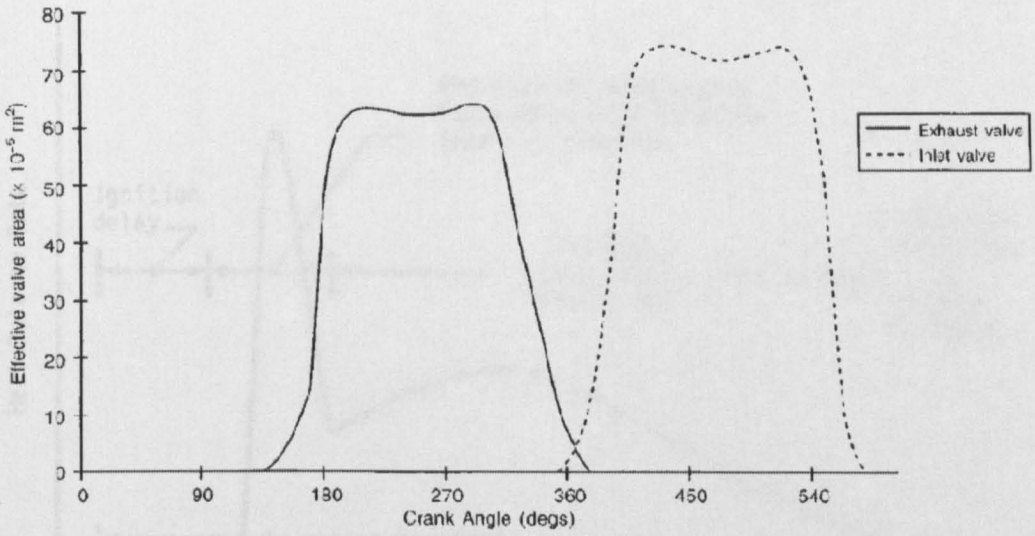

Figure 5.5 Valve effective area profiles, Baranescu, [1999].

5.2.3 Combustion

Combustion is considered as the most important operation in the internal combustion engine where it is responsible for the generation of the thermal energy by burning of the fuel, and then converted to mechanical energy due to engine processes. Many models have been discussed in the literature to simulate this complicated non-linear process, e.g. Watson and Marzouk, [1978]; Watson and Janota, [1982]; Heywood, [1988] and Ramos, [1989]. The single-zone model which is proposed by Watson, [1984] was selected in the present study, because it has wide acceptance and used to predict both pre-mixed and diffusion modes of combustion, as shown in Figure 5.6, to construct the total heat release period due to combustion. These two modes are assumed to proceed concurrently from the ignition point during the combustion period. Initially, the pre-mixed combustion is considered to consume most of the evaporated fuel present in the combustion chamber at the end of the ignition delay period until the fuel air mixture that was prepared and ready to burn prior to ignition is exhausted. The combustion process is then assumed to continue only in the diffusion mode until the end of combustion.

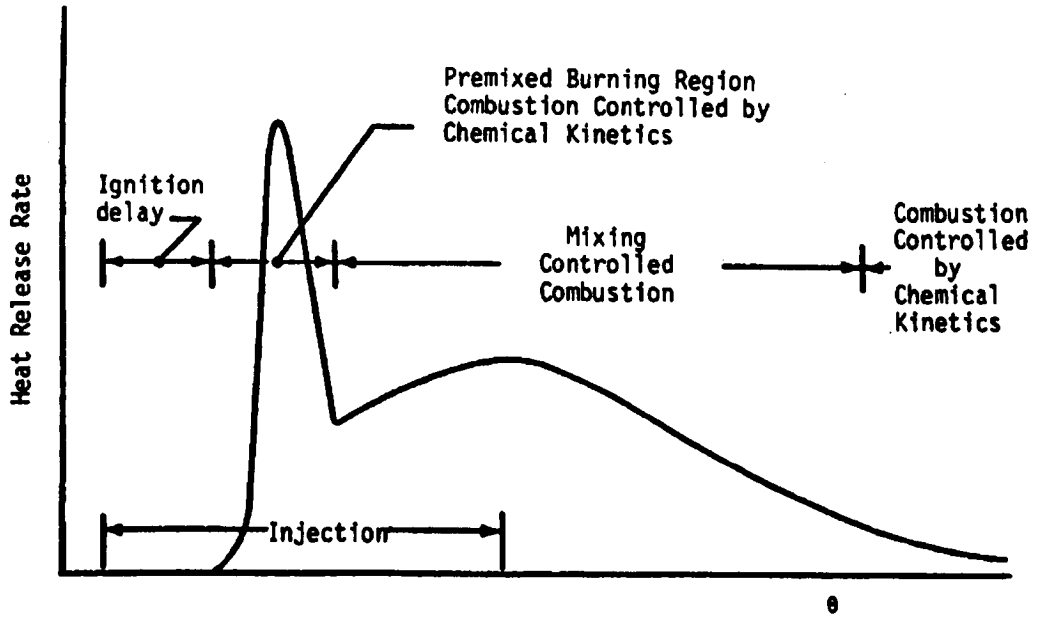

Figure 5.6 Schematic of the heat release in the direct-injection diesel engine, Ramos, [1989]

The ignition delay (ID), which is defined as the time between the start of fuel injection into the combustion chamber and fuel ignition, should be considered in studying the combustion process (determined from the change in slope on the P-θ diagram, or from a heat release analysis of the $P(\theta)$ data). This period is considered as a function of the cylinder pressure and temperature and could be calculated using the following equation given, by Heywood, [1988].

$$ID = 3.45\left(\frac{P}{101.3}\right)^{-1.02} e^{2100/T} \quad \text{(ms)} \qquad \textbf{(5-47)}$$

where P is the cylinder pressure (kPa) and T is the temperature (K).

The values of the different constants in the previous equations were selected based on studies where the fuel was injected into a uniform air environment, where pressure and temperature the only variables. In an engine, pressure and temperature change during the delay period due to compression resulting from piston motion. To account for the effect of changing conditions on the delay the following relationship is usually used:

$$\int_{\theta_{inj}}^{\theta_{ign}} \left(\frac{d\theta}{ID} \right) = 1 \qquad \textbf{(5-48)}$$

where θ_{inj} is the angle at injection and θ_{ign} is the angle at ignition.

Watson, [1984], modelled the combustion process using an empirical relationship that has the advantage of using constants that were developed from a huge number of tests for different engines over a wide range of operating conditions. This approach depended on prediction of the apparent fuel burning rate (the rate at which fuel must be burnt given the assumptions regarding equilibrium thermodynamic, homogeneity, etc), and required matching of experimentally determined cylinder pressure diagrams. The result of calculating and curve fitting of a large number of fuel burning rate diagrams over the two burning modes showed that the relation between the total fuel burning rate and the burning rate in each mode has the following form

$$\left(m'_f\right)_{norm} = \beta \cdot \left(m'_f\right)_{pre} + (1-\beta) \cdot \left(m'_f\right)_{diff} \qquad \textbf{(5-49)}$$

Where $\left(m'_f\right)_{norm}$ is the normalized total fuel burning rate, $\left(m'_f\right)_{pre}$ is the normalized fuel burning rate in the premixed mode and $\left(m'_f\right)_{diff}$ is the normalized fuel burning rate in the diffusion mode. The factor β, was introduced by Watson et al., [1980], to quantify the portion of the fuel consumed in the pre-mixed burning mode. This factor, called the burning factor, depends on the length of the ignition delay period and the overall equivalent ratio prior to the ignition, Fig. The value of β was defined as follows:

$$\beta = \frac{m_{pre}}{m_f} = 1 - 0.926 \cdot F_{ig}^{0.37} \cdot ID^{-0.26} \qquad \textbf{(5-50)}$$

The normalization process was achieved by dividing the expression by the total quantity of fuel injected and the nominal maximum combustion duration (constant in terms of crank angle). The normalized pre-mixed burning rate is written as,

$$\left(m'_f\right)_{pre} = K_{P1} \cdot K_{P2} \cdot \theta_{norm}^{K_{P1}-1}\left(1-\theta_{norm}^{K_{P1}}\right)^{K_{P2}-1} \quad \textbf{(5-51)}$$

where $K_{P1} = 2+1.25\times10^{-8} \cdot \left(ID \times N\right)^{2.4}$

and $K_{P2} = 5000$

In the above equations ID has units in ms and N is given in RPM. The normalized diffusion burning rate is given by

$$\left(m'_f\right)_{diff} = K_{d1} \cdot K_{d2} \cdot \theta_{norm}^{K_{d2}-1} \cdot \exp\left(-K_{d1} \cdot \theta_{norm}^{K_{d2}}\right) \quad \textbf{(5-52)}$$

where $K_{d1} = 14.2/F^{0.644}$

$$K_{d2} = 0.79\times K_{d1}^{0.25}$$

The term θ_{norm} is defined as the non-dimensional normalized angle, increasing from 0 at the start of combustion to 1 at the end of combustion and is defined mathematically as:

$$\theta_{norm} = \frac{\theta-\theta_{ign}}{\theta_{com}} \quad \textbf{(5-53)}$$

where θ_{com} is the combustion duration angle starting at ignition until the end of combustion (usually 125°); Ramos, [1989].

The parameters K_{P1}, K_{P2}, K_{d1} and K_{d2} have been evaluated using correlations with the fundamental factors that have the strongest influence on the combustion rate. The values shown are obtained for a range of direct injection diesel engines from the work presented by Watson, [1984], who showed that the actual fuel burning rate could be given by,

$$m'_{bf} = \frac{m_f \cdot \left(m'_f\right)_{norm}}{\theta_{com}} \quad \textbf{(5-54)}$$

Note that the fuel enthalpy of formation is a very important parameter that liberates the chemical energy that results from the combustion process. The value of enthalpy of formation mainly depends on the fuel composition. Ramos, [1989], provides a correlation for calculating the enthalpy of formation by specifying the low heating value (LHV) in kJ/kg of the fuel at 25°C and 1bar and the injected fuel temperature T_f as follows:

$$h_f = 2.326\left[LHV - 19183 + 0.5(T_f - 537)\right] \quad \text{(kJ/kg)} \qquad \textbf{(5-55)}$$

5.2.4 Cylinder wall heat transfer

The heat transfer mechanism in a diesel engine comprises forced convection and radiation heat transfer. The forced convection appears between the turbulent flow in the cylinder and the combustion chamber walls, whilst radiation heat transfer only takes place when a high temperature difference exists, i.e. between the flame or burning gases and the combustion chamber walls. The total heat transfer rate can thus be expressed as the sum of the two components.

$$Q'_{ht} = Q'_{ht1} + Q'_{ht2} \qquad \textbf{(5-56)}$$

The convective heat transfer Q'_{ht1} at the gas-to-cylinder wall interface will depend on the temperature gradient in the boundary layer at the surface; however, due to the inherent difficulties in calculating the details of turbulent fluid motion in the combustion chamber during the operation cycle of the engine, the convective heat transfer rate will be calculated using the usual expression as.

$$Q'_{ht1} = h_{con} A(T - T_{wall}) \qquad \textbf{(5-57)}$$

where h_{con} is the heat transfer coefficient based on forced convection. Borman and Nishiwaki, [1987], conducted an intensive review of the empirical correlations used to determine the heat transfer coefficient in the internal combustion engine. The first reviewed model was based on the experiments in a spherical bomb and referring the data to the actual engines and indicates the heat transfer coefficient in the convection heat transfer mode as follows

$$h_{con} = 5.41\times10^{-3}\left(1+1.24\cdot N_P\right)\cdot\left(P^2\cdot T\right)^{1/3}\ (\mathrm{kW/m^2\cdot K}) \qquad \textbf{(5-58)}$$

where N_p (m/sec) is the mean piston speed, P (MPa) is the cylinder pressure, T (K) is the cylinder gas temperature. Originally this heat transfer coefficient was intend to predict the time average or steady state flux, but it has often been used for the prediction of the instantaneous heat flux, probably because it was expressed in terms of instantaneous P and T values. This basic correlation had been through many modifications to increase its prediction accuracy. Most of these modifications concentrate on the mean-piston-speed term, e.g. $(3.5+0.185N_P)$ and $(3.22+0.864N_P)$ instead of $(1+1.24N_P)$. As there is insufficient information about the source of experimental data used to obtain these correlations, a comparison was undertaken to establish the most appropriate correlation to use in the present model. As a result of the comparison, the best correlation was as follows:

$$h_{con} = 5.41\times10^{-3}\left(3.22+0.864\cdot N_P\right)\cdot\left(P^2\cdot T\right)^{1/3}\ (\mathrm{kW/m^2\cdot K}) \qquad \textbf{(5-59)}$$

The mean piston speed is a function of the crank shaft rotational speed, N, and the piston stroke value, ST.

$$N_p = \frac{2\cdot N\cdot ST}{60}$$

The primary source of radiative heat transfer in a diesel engine is the high temperature burnt gases and the soot particles which are formed as an intermediate step in the turbulent diffusion controlled diesel flame. Estimates of the relative importance of the radiation mode in cooled diesel engines have varied between a few and 50 percent of the total heat transfer. In general, the radiant heat flux depends on the location on the combustion chamber surface, crank angle, engine load, engine size, and engine design. Following the work of Assanis and Heywood, [1986], the instantaneous radiant heat transfer can be expressed as

$$Q_{ht2} = \varepsilon\cdot\sigma\cdot A\cdot\left(T_{rad}^4 - T_{wall}^4\right) \qquad \textbf{(5-60)}$$

Where σ is the Stephan-Boltzman constant, ε is the apparent grey body emissivity, (its value was assumed to vary linearly between its maximum value 0.9 and zero over the expansion stroke, see Figure 5.7). T_{wall} represents the inside wall surface temperature of the cylinder head, piston or liner. In general, during the intake and compression processes, the radiation heat flux was assumed to be zero where the temperature level is not too high. During combustion, radiation heat transfer will exist with different values depending on the controlling parameters.

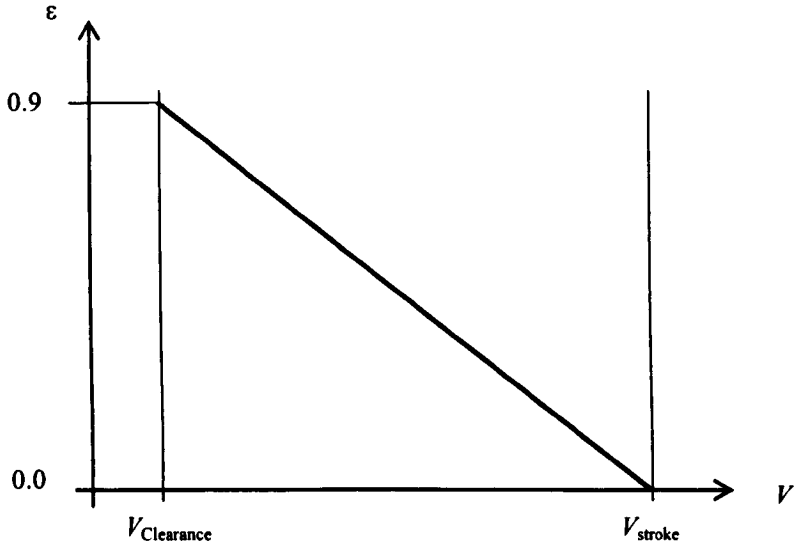

Figure 5.7. The emissivity change with respect to the cylinder volume.

The apparent (bulk) radiant temperature T_{rad}, depends on the adiabatic flame temperature, which can be modelled as the temperature of the slightly rich mixture of fuel and air (F=1.1) zone. However, as combustion progresses and relatively fewer close-to stoichiometeric fuel-air zones are found in the cylinder, this adiabatic flame temperature becomes considerably higher than the apparent radiant temperature; a better estimation was found to be the mean of the adiabatic flame temperature and the average bulk gas temperature, i.e.

$$T_{rad} = \frac{T + T_{F=1.1}}{2} \qquad \textbf{(5-61)}$$

The temperature of the combustion products at F = 1.1 is computed from a correlation of instantaneous gas temperature, T (K), and pressure, P (atm), as shown by Assanis and Heywood, [1986].

$$T_{F=1.1} = [1 + 0.0002317(T - 950)] \times (2726.3 + 0.906P - 0.003233P^2) \quad \textbf{(5-62)}$$

for 800 K < T < 1200K, and

$$T_{F=1.1} = [1 + 0.000249(T - 650)] \times \begin{pmatrix} 2497.3 + 4.7521P \\ -0.11065P^2 + 0.000898P^3 \end{pmatrix} \quad \textbf{(5-63)}$$

for 450 K < T < 800 K

The instantaneous gas temperature T, is calculated assuming adiabatic compression of the air from the start of compression. Because the cylinder wall temperature changes with time throughout the expansion process, the cylinder wall temperature should be updated at each step. This was done using the one-dimensional heat conduction model and the electrical analogy model, shown in Figure 5.7. Based on this, the energy balance can be expressed as follows,

$$Q'_{h1} + Q'_{h2} = \frac{T_{Wall} - T_{coolant}}{R_{WC} + R_W} \quad \textbf{(5-64)}$$

where $R_{WC} = 1/h_{coolant} \cdot A$ is the thermal resistance from wall to coolant fluid. The thermal resistance for conduction through the wall is $R_W = t/K \cdot A$, where t is the wall thickness, A is the inner cylinder area through which heat transfer and K is the thermal conductivity. In solving equations (5-57), (5-60), and (5-64), a fourth order polynomial, (5-65), in T_{Wall} was obtained and by using an iteration technique, the i^{th} solution will give the optimum value for the wall temperature to satisfy this equation. The resulting optimum value is used in the following calculations of the model. The wall temperature equation is shown below:

$$\frac{T - T_{wall}}{R_{gW}} + \varepsilon \cdot \sigma \cdot A\left(T_{rad}^4 - T_{wall}^4\right) = \frac{T_{Wall} - T_{coolant}}{R_{WC} + R_W} \qquad \textbf{(5-65)}$$

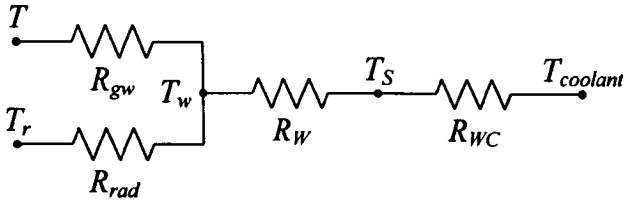

Figure 5.8. Thermal resistance for the cylinder

Finally the total heat transfer from the cylinder is the sum of the convection and radiation heat flux components:

$$Q'_{ht} = Q'_{ht1} + Q'_{ht2}$$

Borman and Nishiwaki, [1987], show a simplified method to calculate the heat transfer between cylinder gases and wall where there is no explicit term for the radiation. The heat transfer has only one term which comprises the convection and radiation effects within the same heat transfer coefficient. This correlation had been tested against natural-aspirated large two-stroke and four-stroke diesel engines. The proposed heat transfer coefficient is shown in the following equation.

$$h_{con} = 7.67 \times 10^{-3} \left(N_P\right)^{1/3} \cdot \left(P \cdot T\right)^{1/2} \ (\text{kW/m}^2 \cdot \text{K}) \qquad \textbf{(5-66)}$$

On the basis of the above relationship, the total instantaneous heat transfer through the cylinder wall was evaluated using the simple heat transfer relation given in equation (5-67)

$$Q'_{ht} = h \cdot A \cdot \left(T - T_{wall}\right) \ (\text{kW}) \qquad \textbf{(5-67)}$$

5.3 ENGINE SIMULATION

The diesel engine is a complex non-linear system, both algebraic and non-linear differential equations have to be solved in order to simulate the engine performance. MATLAB/SIMULINK (Mathworks) was used to model the engine via the SIMULINK graphical interface and the model equations solved in the time domain. The solution to the non-linear differential equations was obtained using the ordinary differential equations solver "ode45" available in MATLAB using a maximum time step size of 0.0001 sec/step.

To simplify the modelling, the programme was split into two parts, namely engine load dynamics and thermodynamics engine modelling. The dynamic modelling part includes the dynamic engine model equations using a lookup table of cylinder pressure as a function of crank angle. This part was verified by comparing output crank angle with the input simulated signal. The second stage includes the integration of the thermodynamic model equation to the engine dynamic simulation code using the output crank angle without feedback in the thermodynamic part. Some tuning was undertaken to obtain the model constants and empirical relationships to optimise the model performance, and the output cylinder pressure signal used as feedback to the dynamic part to finalize a single cylinder engine simulation. This single cylinder engine model was used as the basis for constructing the multi-cylinder engine simulation program. The following sections describe the development of the model.

5.3.1 Single cylinder engine simulation

Figure 5.9 shows the layout of the single cylinder simulation model which comprises three main functional blocks. The geometric parameters and constants are initialised, including cylinder volume and piston displacement which is calculated as a function of the engine crank angle. Some initial constants are assigned values, as listed in Table 5-1. The engine dynamic model deals with the force balance and generates the instantaneous crank angle and speed resulting from the dynamic balance. This block requires the instantaneous cylinder pressure as an input to evaluate the indicated torque resulting from the cylinder pressure acting on the piston. The external load torque is also input to the dynamic model.

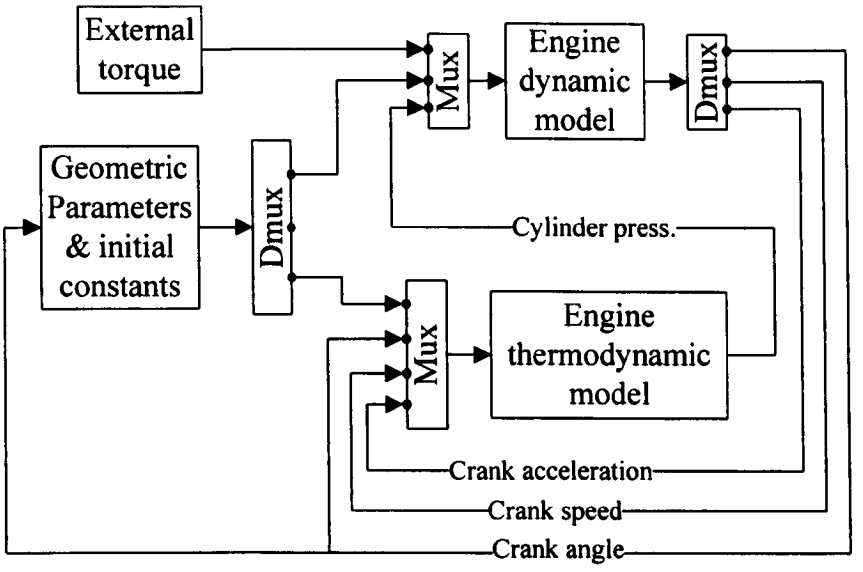

Figure 5.9 Single cylinder engine simulation layout.

Table 5-1 Initial constants used in the simulation model.

Parameter	Symbol	Deutz MAG Engine (single cylinder)	Ford 70PS Engine (four cylinder)
Bore diameter	d	95 mm	93.7 mm
Stroke length	s	95 mm	90.5 mm
Crank radius	r	47.5 mm	45.25 mm
Connecting rod length	L	160 mm	154 mm
Compression ratio	CR	17	20.8
Mass of piston	m_p	0.98 kg	.97 kg
Mass of connecting rod	m_r	0.65 kg	1.312 kg
Mass of reciprocating parts	M	1.18 kg	1.23 kg
Intake valve open (BTDC)		21°	7°
Intake valve closed (ABTD)		62°	45°
Exhust valve open (BBDC)		62°	57°
Exhaust valve close (ATDC)		21°	7°

The thermodynamic relationships include calculations for computing inlet and exit gas mass as well as burnt fuel mass. By applying both mass and energy conservation laws, the properties of the gases within the cylinder can be evaluated instantaneously and cylinder pressure computed and fed into the dynamic sub-system. Consequently, the simulation sub-system generates the instantaneous crank angle and speed change which is required by the other two simulation blocks.

The complexity of the above layout was such that it was necessary to develop the simulation code through several stages. The first stage, which is used to evaluate the geometric parameters, assuming constant engine speed, contains relatively simple algebraic equations which were validated by comparing the output parameters against manually calculated values at several arbitrary input conditions. The dynamic sub-system which includes the force-balance equations for the engine were developed as a second step. A lookup table of the cylinder pressure as a function of the crank angle was initially used to run the model. Figure 5.10 shows the layout of the dynamic sub-system including the interaction between different parameters. Friction torque was considered proportional to the instantaneous crank speed and compression ratio of the engine. The reciprocating parts of the engine modify the inertia of the engine, which was built into the model.

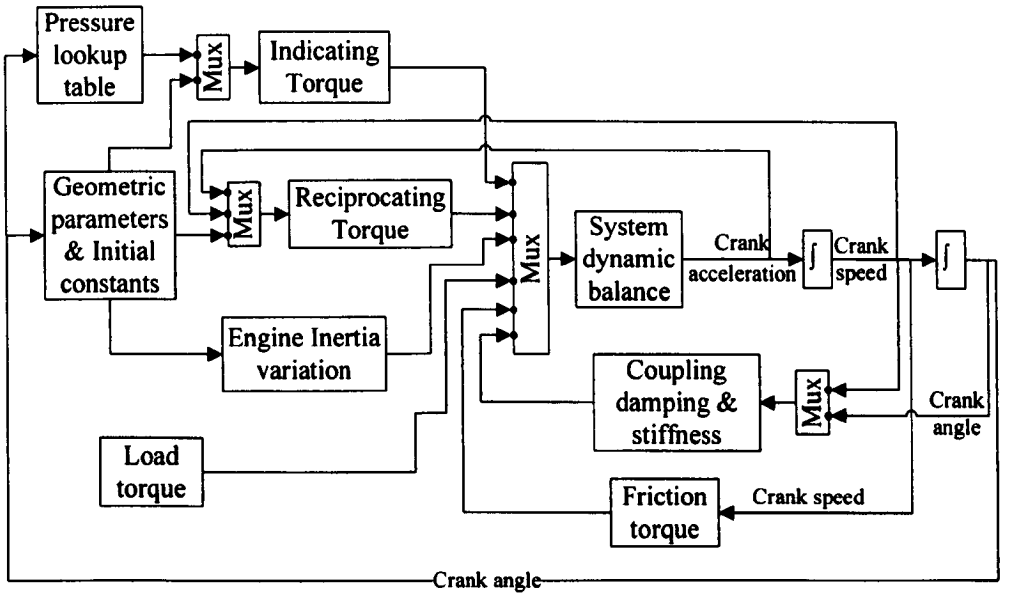

Figure 5.10 Dynamic sub-system layout

The thermodynamic model consists of many components that include both mass and energy balance on different engine processes, such as mass flow rate through the inlet and exhaust valve, burnt fuel mass flow rate in the combustion process, heat transfer through the cylinder walls, and energy and mass change within the cylinder. In view of the dependency on the timing of events to crank angle, the model was triggered with respect to crank angle and not time.

To simplify the development process, the thermodynamic sub-system was constructed initially without using any direct feedback. Appropriate simulated parameters were generated via lookup tables as a function of crank angle using linear interpolation between data points. Validation of the different sub-systems was achieved by comparing the model output parameters with those calculated from the lookup tables and substituted inputs. The different feedback loops were progressively closed and all lookup tables removed. The final thermodynamic subsystem, shown in Figure 5.11, was derived using a simulated crank angle during the final development and tuning stage of the thermodynamic sub-system.

Combining both dynamic and thermodynamic subsystems together with the geometric parameters sub-system was the final step in the single cylinder engine simulation code developments. This code used all the system of equations described within the model description section. The used of empirical correlations was kept within the minimum possible limitations without using any performance empirical equations. The defined engine constants were listed in a data file that was loaded before running the code. This adds an important advantage to the programme code which permits any size of diesel engine to be modelled without major modification.

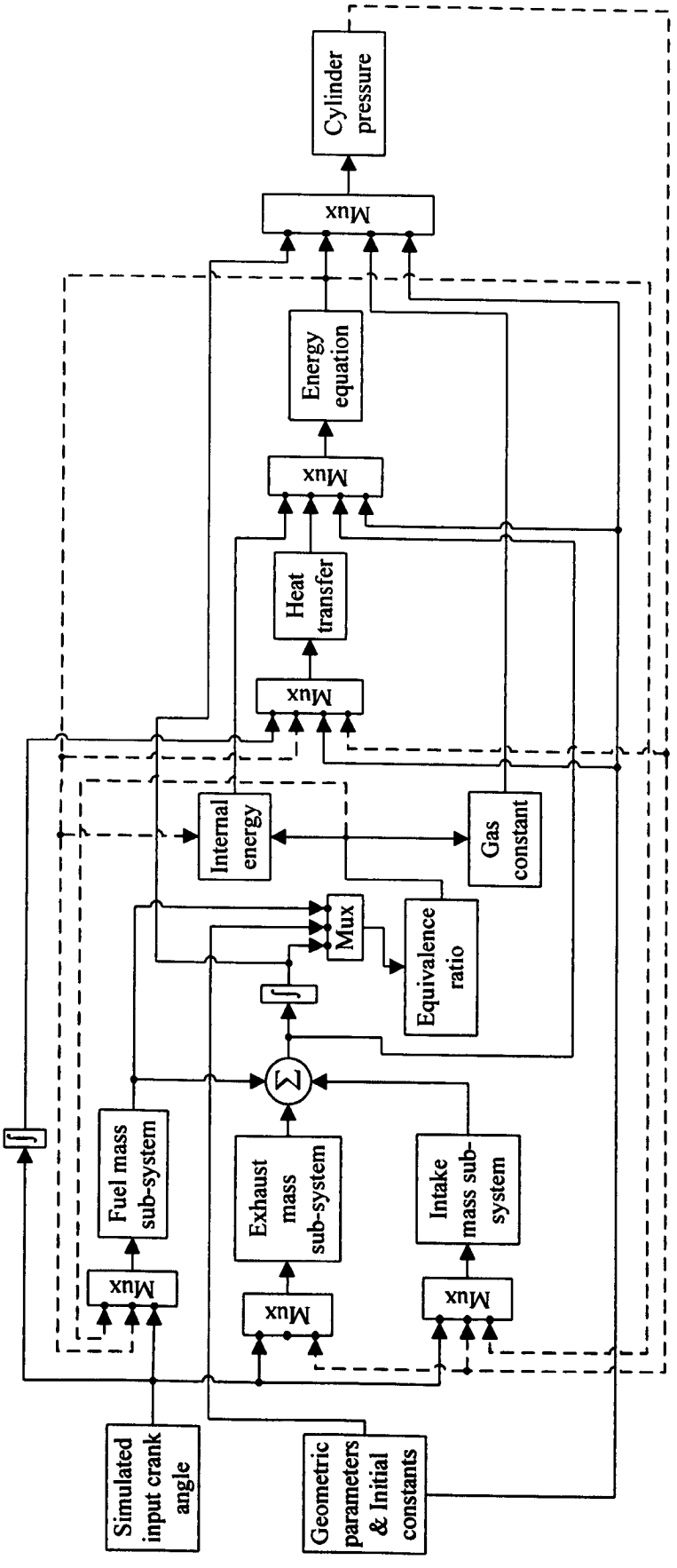

Figure 5.11 Thermodynamic sub-system layout.

5.3.2 Single cylinder engine simulation validation

The validation process for the single cylinder simulation code brought about some challenges as there was no available experimental data available for single cylinder engines. Thus it was decided to validate the simulation in two stages. Initially the trend for different parameters relative to the piston displacement was compared to data for the medium size engines. Then a comparison was undertaken between the simulation model results and published research work on a single cylinder diesel engine of similar size of the engine used in the present study. Cylinder pressure is the direct result of the combustion process in the cylinder; hence, it is very important to validate the simulated pressure value. The results published by Zweiri et al., [2001], were used in the validation by applying the same engine dimensions and fuel limits to the present model. Consequently, the present model successfully reproduces similar results to the work of. An example of the comparison is shown in and Figure 5.12.

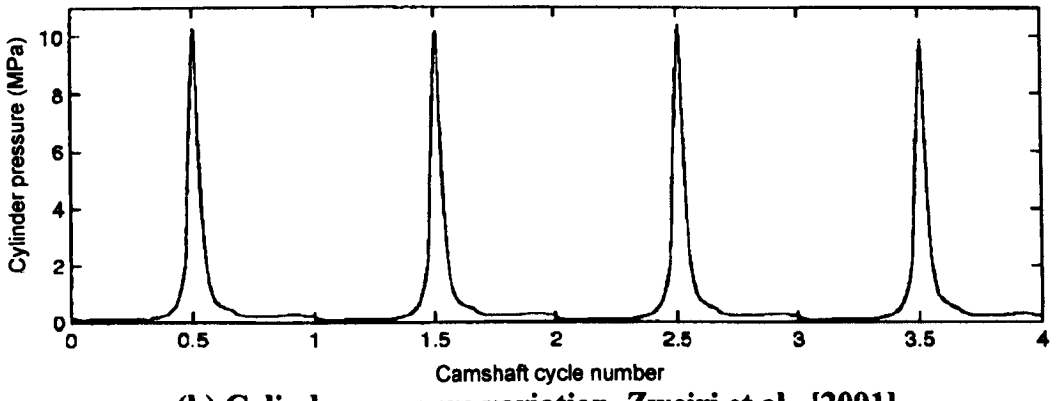

(b) Cylinder pressure variation, Zweiri et al., [2001].

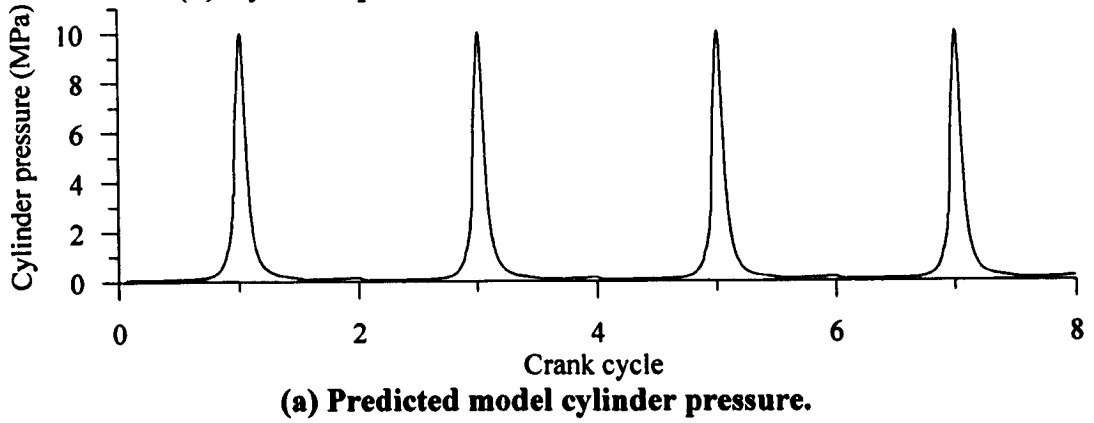

(a) Predicted model cylinder pressure.

Figure 5.12 Comparison of predicted cylinder pressure for a single cylinder engine (at 40mm^3 fuel per cycle).

5.3.3 Four cylinder engine simulation

A four cylinder engine consists of four in-line single cylinder units that are inter-connected through the crankshaft. The four cylinder simulation model was constructed using four of the validated single cylinder models running in parallel. Figure 5.13 shows the layout of the simulation program. The thermodynamic model of the cylinder was utilized to generate the multi cylinder thermodynamic sub-system where each one of the four cylinders has a phase shift of 180° crankshaft angle with respect to the adjacent cylinder. The individual indicated torques of the four cylinders are added to form the total torque applied to the crankshaft. A modified dynamic balance was used for the multi-cylinder engine model to take into account the changes in applied forces to the crankshaft of the single cylinder and multi-cylinder engines.

The dynamic sub-system was integrated to utilize the total indicated torque and inertia and mass constants of the moving engine parts to evaluate the instantaneous engine acceleration of the crankshaft. The dynamic balance take both engine and dynamometer balance into account. In a multi-cylinder engine, it is possible to assume that total inertia relative to the crankshaft is the sum of the individual cylinder inertias. The crank is usually designed to minimise the forces acting on the engine bearings so as to yield smooth engine rotation, nevertheless, the inertia variation still an effective component causing the rotational speed variation.

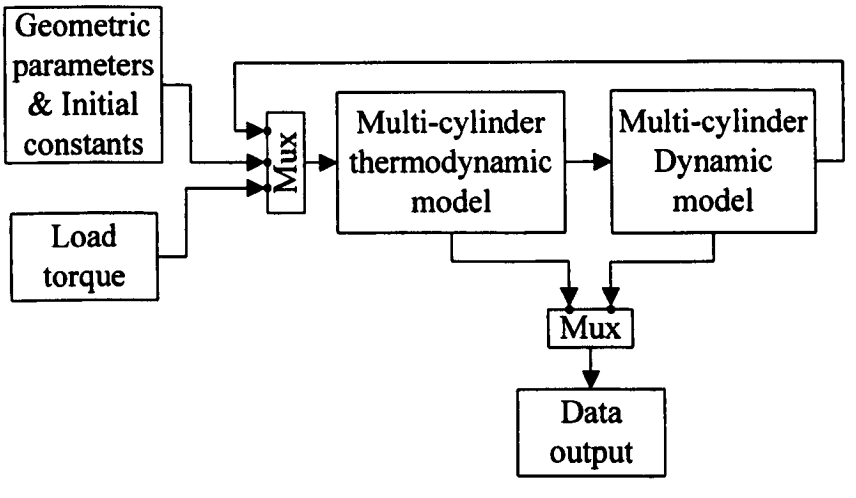

Figure 5.13 The multi-cylinder engine simulation layout

5.3.4 Validation of four cylinder engine simulation

In order to validate the four cylinder model, a set of runs for the simulated model at different operating conditions were undertaken and the results were compared to the experimental data. The cylinder pressure and instantaneous speed were selected for the validation process, based on their relative importance to the combustion process. A sample of the comparison results will be presented and analysed within the following sections. In addition, the power-torque curve for the engine from both experimental and model results were produced and compared to validate the model results.

Changes in the instantaneous speed could be helpful to detect some important faults related to injected fuel and combustion quality. The simulation model was run over different operating conditions of load and fuel consumption rate and the corresponding actual measured fuel consumption was input to the model in order to limit the calculated burnt fuel rate, resulting from the single zone combustion theory. This limitation simulates the fuel injection control valve of the actual engine.

Figure 5.14 represent sample of the comparison results at two different operating conditions. At both small brake load and fuel consumption, the model successfully predicts the engine speed variation at both crest and trough. However, at an increased load of 113 Nm the model correlation is not so good (refer to Figure 5.15), with it being unable to follow the ripple at the crest of the instantaneous speed variation which results from the ratio between applied load and energy stored in the flywheel. A more detailed discussion about speed variation is given in the experimental result analysis section (4.1.1).

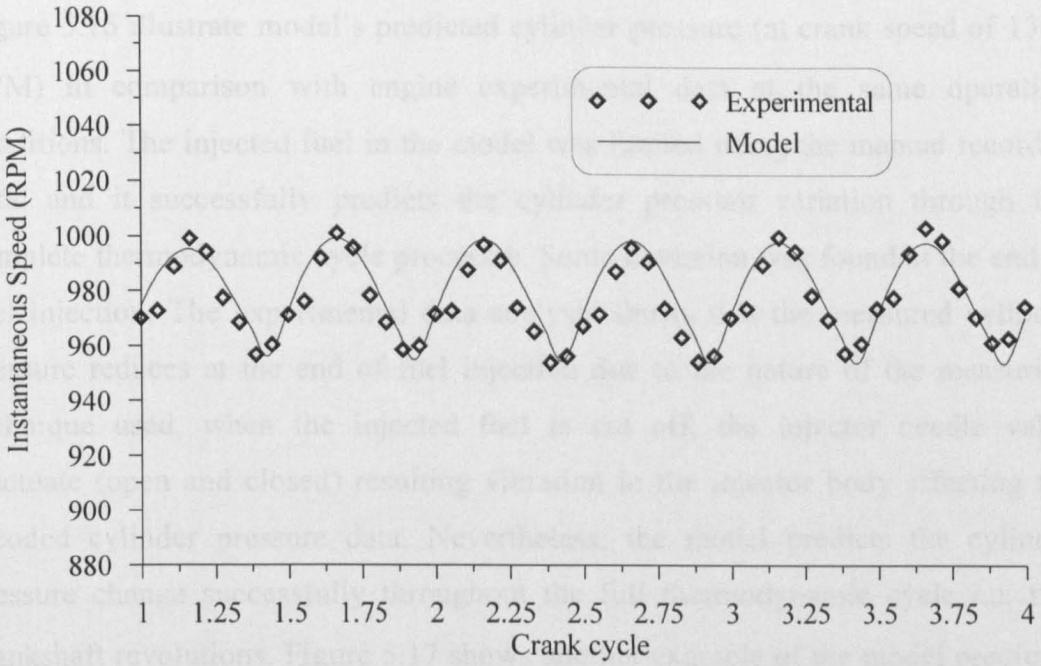

Figure 5.14 Instantaneous crankshaft speed variation at 8 Nm load (0.1528 g/s fuel consumption)

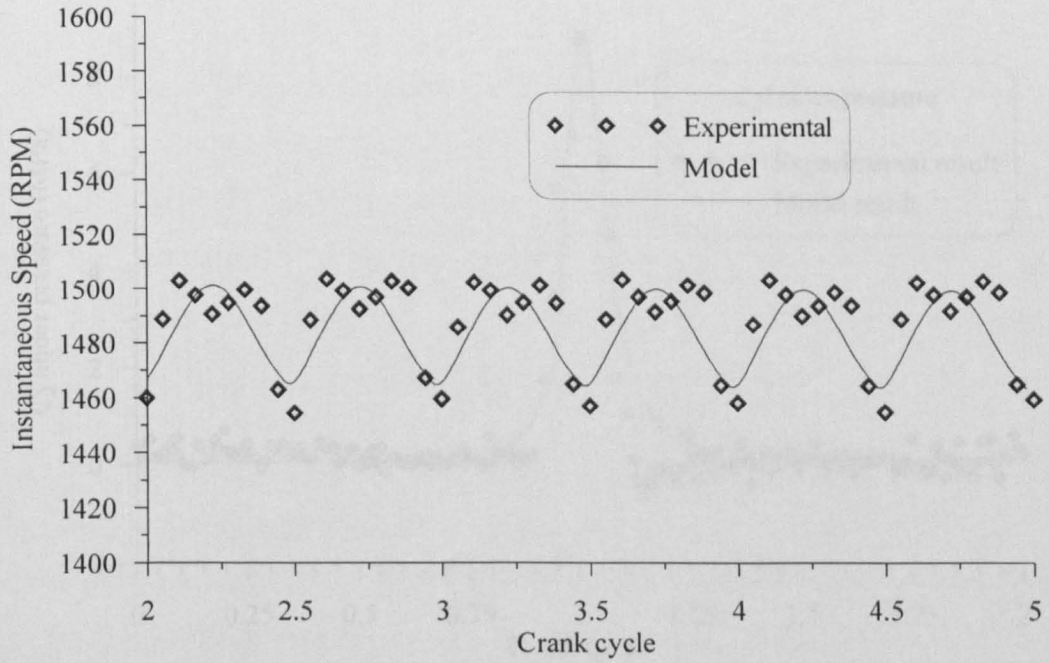

Figure 5.15 Instantaneous crankshaft speed variation at 113 Nm load (1.043 g/s fuel consumption).

The cylinder pressure was also used for the validation process as it is the main driving parameter for the engine and the direct result of the combustion process. The model was executed at a set of different operating conditions in line with experimental tests conditions, and several comparative results follow.

Figure 5.16 illustrate model's predicted cylinder pressure (at crank speed of 1360 RPM) in comparison with engine experimental data at the same operating conditions. The injected fuel in the model was limited using the manual recorded data, and it successfully predicts the cylinder pressure variation through the complete thermodynamic cycle processes. Some deviation was found at the end of fuel injection. The experimental data analysis shows that the measured cylinder pressure reduces at the end of fuel injection due to the nature of the measuring technique used, when the injected fuel is cut off, the injector needle valve fluctuate (open and closed) resulting vibration in the injector body affecting the recoded cylinder pressure data. Nevertheless, the model predicts the cylinder pressure change successfully throughout the full thermodynamic cycle i.e. two crankshaft revolutions. Figure 5.17 shows another example of the model predicted cylinder pressure validations at another operating conditions.

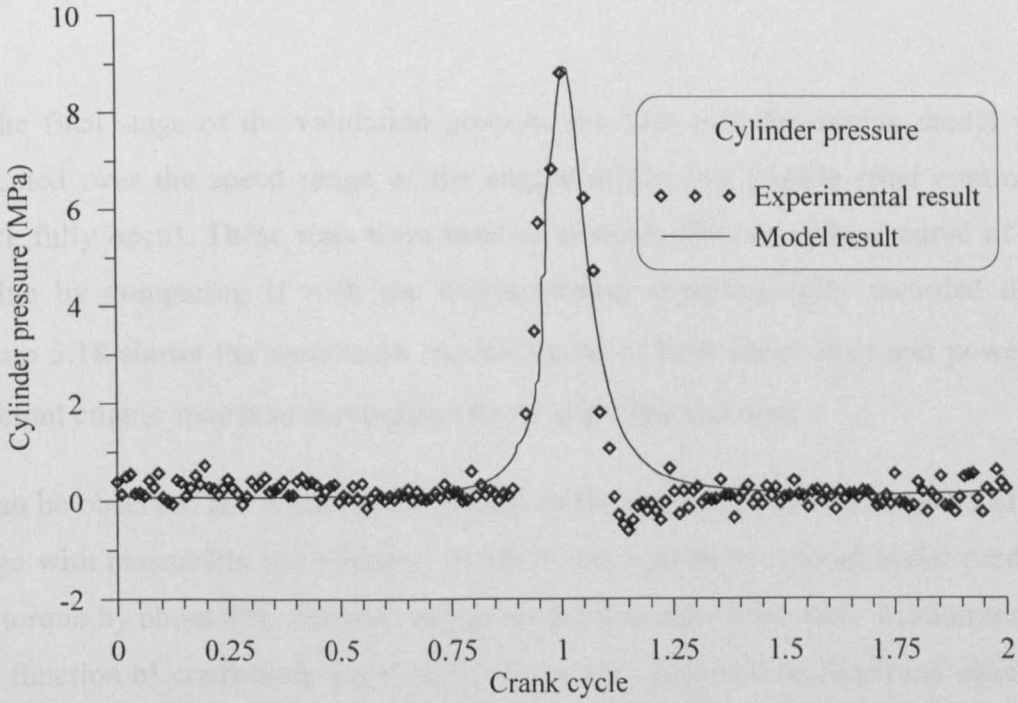

Figure 5.16 Model results validation at 1360 RPM and 21 Nm.

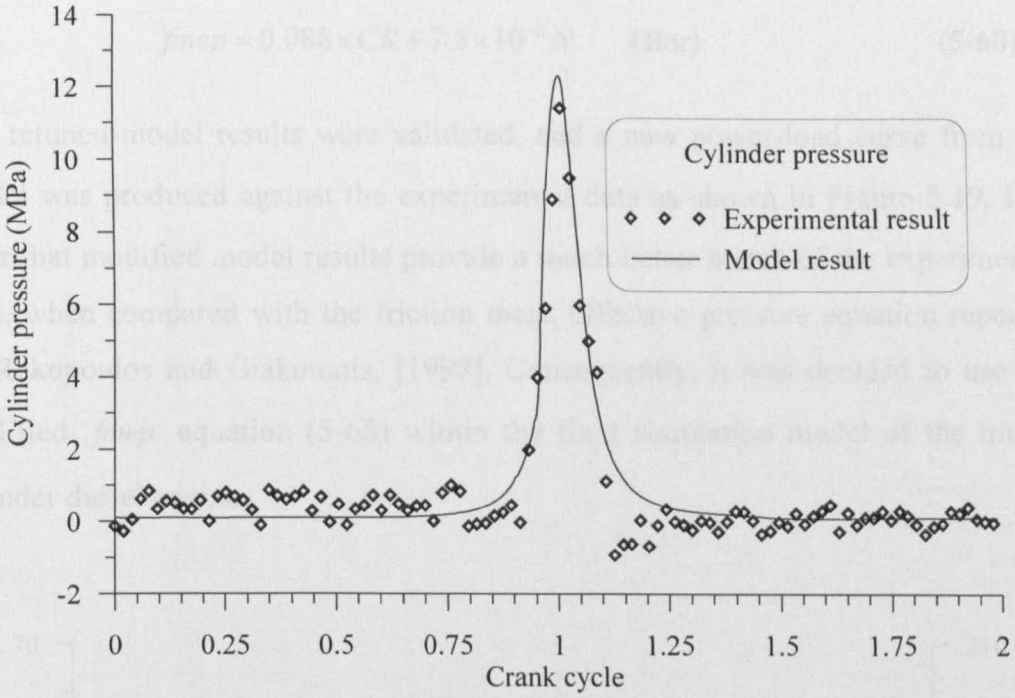

Figure 5.17 Model result validation at 2330 RPM and 61 Nm

In the final stage of the validation process, the four-cylinder engine model was executed over the speed range of the engine at the full throttle (fuel controller valve fully open). These runs were used to evaluate the power-load curve of the engine by comparing it with the corresponding experimentally recorded data. Figure 5.18 shows the simulation model results of both brake load and power at different engine speeds in comparison to the experimental data.

It can be observed the model predicts both brake load and power over most of the range with reasonable correlations. At the lower speeds the model under predicts the torque by about 8%. Analysis of the results indicates that, since friction torque is a function of crankshaft speed and compression ratio and as empirical equation (5-14) does not specify the engine dimensions used to evaluate its constants it was decided to adjust the value of the two constants in equation (5-13) used to evaluate friction mean effective pressure. After some trial and error, the best fit for the experimental data, through the whole speed range of the engine, were obtained using the following equation.

$$fmep = 0.088 \times CR + 7.5 \times 10^{-4} N \quad \text{(Bar)} \qquad \textbf{(5-68)}$$

The retuned model results were validated, and a new power-load curve from the model was produced against the experimental data as shown in Figure 5.19. It is clear that modified model results provide a much better match of the experimental data, when compared with the friction mean effective pressure equation reported by Rakopoulos and Giakoumis, [1998]. Consequently, it was decided to use the modified *fmep* equation (5-68) within the final simulation model of the multi-cylinder diesel engine.

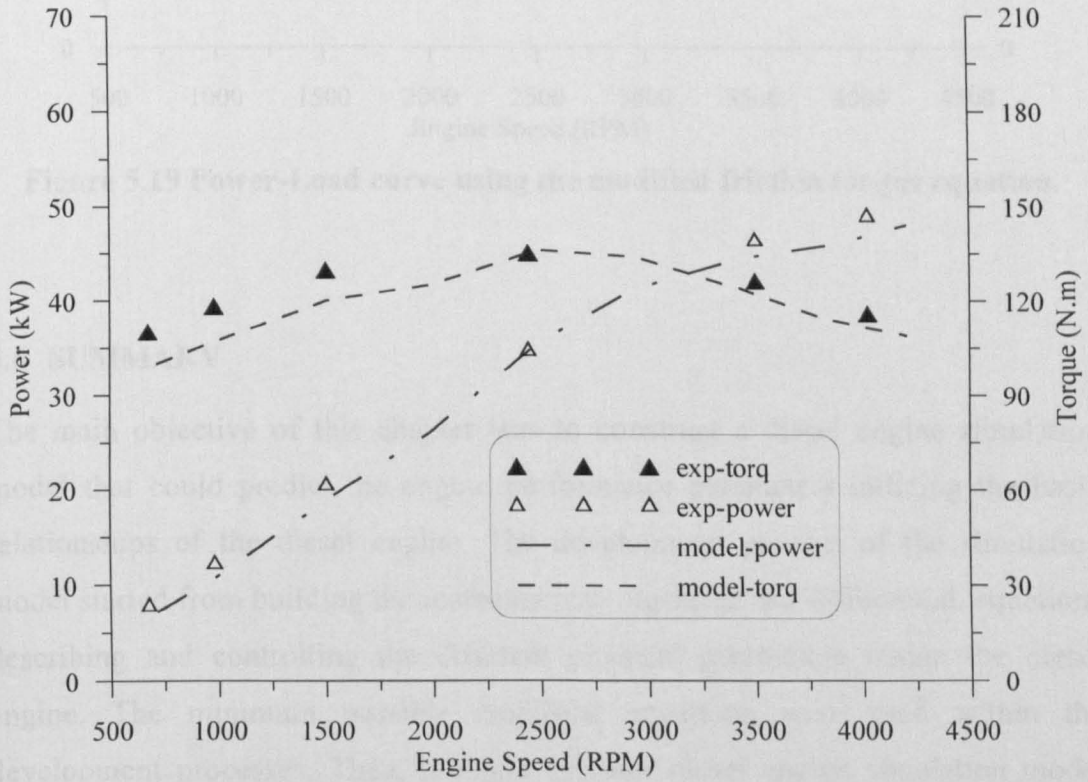

Figure 5.18 Power-Load curve comparison of model and experimental data.

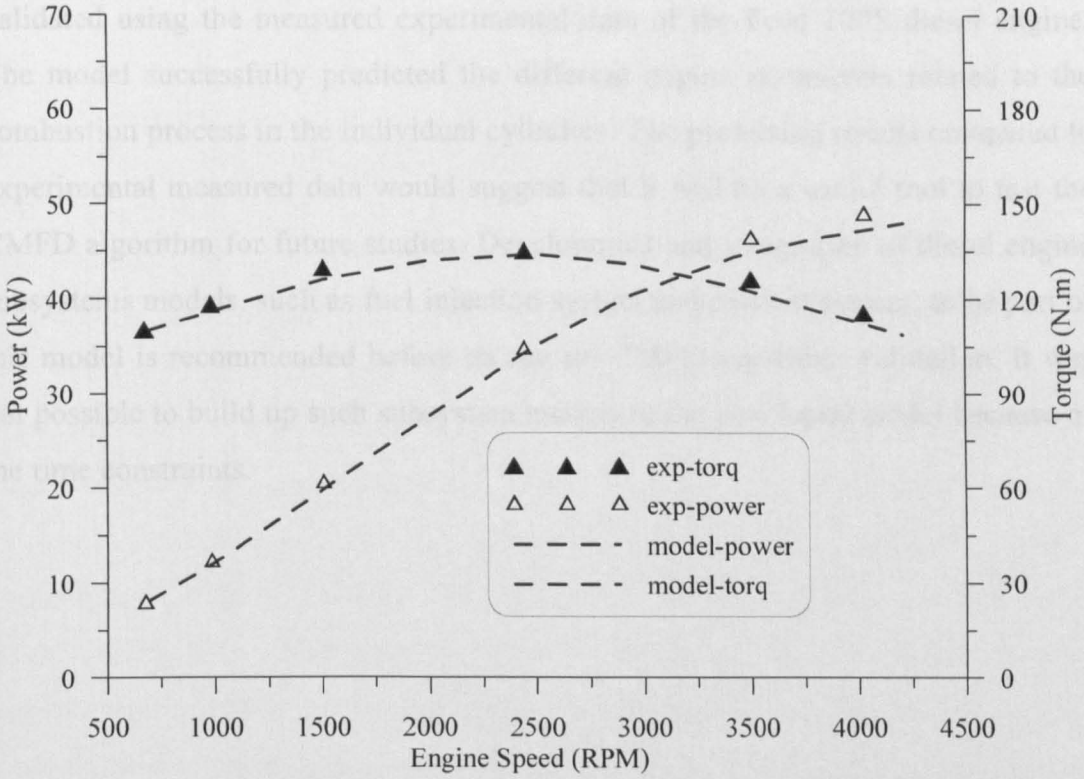

Figure 5.19 Power-Load curve using the modified friction torque equation.

5.4 SUMMARY

The main objective of this chapter was to construct a diesel engine simulation model that could predict the engine performance parameters utilizing the basic relationships of the diesel engine. The development process of the simulation model started from building the mathematical, algebraic and differential, equations describing and controlling the different physical parameters within the diesel engine. The minimum possible empirical equations were used within the development processes. Then, a single cylinder diesel engine simulation model was programmed using the MATLAB/SIMULINK software as the first step toward the multi-cylinder engine simulation. The single cylinder engine model was verified using a literature data where there was no available experimental data for a single cylinder diesel engine.

The validated single cylinder model was utilized to develop the final multi-cylinder diesel engine simulation model. Four-cylinder diesel engine model consists of four parallel unit of the single cylinder model with phase shaft of 180° of the crankshaft revolution. The final four cylinder engine simulation model was

validated using the measured experimental data of the Ford 70PS diesel engine. The model successfully predicted the different engine parameters related to the combustion process in the individual cylinders. The promising results compared to experimental measured data would suggest that it will be a useful tool to test the CMFD algorithm for future studies. Development and integration of diesel engine subsystems models, such as fuel injection system and exhaust system, to be part of this model is recommended before its use for CMFD algorithm validation. It was not possible to build up such subsystem models to the developed model because of the time constraints.

CHAPTER 6

DEVELOPMENT AND VALIDATION OF DIESEL ENGINE NEURO-FUZZY DIAGNOSTIC SYSTEM

The ultimate aim of this research is to develop a system which will be able to perform on-line condition monitoring and fault diagnosis of a diesel engine using a limited number of sensors. This chapter consolidates all of the work conducted during this research and demonstrate how the data is captured and post processed to develop, optimise and validate a diesel engine diagnostic scheme based on a neuro-fuzzy system. As described in Chapter Two, the studies conducted in the recent years have used complex look-up tables, large knowledge base or approximate models to perform diagnosis, and in addition, the sensor outputs have often required normalisation and sophisticated signal processing before diagnosis could be performed.

This work shows how a combination of a neural network and fuzzification can be developed to minimize the need for all of the above and yet offer satisfactory performance of CMFD of the diesel engine. The systems discussed in Chapter Two required a significant degree of computing hardware and software and the need for expensive sensors as well as complicated signal conditioning; another restriction for the CMFD system performance. This work shows how relatively low cost computing hardware and reliable, low-cost sensors can be used develop and run a robust CMFD system. Often neural networks are trained and tested on simulated diesel engine data, Nareid and Lightowler, [2004], with limited research undertaken using experimental data for the signal capture and processing complexity. Nor have they been used to diagnose a wide range of realistic engine faults, e.g. fuel injection problems, and less attention has been paid to the development of fault-symptom relationships for high speed diesel engines.

To ascertain the neural network based diagnostic system practical limitations, the following criteria are defined. The neural network based CMFD system must:

* Be able to be trained on real engine data. This allows the neural network to be trained simultaneously with endurance, reliability and field trial engine

testing which forms part of any engine development programme, as well as making the neural network approach more commercially viable than other forms of CMFD systems such as expert systems.

* Be able to perform an accurate diagnosis with reliable, non-intrusive, cheap instrumentation.

* Have the ability to perform an accurate diagnosis at torques and speeds other than those trained for. If the neural network CMFD algorithm needs to be trained on data generated at all operating conditions, it will not be practically viable.

* Be capable of being integrated with data acquisition software to satisfy the requirements for future integration with commercial diesel engines.

Within the present work, a neuro-fuzzy system was developed to evaluate the engine condition and detect the fault existence. The neural network uses selected key input data to evaluate the engine condition while the fuzzification aims to evaluate the level of fault to enable the user to select a suitable course of action. Several training algorithms and various network architectures were investigated during the development process to evaluate the optimum configuration. The use of sensors with different bandwidths is another challenge in the present work, and a multi-net technique was utilized in which two parallel neural networks were used to accommodate the different data groups and increase the CMFD algorithm performance.

Throughout the development and validation of the neuro-fuzzy system, emphasis was put on the practical application of neural networks to diesel engine fault diagnosis. The neural network was developed using Matlab to enable different training algorithms and network architectures to be evaluated to optimum architecture for diesel engine data.

6.1 SELECTION OF INPUTS FOR NEURAL NETWORK DIAGNOSIS SYSTEM.

The choice of input data is critical to the successful development of a neural network. The analysis of the engine test data and fault symptom relationships were used to select which sensors were able to detect the presence of a particular fault.

It was decided that the neural network CMFD algorithm would use sensors which were easy to install, non-intrusive, relatively low cost and reliable.

Generally, sensors that need high sampling rates to accurately represent the measured parameters were not utilized in the developed neural network CMFD algorithm as high computational power will be required to measure and process the captured data, thus limiting the practical application of the CMFD system. It was decided that the neural network would concentrate on using raw sensors readings, which was considered beneficial because it allowed the sensor data to be passed directly to the networks, thus eliminating the need for pre-processing. Although cylinder pressure and injected fuel pressure are both key diagnostic parameters in the combustion process, they were not directly utilised because at fast engine speed they require high sampling rates and specialist signal processing which means high computational resources and limitations for online market applications, Moro et al., [2002]. The following parameters were chosen as offering suitable inputs for the neural network diagnostic model development.

* Instantaneous speed.
* Average crankshaft speed.
* Average load torque.
* Average consumption fuel mass flow rate.
* Fuel lever position.
* Exhaust gas temperature for individual cylinders.
* Inlet air volume flow rate.

The choice of sensors is of critical importance in the development of any diagnostic system. Sensors should satisfy the requirements of neural network which had been stated above and should give significant and detectable changes in the presence of a fault. The inputs to the CMFD system should be readily indicate fault-symptom relationships. If this is not possible, the degree of success of the artificial intelligence may be compromised. As discussed in Chapter Three, the sensors utilized for measuring all of the above parameters satisfy the requirements of the neural network CMFD algorithm.

6.2 TRAINING OF NEURAL NETWORK CMFD ALGORITHM

The engine test data from the selected sensors were divided into three groups. The first two groups were used for training and validation of the neural network respectively, while the last group was used for testing the developed neural network. The training set of data was selected to cover the full operating range of the engine under for both healthy and faulty conditions. The validation input data comprised randomly selected sets of engines test data. The third group was selected to include healthy and faulty data that represent the entire engine operating range for testing processes. This testing group was not used for the training or validation processes but was used to evaluate the ability of the developed CMFD system to successfully detect the faults on data which it was not trained on.

Supervised neural network training requires input and output data for the training, validation and testing processes. To compliment the training input data a set of neural network outputs were devised to characterize both healthy and faulty modes of engine operation. The selection of the output vector configuration is critical parameter that affects the possible application of the developed neural network. The output vector was added to the recorded data manually for use within the development process. The neural network output will set a flag to indicate the presence of a fault and/or requirements for any maintenance.

The output vector was assumed to contain only two outputs, as shown in Table 6-1, where each one corresponds to a specific fault type. The value of the output will depend on the level of fault severity. Utilizing this output vector improve the flexibility of the developed neural network to evaluate an intermediate fault level, and help to select the critical border of the fault level. However, the training process usually needs a large number of training data sets in order to converge and reduce the error factor.

Table 6-1 Neural network diagnosis outputs vector.

	Neuron 1 (Air fault)	Neuron 2 (Fuel fault)
Healthy	0	0
Air Inlet Blockage 25%	0.25	0
Air Inlet Blockage 50%	0.5	0
Fuel Blockage 50%	0	0.5
Fuel Blockage 80%	0	0.8

6.3 THE CMFD ALGORITHM

According to the nature of the selected input parameters, the developed CMFD algorithm must accommodate different sampling rates for the measured data. The multi-net approach represents a promising solution to this problem. Two parallel neural networks were designed to accommodate this, as shown in Figure 6.1. The inputs were divided into three groups, the first of which was used in both neural networks includes the average signals levels which do not change within the measuring period. The second group, which includes the exhaust gas temperature, was utilized, in parallel with the first group, as the input to the first neural network. Collectively this group of data represents the low bandwidth signals of the measured data. The third group of data is utilized in the second neural network and comprise the instantaneous speed parameter with which to evaluate the individual cylinder contribution along with the averaged parameters (included in the first group of data) input to the second neural network to index the change in instantaneous speed values.

The output of the two parallel neural networks was combined in order to generate a final evaluation of the engine condition and the fault, type and level, using a fuzzy logic structure. The fuzzification aims to improve the overall algorithm performance by evaluating the severity level of the error based on the engine manufacturer test recommendations and produces the required action by the user. More details about the developed fuzzification stage will be included later in this chapter.

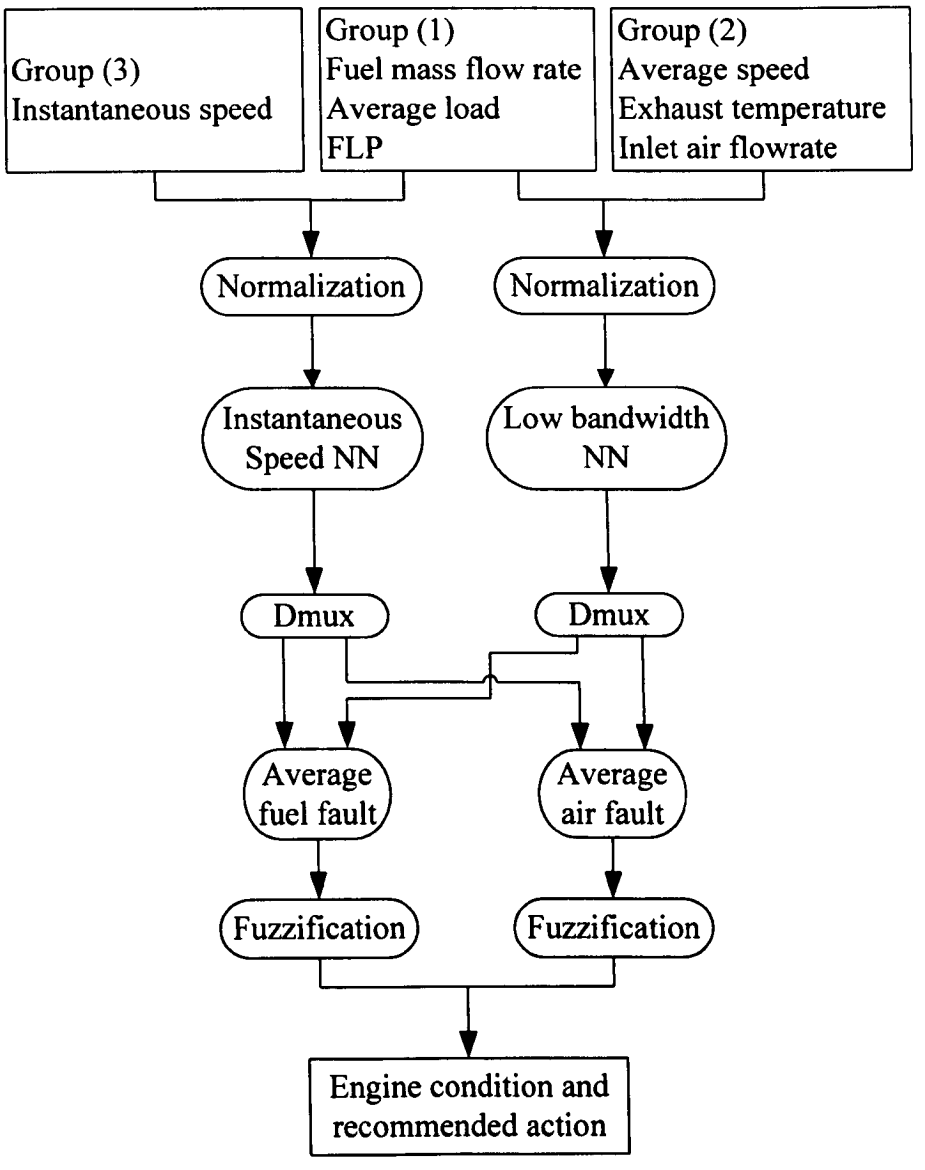

Figure 6.1 The CMFD algorithm layout

The most appropriate neural network architecture for the engine CMFD is the MLP and RBF (see Chapter 2). In the present work, both configurations were compared using the selected input data. The results of the training process indicated that the RBF was not suitable for the particular input data range, as it generates a neuron for each data row in the hidden layer and resulted in extremely large neural networks, which in turn required massive memory and computational time.

As shown from previous research, the performance of the MLP neural network is improved when using only one hidden layer, regardless of the number of neurons used. Accordingly, the MLP neural network was selected for the CMFD system where it was successfully applied. There is no rule with which to select the

optimum number of neurons in the hidden layer. Increasing the number of neuron consequently increases the training time and decrease the response time of the developed neural network, whilst reducing the number of hidden layer neurons reduces the neural network performance. An optimum number of hidden layer neurons can be found by trial and error beyond which an increase in the number of hidden layer neurons does not improve performance.

The training algorithm is another important factor; it is very difficult to know which training algorithm will be most appropriate to a given problem as it depends on many factors, including the complexity of the problem, the number of data points in the training set, the number of weights and biases in the network, the error goal, and whether the network is being used for pattern recognition (discriminate analysis) or function approximation (regression). The diesel engine CMFD is considered to be a pattern recognition problem where a certain data set indicates the engine condition and can evaluate the fault type. Nevertheless, it is difficult to evaluate the optimum training algorithm. A comparison study conducted by Mathworks suggest that *Levenberg-Marquardt (trainlm), and BFGS Quasi-Newton backpropagation (trainbfg)* algorithms are the most suitable in pattern recognition problems. Both training algorithm were tested to establish which one will provide an optimum output.

6.3.1 Low bandwidth (averaged) data neural network

As explained earlier, the averaged neural network inputs comprise of the exhaust gas temperature and average value of speed, load, fuel consumption, and FLP. The data was measured using a sampling rate of 1 kHz and compressed using a window average to an equivalent sampling rate of 0.1 kHz. The measured data was normalized using the maximum expected value of each parameter before the training process. The parameters values used for normalization are shown in Table 6-2.

Table 6-2 Normalization values for input data.

Parameter	Normalization value
Exhaust temperature	450°C
Fuel mass flow rate	1.5 g/s
Average speed	4500 RPM
Load	125 Nm
Inlet air flow rate	2.3 V
Crank cycle	4 cycle

After several trials, the configuration that produces the minimum performance factor consists of one hidden layer with 20 neurons as shown in Figure 6.2. The input layer contains 11 neurons which take the value of the normalized input data while the output layer has 2 neurons corresponding to the engine condition and the fault severity level evaluation. The output layer transfer function was selected to be *LogSig* which is suitable for the output values which vary between 0 and 1. The optimum training algorithm was found to be the *trainlm* which converges to the minimum performance factor in the minimum possible time. The *trainlm* requires 'massive' memory size as the storage of some matrices can be quite large for certain problems; consequently, the training process takes longer. The training performance curve, shown in Figure 6.3, indicates the fast convergence of the selected training algorithm where the performance factor (which is the mean square errors) reduced to 9.8×10^{-5} after only 161 epochs.

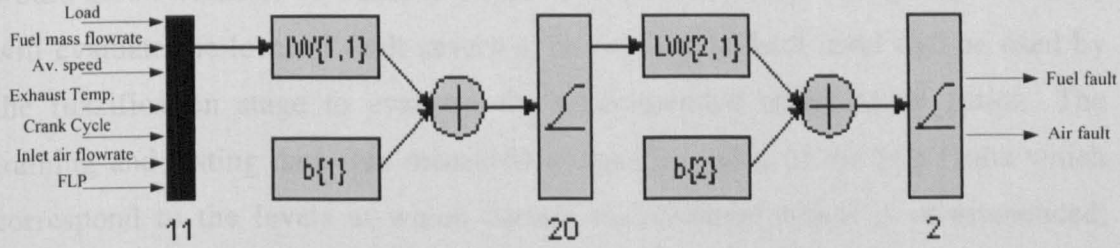

Figure 6.2 Low frequency data neural network layout

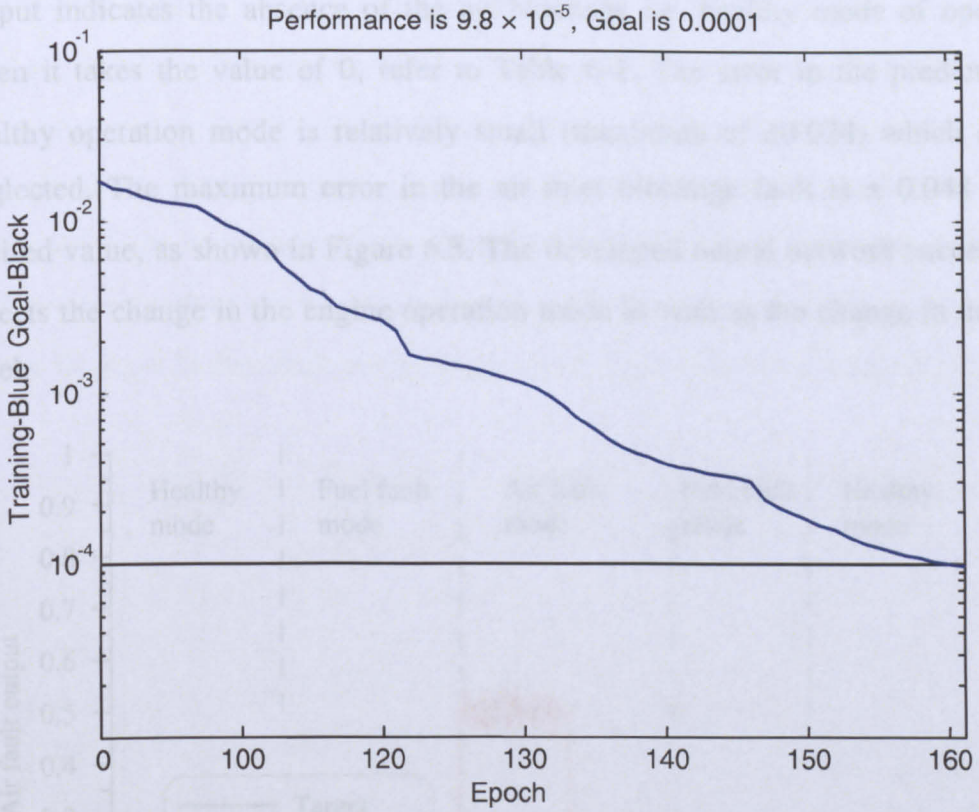

Figure 6.3 The performance factor curve of the training process.

In order to validate the developed neural network, a set of input data, which was not used within the training stage, was given to the neural network. The neural network output is then compared with the desired output to validate the neural network. The data set contains engine data covers the full operating range for both healthy and faulty operation modes. The output from the neural network represents the engine condition; if the engine is working under healthy mode the two outputs would give a value of 0. Under any type of fault the corresponding output (1 or 2) will evaluate the level of fault severity. The evaluated fault level will be used by the fuzzification stage to evaluate the recommended maintenance action. The training and testing data was measured at specific value of the two faults which correspond to the levels at which certain maintenance action is recommended, Refer to section 4.2 for more detail about the testing fault setting.

Figure 6.4 shows the neural network output-1, which evaluates the air inlet blockage, in comparison to the desired output of the test data set. The result indicates an accurate prediction of the fault existence as well as it level. The

output indicates the absence of the air blockage i.e. healthy mode of operation when it takes the value of 0, refer to Table 6-1. The error in the prediction of healthy operation mode is relatively small (maximum of ±0.024) which can be neglected. The maximum error in the air inlet blockage fault is ± 0.048 of the desired value, as shown in Figure 6.5. The developed neural network successfully detects the change in the engine operation mode as well as the change in the fault level.

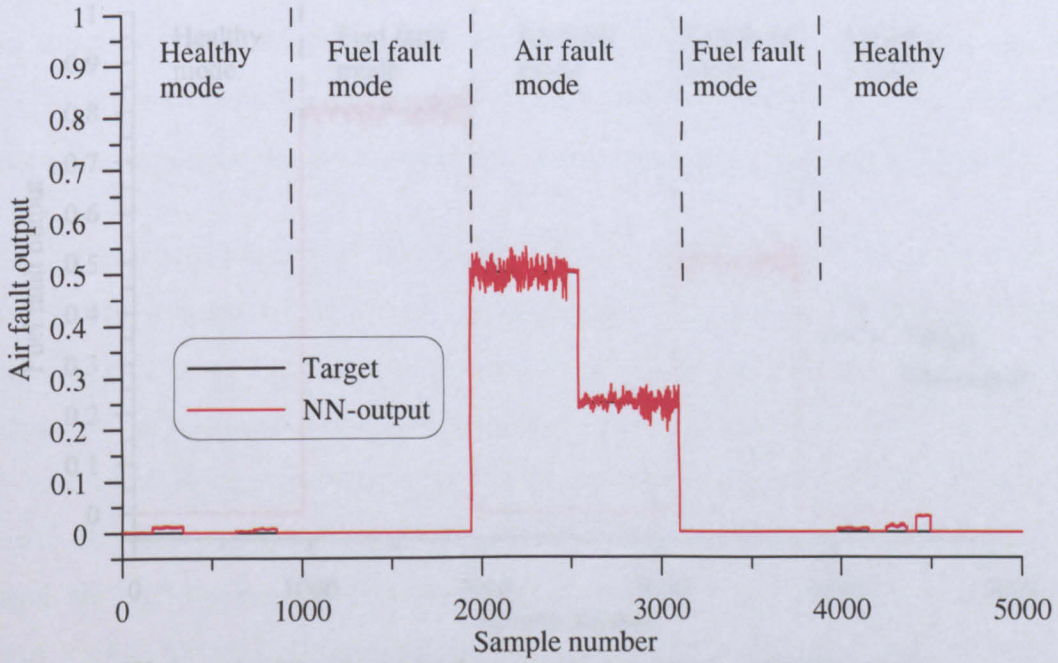

Figure 6.4 Air inlet blockage fault detection validation test.

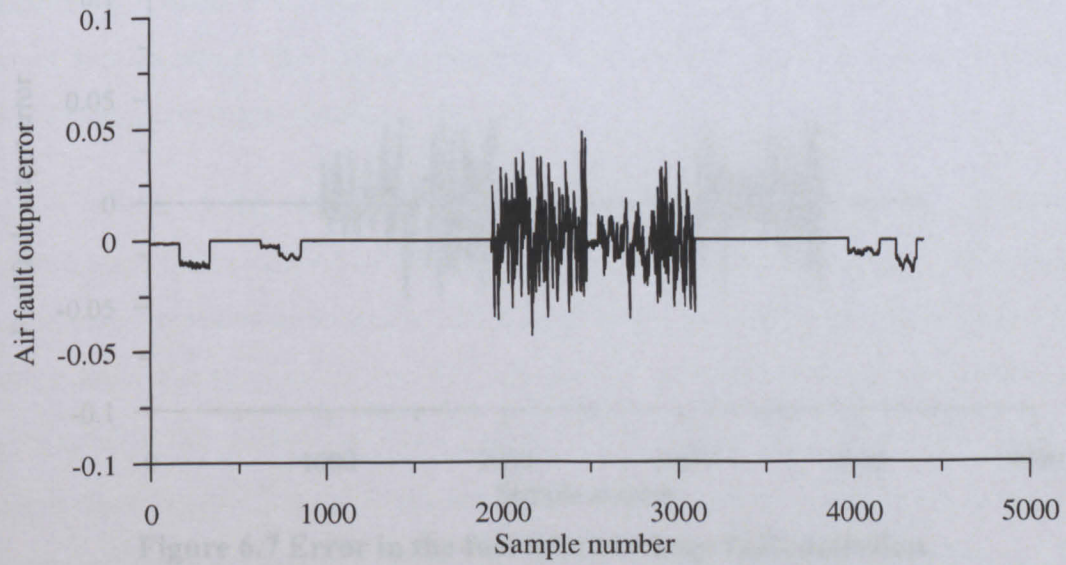

Figure 6.5 Error in the air inlet blockage fault detection.

The second output, corresponding to the fuel fault, was validated using the test data set and the validation results are shown in Figure 6.6. It is concluded that the neural network detected both the fault existence and severity level successfully. It also illustrates that the output value is not affected by the air inlet blocking existence in the test data set (in the range 1960 – 3110 sample number). The value of the second output neuron only changed under the effect of fuel fault. Figure 6.7 shows the error in fuel fault output value which has a maximum value of ±0.047.

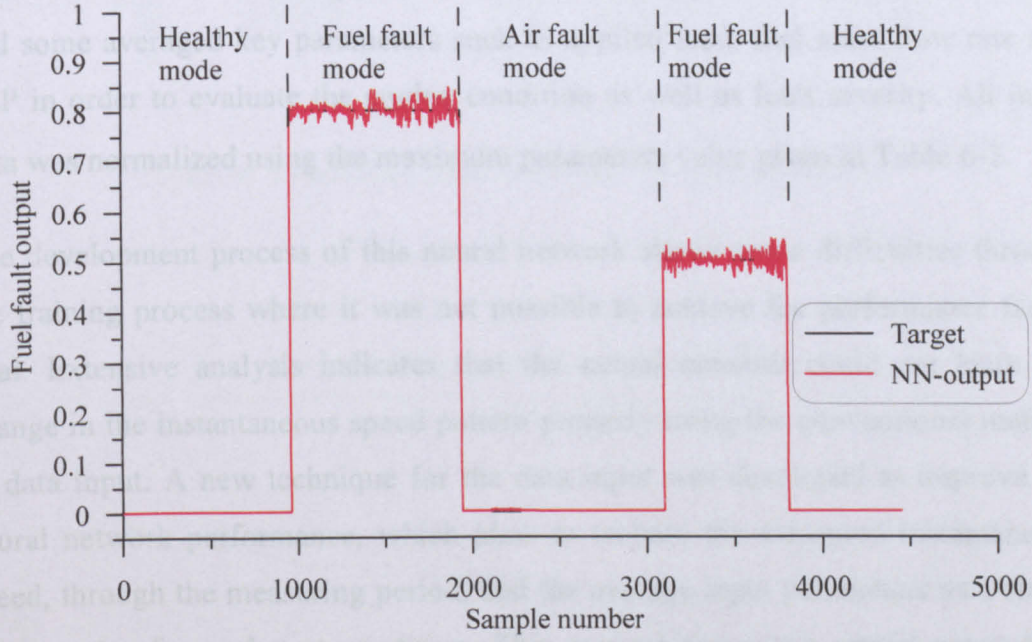

Figure 6.6 The fuel blocking fault detection validation test.

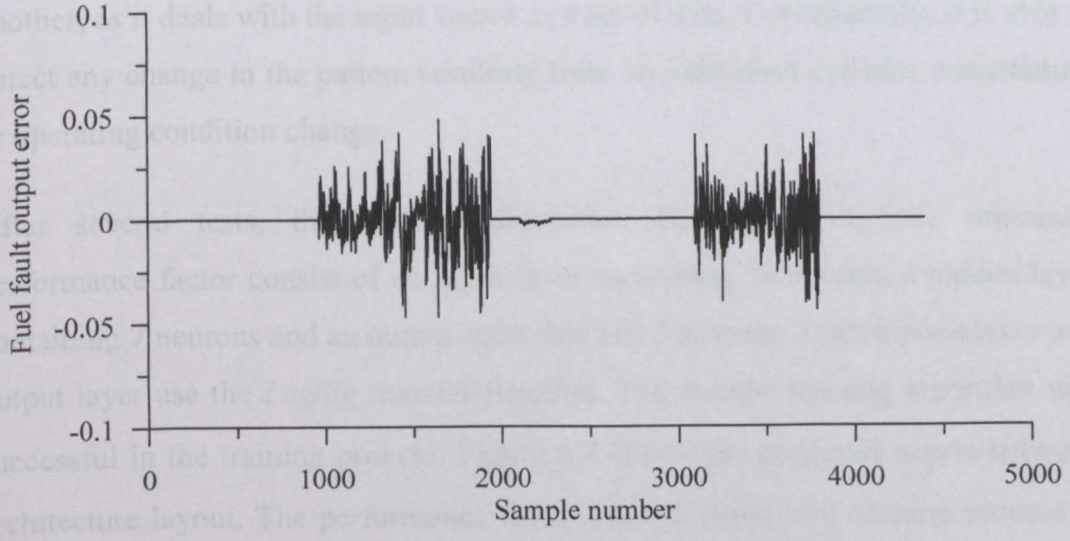

Figure 6.7 Error in the fuel inlet blockage fault detection.

6.3.2 Instantaneous speed neural network

An analysis of the importance of instantaneous speed signal as a key parameter was indicated in Chapter 4. The speed variation throughout the thermodynamic cycle of the engine relates directly the combustion processes quality as well as the contribution from individual cylinders. This signal was measured using a Hall effect proximity sensor which is triggered by the flywheel teeth, thus the rate at which data was captured depends on the engine speed, and thence a separate neural network was developed to monitor the instantaneous speed measurement and some averaged key parameters such as applied load, fuel mass flow rate and FLP in order to evaluate the engine condition as well as fault severity. All input data was normalized using the maximum parameters value given in Table 6-2.

The development process of this neural network shows some difficulties through the training process where it was not possible to achieve the performance factor goal. Extensive analysis indicates that the neural network could not learn the change in the instantaneous speed pattern properly using the conventional method of data input. A new technique for the data input was developed to improve the neural network performance, which aims to include the measured instantaneous speed, through the measuring period, and the average input parameters as a single input vector for each test condition. This method forces the neural network to observe the pattern shape variation of the speed from one testing condition to another, as it deals with the input vector as a set of data. Consequently, it is able to detect any change in the pattern resulting from an individual cylinder contribution or operating condition change.

After several tests, the final configuration that results in the minimum performance factor consist of an input layer containing 76 neuron, a hidden layer containing 7 neurons and an output layer that has 2 neurons. Both hidden layer and output layer use the *LogSig* transfer function. The *trainlm* training algorithm was successful in the training process. Figure 6.8 shows the proposed neural network architecture layout. The performance factor change during the training process is shown in Figure 6.9 where it takes 174 epochs to achieve a final value of 5.8×10^{-5}. Through the training process 105 input data sets were used which represents the

full engine operating range at different loads and speeds, under both healthy and faulty operation modes.

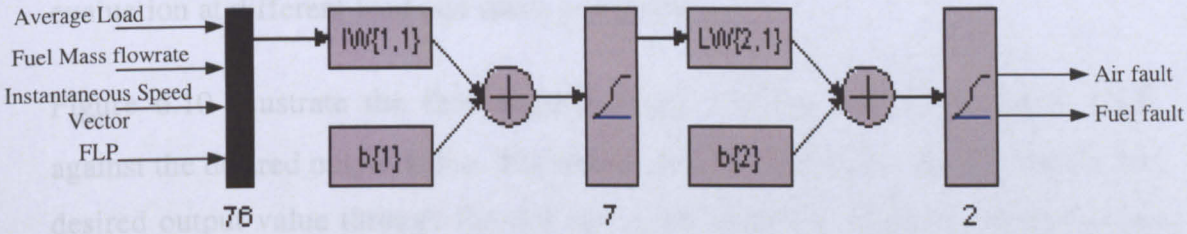

Figure 6.8 Instantaneous speed neural network layout

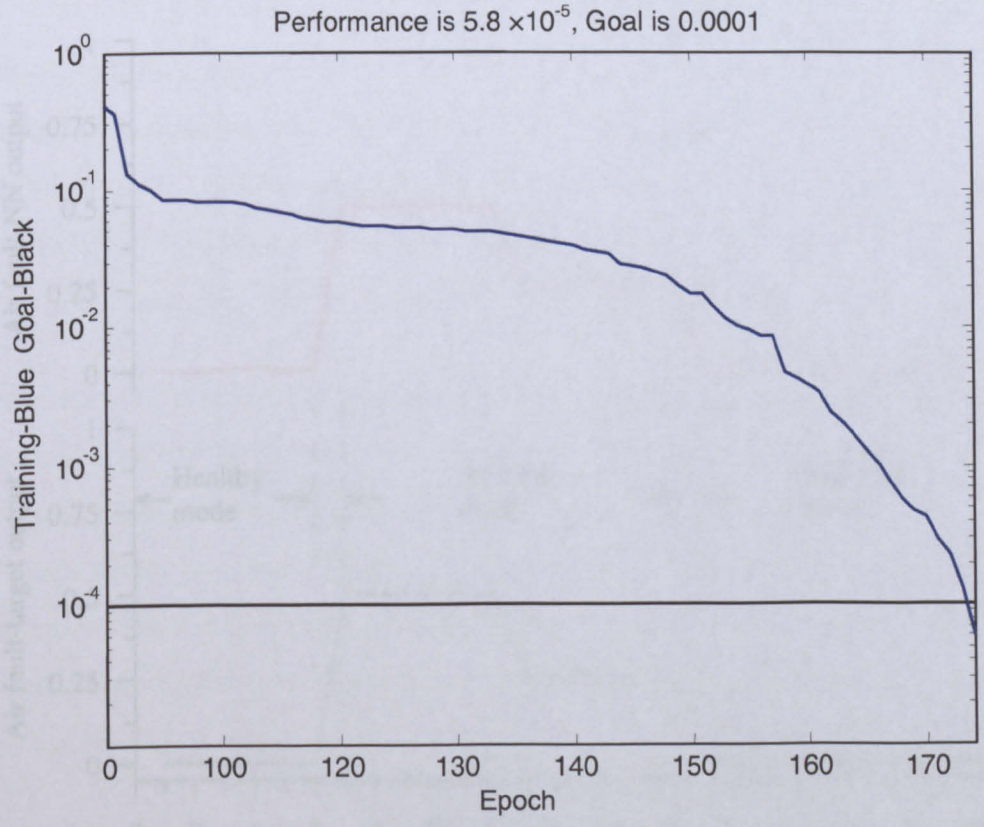

Figure 6.9 Performance factor curve of the training process.

In order to verify the reliability of the developed neural network for engine CMFD, 30 sets of input data covering the different engine operation range under both healthy and faulty mode of operation were applied to the neural network. The comparison between the neural network outputs and the desired target outputs shows the accurate prediction of the engine operating condition and fault level evaluation at different load and speed conditions.

Figure 6.10 illustrate the first output, which evaluates the air blockage level, against the desired output value. The neural network output accurately matches the desired output value through the full set of test samples. When the engine is run under healthy or under fuel fault mode the value of the air blockage fault (output 1) yields a value of 0, whereas in case of air starvation this output evaluate the ratio of the blockage. A relatively low error value was found in the neural network output (maximum of 0.018) as shown in Figure 6.11.

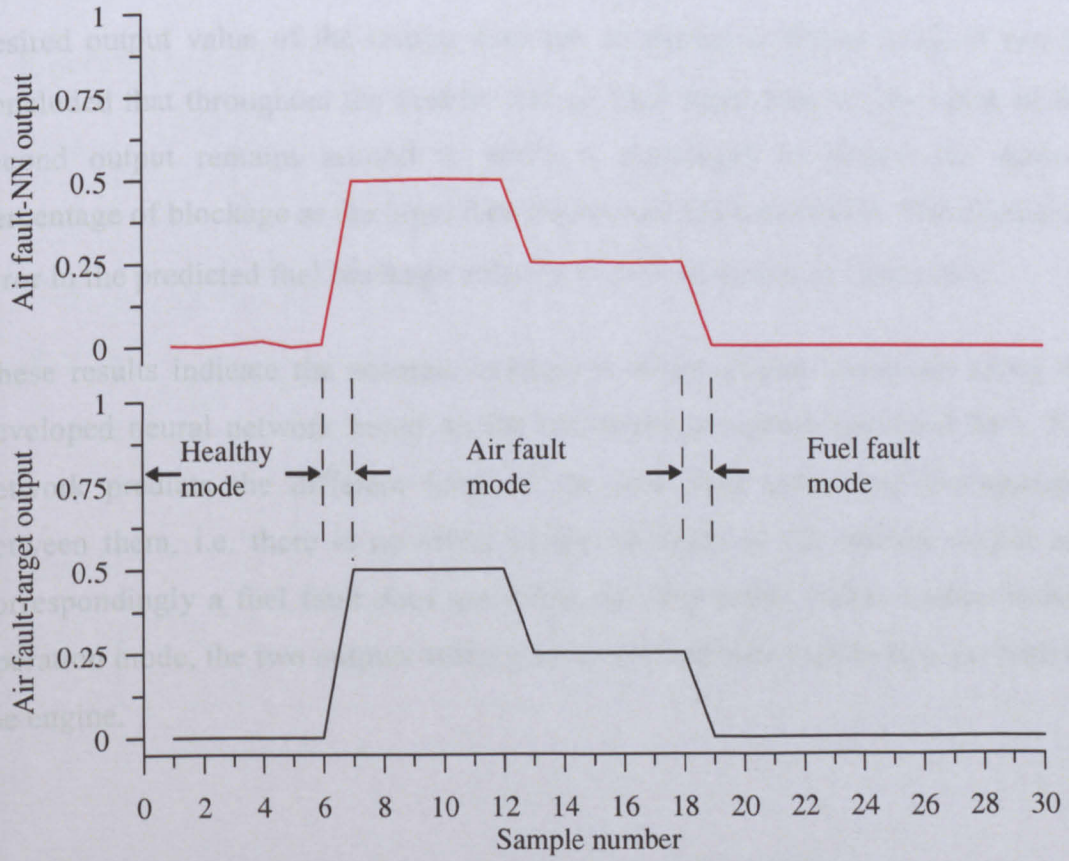

Figure 6.10 Air fault prediction validation using instantaneous NN.

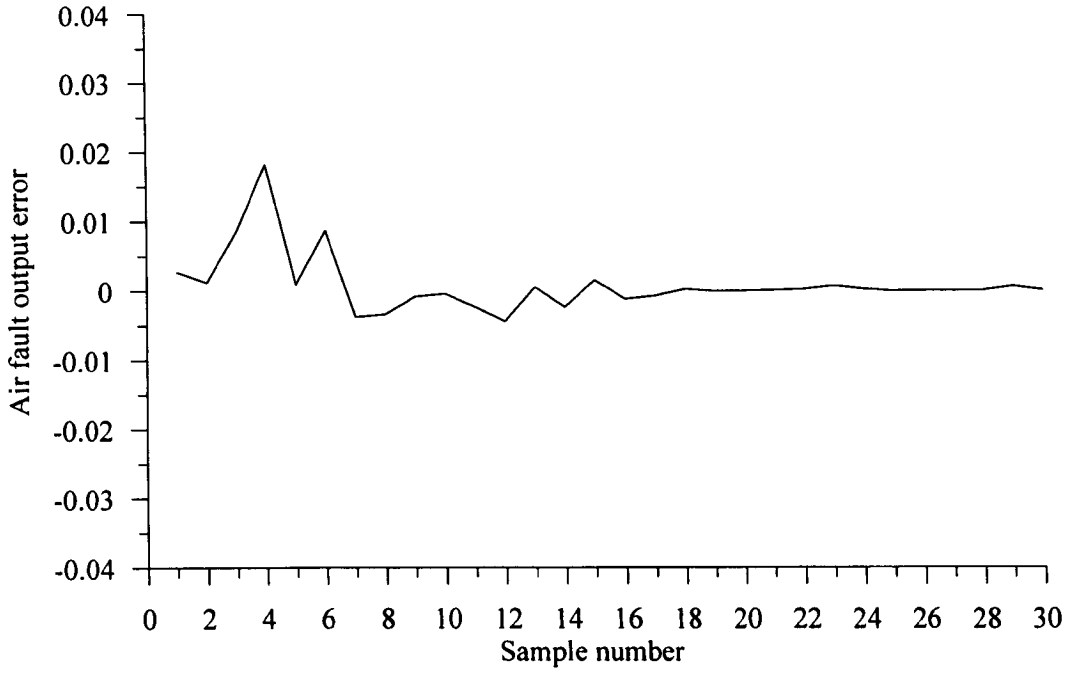

Figure 6.11 Error in the air blockage fault evaluation.

The fuel blockage fault, evaluated by the second output, was verified against the desired output value of the testing data set, as shown in Figure 6.12. It can be concluded that throughout the healthy and air fault input data set the value of the second output remains around 0, while it converged to almost the desired percentage of blockage as the input data shows fuel fault condition. The maximum error in the predicted fuel blockage value is ±0.017 as shown in Figure 6.13.

These results indicate the accurate evaluation of the engine condition using the developed neural network based on the instantaneous speed measured data. The network predicts the different level of the two fault types and distinguishes between them, i.e. there is no effect of the air fault on the second output and correspondingly a fuel fault does not affect the first output value. Under healthy operation mode, the two outputs value goes to 0 to indicate that there is no fault on the engine.

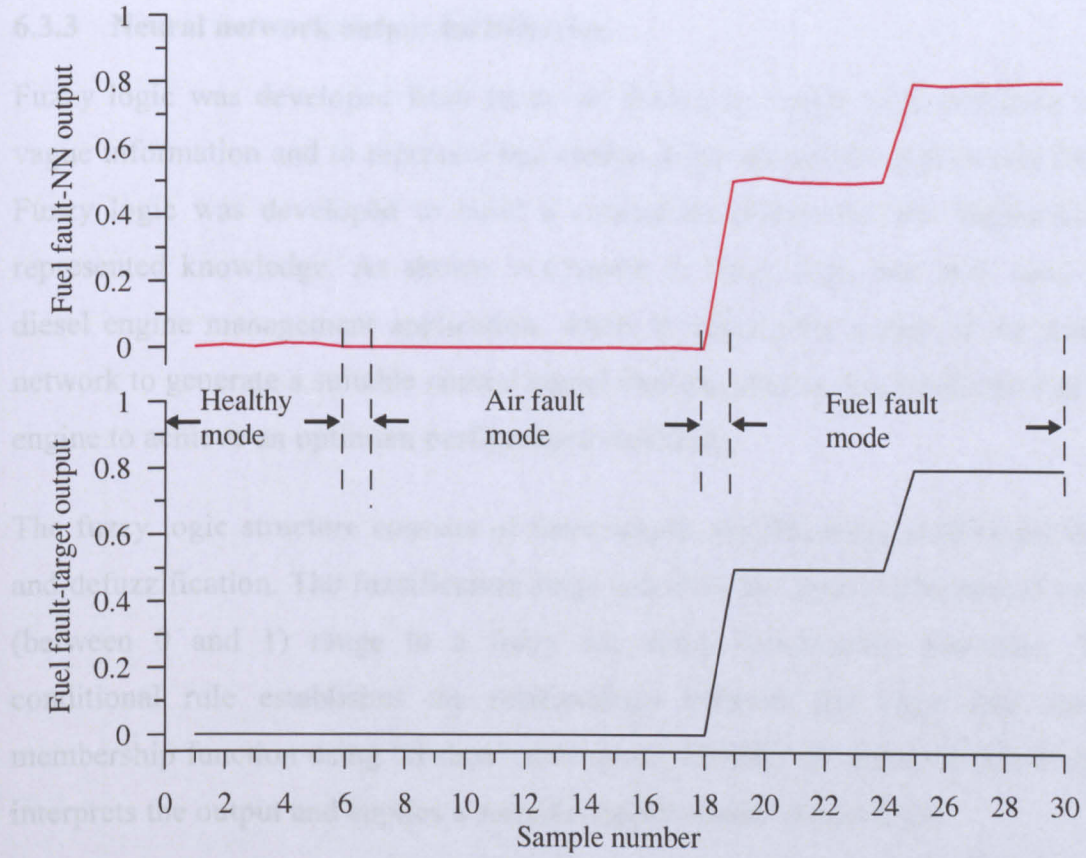

Figure 6.12 Fuel fault validation result using the instantaneous speed NN.

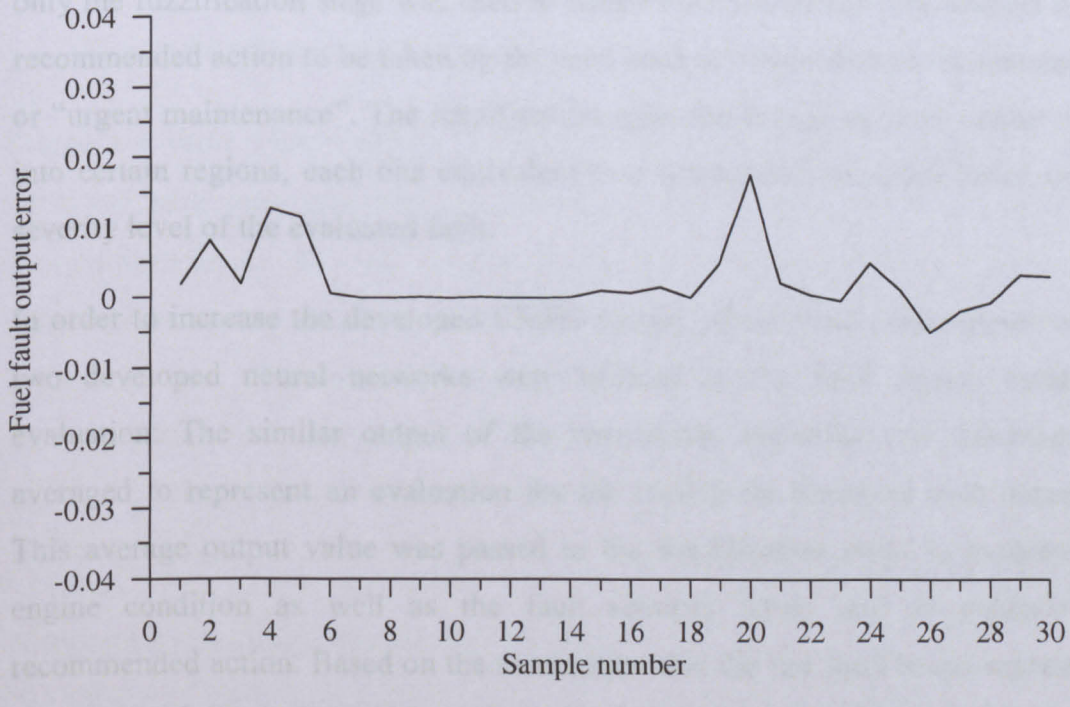

Figure 6.13 Error in the fuel blockage fault evaluation.

6.3.3 Neural network output fuzzification

Fuzzy logic was developed from fuzzy set theory to reason with uncertain and vague information and to represent knowledge in an operationally powerful form. Fuzzy logic was developed to build a conceptual framework for linguistically represented knowledge. As shown in Chapter 2, fuzzy logic has been used for diesel engine management application, where it utilizes the output of the neural network to generate a suitable control signal that can adapt some parameters in the engine to achieve an optimum performance condition.

The fuzzy logic structure consists of three stages, fuzzification, conditional rule, and defuzzification. The fuzzification stage converts the input mathematical value (between 0 and 1) range to a fuzzy set using membership functions. The conditional rule establishes the relationships between the input and output membership function using "if-then" statements. Finally, the defuzzification stage interprets the output and applies a suitable output control signal level.

As the aim of the present work is to develop a CMFD system for the diesel engine, only the fuzzification stage was used to convert the neural network outputs into a recommended action to be taken by the user, such as "maintenance recommended" or "urgent maintenance". The fuzzification splits the neural network output range into certain regions, each one equivalent to a corresponding action based on the severity level of the evaluated fault.

In order to increase the developed CMFD system performance, the outputs of the two developed neural networks were utilized in the final engine condition evaluation. The similar output of the two neural networks was summed and averaged to represent an evaluation for the fault level based on both networks. This average output value was passed to the fuzzification stage to evaluate the engine condition as well as the fault severity level, and to produce the recommended action. Based on the assumption that the test fault levels represent a milestone of the fault severity range, the fuzzification membership function of each output of the neural network was evaluated.

The air inlet blockage fault severity range was divided to three parts. If the blockage is below 25% the engine was considered as healthy (and no action should

be done). Between 25% and 50%, as the air inlet blockage is developed maintenance action is recommended. If it goes over 50%, the engine should be stopped and the air inlet checked. The values of 25% and 50% can be changed based on the manufacturers recommendation within the practical application of the developed CMFD system.

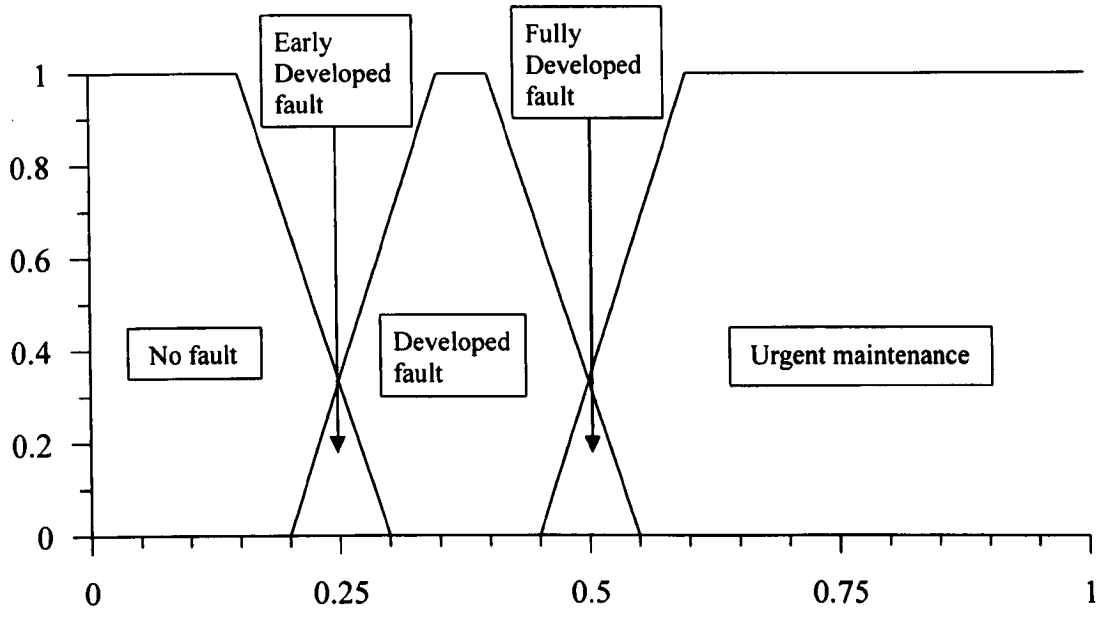

Figure 6.14 The graphical representation of air inlet blockage severity.

Based on these three ranges, the fuzzification memberships of the air inlet blockage fault were generated, as shown in Figure 6.14, using a ±5% variation around each level. The used membership functions generate five regimes for the fault evaluation which can be used to interpret the detected air inlet fault level to inform the user of the recommended action. The fuzzy membership function can be programmed into the algorithm using different techniques such as a lookup table. To simplify the different regimes, it was expressed using "if-then" statements as follows:

If (output-1 < 0.2) then "no air inlet blockage"

If (0.2 ≤ output-1 < 0.3) then "early air inlet blockage"

If (0.3 ≤ output-1 < 0.45) then "developed air inlet blockage"

If (0.45 ≤ output-1 < 0.55) then "fully developed air inlet blockage"

If (0.55 ≤ output-1 < 1) then "urgent maintenance required for air inlet"

These membership functions can be integrated into the developed CMFD algorithm and programmed using the appropriate programming language for the used microcontroller in the practical application.

The fuel fault severity was evaluated using the second output (output-2) of the neural network, and can be used to estimate the suitable action for the engine user. As the fuel starvation level has no specific level at which the different maintenance actions are recommended, some arbitrary values were used within the present study for evaluating the CMFD algorithm application. More detail about the fault testing level selection are found in section 4.2. Using the two testing level values (50% and 80%) as a border line between recommended actions with a ±10% variation around each level; three fuzzy membership functions were assumed as shown in Figure 6.15. The developed fuzzy membership functions generate five regions for the engine conditions at which the suitable maintenance action can be evaluated. As stated before, the fuzzy membership function can be converted to a programmable form depending on the used platform for the practical applications.

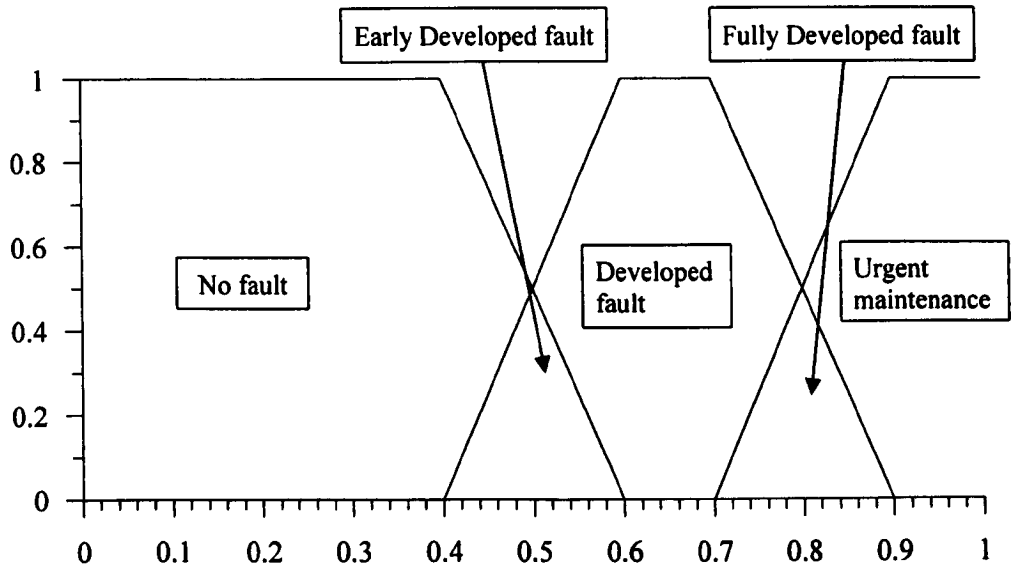

Figure 6.15 The graphical representation of the fuel blockage severity.

6.3.4 Developed CMFD system

The developed neural networks and fuzzification were integrated together to form the developed CMFD algorithm, which was constructed using the MATLAB/SIMULINK platform. A block diagram is included in Appendix B. The MATLAB/SIMULINK developed code can also be integrated into the data acquisition code, which was developed using Labview platform. C-code can be generated using Labview for different applications. Within the present study, the code was only generated under the MATLAB/SIMULINK platform and tested using a set of measured input data.

6.4 SUMMARY

As a result of the measurement data analysis, some key parameters were evaluated that were utilized to detect the two types of fault namely, air inlet and fuel blockage, and to distinguish between the fault type and severity level. These parameters were divided into three groups based on their sampling rate and possible utilization in the developed CMFD algorithm. The groups of key parameters satisfy the requirements for developing a robust CMFD algorithm where the sensors are non-intrusive, cheap, reliable and easy to be integrated on the engine. Some of these sensors are already included in the modern diesel engines, such as engine average speed and total exhaust gas temperature sensors.

Two neural networks were developed to utilize the key parameters in order to evaluate the engine operating condition and the severity level of the fault in case existence. The first neural network evaluates the engine condition based on the exhaust gas temperature plus the average value of some key parameters such as applied load, average engine speed, and FLP setting. The second neural network evaluates the engine condition based on the instantaneous speed and the averaged parameters. The two neural networks work in parallel to improve the performance of the developed CMFD algorithm. In order to prepare the data for training the two neural networks, an output vector was introduced manually into the input data sets which consist of two outputs. Each output represents one type of the two test faults while the output magnitude represents its severity level.

Through the training process of the two neural networks, different training algorithm and network architectures were compared. The *trainlm* training algorithm and MLP network architecture successfully represented the input data and predicted the engine condition. By applying a set of test data at different operating conditions of load and speed, the neural network based on exhaust temperature evaluated the inlet air fault with a maximum error of ±0.048 while the fuel fault maximum error was ±0.047. The second neural network, (based on instantaneous speed), evaluated the air blockage fault and the fuel fault with a maximum error of ±0.018 and ±0.017, respectively.

The output of the two neural networks were combined and averaged to form two outputs, each of which represents one fault type. This method increases the performance of the developed CMFD algorithm by utilizing the two neural networks in parallel. Each of the two averaged outputs was introduced to a fuzzification stage to evaluate the engine condition as well as the recommended user action in the event of a fault existing.

The air fault fuzzification utilizes three membership functions that produce five ranges for the evaluated fault severity levels, which were interpreted into a corresponding message for the user and recommended suitable action. For the present study, the testing levels of the air inlet blockage were utilized to build the membership functions. Five regions were generated at which a message was displayed containing the recommended action and/or the engine condition. Another set of three membership functions were utilized for the fuzzification of the fuel fault output ranges. Five regions for the fuel fault severity levels were generated at which the fuel fault condition or severity levels were displayed for the user. The membership functions for both air inlet and fuel blockage faults could be programmed into the practical applications of the CMFD algorithm with different methods based on the used platform.

The developed CMFD algorithm verifies the hypothesis of the present work by demonstrating the utilization of a limited number of cheap, non-intrusive, reliable and easy installation sensors based on the utilization of neural network and fuzzification combinations.

CHAPTER 7

CONCLUSIONS AND RECOMMENDATIONS

This research has focused on the design, configuration and validation of a system capable of on-line condition monitoring and fault diagnosis of a medium size commercial diesel engine using a neural network based approach. The overall research aim was achieved through the satisfaction of all the research objectives identified in Chapter One. Further to this, the research constitutes original work which has also satisfied recommendations given in previous research.

The work conducted in this research can be summarised as follows

* An available diesel engine was integrated with additional sensors and used as a test facility for experimental measurements required for the development of the key parameters for engine condition evaluation. A hardware signal conditioning and data acquisition program was designed and implemented.
* Automation of an existing manually controlled hydraulic brake dynamometer to improve its loading performance. This includes the integration of actuator, sensors and embedded controller to the hydraulic brake system. The brake was used to simulate the external load applied to the engine through the experimental tests.
* A simulation model for the diesel engine was developed using the basic mathematical relationships that govern the different parameters in the diesel engine. The model includes the dynamic and thermodynamic balancing of the engine and makes use of well defined empirical correlations to predict the engine performance and increase the scope of its utilization. The model was validated using the measured signals.
* A program of experimental tests was undertaken which covers the engine operating range. Tests were performed under healthy condition, and also with two synthetic faults introduced on the engine to establish their individual effect on performances, measured against the healthy state.

* Extensive analysis of the experimental data under both healthy and faulty mode of operation were undertaken to evaluate the fault-symptom relationships. The analysis clarified the key parameters that could be utilized in the engine CMFD system to detect different faults.

* Finally, an intelligent engine CMFD algorithm was developed using a combined neural network and fuzzification approach. Through the development process of the neural network, a multi-network system was utilized to overcome the different sampling rates of the key parameters.

7.1 CONCLUSIONS

The following conclusions can be drawn from the present work:

* A new technique was developed to measure the cylinder and fuel injection pressures by measuring the axial and circumferential strains in the injector body. The sensor calibration was validated through the experimental measurements. The utilization of these signals in the engine CMFD system requires high computational resources which restrict practical application; however, it could be used to measure the peak pressure of fuel injection and cylinder.

* Shortage of fuel and air to the cylinder can be caused by many faults, and directly affects the combustion efficiency and consequently reduces the engine performance.

* Fuel and air faults can be detected on-line by an engine condition monitoring and fault detection system using the following measurements:

    1- Average speed.

    2- Fuel lever position.

    3- Average load torque.

    4- Individual cylinder exhaust temperature.

    5- Single exhaust gas temperature at the exhaust pipe.

    6- Inlet air volume flow rate.

    7- Fuel consumption mass flow rate.

8- Instantaneous engine speed.

* Two neural networks were developed and shown capable of detecting the designated faults and distinguishing different severity levels. Direct measurement sensors were used which do not require sophisticated signal conditioning or data processing. Both neural networks are based on sensors that are cheap, easy installed, and some of which already available in the modern commercial car engines.

* The utilization of the multi-net technique improves the CMFD system performance and provided a reliable tool for fault evaluation in a practical application.

* The fuzzification membership functions transform the different fault level ranges into simple messages that can be presented to the user with a recommended course of action.

* The developed data acquisition and CMFD algorithm can be integrated to form a standalone system as part of portable or fixed diagnostic system.

7.2 VALUE OF THIS RESEARCH

This work has shown that a wide range of diesel engine faults can be successfully diagnosed using a limited number of relatively low cost sensors. Much effort has been directed towards development of testing facilities and experimental tests to select key diagnostic sensors. The developed CMFD system utilizes sensors that are easily installed which allow this system to be practically viable. The application of such system could give the following practical benefits.

* Only equipment which requires attention is dismantled for assessment. This minimises wastage of labour, replacement consumables such gaskets and seals and engine operating time.

* Effective prediction and planning of maintenance operations.

* The rate of development of a fault can be monitored and an informed decision can be made as to when corrective action should take place. This increase reliability, minimises unplanned down-time and allows a fault to

develop until maintenance is forced by safety considerations, catastrophic failure or long term engine damage.

* Measurements of the engine parameters from new to the end of the warranty period and after overhaul give useful comparative data.

This work has made a significant contribution to knowledge in the following areas.

* Development of new direct measuring sensor to measure cylinder and injection fuel pressures which does not change the combustion chamber internal dimensions.
* The approach of developing and configuring a comprehensive, fully automated computer based system to monitor engine condition and detect faults using largely 'off the shelf' software and hardware.
* A detailed analysis of high speed engine instrumentation repeatability and the effect of data sampling and averaging.
* A comprehensive study of commonly occurring high speed diesel engine faults, reasons for their occurrence and quantification of fault severities experienced on in-service engines
* The training and testing of a neural network diagnostic system on real engine data based on low cost easy sensors.
* An assessment of several neural network training algorithm and architectures to give optimum diagnostic performance when applied to a diesel engine.
* Explicit fault-symptom relationships were developed and key diagnostic sensors for high speed engine were identified.
* The utilization of multi-net technique demonstrates that sensors failure can also be detected by comparison of the two neural network outputs.
* Neural network testing on engine speeds and torques which the network has not trained on.
* Utilization of fuzzification at the multi-net output improves the fault severity level detection of the developed engine CMFD system.

7.3 RECOMMENDATION

Finally as a result of this research the following recommendations can be made:

* This research has shown that a neural network-fuzzy structure condition monitoring and fault diagnostic system can successfully be trained to diagnose diesel engine faults on real engine test data generated from one type of diesel engine. Further validation work is required to test this CMFD system on many engines of a similar types and rating engines to establish whether the developed system in this work is generic.

* The variation in environmental condition such as barometric pressure, air inlet temperature, cooling water temperature and relative humidity could affect the engine performance. These parameters were restricted to ranges found in the UK. If this system were to be installed in a practical application it could be affected by the climatic condition variation. Further engine test work and CMFD algorithm validation are required to establish the diagnostic ability of the system under various extremes of climatic conditions.

* The result of this research shows the possibility to indentify the cylinder which suffers from fuel starvation on individual base. However, the tests were undertaken with only one cylinder with that fault. Further tests of the engine with the other cylinders having the same fault will make the experimental data required for training and testing of the CMFD system available. The developed CMFD system could then be trained to indentify the number of cylinder that suffers from that type of faults.

* Some of the key sensors used with the developed system are not currently installed onto the available market diesel engines such as individual exhaust gas temperature sensors; however, the installation of these sensors is easy and will not affect the engine design. Also, the need for high engine efficiencies and low gases emissions will lead the engine development to install more sophisticated instrumentation which will include such type of sensors.

* This research has concentrated on the diagnosis of limited faults. Further work is required to establish the performance of the CMFD system under other faults and multiple faults in the same time.

REFERENCES

Amstutz, A. and Luigi, R. (1995), "EGO sensor based robust output control of EGR in diesel engines", *IEEE Transactions on Control Systems Technology,* 3, 1, 39-48.

Assanis, D. N., Atreya, A., Borgnakke, C., Dowling, D., Filipi, Z., Hoffman, S., Homsy, S., Kanafani, F., Morrison, K., Patterson, D., Syrimis, M., Winton, D., Zhang, G. and Bryzik, W. (1997), "Development of a modular, transient, multi-cylinder diesel engine simulation for system performance and vibration studies", *In Proceedings of Technical Conference of ASME ICE, Colorado, Paper 97-ICE-11,* 87-101.

Assanis, D. N. and Heywood, B. J. (1986), "Development and use of a computer simulation of the turbocompunded diesel system for engine performance and component heat transfer studies", *SAE paper 860329.*

Ayoubi, M. (1998), "Comparison between the dynamic multi-layered perceptron and the generalised Hammerstein model for experimental identification of the loading process in diesel engines", *Control Engineering Practice.,* 6, 2, 271-279.

Ball, J. K., Stone, C. R. and Collings, N. (1999), "Cycle-by cycle modelling of NO formation and comparison with experimental data", *Proc. Instn. Mech. Engrs.,* 213, Part D, 175-189.

Baranescu, C. (1999) "Diesel engine reference book", Second edition, *Elsevier Butterworth Heinemann.*

Bielawski, L. and Lewand, R. (1991) "Intelligent systems design - integrating expert systems, hypermedia, and database technologies", *John Wiely & Sons.*

Borman, G. and Nishiwaki, K. (1987), "Internal combustion engine heat transfer", *Prog. Energy Combust. Sci.,* 13, 1-46.

Chen, M.-Y. and Linkens, D. A. (1998), "A fast fuzzy modelling approach using clustering neural networks", *Proceedings of the IEEE International Conference on Fuzzy Systems,* 2, 1088-1093.

Chow, A. and Wyszynski, M. L. (1999), "Thermodynamic modelling of complete engine systems — a review", *Proc Instn Mech Engrs,* 213, Part D, 403-415.

Chow, M., Sharpe, R. N. and Hung, J. C. (1993), "On the application and design of artificial neural networks for motor fault detection-Part II", *IEEE Transactions on Industrial Electronics,* 40, 2, 189-196.

Crowther, W. J., Edge, K. A., Burrows, C. R., Atkinson, R. M. and Woollons, D. J. (1998), "Fault diagnosis of a hydraulic actuator circuit using neural networks - an output vector space classification approach", *Proc Instn Mech Engrs,* 212 part1, 57-68.

Culliere, T., Titli, A. and Comeu, J. M. (1995), "Neuro-fuzzy modeling of nonlinear systems for control purposes", *Proceedings of the IEEE International Conference on Fuzzy Systems,* 4, 2009-2016.

Drew, S. J., Hesterman, D. C. and Stone, B. J. (1999), "The torsional excitation of variable inertia effects in a reciprocating engine", *Mechanical Systems and Signal Processing,* 13, 1, 125-144.

El-Ghamry, M., Steel, J. A., Reuben, R. L. and Fog, T. L. (2005), "Indirect measurement of cylinder pressure from diesel engines using acoustic emission", *Mechanical Systems and Signal Processing,* 19, 4, 751-765.

Flower, J. O. and Hazell, P. A. (1971), "Sample-data theory applied to the modelling and control analysis of compression ignition engines-part II", *International Journal of Control,* 13, 4, 609-623.

Flower, J. O. and Windett, G. P. (1976), "Dynamic measurements of a large diesel engine using p.r.b.s. technique- part 2. Instrumental, experimental techniques and results", *international journal of control,* 24, 3, 393-404.

Ford (1998) "Engine build specification manual".

Gamo, S. O., Ouladsine, M. and Rachid, A. (1999), "Diesel engine exhaust emissions modelling using artificial neural networks", *SAE paper number 1999-01-1163.*

Gamo, S. O., Rachid, A. and Ouladsine, M. (1998), "GMDH method applied to nonlinear identification of a turbocharged diesel engine", *Proceedings of the American Control Conference,* 962-964.

Gan, C. and Danai, K. (1999), "Fault diagnosis of the IFAC benchmark problem with a model-based recurrent neural network", *Proceedings of the 1999 IEEE, International Conference on Control Applications.,* 1755-1760.

Gelgele, H. L. and Wang, K. (1998), "An expert system for engine fault diagnosis: development and application", *Journal of Intelligent Manufacturing,* 9, 539-545.

Glass, J. W. and Franchek, M. A. (1999), "NARMAX modelling and robust control of internal combustion engines", *international journal of control,* 72, 4, 289-304.

Grimmelius, H. T., Meiler, P. P., Maas, H. L. M. M., Bonnier, B., Grevink, J. S. and van Kuilenburg, R. F. (1999), "Three state-of-the-art methods for condition monitoring", *IEEE Transactions on Industrial Electronics,* 46, 2, 407-416.

Grondin, O., Stobart, R., Chafouk, H. and Maquet., J. (2004), "Modelling the compression ignition engine for control: review and future trends", *SAE paper number 2004-01-0423.*

Gu, F., Jacob, P. J. and Ball, A. D. (1996), "A RBF neural network model for cylinder pressure reconstruction in internal combustion engines", *IEE*

Colloquium on Modeling and Signal Processing for Fault Diagnosis, 18, Part D, 4/1-4/11.

Gu, F., Jacob, P. J. and Ball, A. D. (1999), "Non-parametric models in the monitoring of engine performance and condition Part 2: non-intrusive estimation of diesel engine cylinder pressure and its use in fault detection", *Proc. Instn. Mech. Engrs.,* 213, Part D, 135-143.

Guzzella, L. and Amstutz, A. (1998), "Control of diesel engines", *IEEE Transactions on Control Systems,* 18, 5, 53-71.

Hafner, M., Jost, O. and Isermann, R. (2001), "Mechatronic design approach for engine management systems", *European Journal of Control,* 7, 2-3, 220-247.

Hafner, M., Schuler, M. and Nelles, O. (1999), "Dynamical identification and control of combustion engine exhaust", *Proceedings of the American Control Conference, San Diego, California.*

Hafner, M., Schuler, M., Nelles, O. and Isermann, R. (2000), "Fast neural networks for diesel engine control design", *Control Engineering Practice,* 8, 1211-1221.

Hazell, P. A. and Flower, J. O. (1971a), "Discrete modelling of spark-ignition engines for control purposes", *International Journal of Control,* 13, 4, 625-632.

Hazell, P. A. and Flower, J. O. (1971b), "Sample-data theory applied to the modelling and control analysis of compression ignition engines-part I", *International Journal of Control,* 13, 3, 549-562.

Hendricks, E. (1989a), "The analysis of mean value engine models", *SAE paper number 890563.*

Hendricks, E. (1989b), "Mean value modelling of large turbocharged two-stroke diesel engines", *SAE paper number 890564.*

Hesterman, D. C. and Stone, B. J. (1994), "A systems aproach to the torsional vibration of multi-cylinder reciprocating engines and pumps", *Proc Instn Mech Engrs, Part C, Journal of Mechanical Engineering Science.,* 208, C6, 395-408.

Heywood, J. B. (1988) "Internal combustion engine fundamentals", *McGraw-Hill, New York.*

Jacob, P. J., Gu, F. and Ball, A. D. (1999), "Non-parametric models in the monitoring of engine performance and condition Part 1: modelling of non-linear engine processes", *Proc. Instn. Mech. Engrs.,* 213, Part D, 73-81.

Jensen, J. P., Kristensen, A. F., Sorenson, S. C. and Houbak, N. (1991), "Mean value modeling of a small turbocharged diesel engine", *SAE paper number 910070.*

Jiang, J. (1994), "Optimal gain scheduling controller for a diesel engine", *IEEE Control Systems,* 14, 4, 42-48.

Jiang, J., Gub, F., Gennish, R., Moore, D. J., Harris, G. and Ball, A. D. (2008), "Monitoring of diesel engine combustions based on the acoustic source characterisation of the exhaust system", *Mechanical Systems and Signal Processing,* 22, 1465-1480.

Jones, N. B. and Li, Y.-H. (2000), "A review of condition monitoring and fault diagnosis for diesel engines", *TriboTest,* 6, 3, 267-292.

Kalogirou, S. A. (2003), "Artificial intelligence for the modeling and control of combustion processes: A review", *Progress in Energy and Combustion Science,* 29, 6, 515-566.

Kao, M. and Moskwa, J. J. (1994), "Model-based engine fault detection using cylinder pressure estimates from nonlinear observers", *Proceedings of the 33rd IEEE Conference on Decision and Control,* 3, 2742-2747.

Kao, M. and Moskwa, J. J. (1995), "Turbocharged diesel engine modeling for nonlinear engine control and state estimation", *Transaction of the ASME, Journal of Dynamic Systems, Measurement and Control,* 117, 1, 20-30.

Kim, Y.-W., Rizzoni, G. and Utkin, V. (1998), "Automotive engine diagnosis and control via nonlinear estimation", *IEEE Control Systems,* 18, 5, 84-99.

Kutz, M. (1998) "Mechanical Engineer's Handbook", Second, *John Wiley & Sons, Inc.*

Kwan, C., Lewis, F. L. and Dawson, D. M. (1998), "Robust neural-network control of rigid-link electrically driven robots", *IEEE Transactions on Neural Networks,* 9, 4, 581-588.

Langballe, M., Tonning, L. and Wibrog., T. (1975), "Condition monitroing of diesel engines", *Norwegian Maritime Research,* 3, 2-16.

Lechie, D. (1999) "diesel engine technical manual", *Ford Company.*

Leonard, J. A. and Kramer, M. A. (1991), "Radial basis function networks for classifying process faults", *IEEE Control Systems Magazine,* 11, 31-38.

Leonhardt, S., Ludwig, C. and Schwarz, R. (1995), "Real-time supervision for diesel engine injection", *Control Eng. Practice,* 3, 7, 1003-1010.

Li, H. and Stone, B. J. (1999), "Time domain modelling of reciprocating engine", *Mechanical Systems and Signal Processing,* 13, 1, 169-178.

Lucking, W. G., Darnell, M. and Chesmore, E. D. (1994), "Acoustical condition monitoring of a mechanical gearbox using artificial neural networks", *IEEE International Conference on Neural Networks, World Congress on Computational Intelligence,* 5, 3307-3311.

Ludwig, C. and Ayoubi, M. (1995), "Fault detection schemes for diesel engine turbocharger", *Proceeding of the Amerian Control Conference,* 3, 2118-2122.

Majors, M., Stori, J. and Cho, D. (1994), "Neural network control of automotive fuel-injection systems", *IEEE Control Systems Magazine,* 14, 31-36.

Mariani, F. and Postrioti, L. (1996), "Modelling diesel engine using KIVA II 3D-code: validation of a new global combustion model and its sensitivity to the spatial discretization", *SAE paper number 960872.*

Meireles, M. R. G., Almeida, P. E. M. and Simés, M. G. (2003), "A comprehensive review for industrial applicability of artificial neural networks", *IEEE Transactions on Industrial Electronics,* 50, 3, 585-601.

Miller, W. T. (1989), "Real-Time Application of neural networks for sensor-based control of robots with vision", *IEEE Transactions on Systems, Man, and Cybernetics,* 19, 4, 825-831.

Morita, S. (1993), "Optimization control for combustion parameters of petrol engines using RBF-networks", *International journal of vehicle design,* 14, 5/6, 552-562.

Moro, D., Cavina, N. and Ponti, F. (2002), "In-cylinder pressure reconstruction based on instantaneous engine speed signal", *Transaction of the ASME, Journal of Engineering for Gas Turbines and Power,* 124, 220-225.

Nareid, H. and Lightowler, N. (2004), "Detection of engine misfire events using an artificial neural network", *SAE paper number 2004-01-1363.*

Narendra, K. S. and Parthasarathy, K. (1990), "Identification and control of dynamical systems using neural networks", *IEEE Transactions on neural networks.,* 1, 1, 4-27.

Nguyen, D. H. and Widrow, B. (1990), "Neural networks for self-learning control systems", *IEEE Control Systems Magazine,* 10, 18-23.

P. J. Edwards, Murray, A. F., Papadopoulos, G., Wallace, A. R., Barnard, J. and Smith, G. (1999), "The application of neural networks to the papermaking industry", *IEEE Transactions on neural networks,* 10, 6, 1456-1464.

Rakopoulos, C. D. and Giakoumis, E. G. (1998), "Simulation and analysis of a naturally aspirated IDI diesel engine under transient conditions comprising the effect of various dynamic and thermodynamic parameters", *Energy Convers. Mgmt,* 39, 5/6, 465-484.

Ramos, J. I. (1989) "Internal combustion modelling", *Hemishere, New York.*

Rao, S. S. (1990) "Mechanical vibration", *Addison-Wesley, Reading, Massachusetts.*

Rosentblatt, F. (1958), "The perceptron: A probabilistic model for information storage and organization in the brain." *Psychological Review,* 65, 386–408.

Sardy, S., Ibrahim, L. and Yasuda, Y. (1993), "A application of vision system for the identification and defect detection on woven fabrics by using artificial neural networks", *Proceedings of 1993 International Joint Conference on Neural Networks*, 2141-2144.

Sharkey, A. J. C., Chandroth, G. O. and Sharkey, N. E. (2000a), "Acoustic emission, cylinder pressure and vibration: a multisensor approach to robust fault diagnosis", *Proceedings of the IEEE-INNS-ENNS International Joint Conference on Neural Networks,* 6, 223-228.

Sharkey, A. J. C., Chandroth, G. O. and Sharkey, N. E. (2000b), "A multi-net system for the fault diagnosis of a diesel engine." *Neural computing & applications,* 9, 152-160.

Sharkey, A. J. C., Sharkey, N. E. and Chandroth, G. O. (1996), "Diverse neural-net solutions to fault diagnosis problem." *Neural computing & applications,* 4, 10, 1405-1415.

Shi, W., Yang, J. and Tang, T. (2005), "RBF NN Based marine diesel engine generator modelling", *Proceeding of the Amican Control Onference,* 4, 8-10, 2745-2749.

Silva, L. E. B., Bose, B. K. and Pinto, J. O. P. (1999), "Recurrent-neural-network-based implementation of a programmable cascaded low-pass filter used in stator flux synthesis of vector-controlled induction motor drive", *IEEE Transactions on Industrial Electronics,* 46, 3, 662-665.

Sletmo, K. (1978), "Condition monitoring of marine diesel engines." *ASEA journal,* 51, 6, 143-146.

Sood, A. K., Fahs, A. A. and Henein, N. A. (1983), "A real-time microprocessor based system for engine deficiency analysis", *IEEE Transactions on Industrial Electronics,* 30, 2, 159-163.

Specht, D. (1990), "Probabilistic neural networks", *Neural Networks,* 3, 1, 109-118.

Szu, H. H. (1993), "Automatic fault recognition by image correlation neural network techniques", *IEEE Transactions on industrial Electronics.,* 40, 2, 197-208.

Teeter, J. and Chow, M. Y. (1998), "Application of functional link neural network to HVAC thermal dynamic system identification", *IEEE Transactions on Industrial Electronics,* 45, 1, 170-176.

Tjong, J. S., Lau, T. H. K., Chang, D. K. and Reif, Z. F. (1993) In *Proceeding of 11th international model analysis conference*, Vol. 1 & 2, pp. 1252-1258.

Twiddle, J. A. and Jones, N. B. (2002), "Fuzzy model-based condition monitoring and fault diagnosis of a diesel engine cooling system", *Proc Instn Mech Engrs,* 216, Part I: J Systems and Control Engineering, 215-224.

Wang, Y. Y., Krishnaswami, V. and Rizzoni, G. (1997), "Event-based estimation of indicated torque for IC engines using sliding-mode observers", *Control Eng. Practice,* 5, 8, 1123-1129.

Watson, N. (1982), "Transient performance simulation and analysis of turbocharged diesel engines", *SAE paper number 810338.*

Watson, N. (1984), "Dynamic turbocharged diesel engine simulator for electronic control system development", *Transaction of the ASME, Journal of Dynamic Systems, Measurement and Control,* 106, 1, 27-45.

Watson, N. and Janota, M. S. (1982) "Turbocharging the internal combustion engine", *MacmillN, London.*

Watson, N. and Marzouk, M. (1978), "A non-liner digital simulation of turbocharged diesel engines under transient conditions", *SAE paper number 770123.*

Watson, N., Pilley, A. D. and Marzouk, M. (1980), "A combustion correlation for diesel engine simulation", *SAE paper number 800029.*

Whiteley, J. R., Davis, J. F., Mehrotra, A. and Ahalt, S. C. (1996), "Observations and problems applying ART2 for dynamic sensor pattern interpretation", *IEEE Transactions on Systems, Man, and Cybernetics-Part A: Systems and Humans,* 26, 4, 423-437.

Wu, A. and Tam, P. K. S. (1999), "A simplified model of fuzzy inference system constructed by using RBF neurons", *Proceedings of the IEEE International Conference on Fuzzy Systems,* 1, 50-54.

Wu, S., Er, M. J. and Gao, Y. (2001), "A fast approach for automatic generation of fuzzy rules by generalized dynamic fuzzy neural networks", *Proceedings of the IEEE International Conference on Fuzzy Systems,* 9, 4.

Yin, Y., Wang, W., Yan, X., Xiao, H. and Wang, C. (2003), "An integrated on-line oil analysis method for condition monitoring", *Measurement Science and Technology,* 14, 1973-1977.

Yoo, S. I. and Kim, I. K. (1992), "DIAS1: An expert system for diagnosing automobiles with electronic control units", *Expert system with application,* 4, 1, 69-78.

Zhang, J., Kang, J. and Wang, M. (2003), "Fuzzy modelling of diesel engine using Modified Self-Organizing MAP network", *System Analysis Modelling Simulation,* 43, 8, 1107-1117.

Zurada, J. M. (1995) "Introduction to artificial neural Systems", *Pws Pub Co.*

Zweiri, Y. H., Whidborne, J. F. and Seneviratne, L. D. (2001), "Detailed analytical model of a single-cylinder diesel engine in the crank angle domain", *Proceedings of the Institution of Mechanical Engineers, Part D: Journal of Automobile Engineering,* 215, 11, 1197-1216.

Zweiri, Y. H., Whidbrone, J. F. and Seneviratne, L. D. (1998), "A mathematical transient model for the dynamics of single cylinder diesel engine", *International Conference on Simulation, York, Oct. 98*, 145-151.

Zweiri, Y. H., Whidbrone, J. F. and Seneviratne, L. D. (1999), "Dynamic simulation of single-cylinder diesel engine including dynamometer modelling and friction", *Proc. Instn Mech. Engrs,* 213, Part D, 391-402.

Zweiri, Y. H., Whidbrone, J. F. and Seneviratne, L. D. (2000), "Instantaneous Friction Components Model for Transient Engine Operation", *Proc. Instn Mech. Engrs,* 214, Part D, 809-824.

APPENDIX A. TECHNICAL DATA OF HARDWARE

A.1 LOAD CELL

Omega high accuracy S-Type load cell model number (LCCA-200)
Maximum load capacity: 200 lb
Rated Output: 3mV/V ±0.0075mV/V actual output supplied with each load cell)
Excitation: 10 Vdc (15 Vdc maximum)
Accuracy: 0.037% Full Scale
Linearity: 0.03% FS
Hysteresis: 0.02% FS
Repeatability: 0.01% FS
Zero Balance: 1% FS
Creep in 20 min: 0.03% FS
Operating Temperature: 0 to 150°F
Compensated Temperature: 0 to 150°F
Thermal effects: Zero - 0.0015% FS/°F Span - 0.0008% RDG/°F
Maximum Load: Safe, 150%; Ultimate, 300%
Bridge Resistance: 350 Ohms nominal
Full Scale Deflection: 0.010 in to 0.020 in
Construction: Nickel Plated Carbon Steel
Cable: 20 ft 4-conductor shielded 22-gage wire

A.2 SPEED SENSOR

Omron manufacture
Model number: EE-SX673AXSM
Supply voltage: 5-24 V(DC)
Depth: 12.8 mm
Height: 28.4 mm
IP rating: IP50
Output type: L, D/O
Selectable light/Dark: yes
Switch current: 100 mA
Switching mode: Light Off/On
Slot width: 13.4 mm
Slot depth: 9 mm

A.3 LIMITING SWITCH

Brand: SUNX
Manufacture number: PM-L54P (PNP)
Orientation: Upright
Detector type: Through Beam
Supply voltage: 5 to 24V(dc)
Switching current: 50mA
Sensing distance: 5mm

Output type: PNP
Switching frequency: 1kHz

A.4 STEPPER MOTOR

Type: RAPID SYN
Model: 34D-9209FC.
Step angle: 1.8° (200 step/cycle).
Rated voltage: 2.5 VDC.
Rated current: 4.6 A/phase.
No. of wires: 8 wire.

A.5 MOTOR ENCODER

Hp quick assembly three channel optical encoder
Type: HEDS-5540 A06
Number channel: 3 ch.
Resolution: 500 counts/revelution
Supply voltage: -0.5 V to 7 V
High level output voltage: 2.4 V
Low level output voltage: 0.4 V
Supply current: 30 (min) to 85 (max) mA
Output current: -1.0 to 5 mA per channel.
Velocity: 30000 RPM
Rise time: 180 ns
Fall time: 40 ns
Shaft diameter: 0.25 in

A.6 PC-104

Manufacturer: Arcom
Model: AIM104-386EX
Processor: Intel 386EX 33MHz
RAM: 1Mb SRAM
FLASH: 1Mb (512kb × 2)
Connections: 3 × RS232 serial ports
1 × RS485 port
Real Time Clock chip with off-board battery back-up
10 Way header for TTL I/O
16-bit PC/104 data bus
5VDC only operation
Power consumption: 500mA @ +5V
Power-down mode: 150mA @ +5V

A.7 MOTION MODULE

Manufacturer: Arcom
Model: AIM104-MOTION-1
Operation mode: Full step and Half step.

Driver commutator control signals available for external amplification.
Stepper drive current: 0.7A or less).
2 or 3 channel rotary incremental encoder should be used.

A.8 MULTI I/O MODULE

DAC
Two 12-bit analogue outputs: Current sink: 0-25mA AND
Bipolar voltage: -5v to +5v
Channel Output impedance: Vout = <10W
Voltage overhead at Iout pin 7.5V(MIN)
Channel update time: 320msec/channel
Calibration accuracy @ 25°C: ±2 LSB (MAX) (REF=5.0V)
Linearity: Differential Non-linearity = ±0.5LSB (MAX)
Integral Non-linearity = ±3.5LSB (MAX)
Offset error ±4mV (-20°C to +70°C typ/0°C to 70°C max)
Gain error (cal @ 25°) 0.35% (-20°C to +70°C typ/0°C to 70°C max)
ADC
Bipolar analogue input range: -5v to +5v
12-bit analogue inputs configured as: 16 channel single ended OR
8 channel differential
Channel Input impedance: 10MW//10pF typ
Conversion time: 500msec/channel
Calibration accuracy @ 25°C: Adjustable
Relative accuracy @ 25°C: ±2LSB (-5V to +5V)
Linearity: Differential Non-linearity = ±1LSB (No missing codes)
Gain error (cal @ 25°) 0.5% (-20°C to +70°C typ/0°C to 70°C max)
8 channels of isolated digital input.
Digital input switching voltage range: 10V to 30V
Maximum digital input frequency: 50Hz
Debounce filter time constant: 10ms
All digital inputs include reverse input protection diodes.
Module access LED (on all decoded addresses)
8-bit PC/104 (IEEE996) bus interface.
Operating temperature range, -20°C to +70°C.
Power consumption from the PC/104 host: Max 480mA @+5v

A.9 STRAIN GAUGE

Micro-Measurements Division
Type: WK-06-062AP 350
Resistance: 350 ±0.3%
Gage factor: 2.04 ±1.0%
Transverse sensitivity : -1 ±0.2% at 24°C

APPENDIX B. CIRCUIT SCHEMATIC DIAGRAM

B.1 THE ENGINE SENSOR LAYOUT

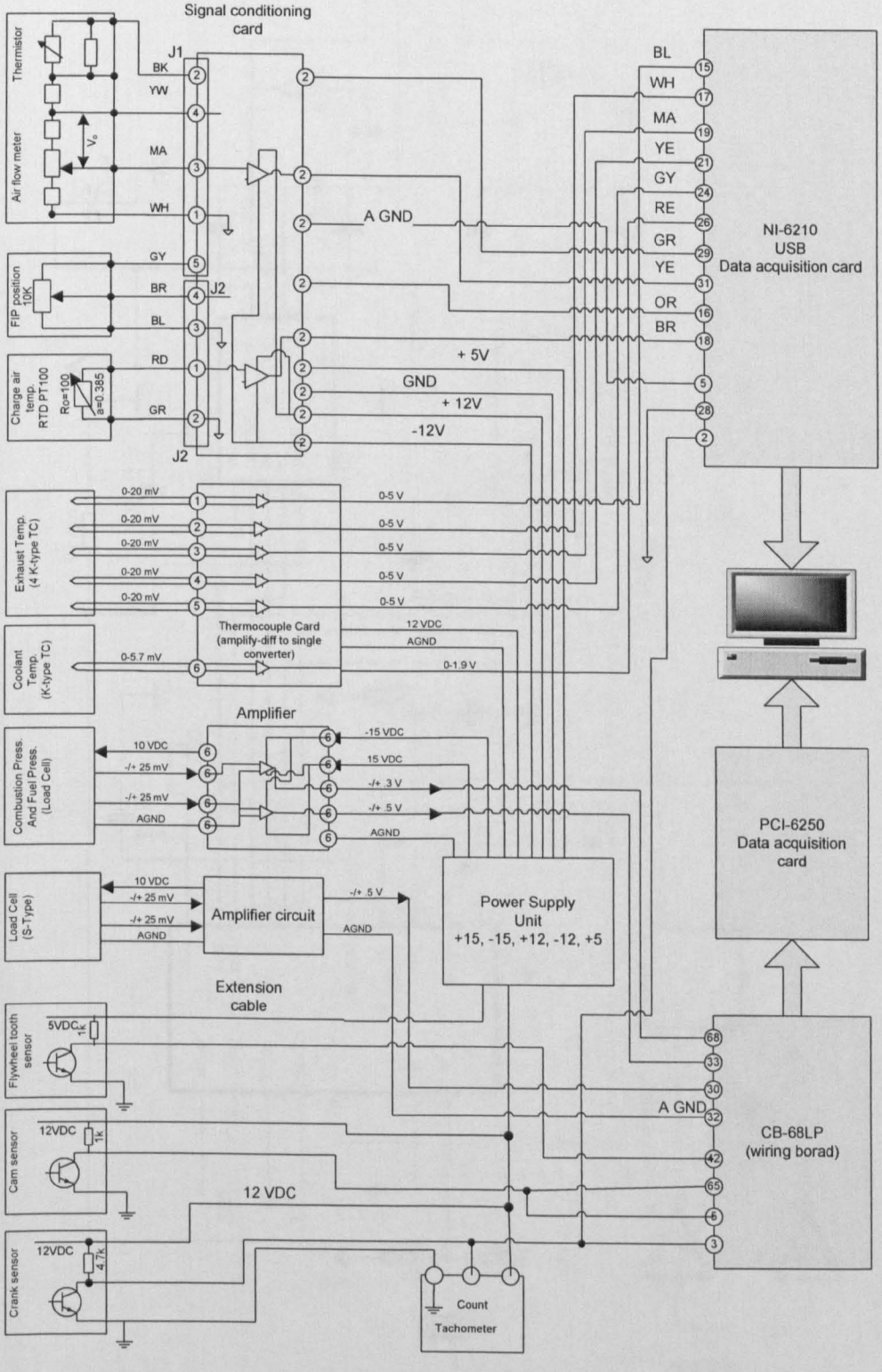

B.2 STEPPER MOTOR MANUAL DRIVER SCHEMATIC DIAGRAM

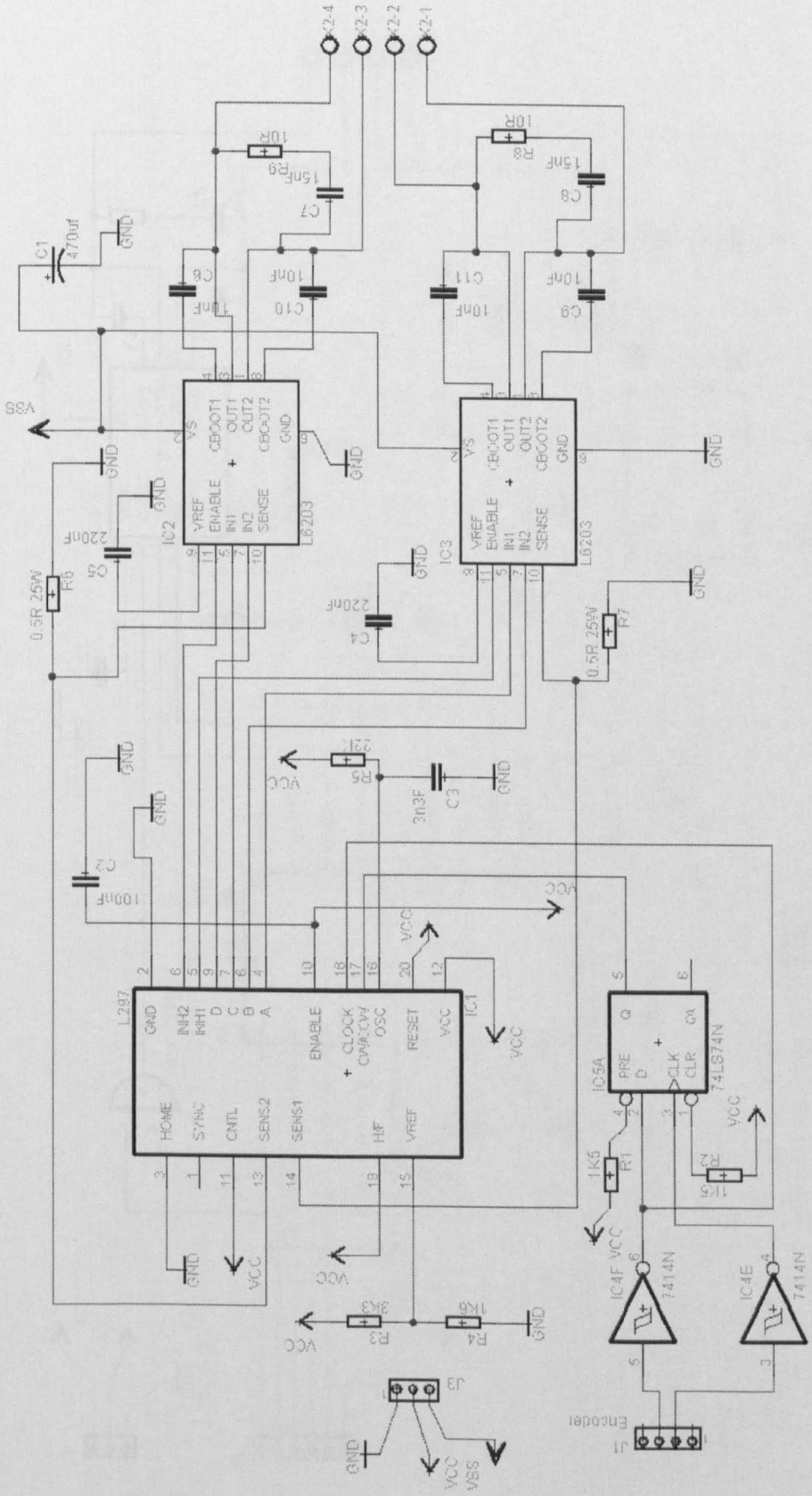

B.3 STEPPER MOTOR AUTOMATIC DRIVER SCHEMATIC DIAGRAM

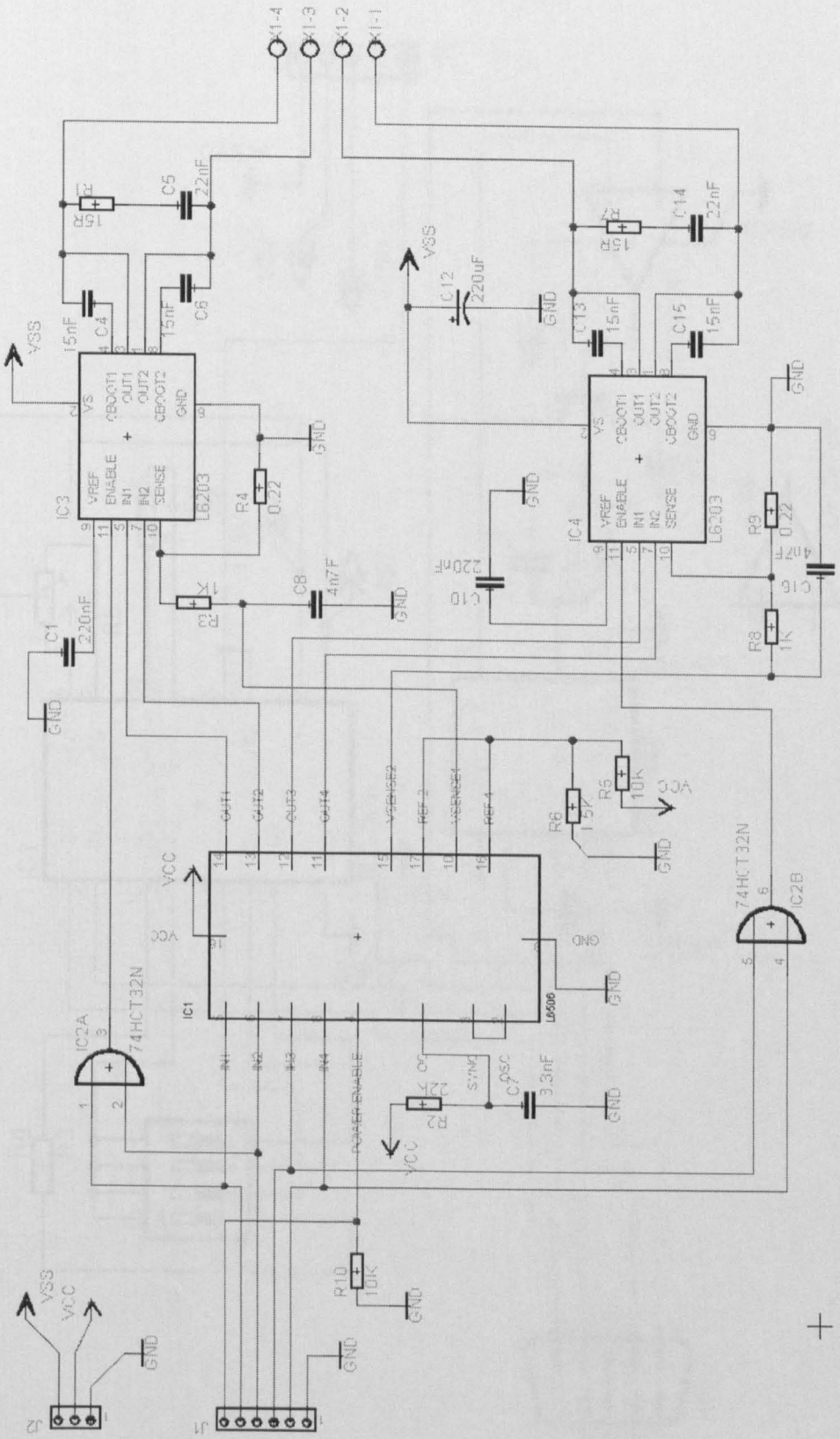

B.4 LOAD CELL AMPLIFIER SCHEMATIC CIRCUIT DIAGRAM

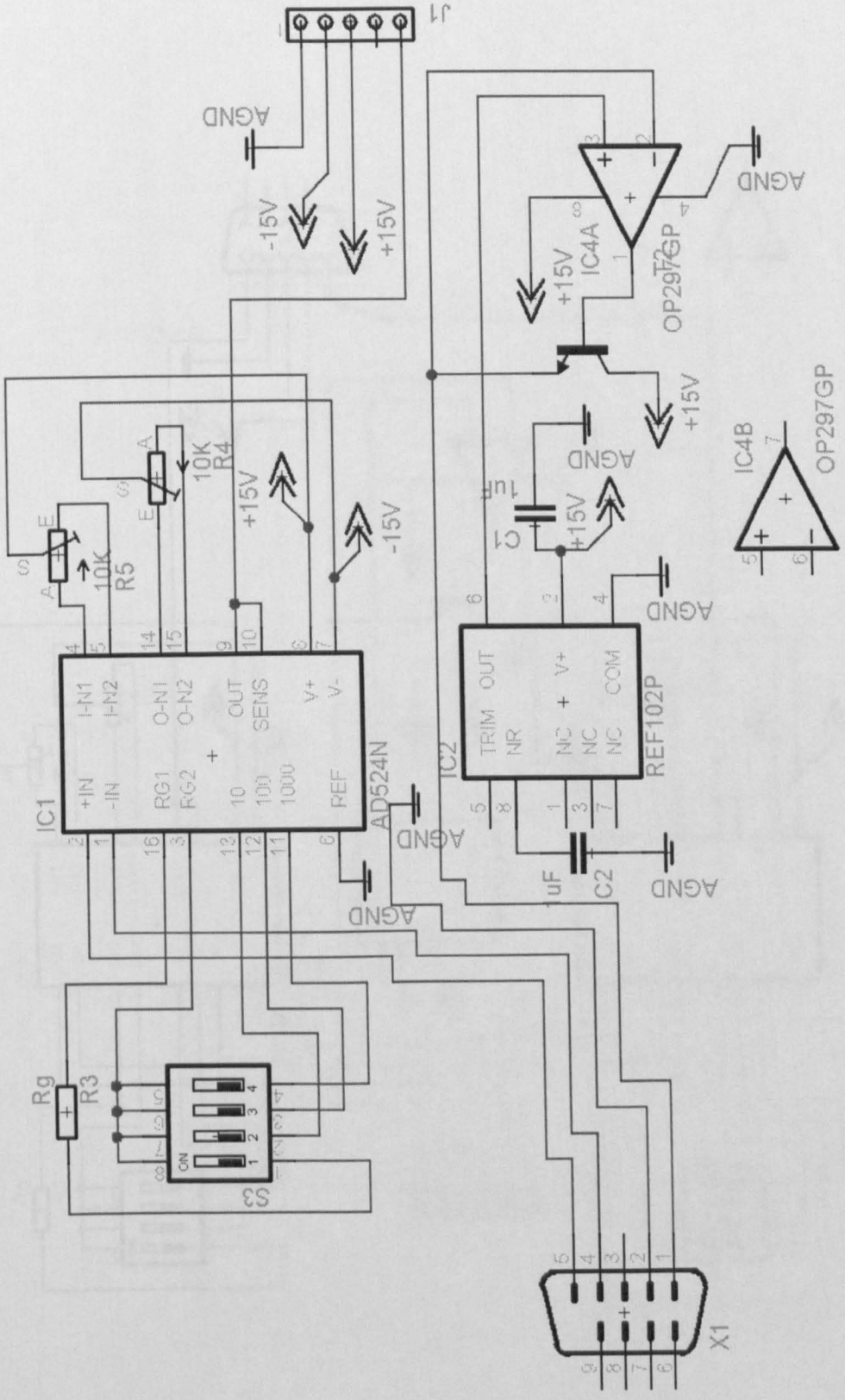

B.5 SCHEMATIC DIAGRAM OF CYLINDER PRESSURE SENSOR AMPLIFIER CIRCUIT

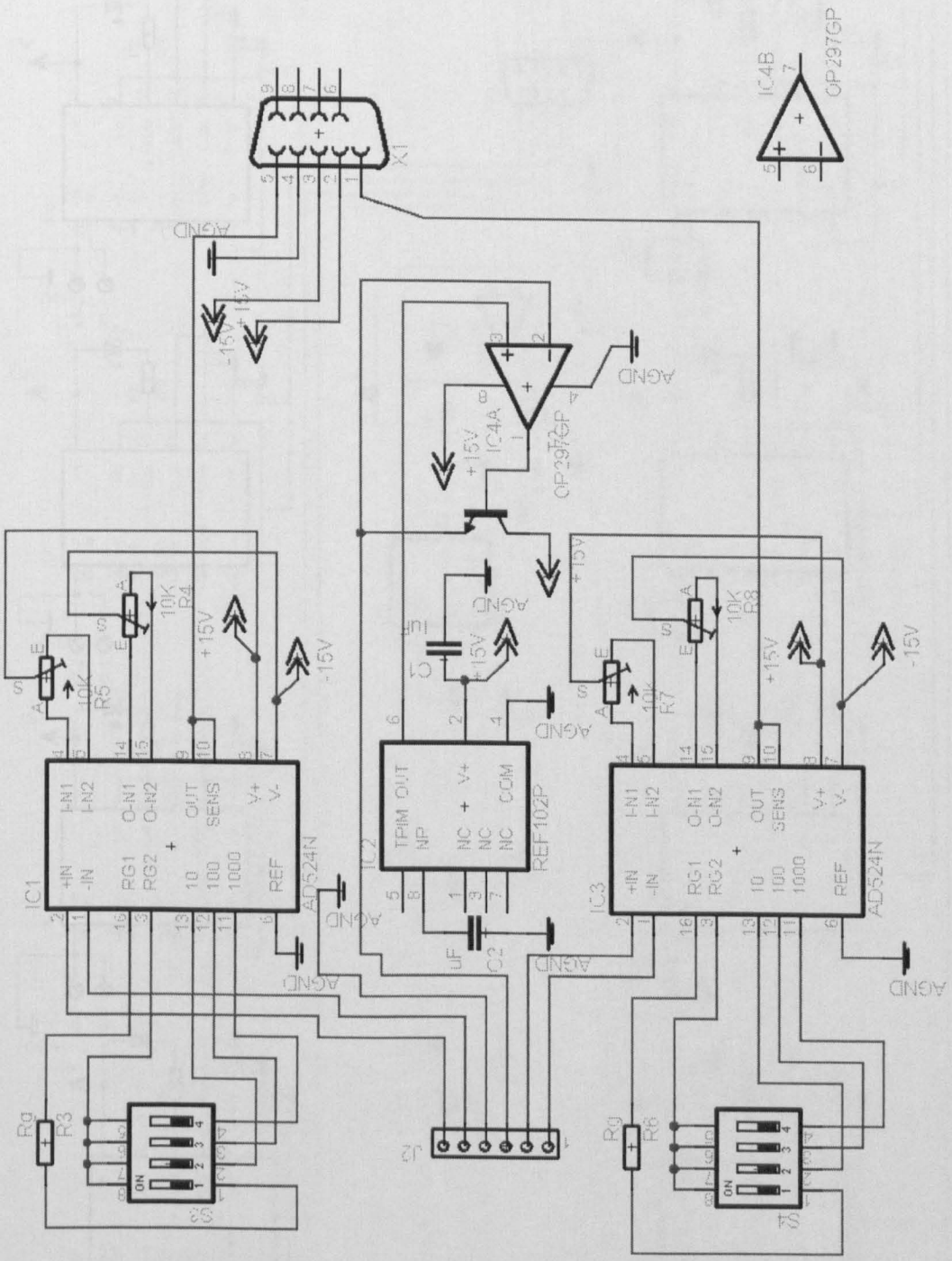

B.6 THERMOCOUPLE SIGNAL CONDITIONING CIRCUIT DIAGRAM

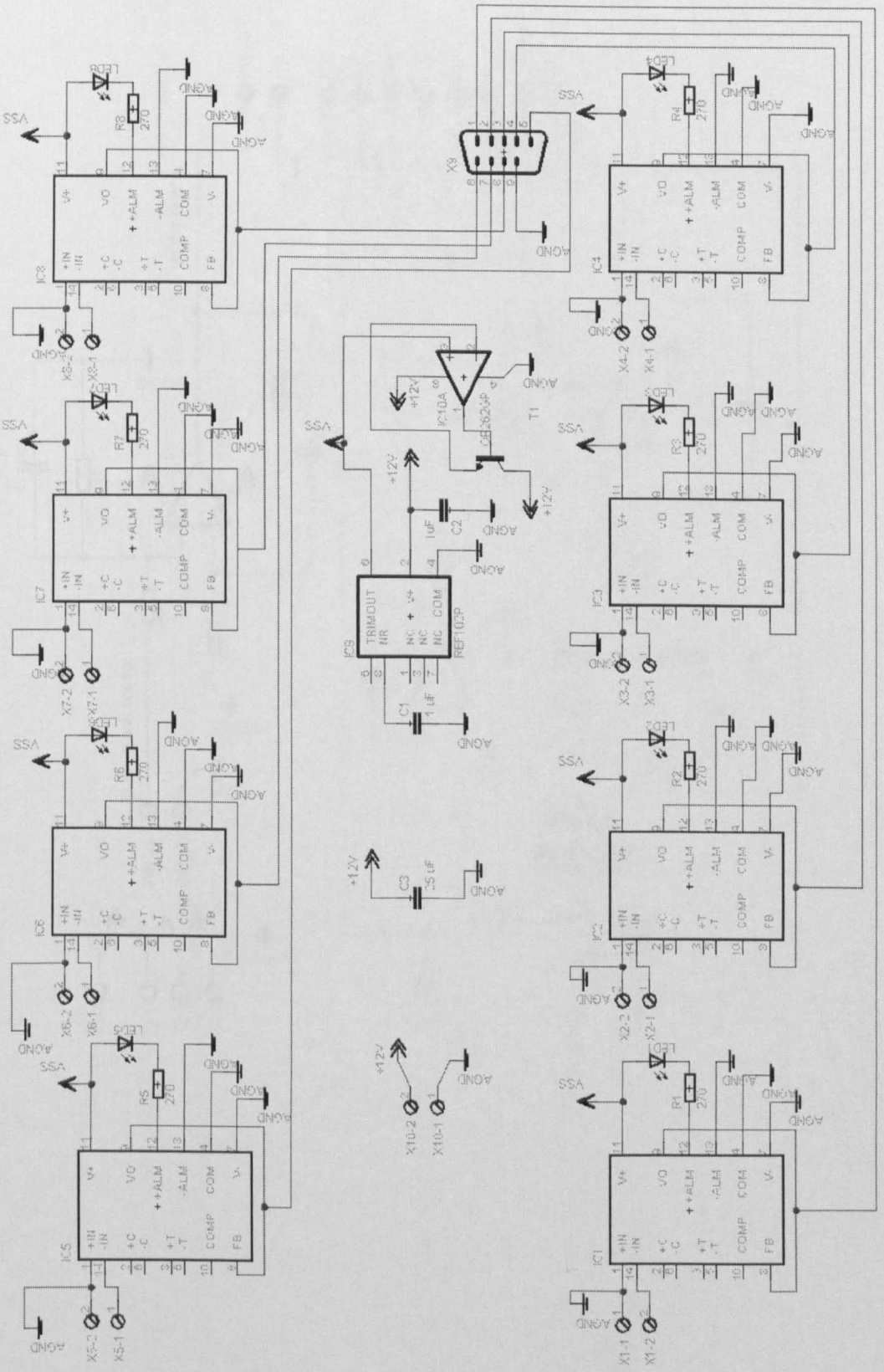

B.7 DETAILED SCHEMATIC DIAGRAM OF SIGNAL CONDITIONING

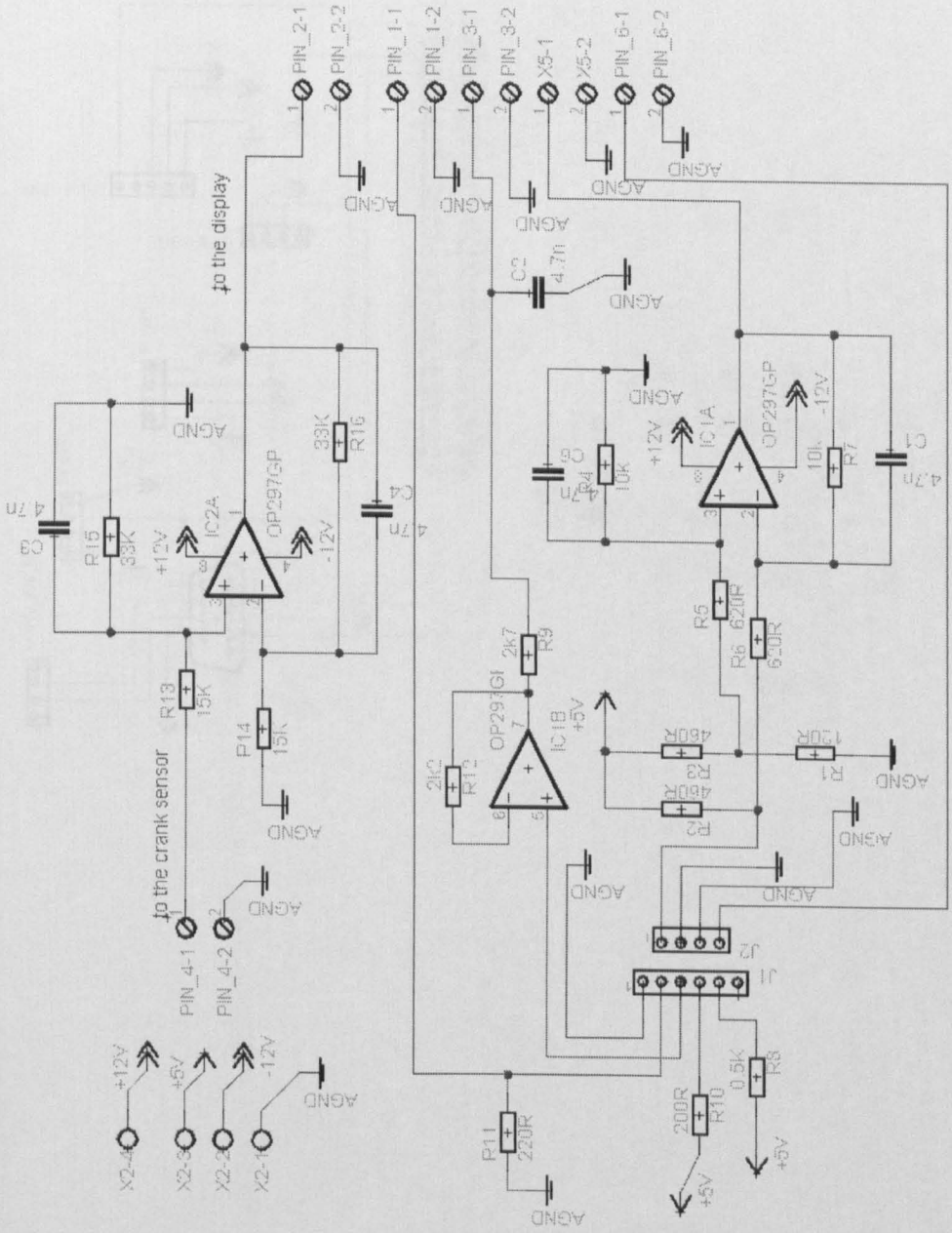

B.8 EXTENSION CARD CONTAINING THE RELAY CIRCUIT DIAGRAM

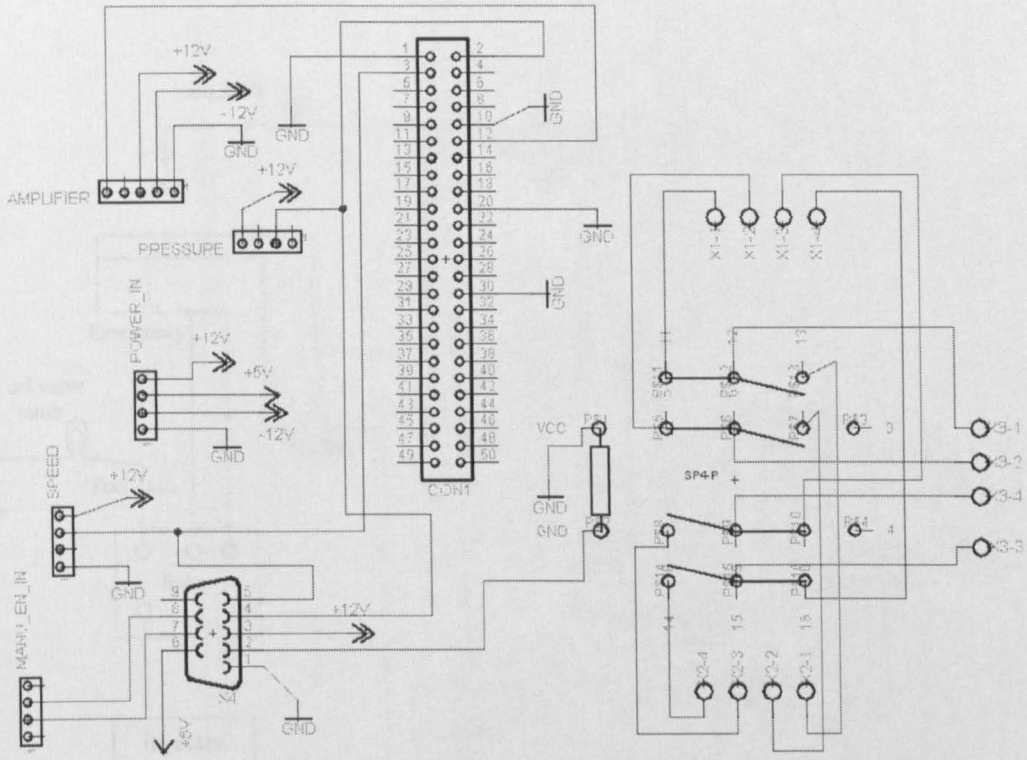

B.9 THE CIRCUIT SCHEMATIC DIAGRAM OF THE ENGINE STARTING PANEL

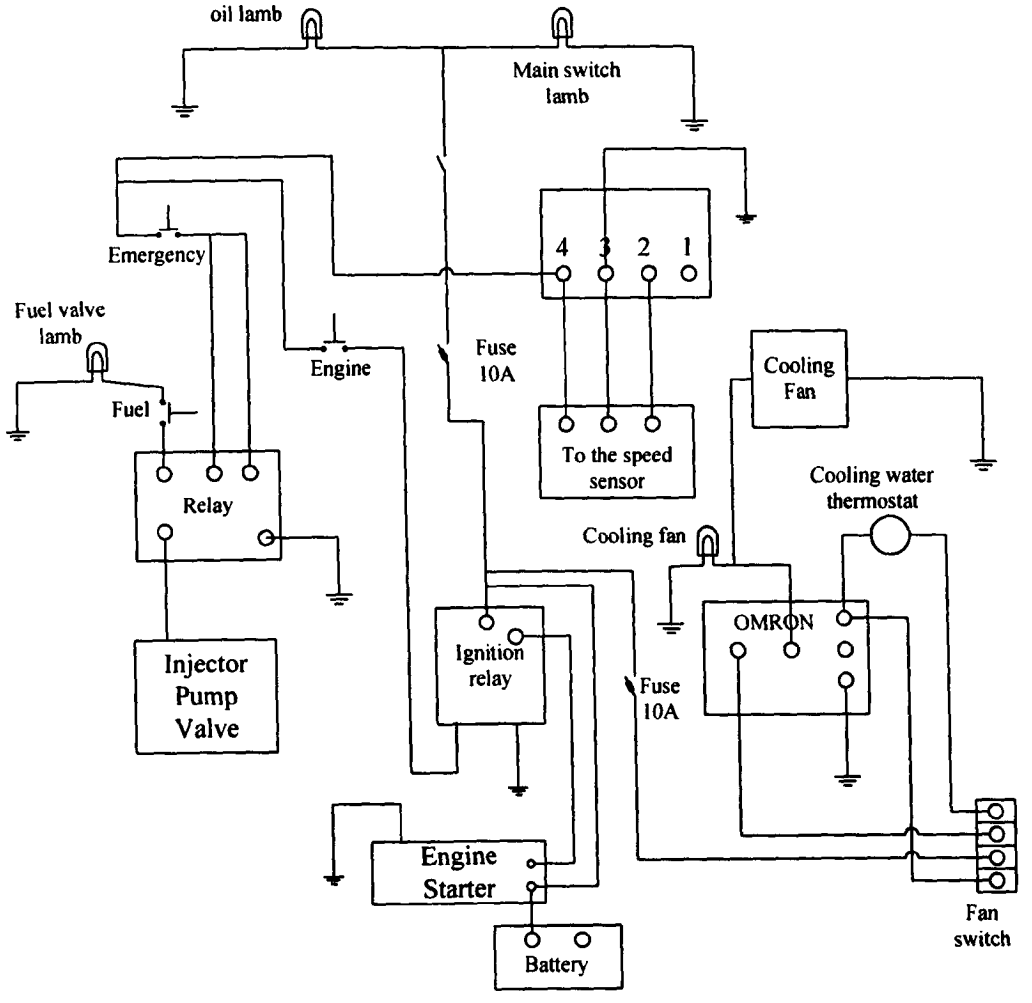

The data acquisition Labview code

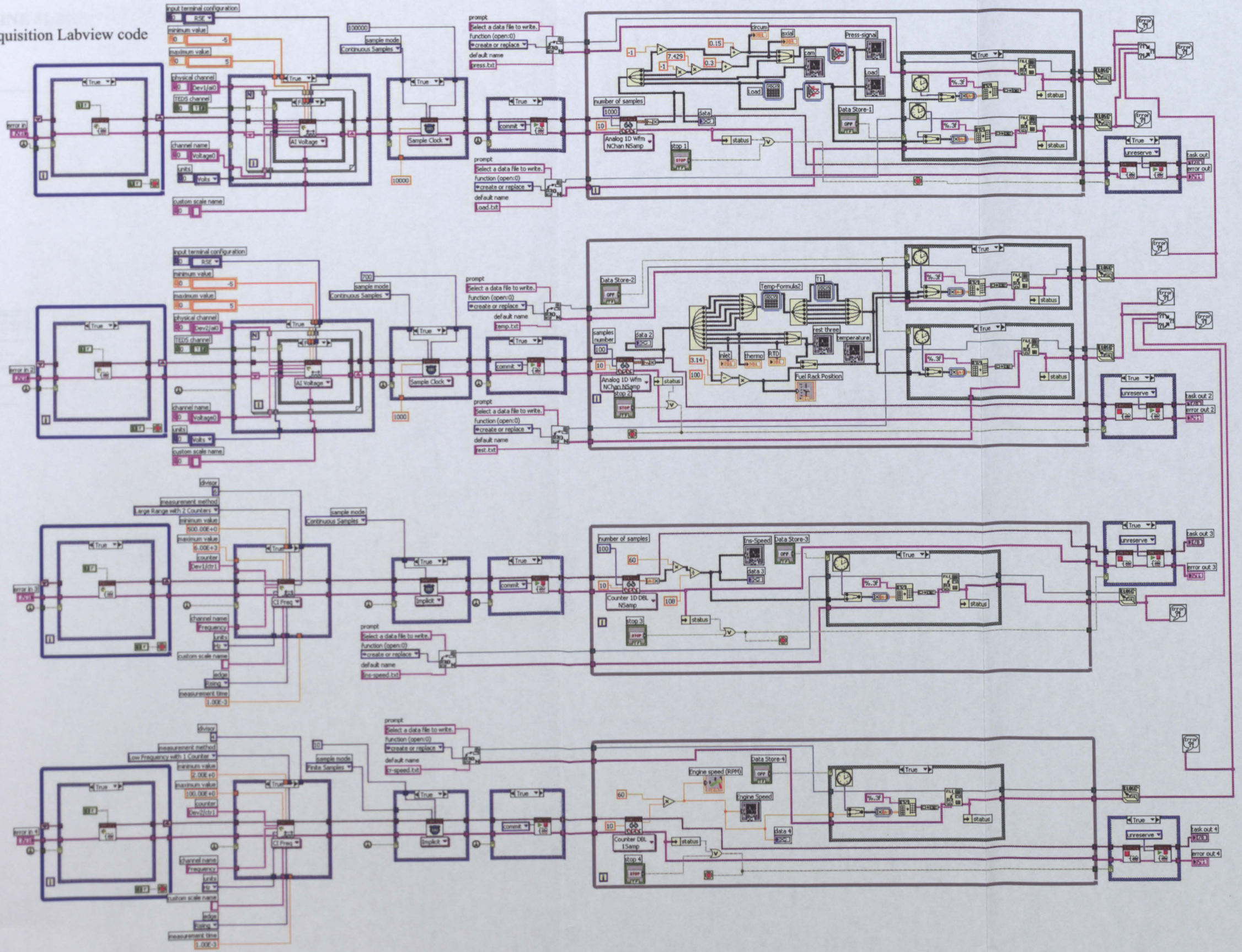

B.10 ENGINE MODEL SIMULINK BLOCK DIAGRAM

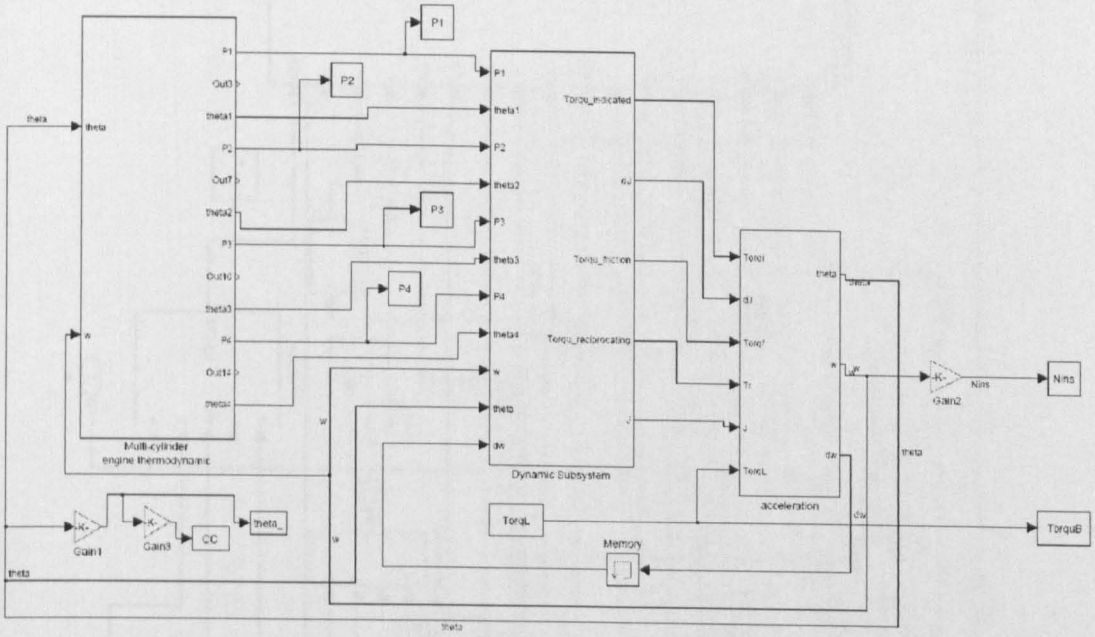

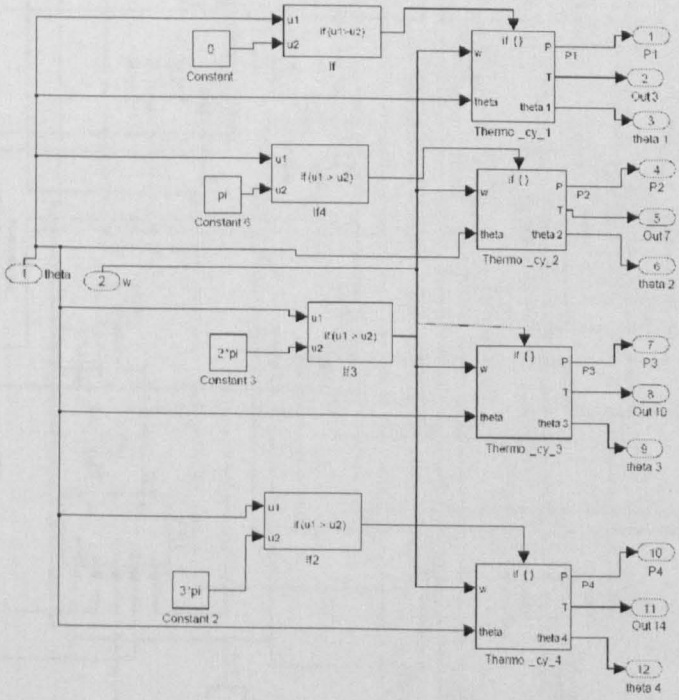

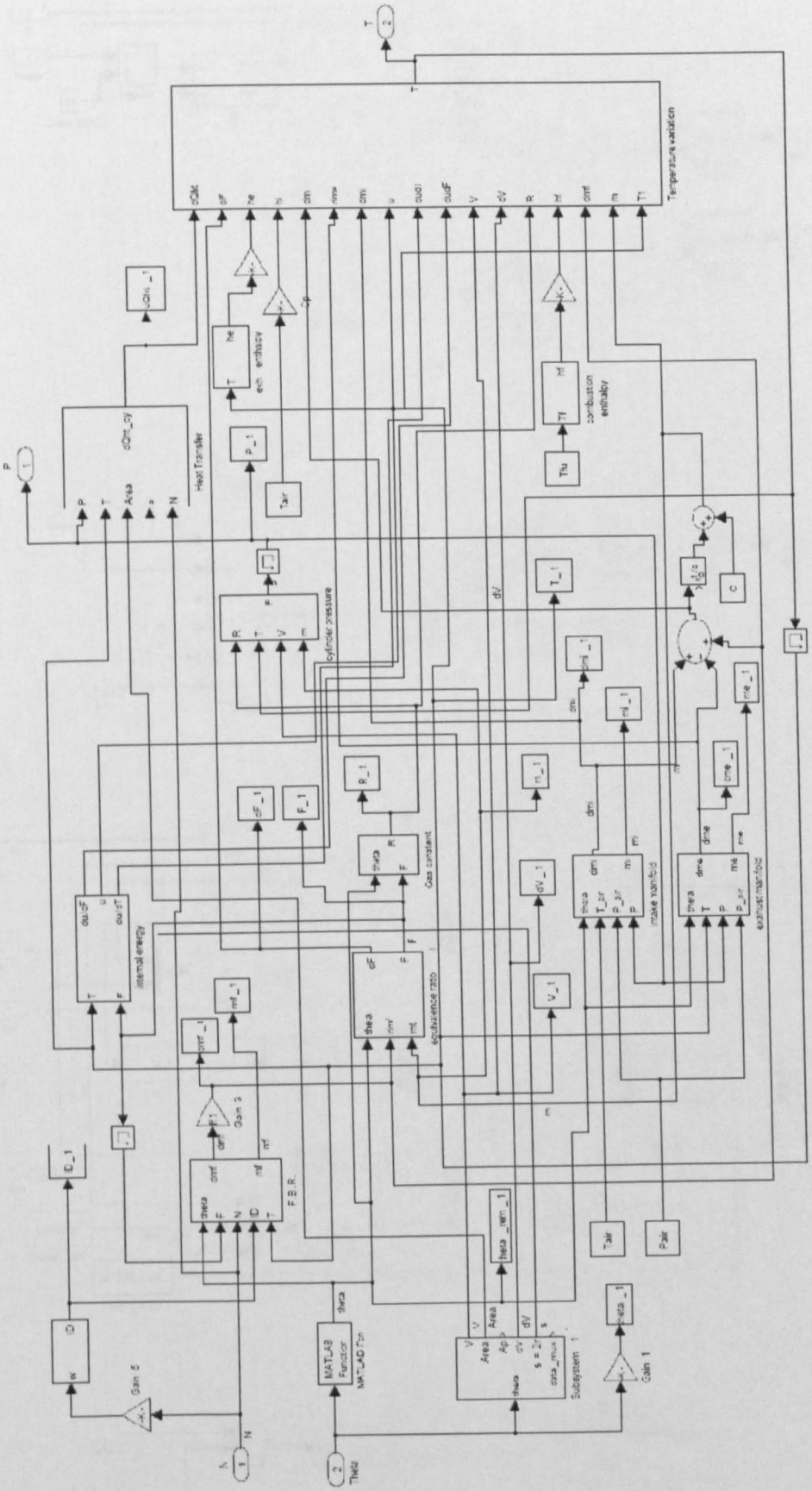
Temperature variation
Heat Transfer
Cylinder pressure
Gas constant
equivalence ratio
internal energy
make manifold
exhaust manifold
F.B.R.
Subsystem 1
MATLAB Function
Gain 1
Gain 3
Gain 6

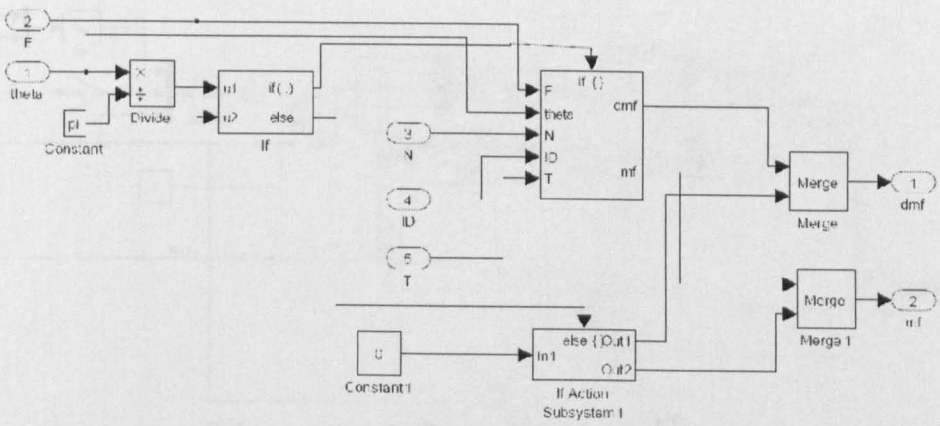
2
F
1
theta
Divide
pi
Constant
u1
u2
if( )
else
If
if ( )
F
theta
N
ID
T
cmf
mf
3
N
4
ID
5
T
Merge
Merge
1
dmf
Merge 1
2
mf
u
Constant1
else ( )
In1
Out1
Out2
If Action
Subsystem 1

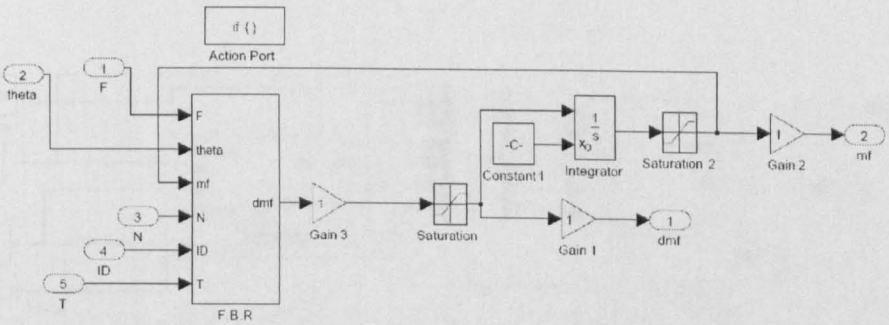
if ( )
Action Port
2
theta
1
F
F
theta
mf
N
ID
T
dmf
F.B.R
3
N
4
ID
5
T
Gain 3
Saturation
-C-
Constant 1
1
s
Integrator
Saturation 2
Gain 2
2
mf
Gain 1
1
dmf

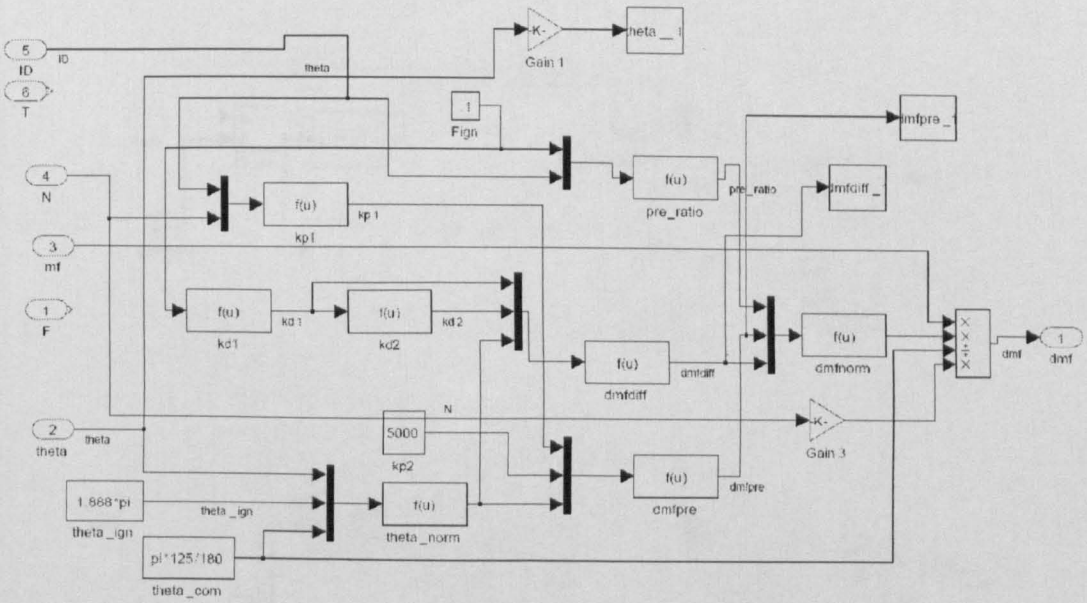
5
ID
ID
6
T
theta
Gain 1
theta_1
1
Fign
dmfpre_1
4
N
3
mf
1
F
f(u)
kp1
kp 1
pre_ratio
pre_ratio
dmfdiff_
f(u)
kd1
kd 1
f(u)
kd2
kd 2
f(u)
dmfdiff
dmfdiff
f(u)
dmfnorm
dmf
1
dmf
2
theta
theta
5000
kp2
N
Gain 3
1.888*pi
theta_ign
theta_ign
f(u)
theta_norm
f(u)
dmfpre
dmfpre
pi*125/180
theta_com

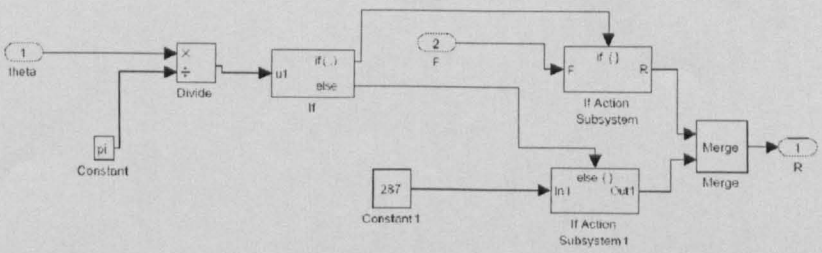
1
theta
Divide
pi
Constant
u1
if( )
else
If
2
F
if ( )
F
R
If Action
Subsystem
Merge
Merge
1
R
287
Constant 1
else ( )
In1
Out1
If Action
Subsystem 1

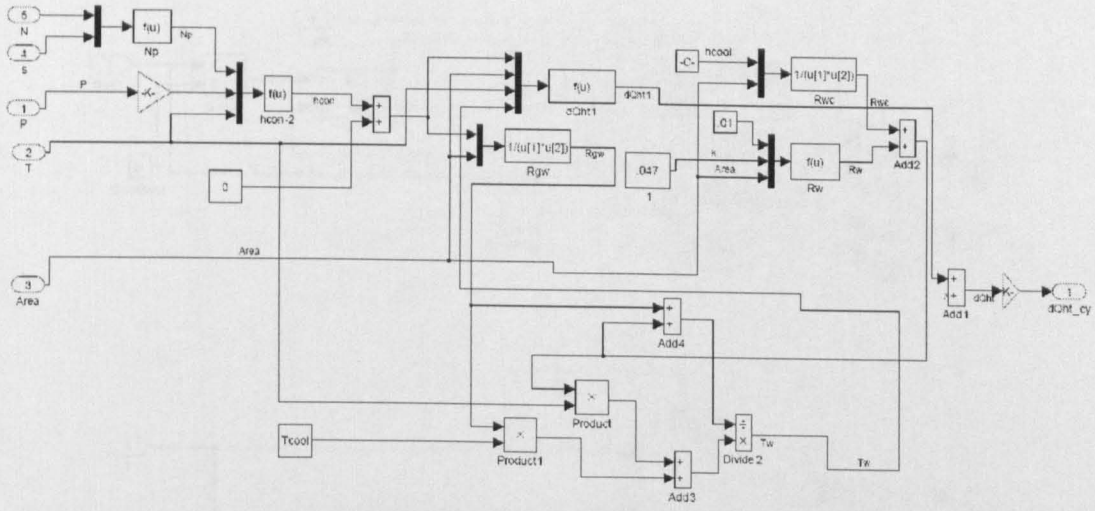
N
s
P
T
Np
hcon-2
dQint1
Rwc
Rgw
Rw
Add2
Area
Add1
dQint_cy
Add4
Product
Product1
Divide2
Add3
Tcool
Tw

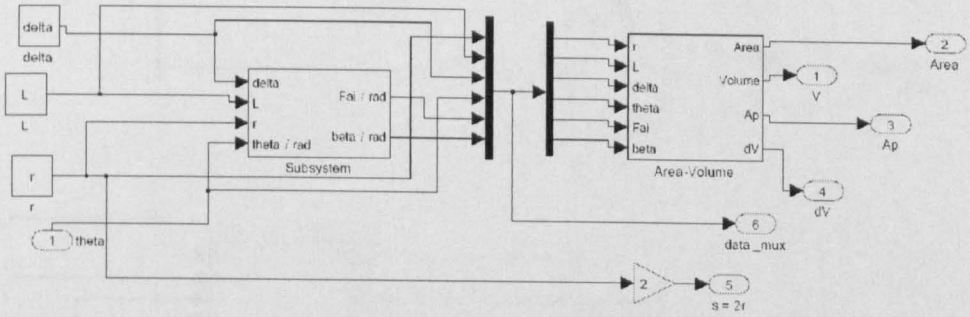
delta
L
r
theta
Subsystem
Fai / rad
beta / rad
Area-Volume
Area
Volume
Ap
dV
V
data_mux
s = 2r

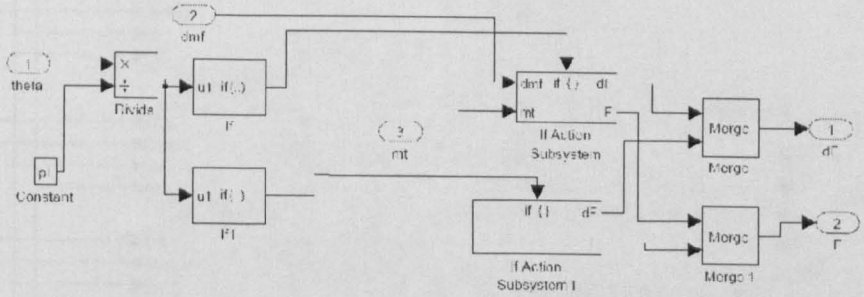
dmf
theta
Divide
Constant
If
If1
mt
If Action Subsystem
If Action Subsystem1
Merge
Merge1
df
dr

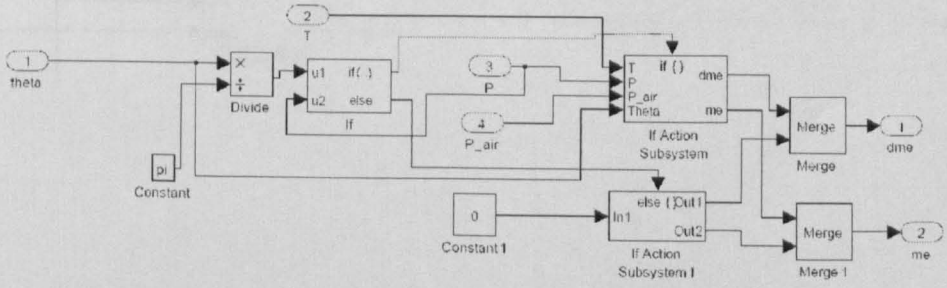
T
theta
Divide
pi
Constant
If
P
P_air
Constant1
If Action Subsystem
If Action Subsystem1
Merge
Merge1
dme
me

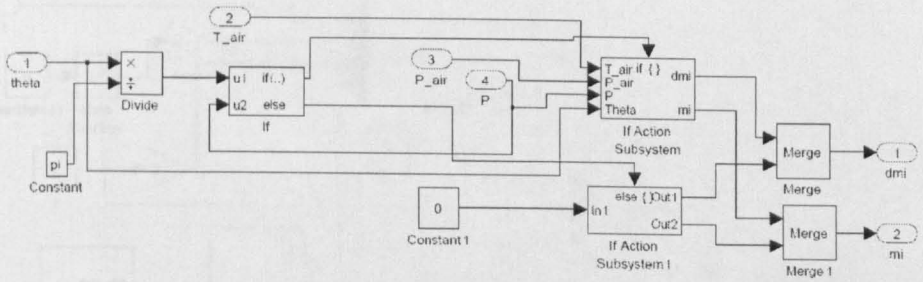
2
T_air
1
theta
Divide
u1 if(..)
u2 else
If
3
P_air
4
P
T_air if { }
P_air
P
Theta
dmi
mi
If Action
Subsystem
pi
Constant
0
Constant 1
else { }Out1
In1
Out2
If Action
Subsystem 1
Merge
Merge
1
dmi
Merge 1
2
mi

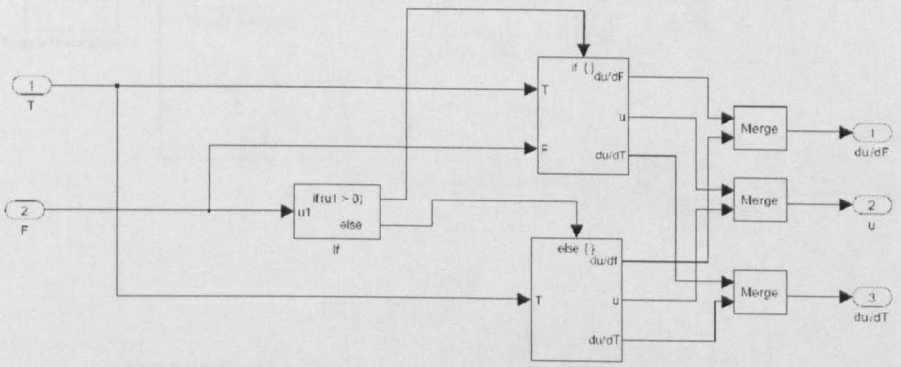
1
T
2
F
if (u1 ~ 0)
u1
else
If
if { }
T
F
du/dF
u
du/dT
Merge
1
du/dF
Merge
2
u
else { }
du/dT
T
u
du/dT
Merge
3
du/dT

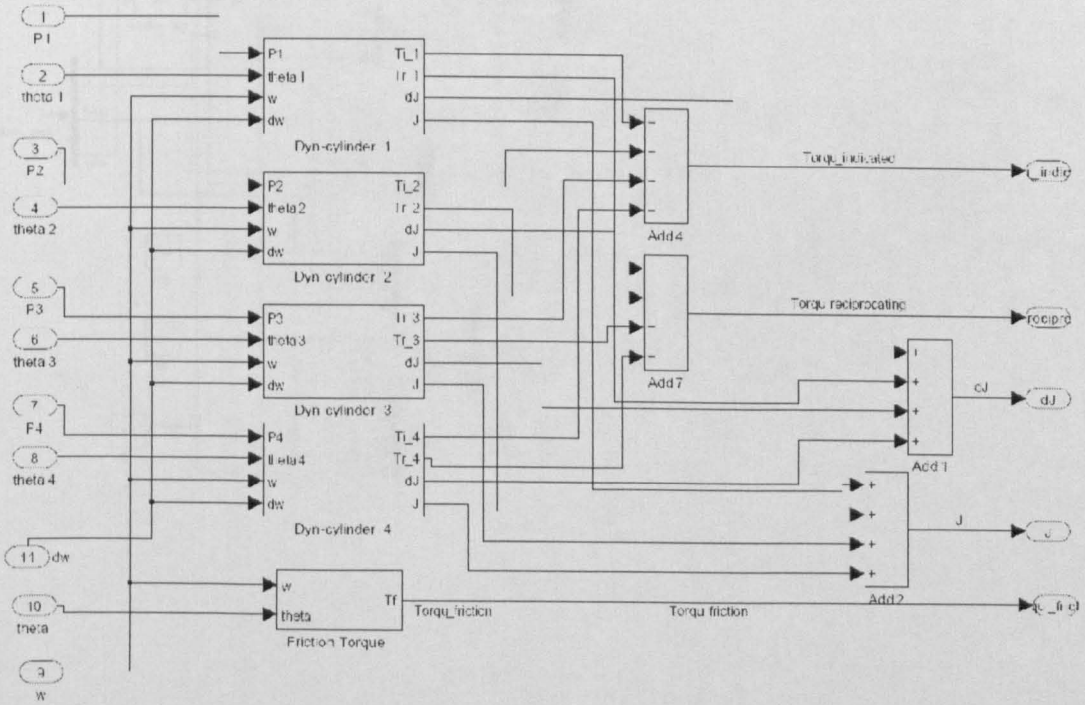
1
P1
2
theta 1
3
P2
4
theta 2
5
P3
6
theta 3
7
P4
8
theta 4
11
dw
10
theta
9
w
P1
theta 1
w
dw
TL_1
Tr_1
dJ
J
Dyn-cylinder 1
P2
theta2
w
dw
TL_2
Tr_2
dJ
J
Dyn cylinder 2
P3
theta3
w
dw
TL_3
Tr_3
dJ
J
Dyn cylinder 3
P4
theta4
w
dw
TL_4
Tr_4
dJ
J
Dyn-cylinder 4
w
theta
Tf
Friction Torque
Torqu_friction
Torqu friction
Add4
Torqu_indicated
Add7
Torqu reciprocating
Add1
dJ
Add2
J

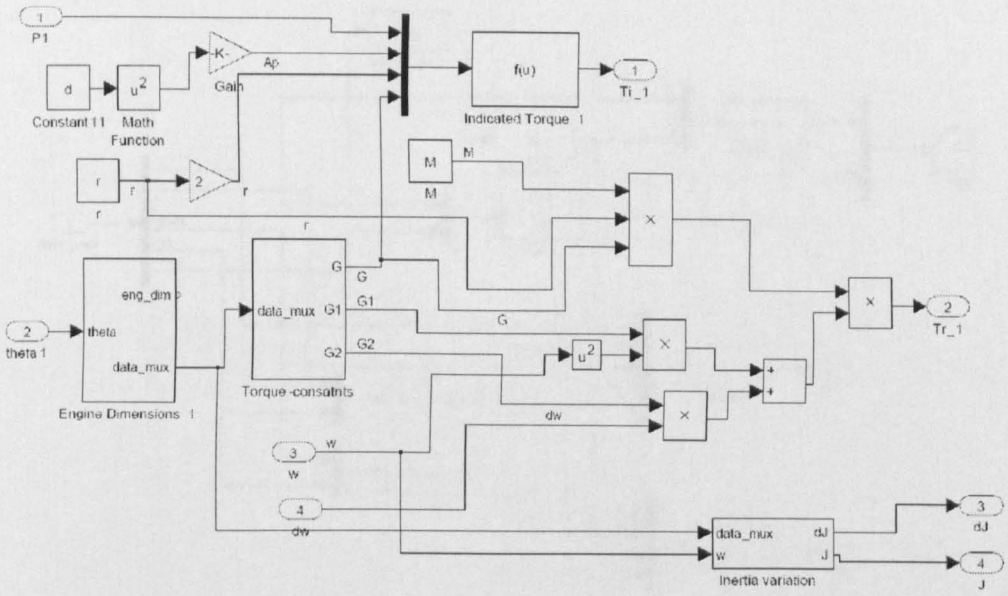
P1
d
Constant 11
u²
Math Function
K
Gain
Ap
f(u)
Indicated Torque 1
Ti_1
r
2
r
M
M
G
G1
G2
data_mux
Torque-consatnts
eng_dim
theta
data_mux
Engine Dimensions 1
theta 1
u²
dw
w
dw
data_mux
dJ
w
J
Inertia variation
Tr_1
dJ
J

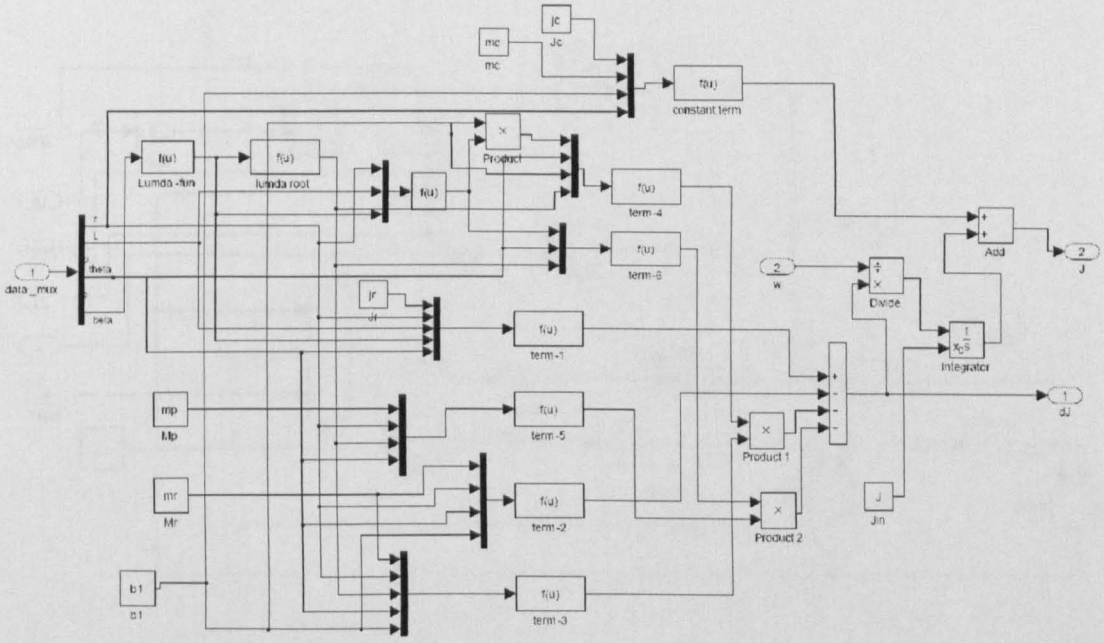
mc
Jc
f(u)
constant term
Product
Lumda -fun
lumda root
term-4
term-6
data_mux
theta
beta
jr
term-1
mp
Mp
mr
Mr
b1
term-5
term-2
term-3
Product 1
Product 2
Add
Divide
Integrator
w
J
dJ
Jin

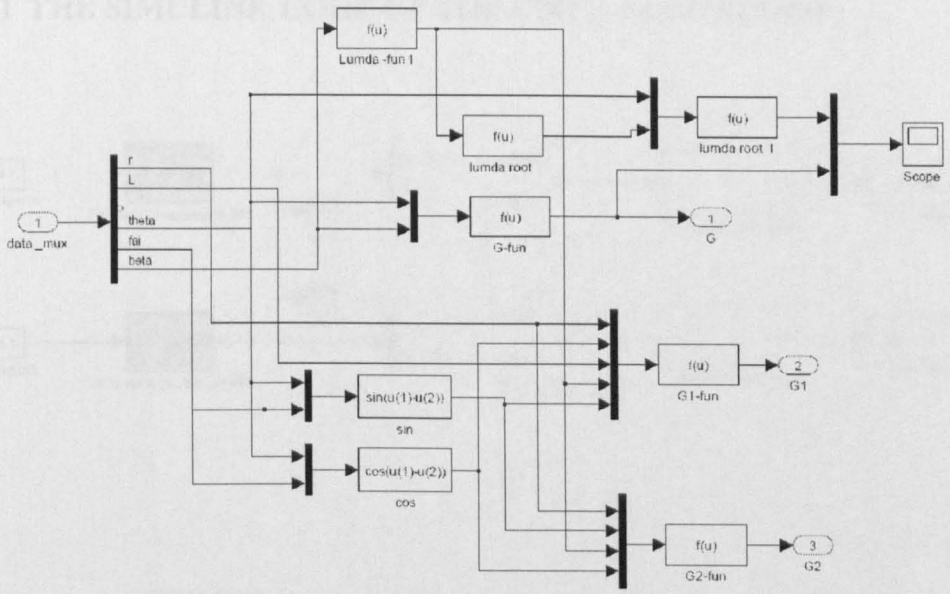
f(u)
Lumda -fun 1
f(u)
lumda root
f(u)
lumda root 1
Scope
r
L
theta
fai
beta
1
data _mux
f(u)
G-fun
1
G
f(u)
G1-fun
2
G1
sin(u(1)+u(2))
sin
cos(u(1)+u(2))
cos
f(u)
G2-fun
3
G2

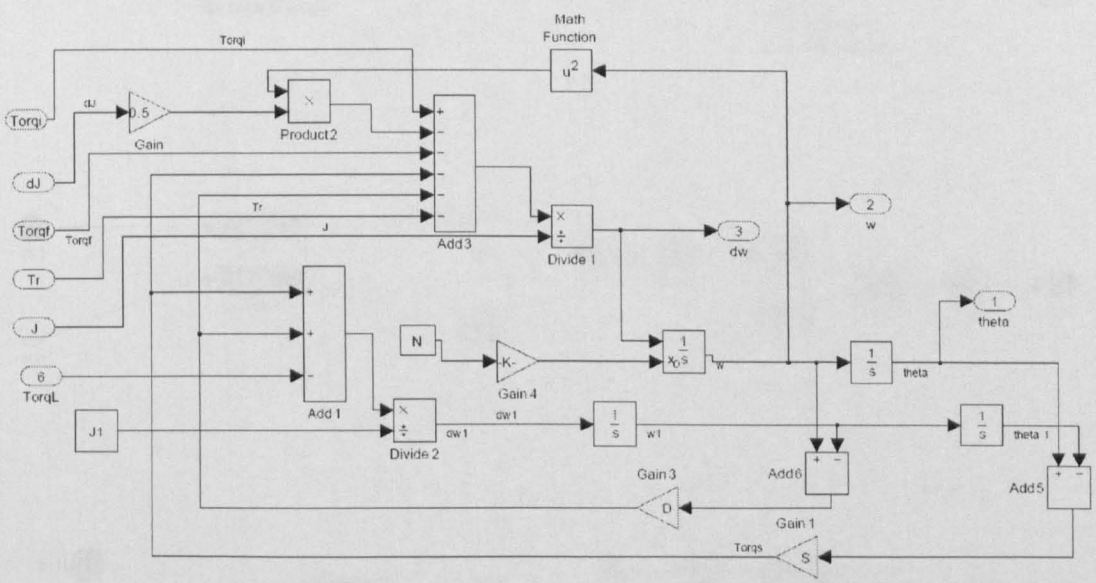
Math
Function
u^2
Torqi
dJ
0.5
Gain
Product2
dJ
Torqf
Torqf
Tr
J
Add3
Divide 1
2
w
3
dw
Tr
J
6
TorqL
Add 1
N
K
Gain 4
$\frac{1}{s}$
w
$\frac{1}{s}$
theta
1
theta
J1
Divide 2
dw1
dw1
$\frac{1}{s}$
w1
$\frac{1}{s}$
theta 1
Gain 3
D
Add6
Add5
Gain 1
Torqs
S

B.11 THE SIMULINK CODE OF THE CMFD ALGORITHM

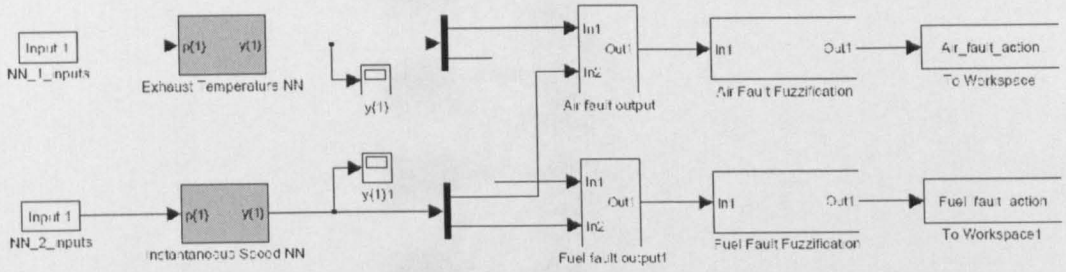

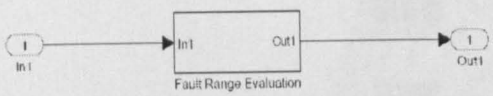

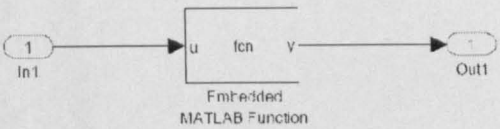

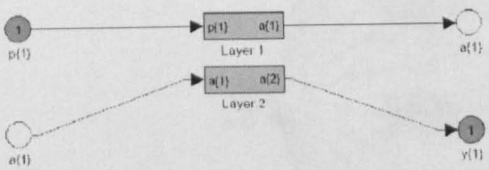

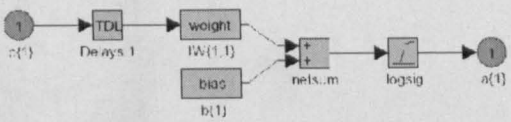

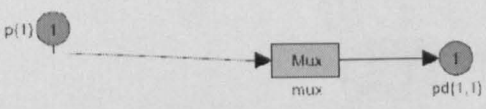

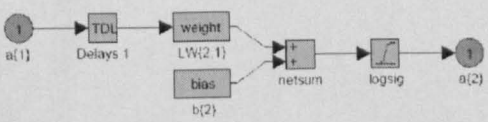

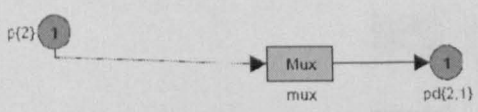

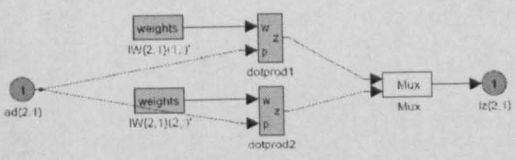

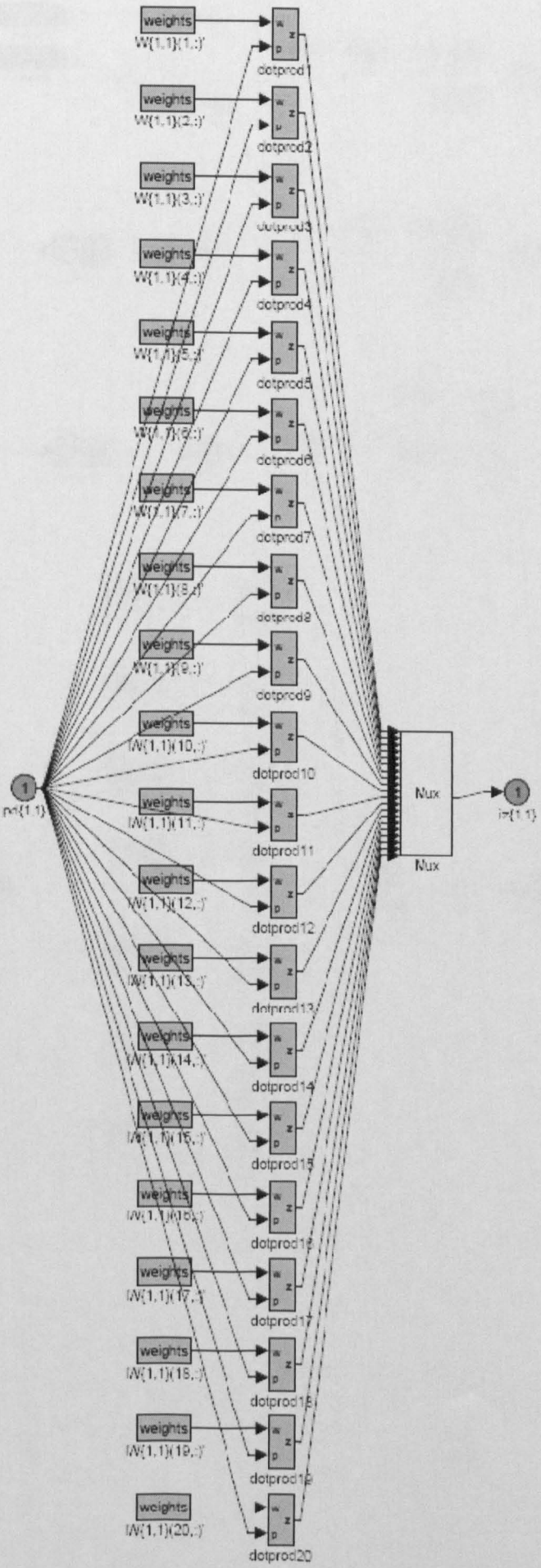
weights
W{1,1}(1,:)'
dotprod1
weights
W{1,1}(2,:)'
dotprod2
weights
W{1,1}(3,:)'
dotprod3
weights
W{1,1}(4,:)'
dotprod4
weights
W{1,1}(5,:)'
dotprod5
weights
W{1,1}(6,:)'
dotprod6
weights
W{1,1}(7,:)'
dotprod7
weights
W{1,1}(8,:)'
dotprod8
weights
W{1,1}(9,:)'
dotprod9
weights
W{1,1}(10,:)'
dotprod10
weights
W{1,1}(11,:)'
dotprod11
weights
W{1,1}(12,:)'
dotprod12
weights
W{1,1}(13,:)'
dotprod13
weights
W{1,1}(14,:)'
dotprod14
weights
W{1,1}(15,:)'
dotprod15
weights
W{1,1}(16,:)'
dotprod16
weights
W{1,1}(17,:)'
dotprod17
weights
W{1,1}(18,:)'
dotprod18
weights
W{1,1}(19,:)'
dotprod19
weights
W{1,1}(20,:)'
dotprod20
1
p{1,1}
Nux
Nux
1
i={1,1}

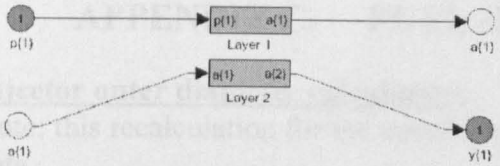
p{1}
Layer 1
a{1}
Layer 2
a{2}
y{1}

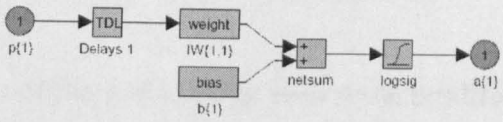
p{1}
Delays 1
weight
IW{1,1}
bias
b{1}
netsum
logsig
a{1}

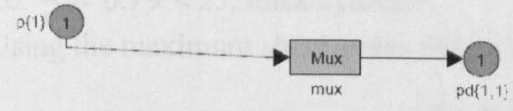
p{1}
Mux
mux
pd{1,1}

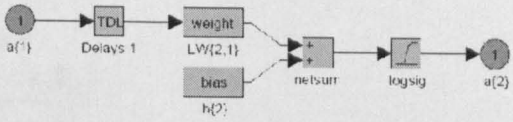
a{1}
Delays 1
weight
LW{2,1}
bias
b{2}
netsum
logsig
a{2}

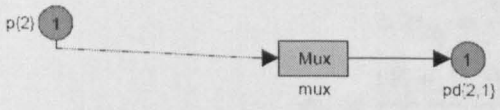
p{2}
Mux
mux
pd{2,1}

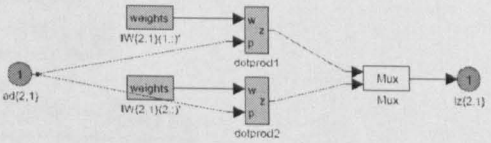
weights
IW{2,1}{1,:}'
dotprod1
pd{2,1}
weights
IW{2,1}{2,:}'
dotprod2
Mux
Mux
iz{2,1}

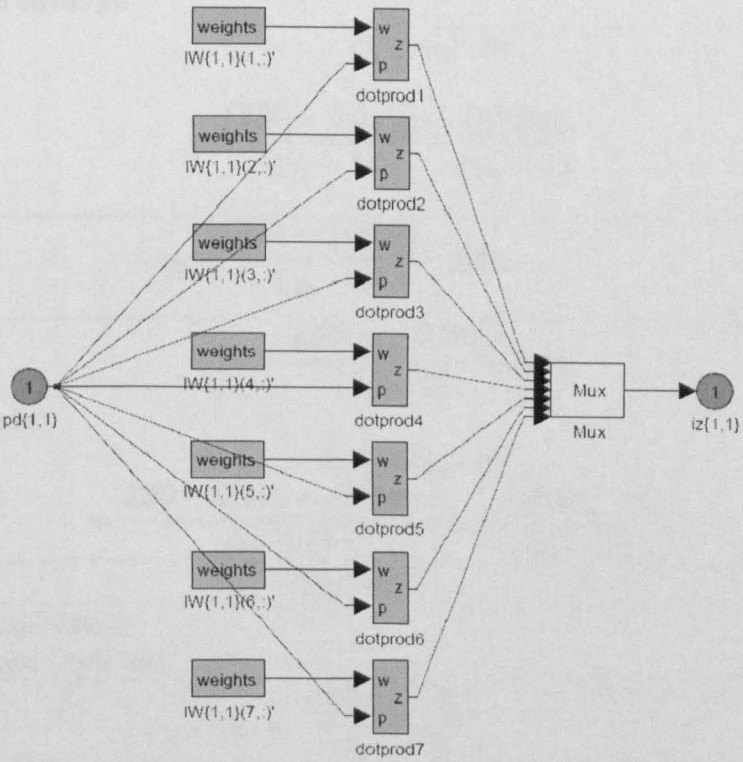
weights
IW{1,1}{1,:}'
dotprod1
weights
IW{1,1}{2,:}'
dotprod2
weights
IW{1,1}{3,:}'
dotprod3
weights
IW{1,1}{4,:}'
dotprod4
weights
IW{1,1}{5,:}'
dotprod5
weights
IW{1,1}{6,:}'
dotprod6
weights
IW{1,1}{7,:}'
dotprod7
pd{1,1}
Mux
Mux
iz{1,1}

APPENDIX C. FUEL INJECTOR CALCULATIONS

Injector outer diameter calculation:

Note: this recalculation for the outer diameter of the fuel injector with some modified data.

$D_i = 2.7$ mm $\quad D_o = 9.5$ mm $\quad t = 3.4$ mm

i.e. $\frac{D_i}{t} = 0.79 < 25$, thick cylinder

Using the maximum shear stress failure theory

$$\sigma_m = \frac{(P_i - \gamma_o P_o)}{(\gamma_o - 1)}$$

Take: $P_i = 2000$ bar $= 200$ MPa [Diesel Ref. Handbook]

$P_o = 1$ bar $= 0.1$ MPa (atmospheric pressure)

$$\therefore \sigma_m = \frac{(200 - 0.1\gamma_o)}{(\gamma_o - 1)}$$

$$\sigma_v = \frac{(P_i - P_o)\gamma_o}{(\gamma_o - 1)} = \frac{(200 - 0.1)\gamma_o}{(\gamma_o - 1)}$$

Known that at the critical bore $\gamma = 1$ and using the theory principles.

The tangential stress is:

$$\sigma_t = \sigma_m + \sigma_v$$

$$= \frac{(200 - 0.1\gamma_o)}{(\gamma_o - 1)} + \frac{199.9\gamma_o}{(\gamma_o - 1)}$$

$\therefore \sigma_t = \frac{200 - 199.8\gamma_o}{(\gamma_o - 1)}$ MPa	(1)

$$\therefore \sigma_t = \frac{200 - 199.8\gamma_o}{(\gamma_o - 1)} \text{ MPa}$$

The radial stress:

$$\sigma_r = \sigma_m - \sigma_v$$

$$= \frac{200 - 0.1\gamma_o - 199.9\gamma_o}{(\gamma_o - 1)} = \frac{-200(\gamma_o - 1)}{(\gamma_o - 1)}$$

$\sigma_r = -200$ MPa	(2)

The axial stress:

For closed cylinder

$\sigma_a = \sigma_m = \frac{(200 - 0.1\gamma_o)}{(\gamma_o - 1)}$	(3)

From equation (1), (2) and (3)

$$\sigma_{max} = \sigma_a$$

$$\sigma_{min} = \sigma_r$$

Then, the equivalent stress is:

$$\sigma_e = \sigma_{max} - \sigma_{min}$$

$$\sigma_e = \frac{(200 - 0.1\gamma_o)}{(\gamma_o - 1)} - (-200) = \frac{199.9\gamma_o}{(\gamma_o - 1)}$$

Let the design stress of the injector body material to be 250 MPa by using safety factor of about 2.5

$$\therefore \sigma_e = \frac{199.9\gamma_o}{(\gamma_o - 1)} = 250$$

$$\therefore 250 = 50.1\gamma_o$$

$$\therefore \gamma_o = 4.99$$

$$\text{but } \gamma_o = \left(\frac{D_o}{D_i}\right)^2$$

$$D_o)_{min} = D_i\sqrt{\gamma_o}$$

$$D_i = 2.7 \text{ mm}$$

$$D_o)_{min} = 2.7\sqrt{4.99} = 6.03 \text{ mm}$$

Then the minimum outer diameter is 6 mm, i.e. the outer diameter of the injector could be reduced by 3.5 mm (1.75 in the reduce)

Using the maximum shear stress failure (the stress due to fuel)

$$\sigma_t)_f = \frac{(P_f - P_{atm})\gamma}{\gamma - 1}$$

$$\sigma_r)_f = P_f$$

$$\sigma_a)_f = \frac{P_f - P_{atm}\gamma}{\gamma - 1}$$

The stress due to cylinder pressure is in axial direction only, therefore,

$$\sigma_a)_{cy} = P_{cy}$$

$$\therefore \varepsilon_a = \frac{1}{E}[\sigma_a)_{total} - \nu\{\sigma_r + \sigma_t\}]$$

$$\& \quad \varepsilon_t = \frac{1}{E}[\sigma_t - \nu\{\sigma_r + \sigma_a)_{total}\}]$$

$$\& \quad \varepsilon_r = \frac{1}{E}[\sigma_r - \nu\{\sigma_a)_{total} + \sigma_t\}]$$

Also,

$\frac{\Delta R}{R} = 2.04\,\varepsilon$ For used strain gage.

$\& \; V_o = V_s\left(\frac{\Delta R}{2R+\Delta R}\right)$ Strain gauge bridge balance

V_s =10 volt & R = 350 ohm

$$\therefore \frac{\Delta R}{2R + \Delta R} = \frac{V_o}{V_s}$$

$\therefore \Delta R = \frac{70V_o}{1 - 0.1V_o}$	(4)
$but\ \Delta R = 714\,\varepsilon$	(5)

From equations (4) & (5)

$\therefore \varepsilon = \frac{70V_o}{714(1 - 0.1V_o)}$	(6)

Strain in axial direction (E = 210 GN/m^2, ν = 0.3 for steel)

$\varepsilon_a = \frac{1}{E}[-0.454P_f + P_{cy} - 83730]$	(7)

Strain in tangential direction

$\varepsilon_t = \frac{1}{E}[0.846P_f - 0.3P_{cy} - 84900]$	(8)

From equation (7)

$P_{cy} = E\,\varepsilon_a + 0.454P_f + 83730$	(9)

Substitute into equation (8)

$$\therefore E\varepsilon_t = 0.846P_f - 84900 - 0.3[E\,\varepsilon_a + 0.454P_f + 83730]$$

$$P_f = 1.409[E\,\varepsilon_t + 0.3E\,\varepsilon_a + 110019] \quad (10)$$

From equation (9)

$$P_{cy} = E\,\varepsilon_a + 83730 + 0.6396[E\,\varepsilon_t + 0.3E\,\varepsilon_a + 110019] \quad (11)$$

The value of E = 195 GN/m^2 to 210 GN/m^2

The value of E has a big effect on the results

APPENDIX D. EXPERIMENTAL RESULTS

D.1 INSTANTANEOUS SPEED

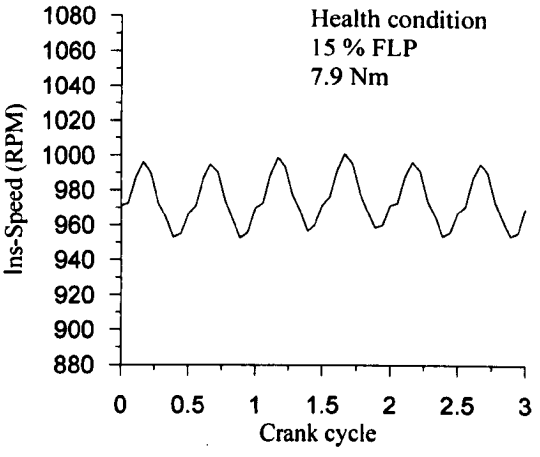

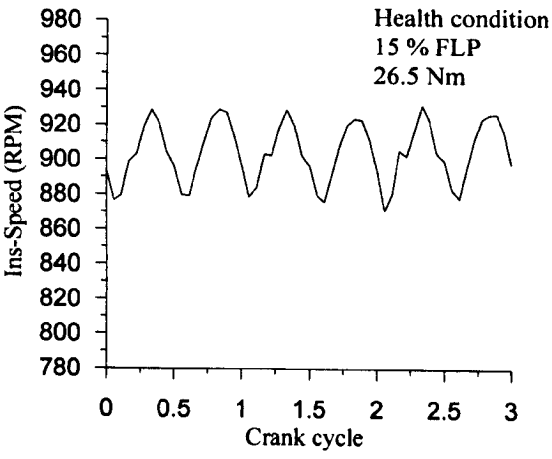

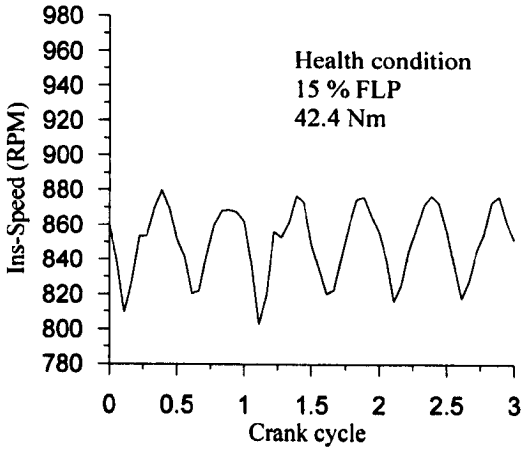

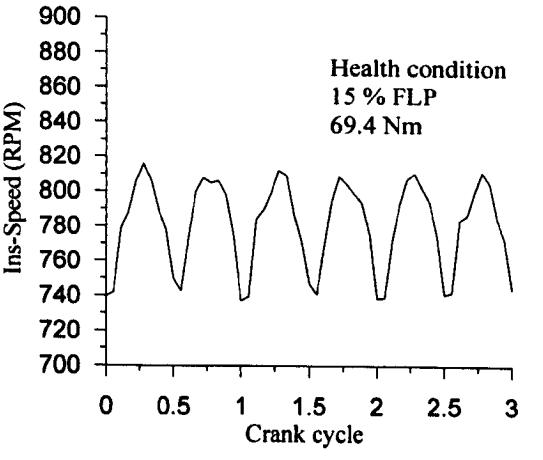

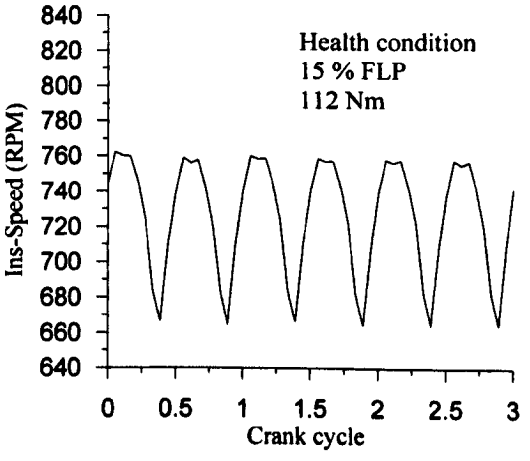

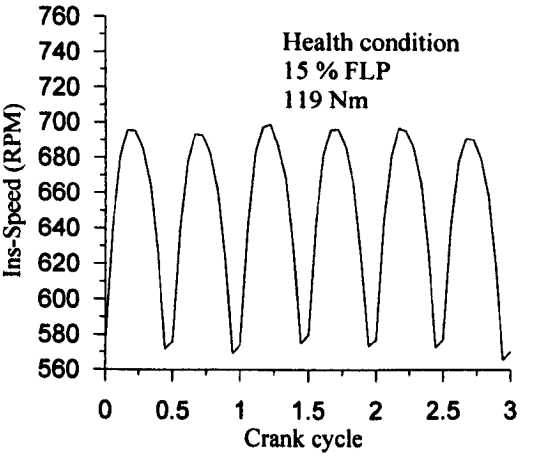

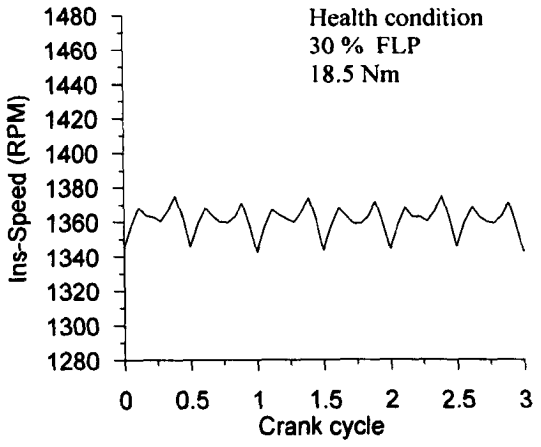
Health condition
30 % FLP
18.5 Nm
Ins-Speed (RPM)
Crank cycle

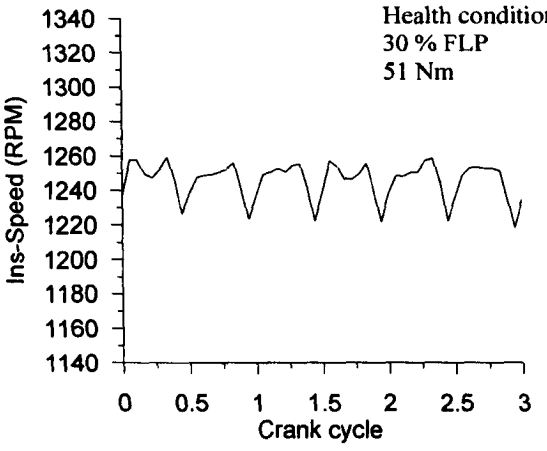
Health condition
30 % FLP
51 Nm
Ins-Speed (RPM)
Crank cycle

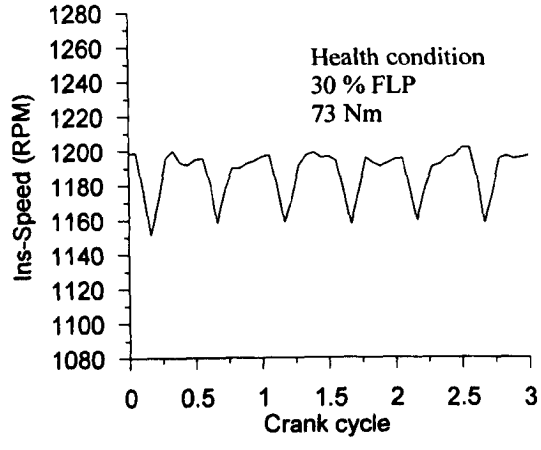
Health condition
30 % FLP
73 Nm
Ins-Speed (RPM)
Crank cycle

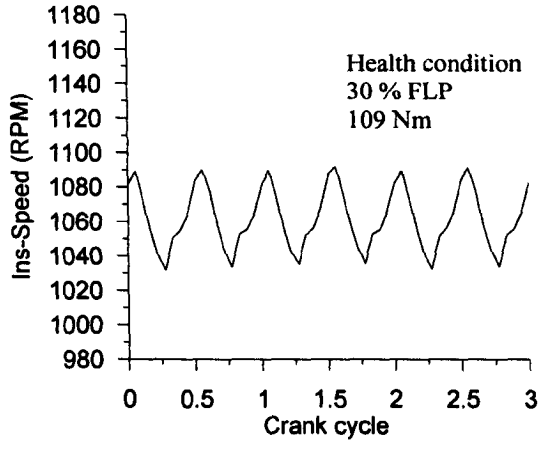
Health condition
30 % FLP
109 Nm
Ins-Speed (RPM)
Crank cycle

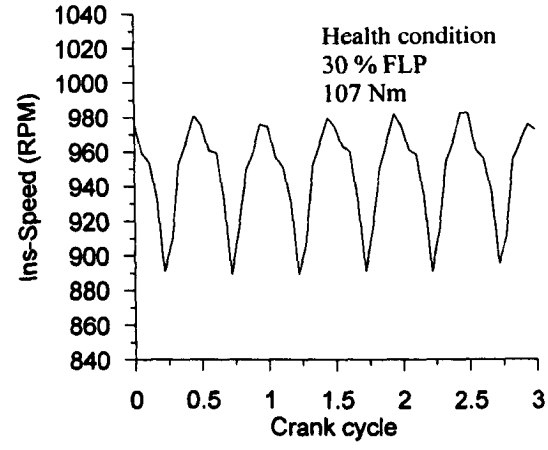
Health condition
30 % FLP
107 Nm
Ins-Speed (RPM)
Crank cycle

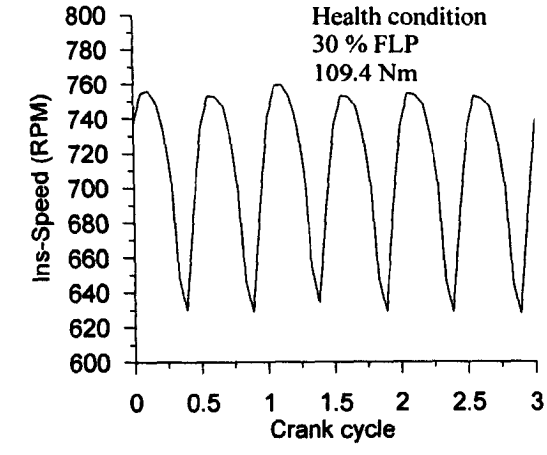
Health condition
30 % FLP
109.4 Nm
Ins-Speed (RPM)
Crank cycle

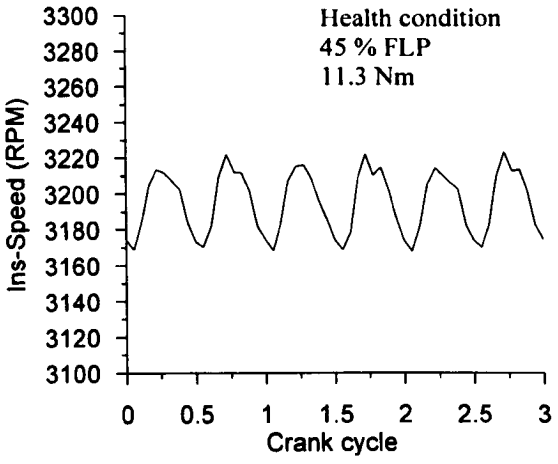
Health condition
45 % FLP
11.3 Nm
Ins-Speed (RPM)
3300
3280
3260
3240
3220
3200
3180
3160
3140
3120
3100
0 0.5 1 1.5 2 2.5 3
Crank cycle

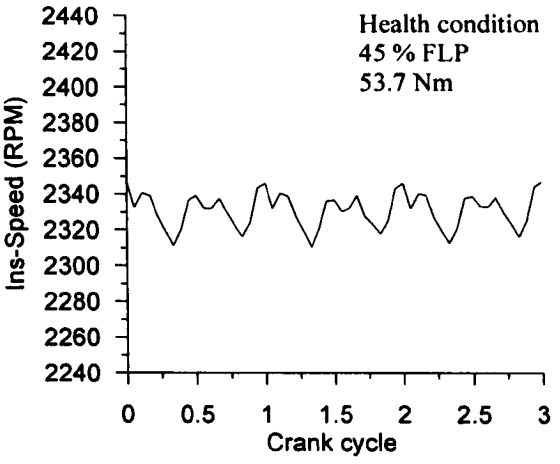
Health condition
45 % FLP
53.7 Nm
Ins-Speed (RPM)
2440
2420
2400
2380
2360
2340
2320
2300
2280
2260
2240
0 0.5 1 1.5 2 2.5 3
Crank cycle

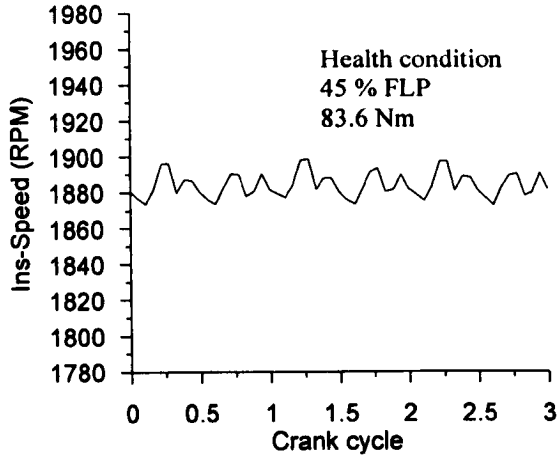
Health condition
45 % FLP
83.6 Nm
Ins-Speed (RPM)
1980
1960
1940
1920
1900
1880
1860
1840
1820
1800
1780
0 0.5 1 1.5 2 2.5 3
Crank cycle

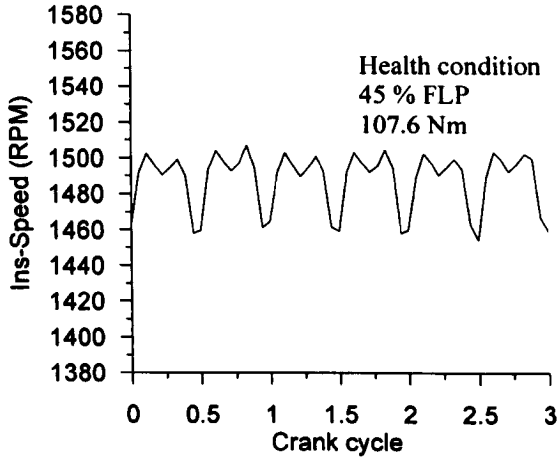
Health condition
45 % FLP
107.6 Nm
Ins-Speed (RPM)
1580
1560
1540
1520
1500
1480
1460
1440
1420
1400
1380
0 0.5 1 1.5 2 2.5 3
Crank cycle

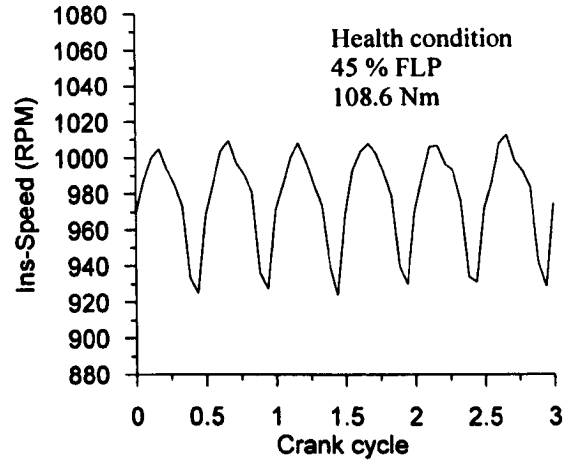
Health condition
45 % FLP
108.6 Nm
Ins-Speed (RPM)
1080
1060
1040
1020
1000
980
960
940
920
900
880
0 0.5 1 1.5 2 2.5 3
Crank cycle

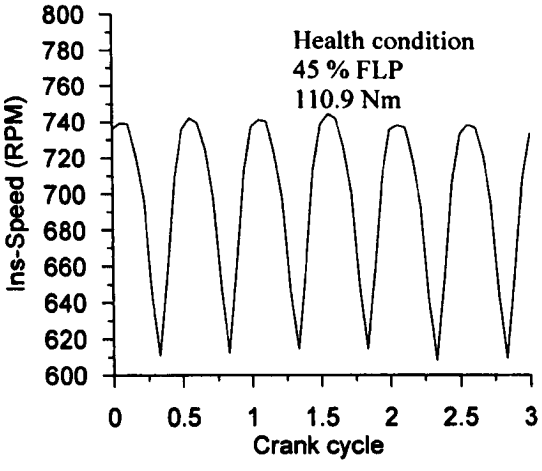
Health condition
45 % FLP
110.9 Nm
Ins-Speed (RPM)
800
780
760
740
720
700
680
660
640
620
600
0 0.5 1 1.5 2 2.5 3
Crank cycle

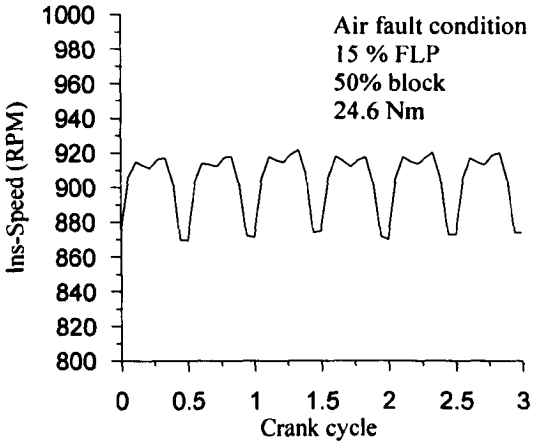
Air fault condition
15 % FLP
50% block
24.6 Nm
Ins-Speed (RPM)
Crank cycle

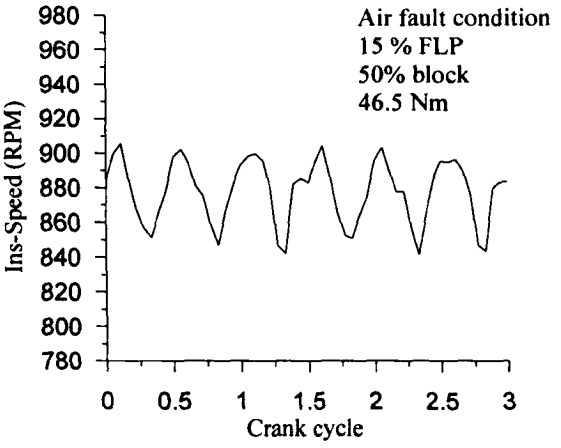
Air fault condition
15 % FLP
50% block
46.5 Nm
Ins-Speed (RPM)
Crank cycle

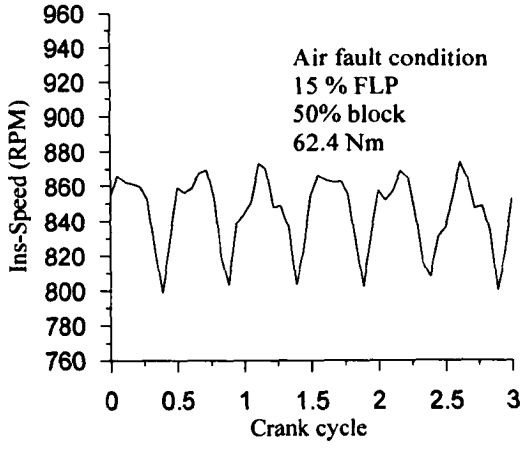
Air fault condition
15 % FLP
50% block
62.4 Nm
Ins-Speed (RPM)
Crank cycle

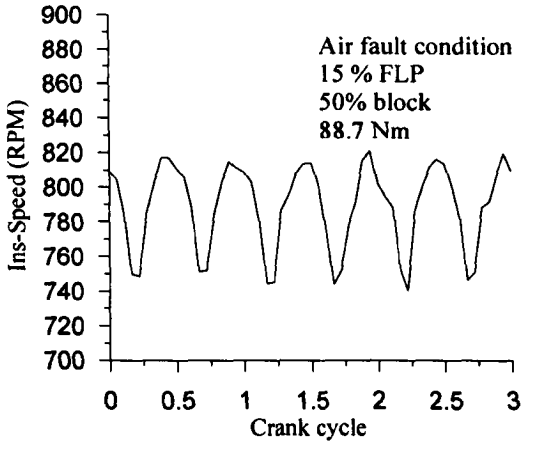
Air fault condition
15 % FLP
50% block
88.7 Nm
Ins-Speed (RPM)
Crank cycle

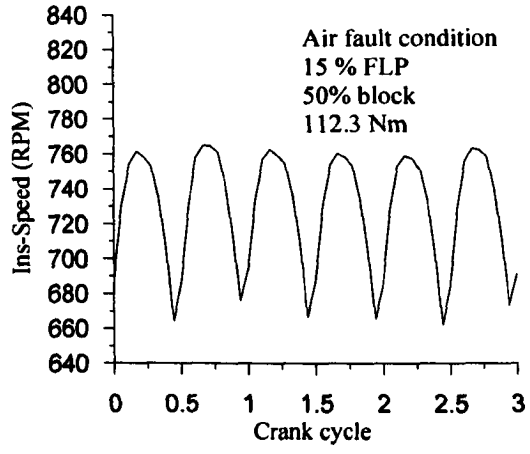
Air fault condition
15 % FLP
50% block
112.3 Nm
Ins-Speed (RPM)
Crank cycle

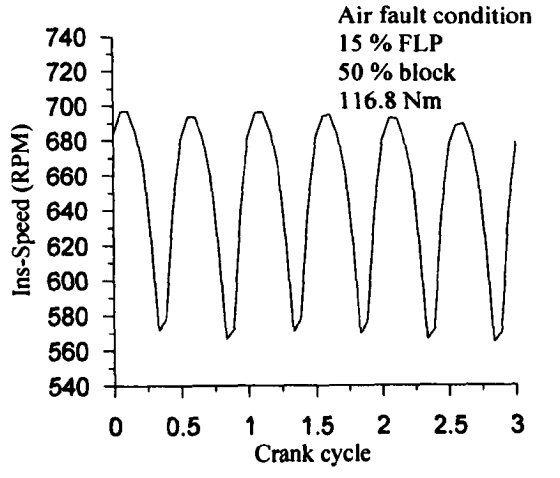
Air fault condition
15 % FLP
50 % block
116.8 Nm
Ins-Speed (RPM)
Crank cycle

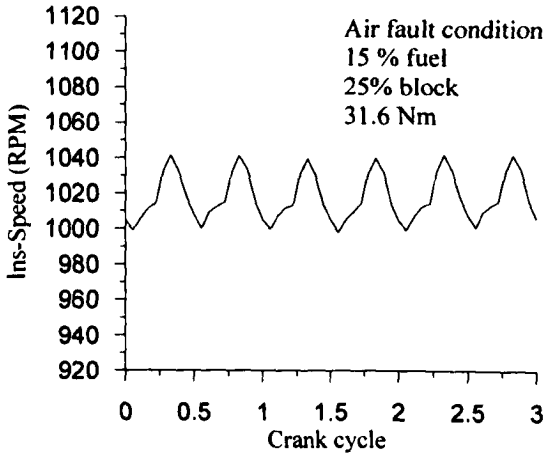
Air fault condition
15 % fuel
25% block
31.6 Nm
Ins-Speed (RPM)
Crank cycle

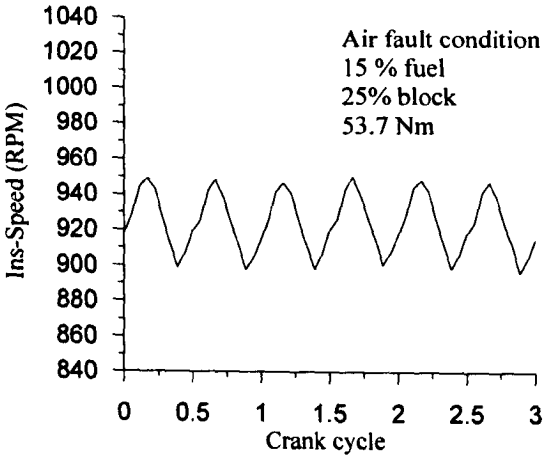
Air fault condition
15 % fuel
25% block
53.7 Nm
Ins-Speed (RPM)
Crank cycle

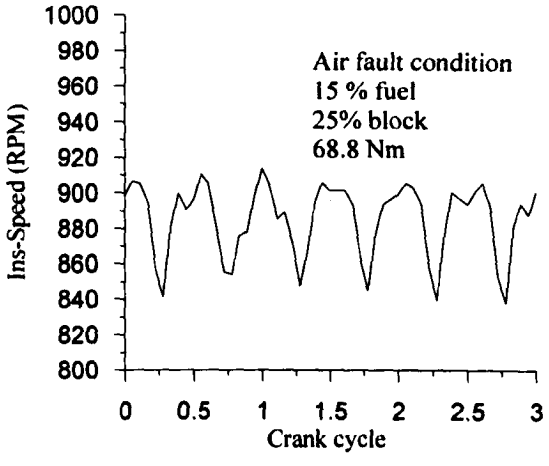
Air fault condition
15 % fuel
25% block
68.8 Nm
Ins-Speed (RPM)
Crank cycle

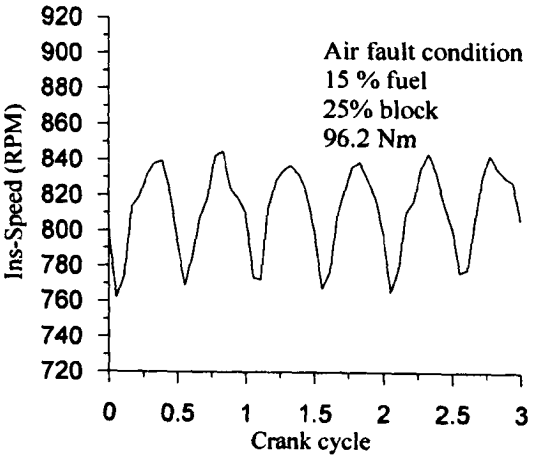
Air fault condition
15 % fuel
25% block
96.2 Nm
Ins-Speed (RPM)
Crank cycle

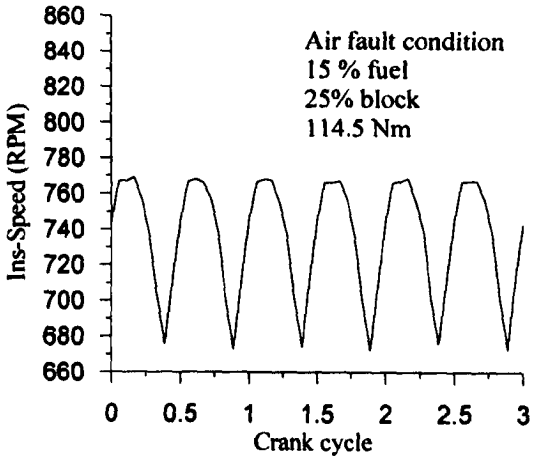
Air fault condition
15 % fuel
25% block
114.5 Nm
Ins-Speed (RPM)
Crank cycle

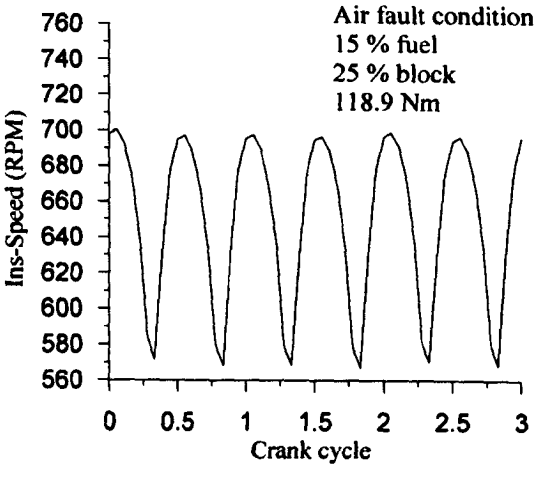
Air fault condition
15 % fuel
25 % block
118.9 Nm
Ins-Speed (RPM)
Crank cycle

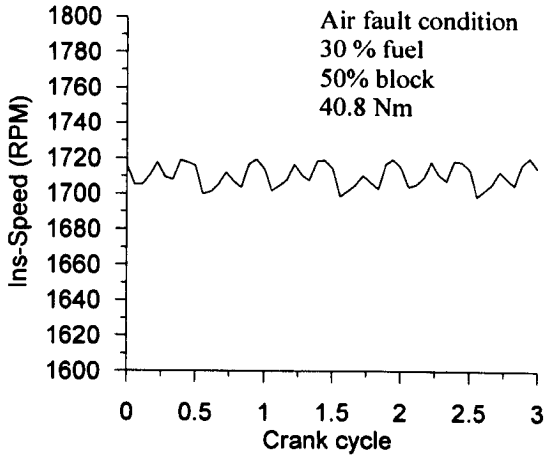
Air fault condition
30 % fuel
50% block
40.8 Nm
Ins-Speed (RPM)
Crank cycle

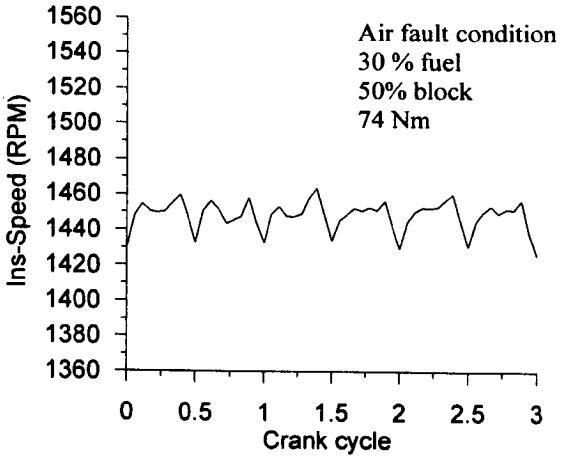
Air fault condition
30 % fuel
50% block
74 Nm
Ins-Speed (RPM)
Crank cycle

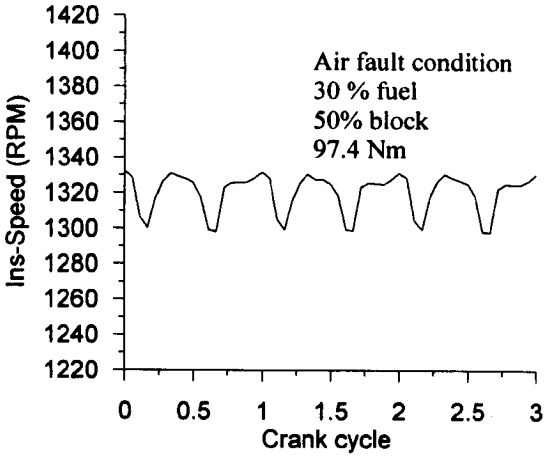
Air fault condition
30 % fuel
50% block
97.4 Nm
Ins-Speed (RPM)
Crank cycle

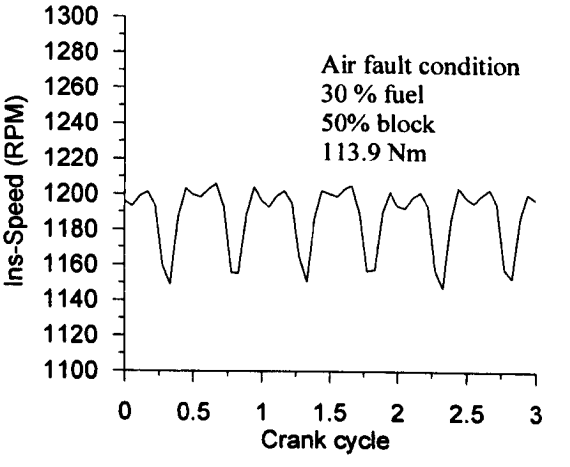
Air fault condition
30 % fuel
50% block
113.9 Nm
Ins-Speed (RPM)
Crank cycle

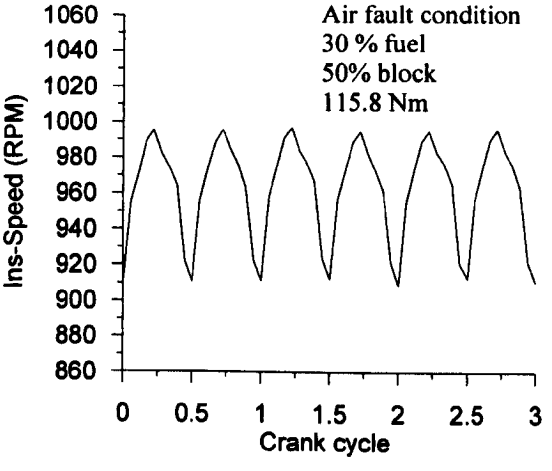
Air fault condition
30 % fuel
50% block
115.8 Nm
Ins-Speed (RPM)
Crank cycle

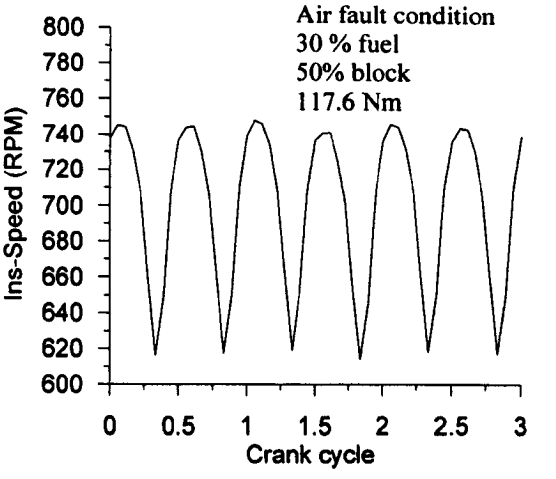
Air fault condition
30 % fuel
50% block
117.6 Nm
Ins-Speed (RPM)
Crank cycle

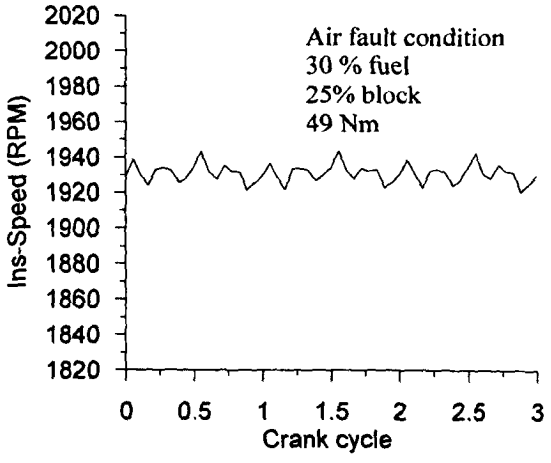
Air fault condition
30 % fuel
25% block
49 Nm
Ins-Speed (RPM)
Crank cycle

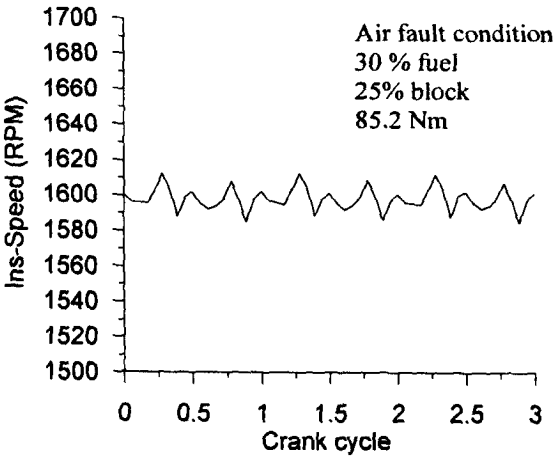
Air fault condition
30 % fuel
25% block
85.2 Nm
Ins-Speed (RPM)
Crank cycle

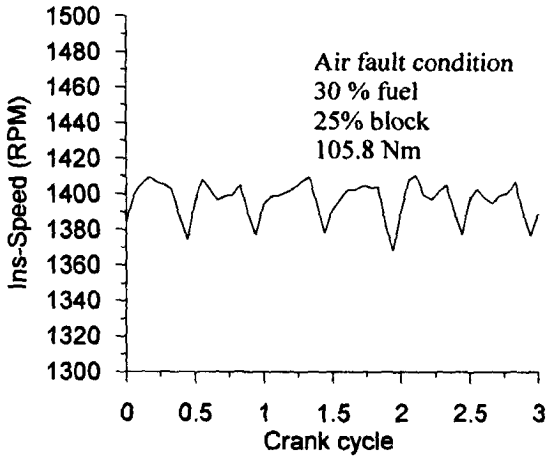
Air fault condition
30 % fuel
25% block
105.8 Nm
Ins-Speed (RPM)
Crank cycle

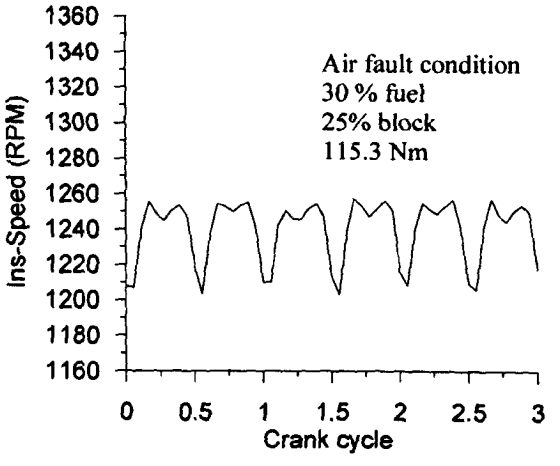
Air fault condition
30 % fuel
25% block
115.3 Nm
Ins-Speed (RPM)
Crank cycle

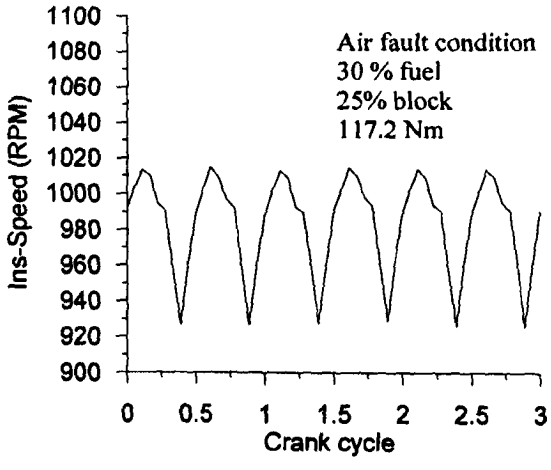
Air fault condition
30 % fuel
25% block
117.2 Nm
Ins-Speed (RPM)
Crank cycle

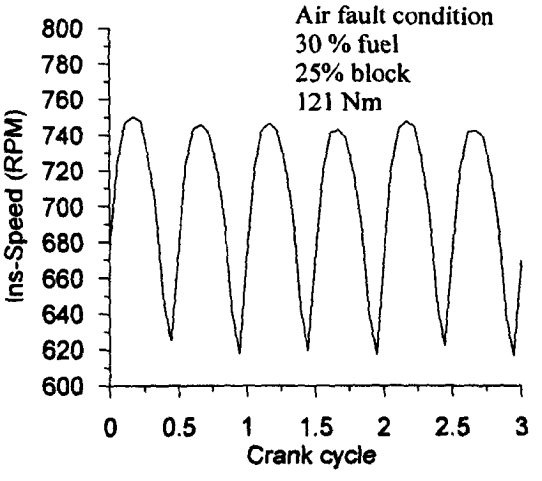
Air fault condition
30 % fuel
25% block
121 Nm
Ins-Speed (RPM)
Crank cycle

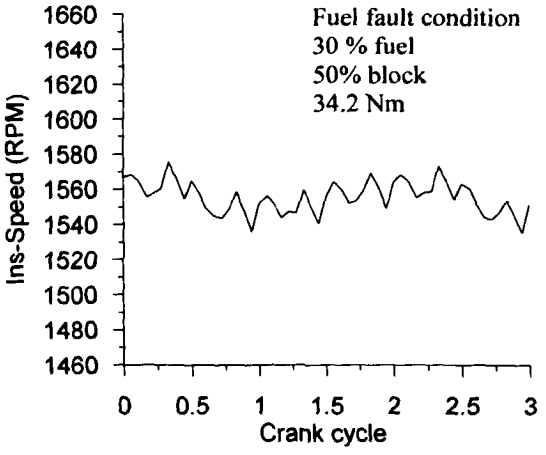
Fuel fault condition
30 % fuel
50% block
34.2 Nm
Ins-Speed (RPM)
Crank cycle

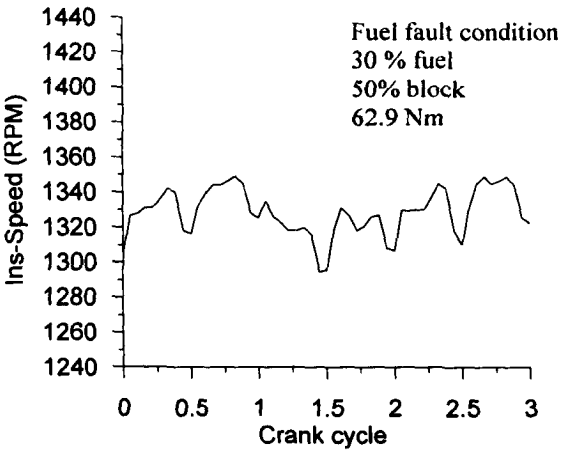
Fuel fault condition
30 % fuel
50% block
62.9 Nm
Ins-Speed (RPM)
Crank cycle

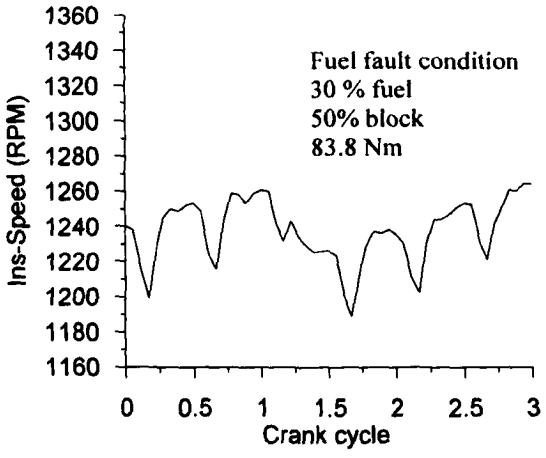
Fuel fault condition
30 % fuel
50% block
83.8 Nm
Ins-Speed (RPM)
Crank cycle

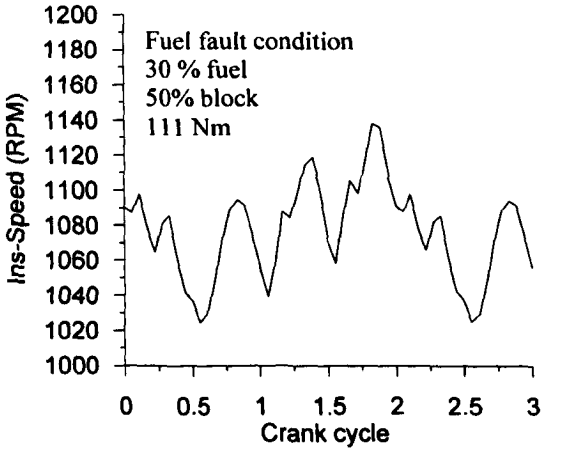
Fuel fault condition
30 % fuel
50% block
111 Nm
Ins-Speed (RPM)
Crank cycle

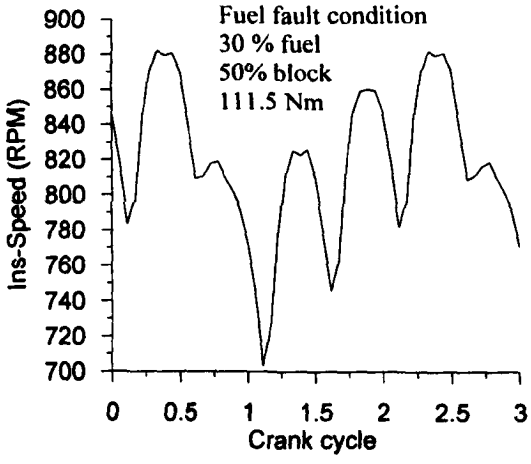
Fuel fault condition
30 % fuel
50% block
111.5 Nm
Ins-Speed (RPM)
Crank cycle

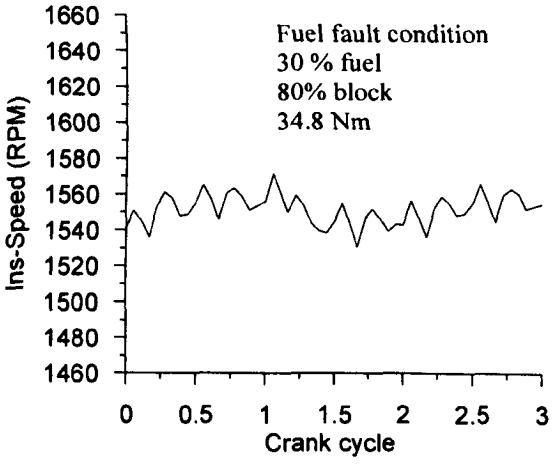
Fuel fault condition
30 % fuel
80% block
34.8 Nm
Ins-Speed (RPM)
Crank cycle

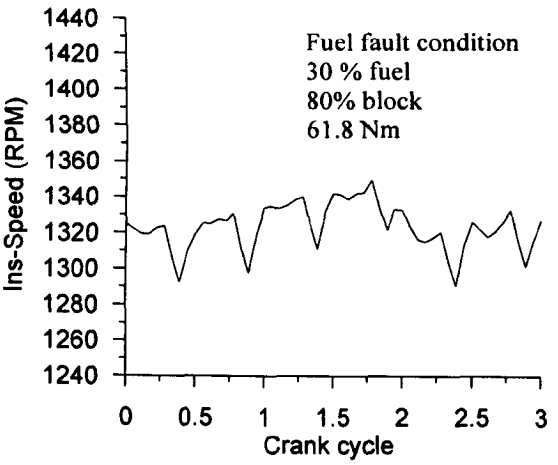
Fuel fault condition
30 % fuel
80% block
61.8 Nm
Ins-Speed (RPM)
Crank cycle

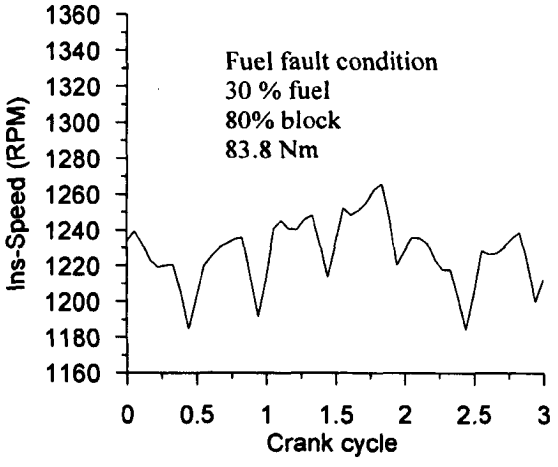
Fuel fault condition
30 % fuel
80% block
83.8 Nm
Ins-Speed (RPM)
Crank cycle

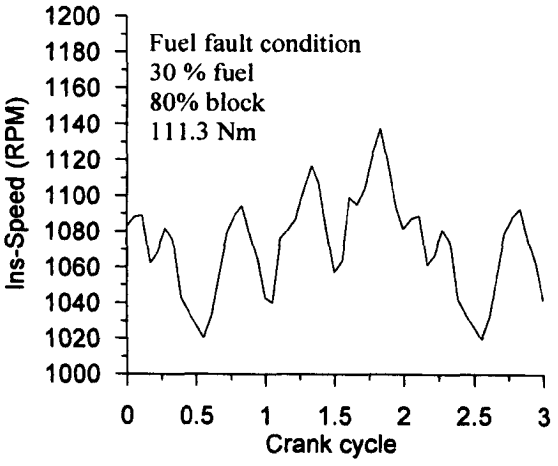
Fuel fault condition
30 % fuel
80% block
111.3 Nm
Ins-Speed (RPM)
Crank cycle

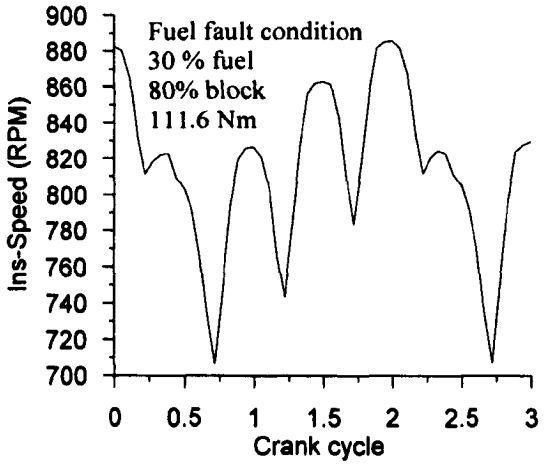
Fuel fault condition
30 % fuel
80% block
111.6 Nm
Ins-Speed (RPM)
Crank cycle

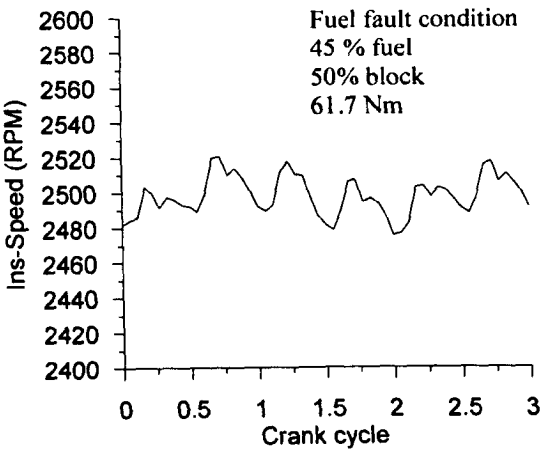
Fuel fault condition
45 % fuel
50% block
61.7 Nm
Ins-Speed (RPM)
2600
2580
2560
2540
2520
2500
2480
2460
2440
2420
2400
0 0.5 1 1.5 2 2.5 3
Crank cycle

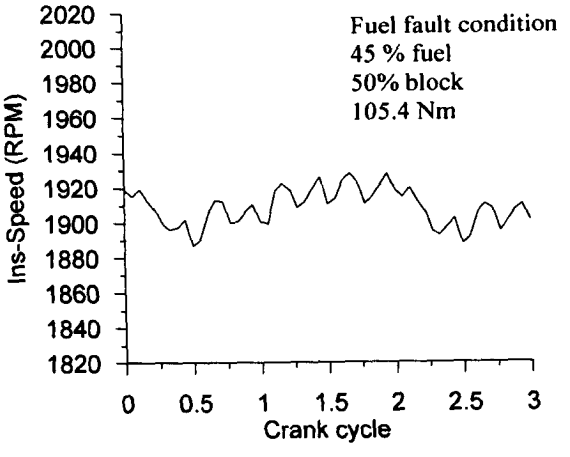
Fuel fault condition
45 % fuel
50% block
105.4 Nm
Ins-Speed (RPM)
2020
2000
1980
1960
1940
1920
1900
1880
1860
1840
1820
0 0.5 1 1.5 2 2.5 3
Crank cycle

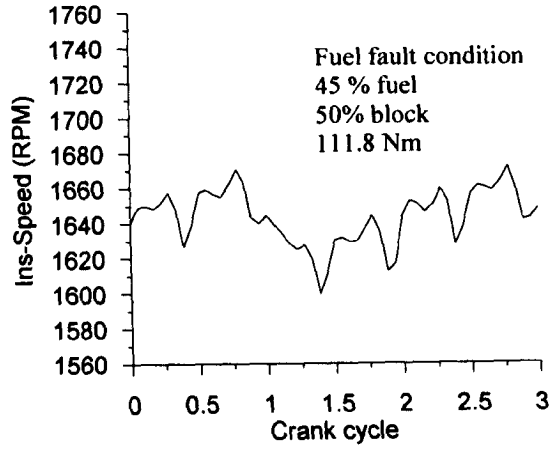
Fuel fault condition
45 % fuel
50% block
111.8 Nm
Ins-Speed (RPM)
1760
1740
1720
1700
1680
1660
1640
1620
1600
1580
1560
0 0.5 1 1.5 2 2.5 3
Crank cycle

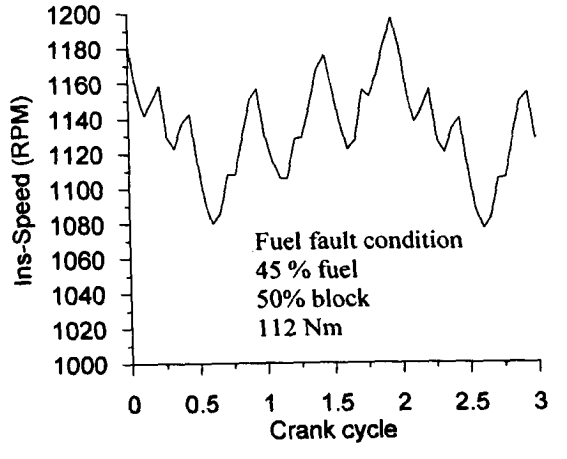
Fuel fault condition
45 % fuel
50% block
112 Nm
Ins-Speed (RPM)
1200
1180
1160
1140
1120
1100
1080
1060
1040
1020
1000
0 0.5 1 1.5 2 2.5 3
Crank cycle

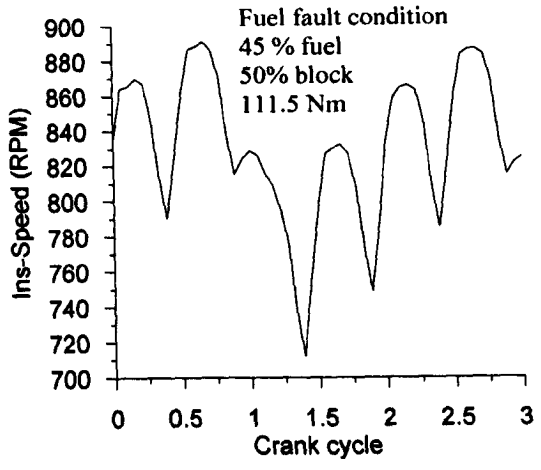
Fuel fault condition
45 % fuel
50% block
111.5 Nm
Ins-Speed (RPM)
900
880
860
840
820
800
780
760
740
720
700
0 0.5 1 1.5 2 2.5 3
Crank cycle

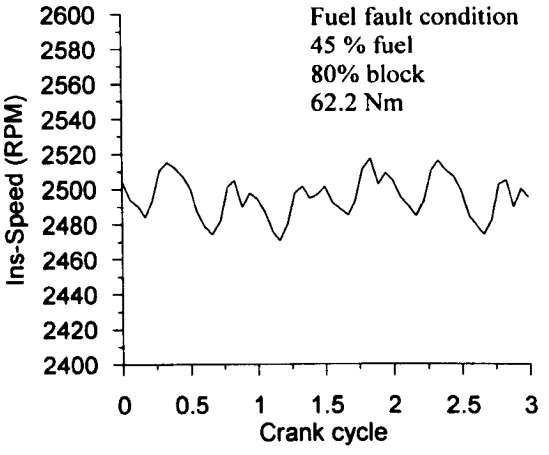
Fuel fault condition
45 % fuel
80% block
62.2 Nm
Ins-Speed (RPM)
Crank cycle

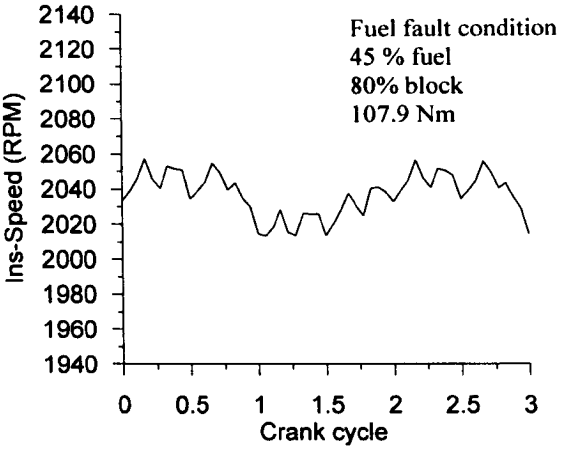
Fuel fault condition
45 % fuel
80% block
107.9 Nm
Ins-Speed (RPM)
Crank cycle

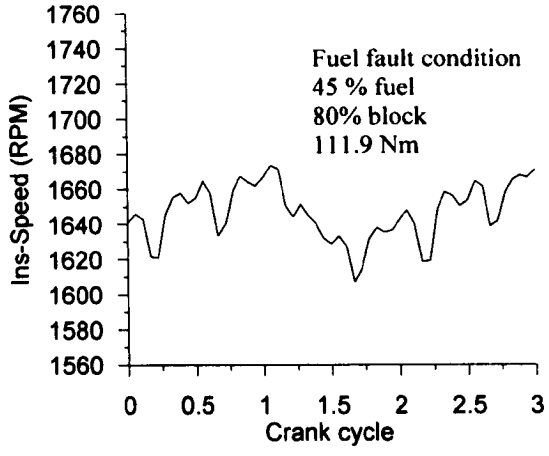
Fuel fault condition
45 % fuel
80% block
111.9 Nm
Ins-Speed (RPM)
Crank cycle

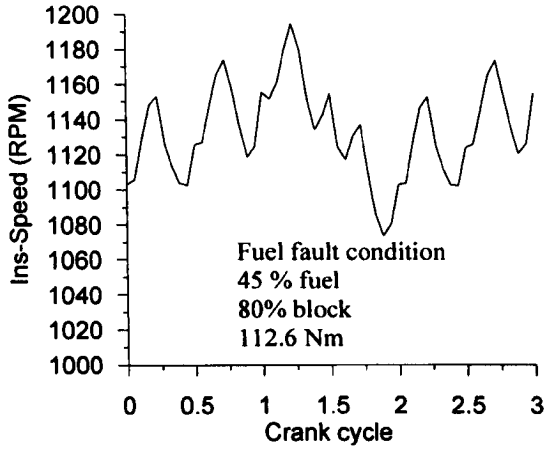
Fuel fault condition
45 % fuel
80% block
112.6 Nm
Ins-Speed (RPM)
Crank cycle

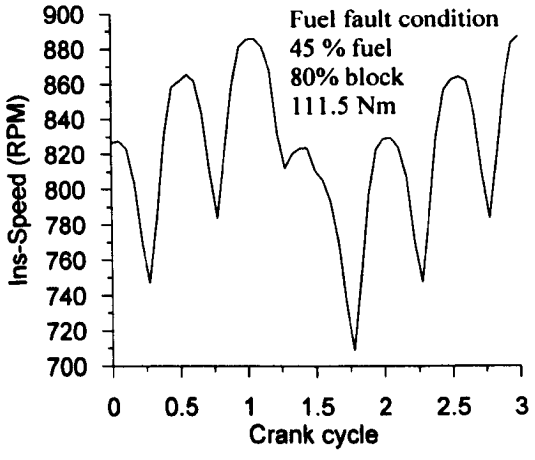
Fuel fault condition
45 % fuel
80% block
111.5 Nm
Ins-Speed (RPM)
Crank cycle

D.2 EXHAUST TEMPERATURE

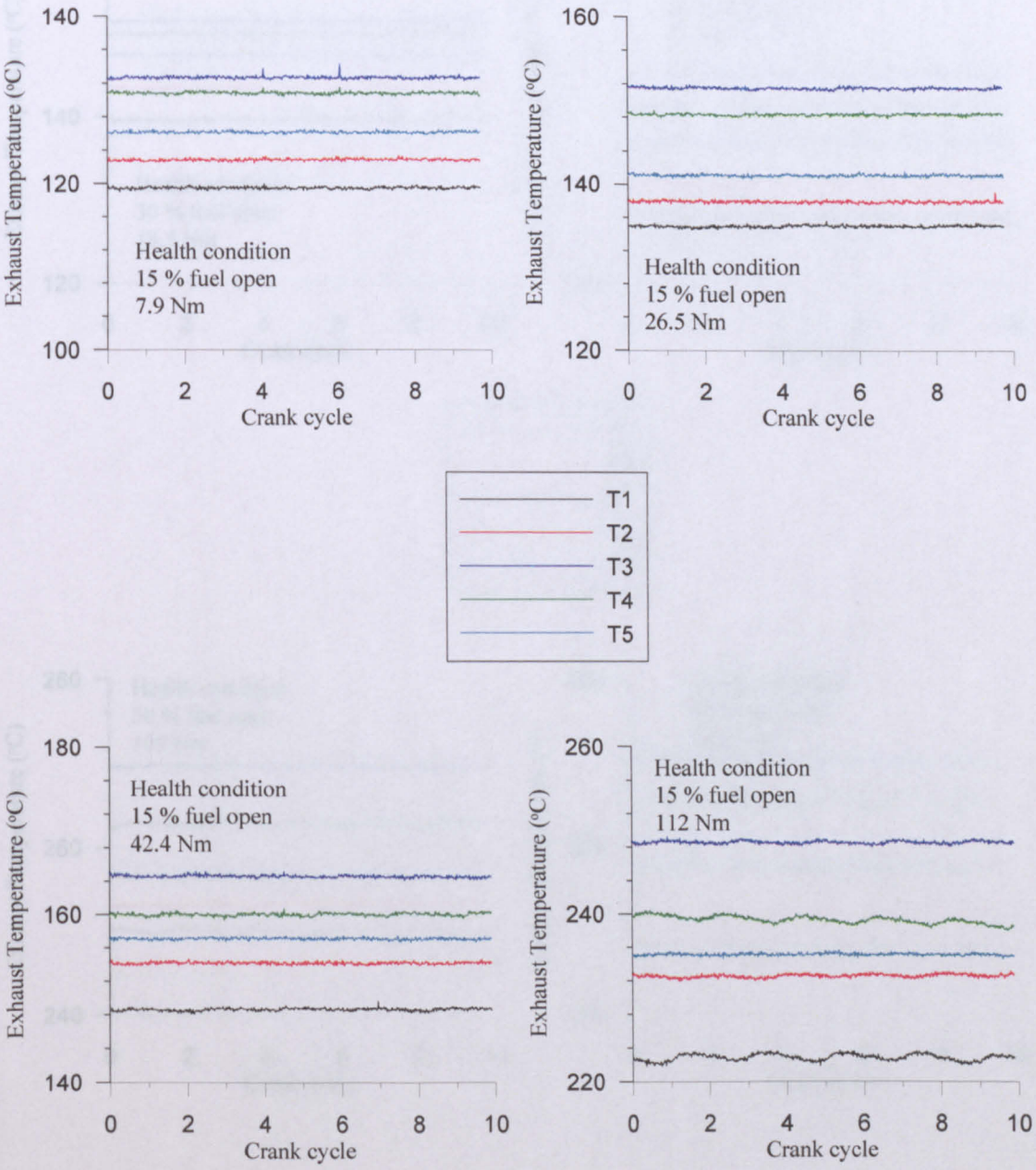

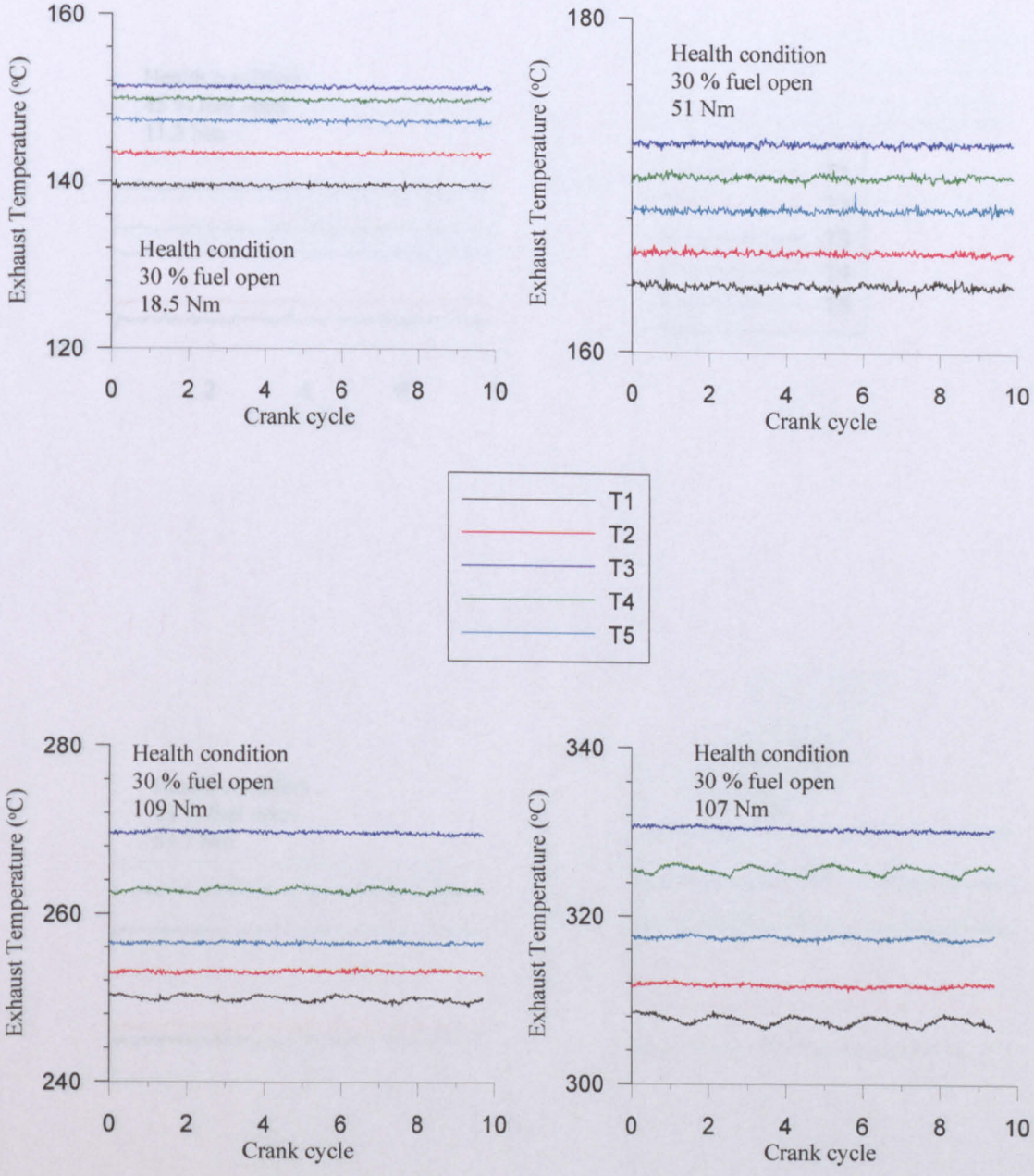
Exhaust Temperature (°C)
160
140
120
Health condition
30 % fuel open
18.5 Nm
0
2
4
6
8
10
Crank cycle
Exhaust Temperature (°C)
180
160
Health condition
30 % fuel open
51 Nm
0
2
4
6
8
10
Crank cycle
T1
T2
T3
T4
T5
Exhaust Temperature (°C)
280
260
240
Health condition
30 % fuel open
109 Nm
0
2
4
6
8
10
Crank cycle
Exhaust Temperature (°C)
340
320
300
Health condition
30 % fuel open
107 Nm
0
2
4
6
8
10
Crank cycle

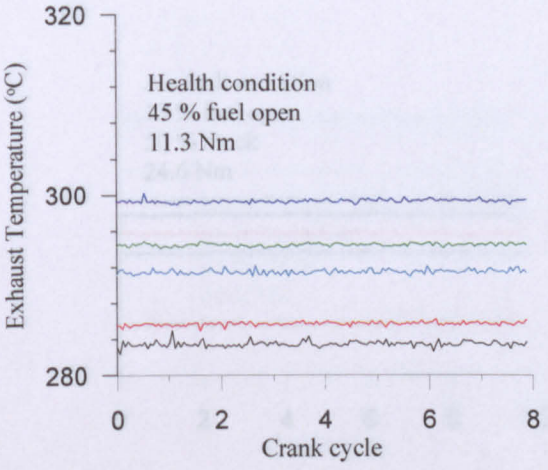
Health condition
45 % fuel open
11.3 Nm
Exhaust Temperature (°C)
320
300
280
0
2
4
6
8
Crank cycle

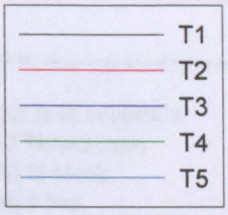
T1
T2
T3
T4
T5

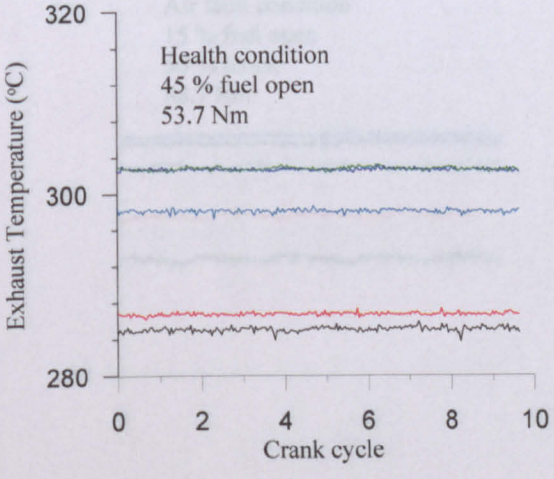
Health condition
45 % fuel open
53.7 Nm
Exhaust Temperature (°C)
320
300
280
0
2
4
6
8
10
Crank cycle

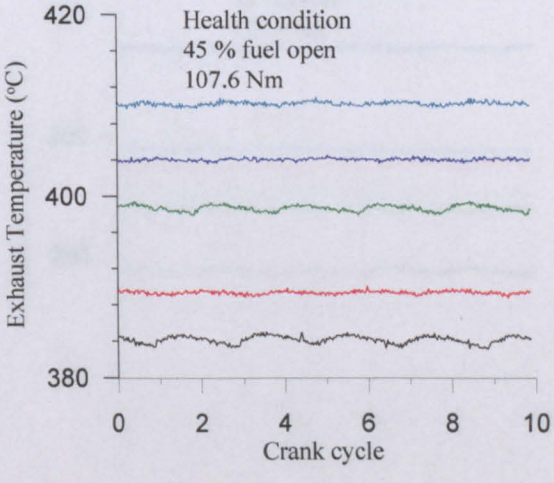
Health condition
45 % fuel open
107.6 Nm
Exhaust Temperature (°C)
420
400
380
0
2
4
6
8
10
Crank cycle

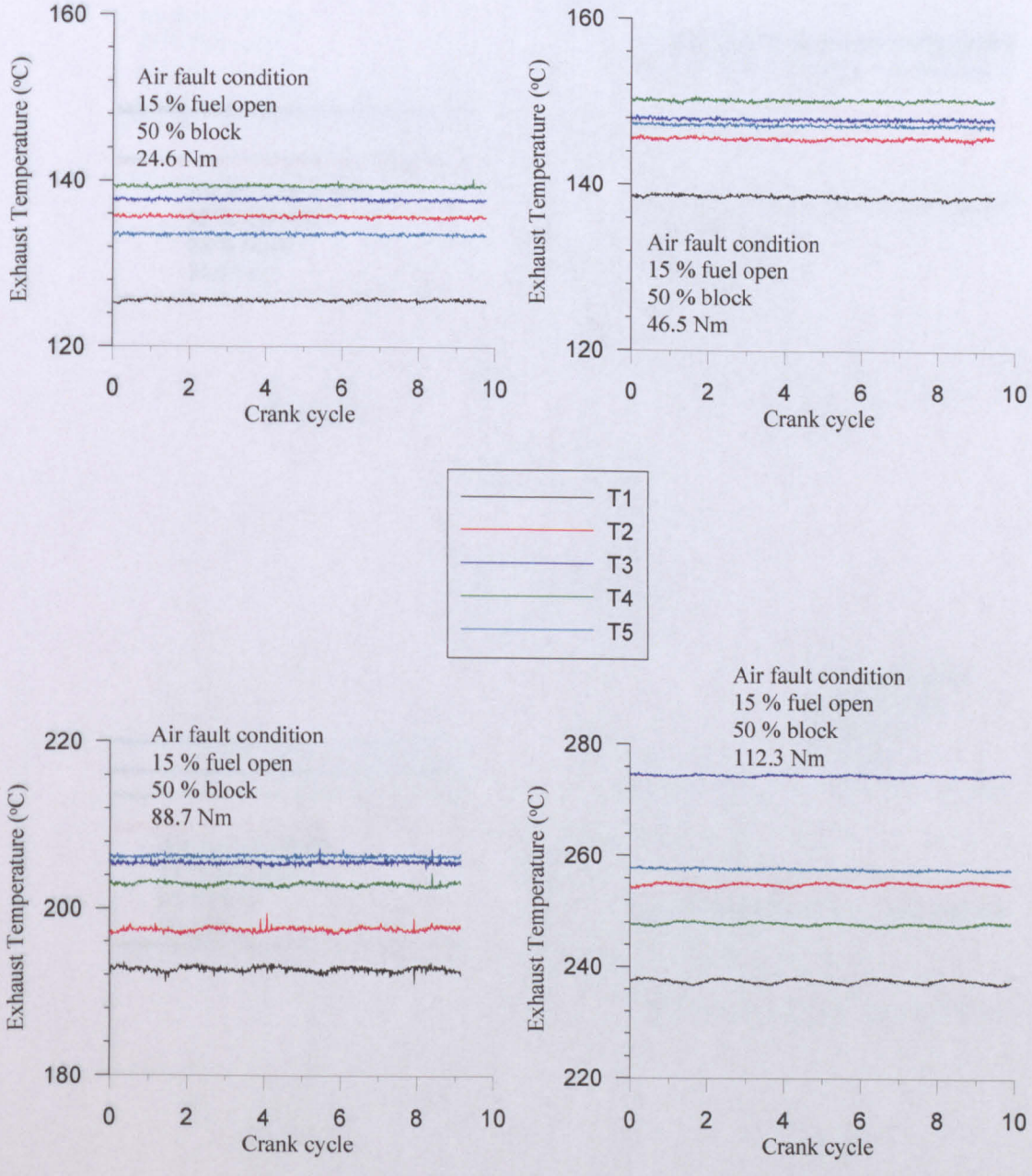
Air fault condition
15 % fuel open
50 % block
24.6 Nm
Exhaust Temperature (°C)
Crank cycle
Air fault condition
15 % fuel open
50 % block
46.5 Nm
T1
T2
T3
T4
T5
Air fault condition
15 % fuel open
50 % block
88.7 Nm
Air fault condition
15 % fuel open
50 % block
112.3 Nm

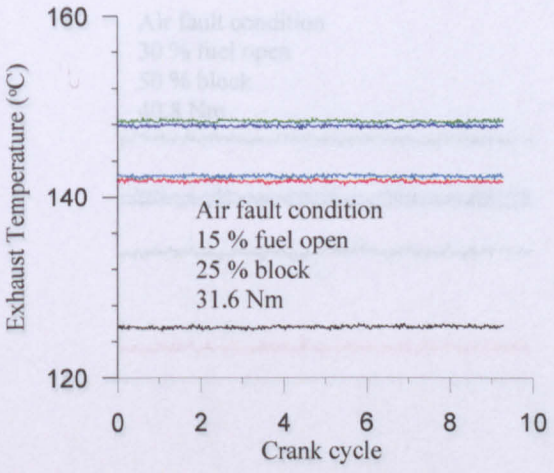
160
140
120
Exhaust Temperature (°C)
Air fault condition
15 % fuel open
25 % block
31.6 Nm
0
2
4
6
8
10
Crank cycle

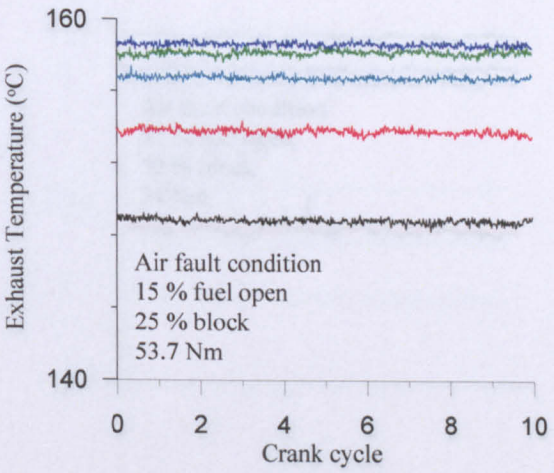
160
140
Exhaust Temperature (°C)
Air fault condition
15 % fuel open
25 % block
53.7 Nm
0
2
4
6
8
10
Crank cycle

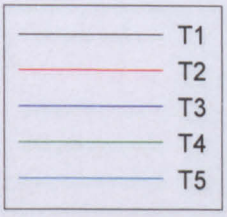
T1
T2
T3
T4
T5

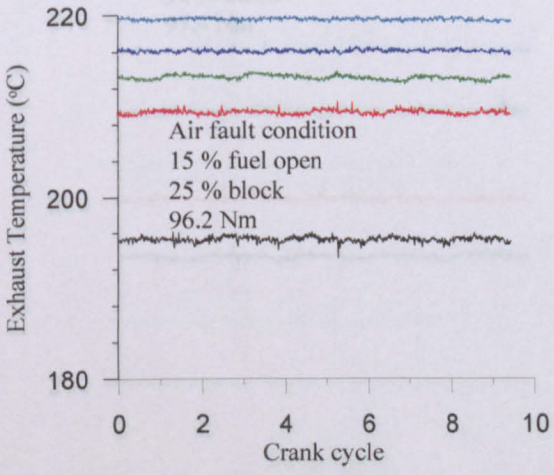
220
200
180
Exhaust Temperature (°C)
Air fault condition
15 % fuel open
25 % block
96.2 Nm
0
2
4
6
8
10
Crank cycle

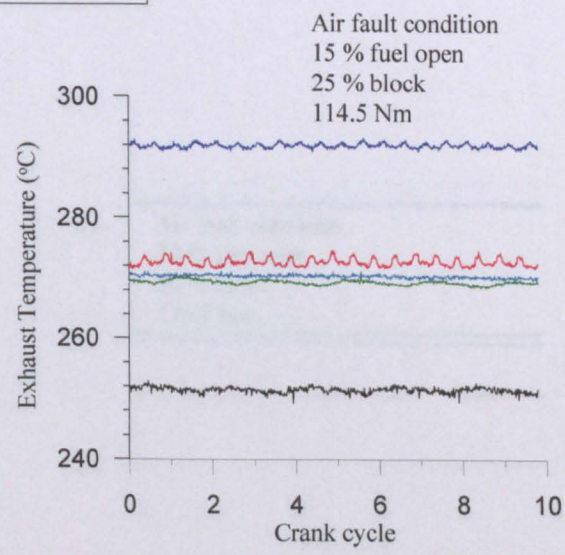
300
280
260
240
Exhaust Temperature (°C)
Air fault condition
15 % fuel open
25 % block
114.5 Nm
0
2
4
6
8
10
Crank cycle

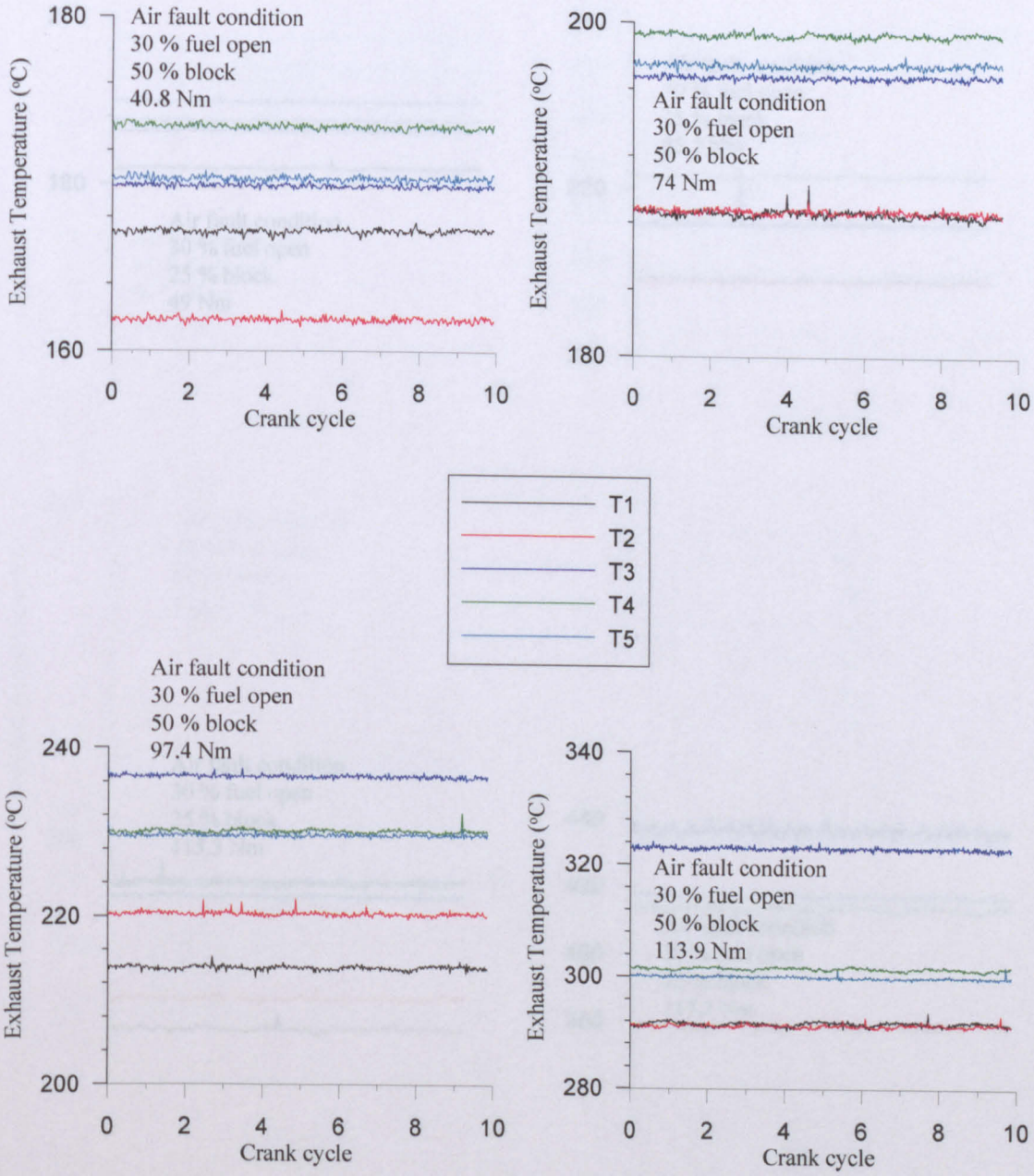
Air fault condition
30 % fuel open
50 % block
40.8 Nm
Exhaust Temperature (°C)
Crank cycle
Air fault condition
30 % fuel open
50 % block
74 Nm
Exhaust Temperature (°C)
Crank cycle
T1
T2
T3
T4
T5
Air fault condition
30 % fuel open
50 % block
97.4 Nm
Exhaust Temperature (°C)
Crank cycle
Air fault condition
30 % fuel open
50 % block
113.9 Nm
Exhaust Temperature (°C)
Crank cycle

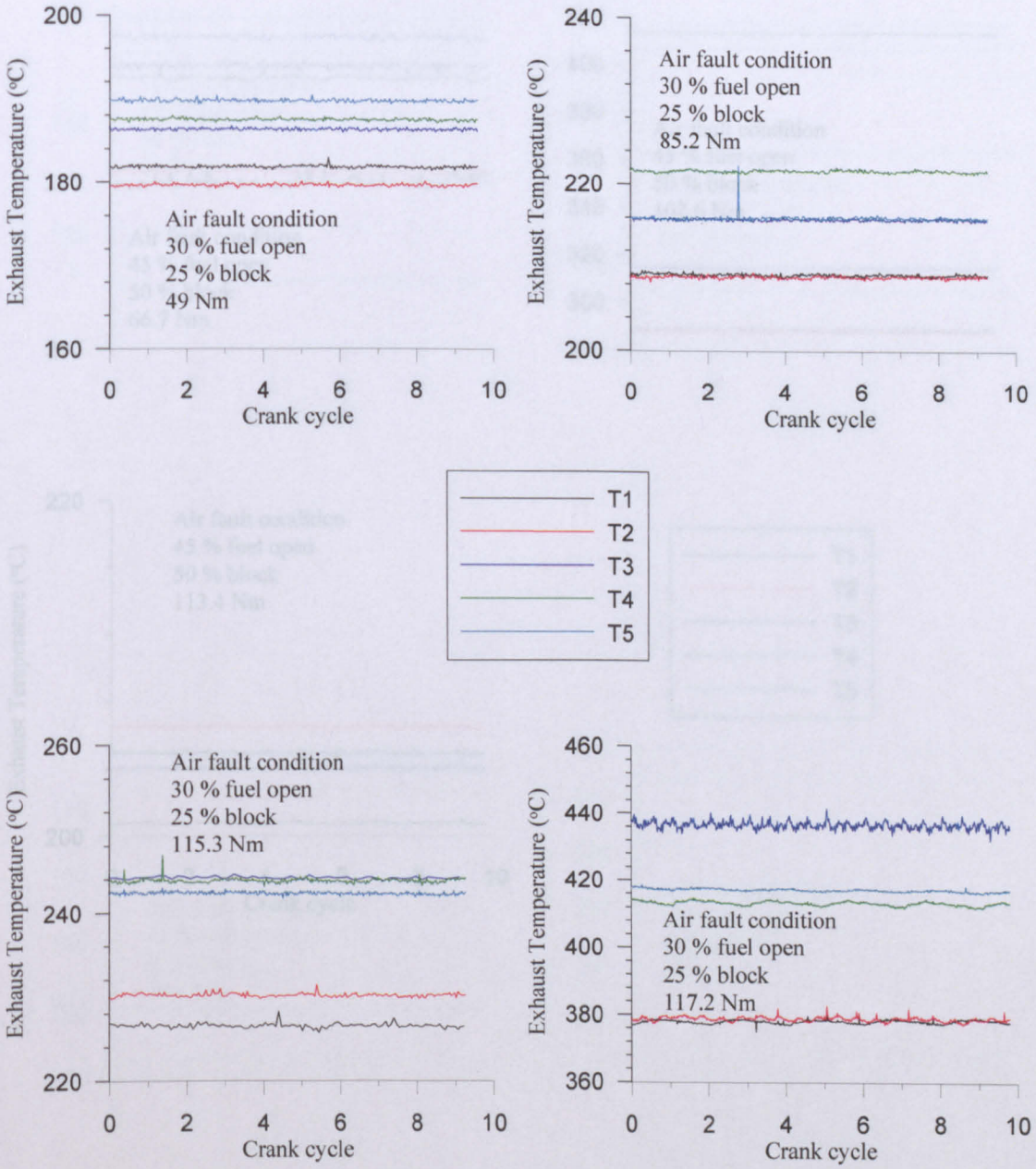
Exhaust Temperature (°C)
Crank cycle
Air fault condition
30 % fuel open
25 % block
49 Nm
Air fault condition
30 % fuel open
25 % block
85.2 Nm
T1
T2
T3
T4
T5
Air fault condition
30 % fuel open
25 % block
115.3 Nm
Air fault condition
30 % fuel open
25 % block
117.2 Nm

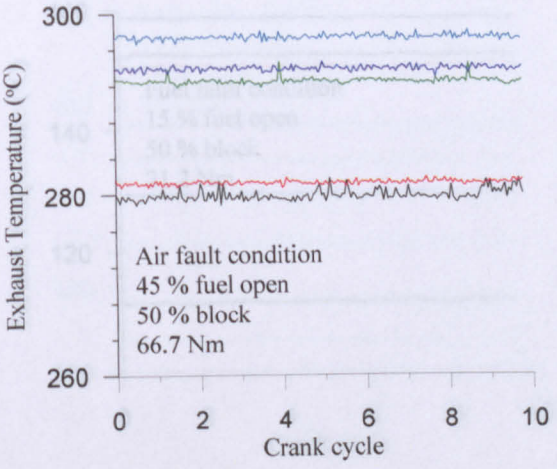
300
280
260
Exhaust Temperature (°C)
Air fault condition
45 % fuel open
50 % block
66.7 Nm
0
2
4
6
8
10
Crank cycle

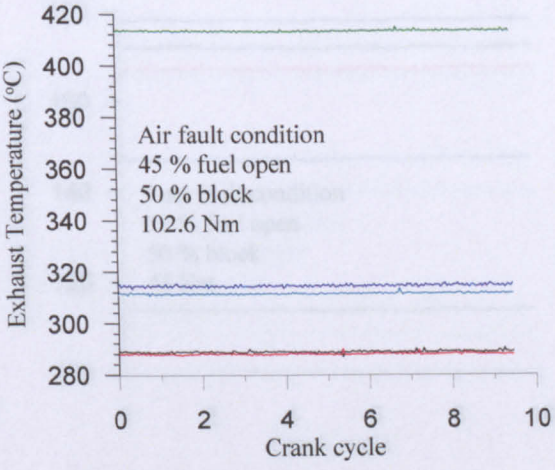
420
400
380
360
340
320
300
280
Exhaust Temperature (°C)
Air fault condition
45 % fuel open
50 % block
102.6 Nm
0
2
4
6
8
10
Crank cycle

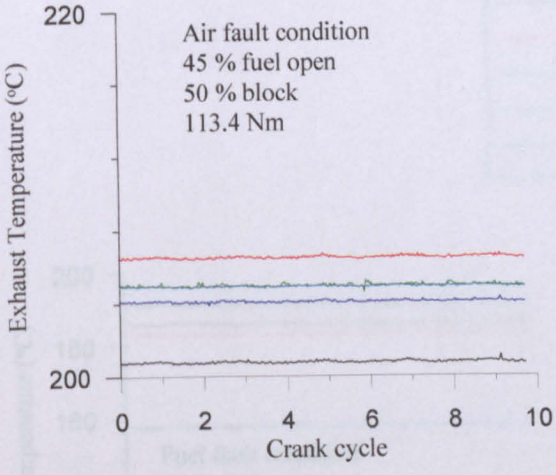
220
200
Exhaust Temperature (°C)
Air fault condition
45 % fuel open
50 % block
113.4 Nm
0
2
4
6
8
10
Crank cycle

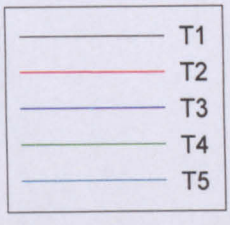
T1
T2
T3
T4
T5

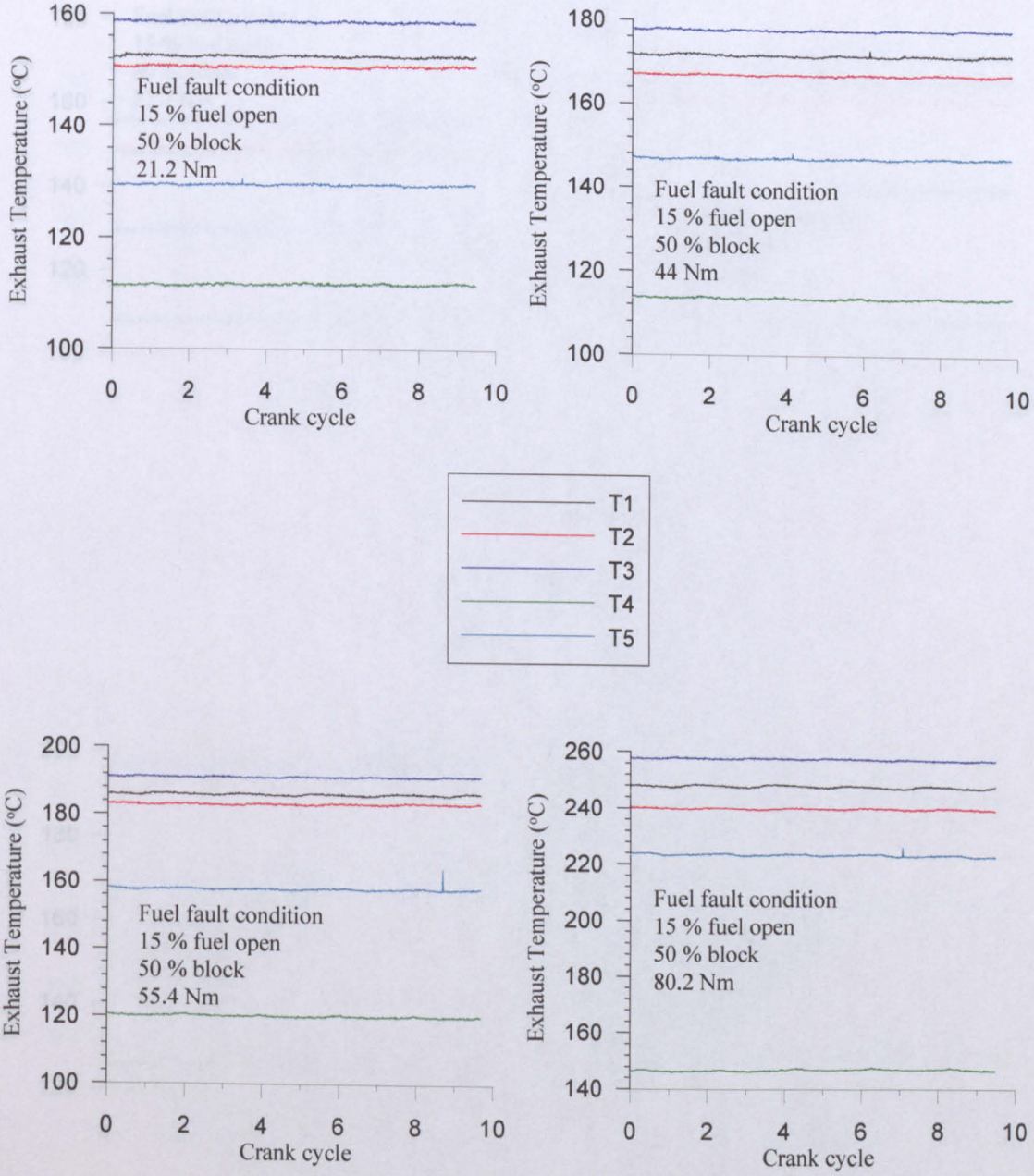
Exhaust Temperature (°C)
Crank cycle
Fuel fault condition
15 % fuel open
50 % block
21.2 Nm
Fuel fault condition
15 % fuel open
50 % block
44 Nm
T1
T2
T3
T4
T5
Fuel fault condition
15 % fuel open
50 % block
55.4 Nm
Fuel fault condition
15 % fuel open
50 % block
80.2 Nm

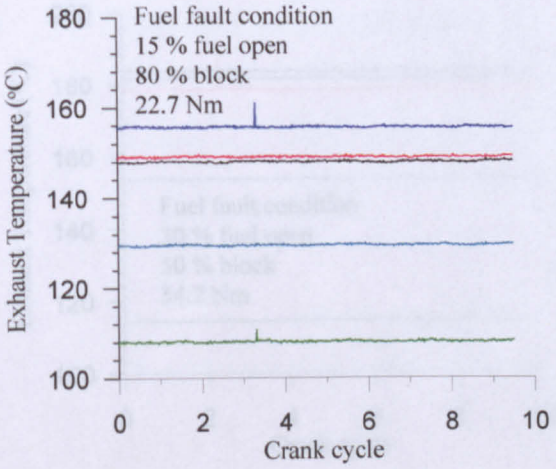
Fuel fault condition
15 % fuel open
80 % block
22.7 Nm
Exhaust Temperature (°C)
Crank cycle

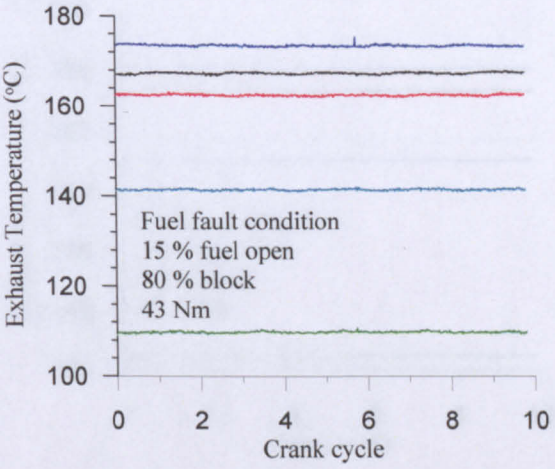
Fuel fault condition
15 % fuel open
80 % block
43 Nm
Exhaust Temperature (°C)
Crank cycle

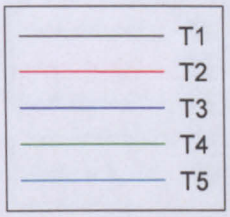
T1
T2
T3
T4
T5

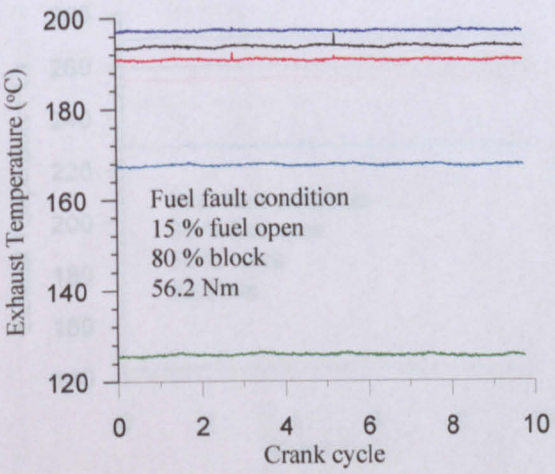
Fuel fault condition
15 % fuel open
80 % block
56.2 Nm
Exhaust Temperature (°C)
Crank cycle

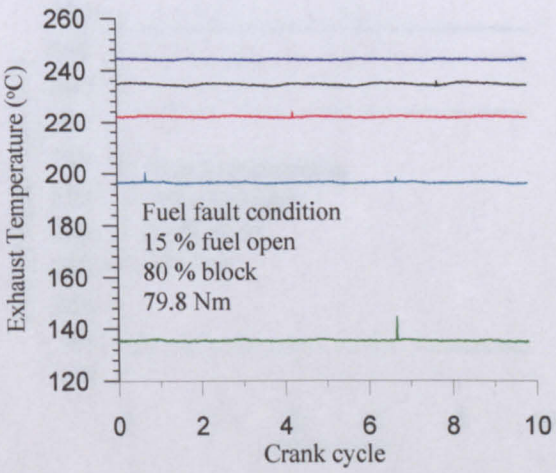
Fuel fault condition
15 % fuel open
80 % block
79.8 Nm
Exhaust Temperature (°C)
Crank cycle

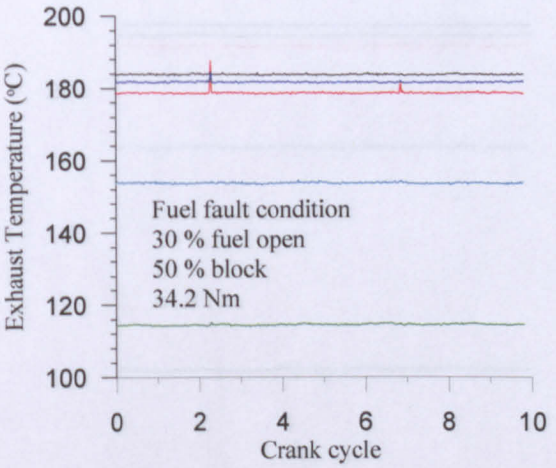
Exhaust Temperature (°C)
200
180
160
140
120
100
0
2
4
6
8
10
Crank cycle
Fuel fault condition
30 % fuel open
50 % block
34.2 Nm

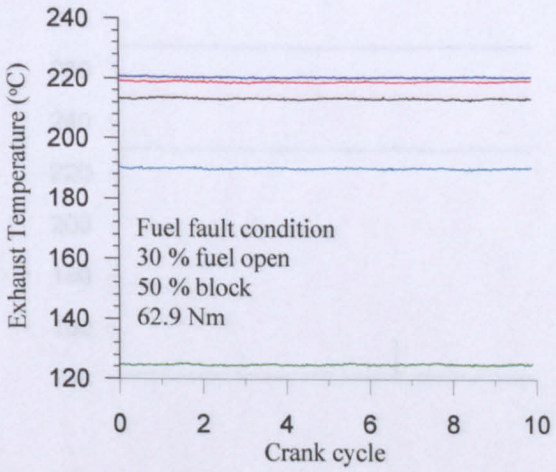
Exhaust Temperature (°C)
240
220
200
180
160
140
120
0
2
4
6
8
10
Crank cycle
Fuel fault condition
30 % fuel open
50 % block
62.9 Nm

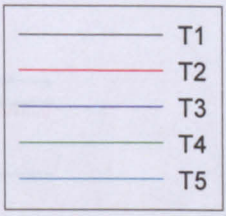
T1
T2
T3
T4
T5

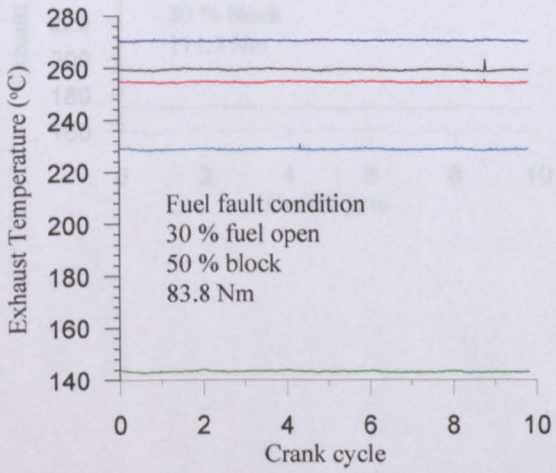
Exhaust Temperature (°C)
280
260
240
220
200
180
160
140
0
2
4
6
8
10
Crank cycle
Fuel fault condition
30 % fuel open
50 % block
83.8 Nm

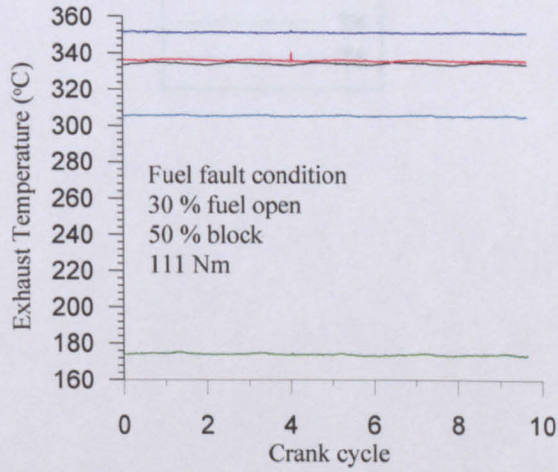
Exhaust Temperature (°C)
360
340
320
300
280
260
240
220
200
180
160
0
2
4
6
8
10
Crank cycle
Fuel fault condition
30 % fuel open
50 % block
111 Nm

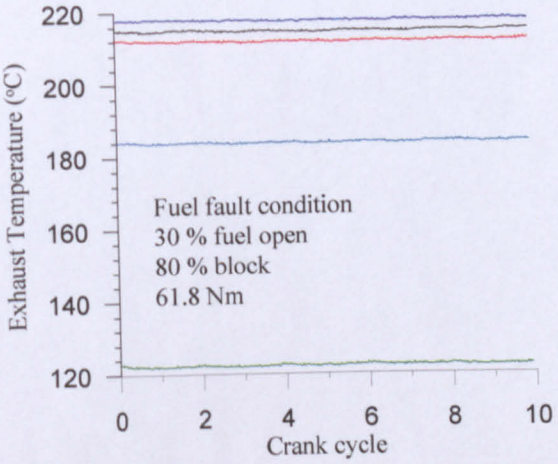
Exhaust Temperature (°C)
220
200
180
160
140
120
0
2
4
6
8
10
Crank cycle
Fuel fault condition
30 % fuel open
80 % block
61.8 Nm

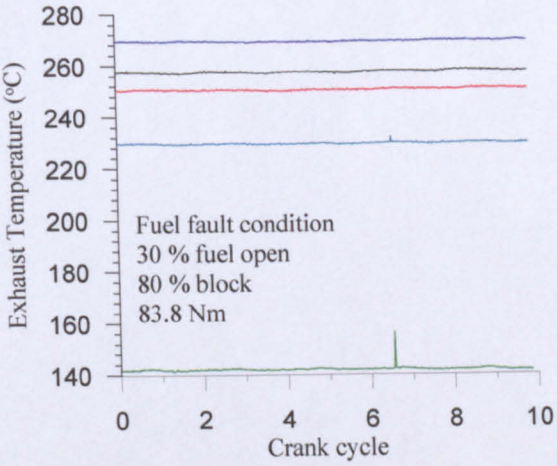
Exhaust Temperature (°C)
280
260
240
220
200
180
160
140
0
2
4
6
8
10
Crank cycle
Fuel fault condition
30 % fuel open
80 % block
83.8 Nm

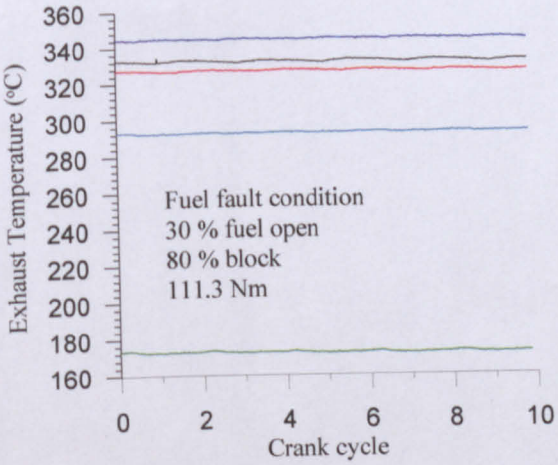
Exhaust Temperature (°C)
360
340
320
300
280
260
240
220
200
180
160
0
2
4
6
8
10
Crank cycle
Fuel fault condition
30 % fuel open
80 % block
111.3 Nm

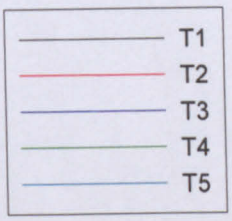
T1
T2
T3
T4
T5